NASA Contractor Report 3230

Turbulence, Combustion, Pollutant, and Stability Characterization of a Premixed, Step Combustor

A. T. Ganji and R. F. Sawyer

GRANT NSG-3028
JANUARY 1980

NASA

NASA Contractor Report 3230

Turbulence, Combustion, Pollutant, and Stability Characterization of a Premixed, Step Combustor

A. T. Ganji and R. F. Sawyer
University of California
Berkeley, California

Prepared for
Lewis Research Center
under Grant NSG-3028

National Aeronautics
and Space Administration

Scientific and Technical
Information Office

1980

PREFACE

This report has been prepared from the doctoral thesis of A.R. Ganji. Both editorial and interpretative changes have been made. The thesis contains additional detail on the design of the step, the reduction and analysis of experimental data, the correction of chemiluminescent analyzer data, and reporting of compiled experimental data. The reader who may be interested in these details may obtain the thesis, "Combustion and Stability Characteristics of a Premixed Vortex Dominated Two Dimensional Flow," from University Microfilms, Ann Arbor, Michigan.

TABLE OF CONTENTS

CHAPTER 1

INTRODUCTION

1.1 Premixed Prevaporized Combustor Concept: Advantages and Drawbacks

This research is part of an effort to understand the fluid dynamics and chemistry of lean premixed flames which might eventually be used in gas turbine combustors. The use of lean premixed prevaporized combustion in aircraft gas turbine engines is one possible approach to reduction of oxides of nitrogen and particulate emission and to improvement of turbine inlet temperature patterns at higher power and cruise modes of operation of gas turbine combustors. At the idle mode of operation, lean premixed prevaporized combustion reduces unburned hydrocarbon and carbon monoxide emission levels. Conventional gas turbine combustors work on the basis of diffusion flames. Fuel is injected by fuel atomizers into the primary zone of the combustor where the flame is stabilized through air swirl created recirculation zones. The resulting near stoichiometric burning of fuel and air produces the maximum possible temperature inside the combustor. In lean premixed prevaporized combustors, the temperature in the primary zone corresponds to the mixture ratio of the zone which is below the stoichiometric condition (by about a factor of two). Lower emission levels of oxides of nitrogen from lean premixed prevaporized combustors is due to lower peak combustion temperature compared to the peak temperature in the primary zones of conventional combustors, Sawyer, et al. (1973).

Reduction of particulates, carbon monoxide, and hydrocarbons is due to the prevaporization of fuel and air, the more uniform combustion in the primary zone of the combustion chamber, and an excess of air. Figure 1.1 shows the pollutants, their cause and cure in the two extremes of power level of an aircraft gas turbine combustor.

Jones (1978) discusses the achievements of advanced technology combustors in reduction of NO_x, CO, unburned hydrocarbons and smoke in different modes of operation of gas turbine engines. He concludes that the desired low levels of NO_x, EPA (1976), cannot be satisfied with the conventional technology for combustors. One of the most promising approaches to the solution of this problem is premixed prevaporized combustion, Figure 1.2 The achievements of using lean premixed prevaporized combustion for gas turbines are likely to be obtained only with the introduction of new or increased problems of stability, flashback and autoignition. The advantages and problems for application of lean premixed prevaporized combustion to gas turbine combustors have been discussed in detail by Lefebvre (1977).

Although there has been extensive and thorough experimental research on turbulent flame propagation and stability in the past, see,for example, Williams, et al. (1949) and Wright and Zukoski (1961), investigation of these processes in the light of the new findings in turbulent flow research has become of renewed basic interest. The problem of autoignition for these type of combustors has been studied to much less extent. Spadaccini (1977) has summarized the literature on the subject up to the cited date. He also discussed the current experimental effort pertinent to the autoignition of premixed reactants in gas turbine combustors. Flashback literature in premixed prevaporized combustors has been reviewed by

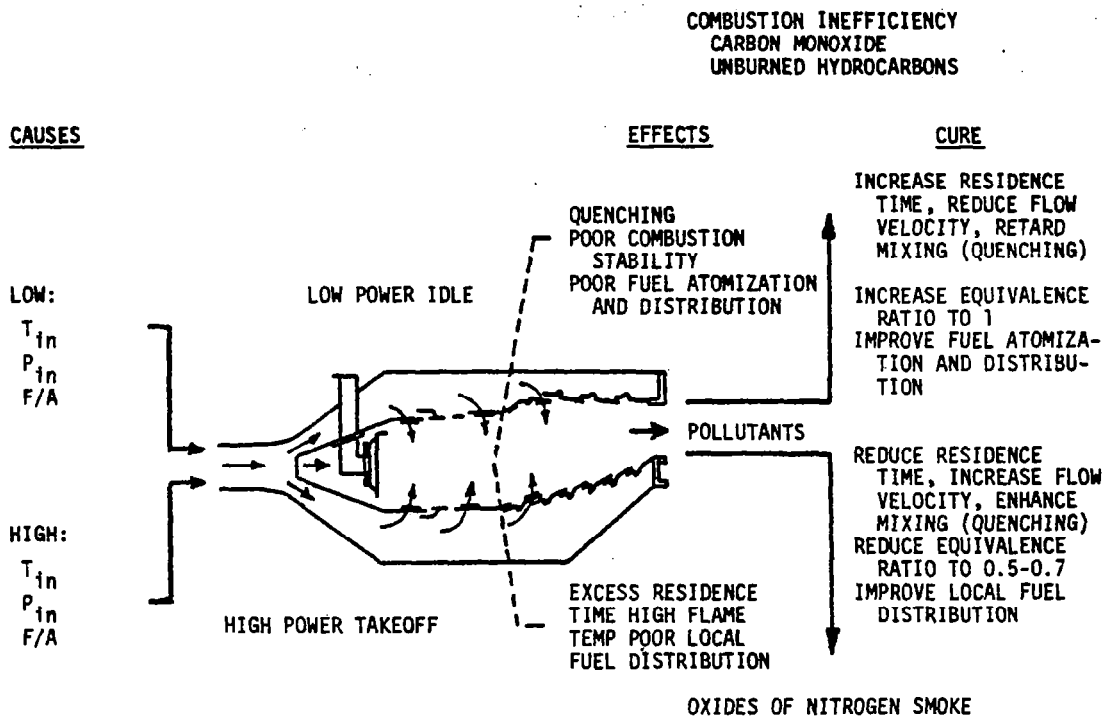

Fig. 1.1 Combustion emission considerations from conventional gas turbine combustors (Jones, 1978).

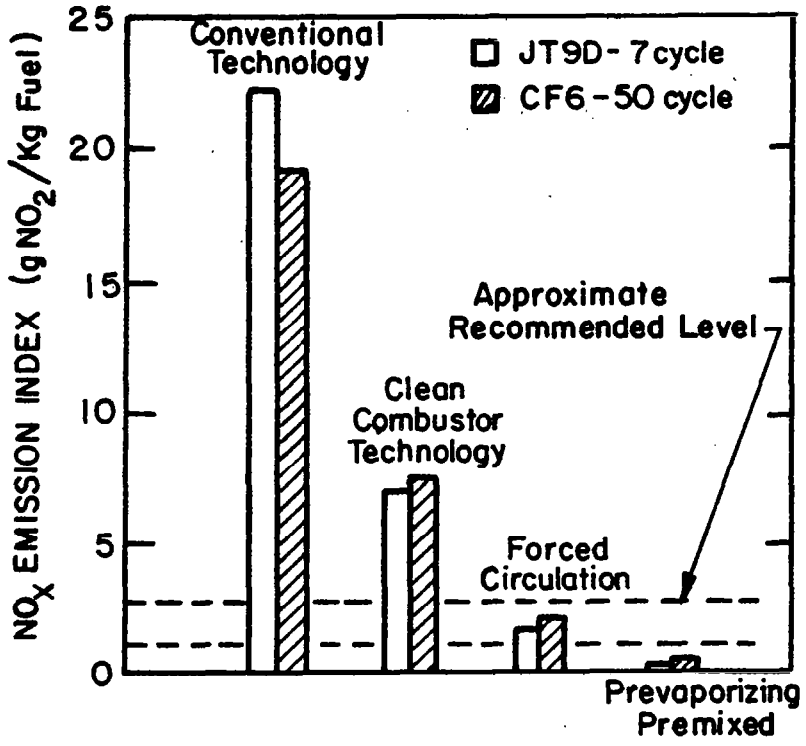

Fig. 1.2 NO_X emissions forecast for subsonic cruise, Mach number - 0.85 at 10.7 km altitude (Lefebvre, 1977).

Plee and Mellor (1978b). They have tried to correlate the existing flashback data in the literature according to a flashback parameter derived from the work of Lefebvre (1966). The scatter in the data prohibits them from drawing definite conclusions from the correlations.

This work is an experimental study of the combustion of a premixed flame stabilized by a rearward facing step. The limits at which the blowout or flashback occur and the formation of gaseous pollutants have been investigated. The experimental facility is a two dimensional premixed prevaporized combustion tunnel, with full optical and probing access to the flame. Propane is used for fuel and air for the oxidizer. The mixing layer in which combustion occurs is close to a free shear layer. The complexities of obtaining a true free shear layer which would require a pilot flame or hot gases on one side of the flow have been avoided. The latter experiment is to be done at Berkeley in the near future, Daily (1978).

1.2 Two Dimensional Shear Layers

The process of combustion in almost all high intensity burners is turbulent in nature. Turbulent flows augment the process of mixing and as a result enhance the intensity of combustion. Fundamental understanding of this mixing process and its interaction with combustion chemistry is currently the biggest challenge to experimentalists and theoreticians in the field. Despite great efforts in research in the field of turbulent flows, there is still no universal approach to the problems in this field, Tennekes and Lumley (1972). This is partly due to the enormous complexity and variations of turbulent flows and partly to the lack of a body of reliable fundamental measurements. Recent developments in optical

diagnostics, advances in computers and data processing methods and the great deal of research in this direction promises new and qualitative advancements in the knowledge of turbulent flows.

Until recently it was thought that free shear layers consisted of two regions, one turbulent and the other nonturbulent, with the turbulent region being characterized by random, three dimensional motions and the presence of vorticity fluctuations. Viscous forces were continously propagating these vorticity fluctuations into the nonturbulent region along the interface between the two regions ("entrainment by nibbling").

Recent experiments on some simple nonreacting turbulent flows, such as free shear layers and jets, has resulted in some new views of the structure of these turbulent flows. Laufer (1975) has concluded that "these turbulent flows are not as chaotic as have been previously assumed, and that there is some order in their motion with an observable chain of events reoccurring randomly with a statistical definable mean period". The new view suggests, "that with every shear flow is associated an identifiable, characteristic structure and that the development of the flow is controlled by the interaction of these structures with each other", Roshko (1976). These views of the structure of turbulence have strong experimental support in free shear layers, Brown and Roshko (1974), in circular jets, Yule (1978), in turbulent wakes, Papailiou and Lykoudis (1974) and in boundary layers, Offen and Kline (1974). The basic findings of this research has established the concept of "coherent large scale structures" in turbulent shear flows. This is more or less a deterministic approach. By deterministic it is meant that, "eddies have a characteristic shape, size and convective motion that can be determined within a relatively small standard deviation," Laufer (1975). The subject of the new trends in

studying turbulent flows has been reviewed by Laufer (1975) and Davies and Yule (1975).

In nonreacting free shear layers behind a splitter plates, Brown and Roshko (1974) and Winnant and Browand (1974) have clearly shown that large eddies are formed in a quasi-orderly fashion, are carried through the mixing layer, and grow through coalescence and engulfment. It is in these processes that the irrotational fluid is ingested and enfolded in the large scale structures. Meanwhile internal mixing occurs by the action of the small scale turbulence and viscosity and the new fluid is digested and incorporated into the structure, Roshko (1976). It is now suggested that these large coherent structures have the prime role in the development and growth of turbulent free shear layers.

There has been far less evidence, experimental work and even effort in the application of these concepts to reacting flows such as combustion. In their pioneering work on bluff body flame stabilzation based on the similarity between nonreacting and reacting flows behind bluff bodies, Nicholson and Field (1949) suggested that "some sort of eddies or vortices or at least curvilinear flow patterns do exist in the burning region" and also "that mixing can be accomplished solely by the well ordered quasi-streamlined flow in the vortex trail." Only recently have there been efforts to apply the concept of "coherent large scale structures" and some related quantitive results of nonreacting shear flows to reacting shear layers. Konrad (1976) has applied measured probability density functions in nonreacting flows to predict reaction rates for similar fast reacting flows. Marble and Broadwell (1977) have predicted the fuel consumption rate for diffusion flames in the mixing region between two streams and also for turbulent fuel jets. Experimental evidence of the

existence of large coherent structures in reacting flows and the effect of combustion on these structures has not been reported. Contemporaneous work by Chigier and Yule (1978) published in the final stages of this work confirms the existence of coherent large structures in the transition region of a turbulent jet diffusion flame.

One of the purposes of the present work is to investigate the importance of large scale coherent structures in a shear flow both with and without combustion.

1.3 Scope of Research and Thesis Content

The experimental facility and equipment which was designed and constructed is described in Chapter 2. Results of cinematography of the flow field by schlieren and shadowgraph techniques are presented and discussed in Chapter 3. These visualization methods were used to observe the flow process and to study such features of the flow as formation, development and convection of large scale structures in reacting and nonreacting flows inside the combustor. The parameters studied are eddy formation period, eddy formation position, and rate of eddy survival as they move downstream. The variation of above parameters has been studied for three values of reference velocity (between 9.0 and 22.5 m/sec), two values of temperature (295, 454 K), and three values of equivalence ratio between the blowout and flashback limits of the flame. The same parameters have also been studied for nonreacting flow behind the step. The effect of tripping the approaching boundary layer on the flow behind the step is also described in Chapter 3. The behavior of the flame in transition to and at the extreme modes of operation (blowout and flashback) is discussed in Chapter 4. In Chapter 5 time averaged, space resolved probe measurements inside the flame are presented and discussed.

Temperature, velocity and concentrations of CO, CO_2, HC, NO and NO_x have been mapped in the flame zone and from these results pointwise efficiency has been calculated. The effect of inlet temperature and velocity on the above parameters has been investigated. Geometry, pressure (one atmosphere), and reactants (premixed propane/air) were held constant for all experiments. In Chapter 6, the results of the three preceeding chapters are summarized and some related theoretical works are briefly mentioned.

CHAPTER 2

EXPERIMENTAL FACILITIES AND PROCEDURES

2.1 Experimental Apparatus

A schematic diagram of the experimental facility is shown in Figure 2.1. Air is supplied by a compressor at a maximum rate of .5 kg-sec^{-1} and maximum pressure of 8 x 10^5 N/m^2. Compressed air is dried in a dessicant dryer to reduce the incoming air humidity to less than 20%. Air can be heated with a three element 90 kw resistance heater to a temperature corresponding to maximum test section inlet temperature of 600 K (at high flow rates), and then filtered through a porous (.6 μm hole) high temperature filter (Microfibre Filter Tubes, grade A, Bolston Filter Products, Lexington, Mass.). Air is distributed into three lines.. Two go to the mixing chamber and the third is used for cooling the test section. The pressure and flow in these lines are controlled by three high temperature globe valves.

In each line the air is measured by interchangeable critical flow nozzles designed according to the ASME standards (ASME, 1959). The advantages of this type of flow meter are discussed by Arnberg (1962). Three different size nozzles of 5.08, 7.62 and 12.70 mm throat diameter were manufactured and calibrated at Alameda Naval Air Station according to the Bureau of Stanadards procedure. They are accurate within .2% at ambient temperatures. The diameter of pipes upstream and downstream of the nozzles is 51 mm, so the temperature and pressure measured upstream of the nozzles are considered to be at their stagnation values. The two

1 - FLAME DETECTOR
2 - OVER PRESSURE CONTROL
3 - OVER TEMPERATURE CONTROL
4 - WATER PRESSURE CONTROL
5 - UNDER TEMPERATURE CONTROL
6 - AIR FLOW CONTROL
7 - FUEL LEAK CONTROL

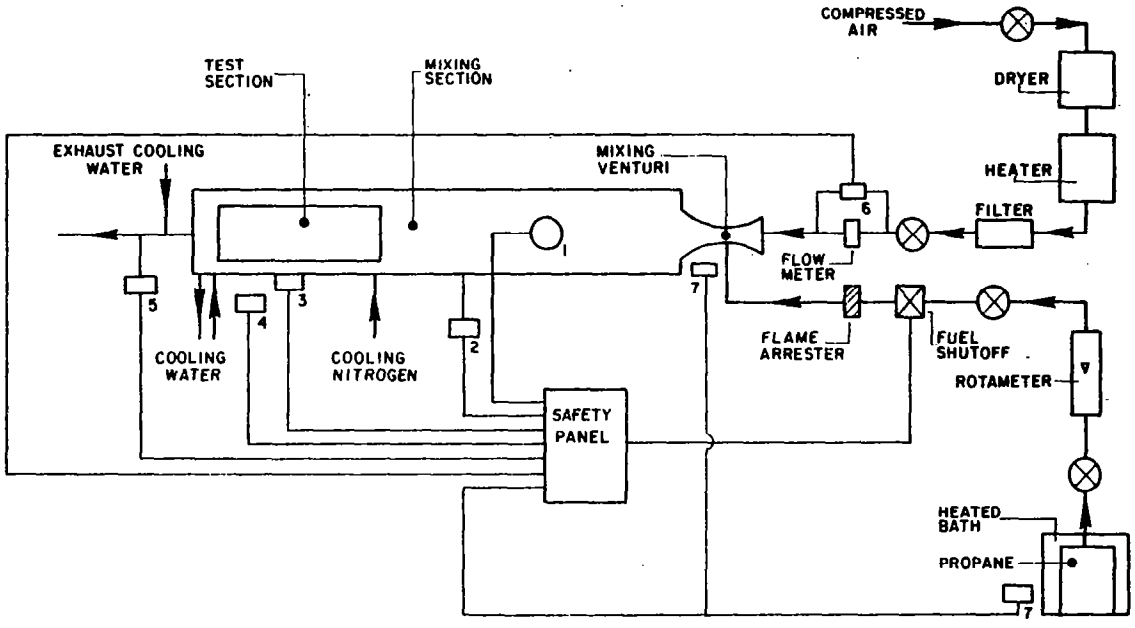

Fig. 2.1 Flow schematic of the two dimensional combustor facility. Safety system sensors for automatic fuel shutoff are given at the top of the page.

streams of air enter the air manifold from two opposite sides. The air manifold then directs the air to the three mixing venturi nozzles.

The fuel system consists of two propane tanks (fuel composition is given in Table 2.1) immersed in water baths, which are heated by steam coils. The purpose of heating is to provide the propane latent heat of vaporization. Otherwise extraction of propane at high flow rates, as is the case in these experiments, results in reduction of temperature and pressure in the tanks which can lead to flame extinction. Fuel is measured by a calibrated rotameter (Fisher & Porter Rotameter No. FP-314-27-G10/86). Fuel flow rate is controlled by a needle valve downstream of the rotameter. Fuel then flows through an automatic shut off valve. This valve can be activated by a number of default detectors through a safety circuit. These detectors are also shown in Figure 2.1. After passing through a flame arrester the fuel mixes with air in the venturi nozzles.

Table 2.1

Typical Analysis of the Fuel
Used for the Experiments

Components	Mass per-cent
Ethane	1.5
Propylene	2.5
Propane	95.8
Isobutane	.2
Isopentane & Hexane	trace
N-Butane	trace

The cross section of the experimental apparatus is shown in Figure 2.2. Air and fuel mix in three venturi nozzles at the throat of the venturies. This method of mixing has proved to be an effective way of intermixing

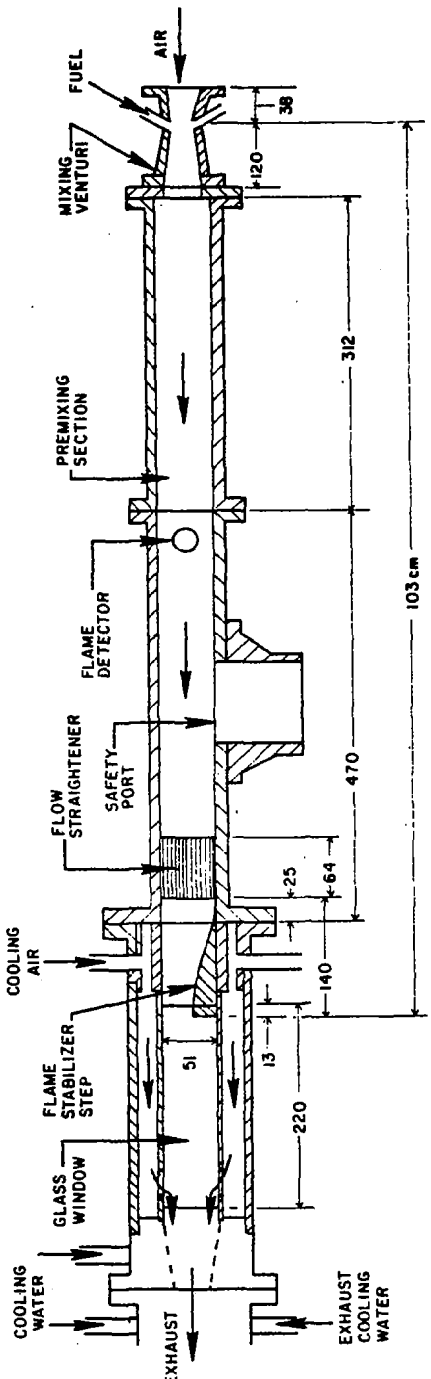

EXPERIMENTAL APPARATUS

Fig. 2.2 Two dimensional combustor test section. Dimensions in mm.

two gases, Schefer (1976). The mixture then enters the premixing chamber that is about one meter long. The premixing chamber has a rectangular cross section 51 mm high and 173 mm wide. It was attempted to make the premixing section as smooth as possible and without any obstruction to the flow. The premixing section is equipped with a photoconductive, cadmium selenide cell (Type CL 703, Clairex Electronix, Inc., N.Y.) flame detector, an adjustable over pressure detector (set normally at 2×10^5 N $/m^2$) and an 89 mm brass foil blowout disc (experimentally tested for 2.7×10^5 N $/m^2$) at the bottom of the premixing section. The blow out port is connected to the laboratory exhaust trench by a pipe of the same diameter. A 1.5 mm square cell ceramic flow straightener (Celcor, 200 square cells/in^2, Corning glass products, N.Y.), with 31% blockage has been used to smooth any large flow discontinuities. The dimension of the cells is less than the quenching distance for operational limits of the equivalence ratio ($.4 < \phi < .8$) at ambient temperature, Fristrom and Westenberg (1965). Therefore, the flow straightener also acts as an effective flame arrester preventing the flame from flashing back into the premixing chamber.

The test section entrance is equipped with a step which is streamlined in the upstream direction and has a blockage ratio of 0.5. The step, designed according to the procedure of Libby and Reiss (1951), delivers a uniform entrance velocity and also stabilizes the flame. As shown in Figure 2.2 the step is mounted at the bottom of the combustor. A photograph of the step is shown in Figure 2.3.

The top and bottom of the test section is constructed of 3.2 mm thick inconnel plates which are reinforced by welding three 25.4 mm by 25.4 mm bars along them. These bars were found to be necessary because

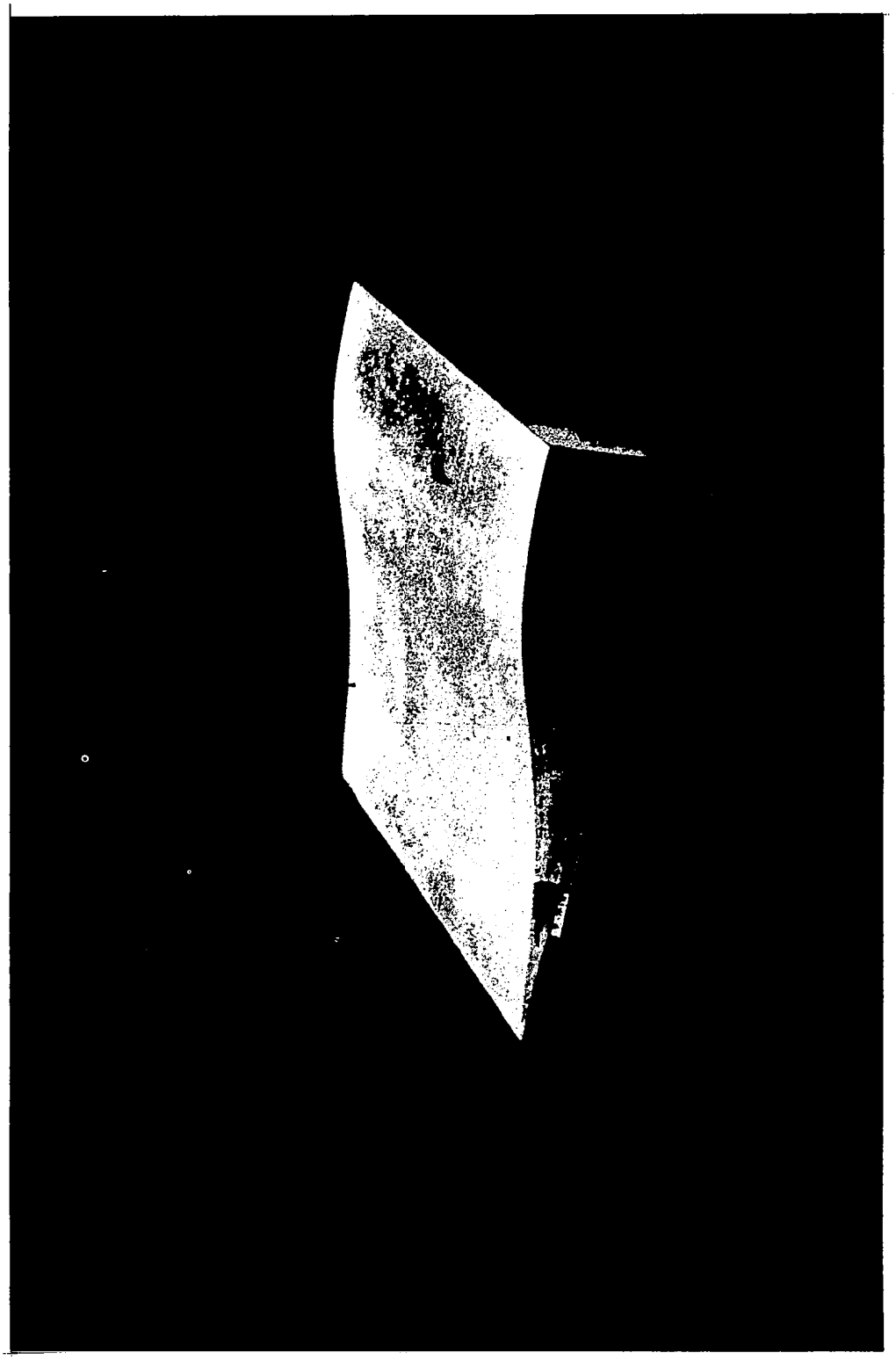

Fig. 2.3 Step profile.

otherwise warping of the plates occurs due to the temperature gradient which is created in the plates during the operation of the experiment. These re-enforcement bars are not attached to the 12.5 mm thick outer plates, to minimize thermal distortion. Air pathways for cooling the top and bottom plates have been provided, but their use was found to be unnecessary.

Optical access to the test section is provided by two 12.7 mm thick fused quartz (G.E. Type 124 Clear Fused Quartz more than 99.97% pure SiO_2) windows on the sides of the test section. Nitrogen cooling of the internal surfaces of the windows has been provided. During the course of experiment it was found that it is not essential to cool the windows.

As shown in Figure 2.2 the exhaust section is water cooled. The products of combustion pass through a contraction of 73 mm by 73 mm into the exhaust trench. The products are cooled by three water sprays to a temperature of about 400 K. The exhaust trench is at about 38 mm of water vacuum.

Initial ignition of the system is provided by a conventional rod ignitor and a 10,000 volt, 23 mA ignition transformer. The rod is located 5 cm downstream of the step edge and 6.4 cm off center from the plane of symmetry.

Gas temperatures were measured by chromel alumel thermocouples at the following locations:

1. - main air manifold
2. - 75 mm upstream of each air nozzle
3. - 100 mm downstream of fuel rotameter outlet
4. - the throat of the middle venturi
5. - 64 mm upstream of the edge of the step

The thermocouples were connected to a digital thermometer (Model 250 Omega Digital Thermometer) with a reference junction compensator and accuracy within ± 1 K.

Pressure of the gases was measured and could be recorded at the following positions in the system:

1. - Main air manifold
2. - 75 mm upstream of each air nozzle
3. - 75 mm downstream of fuel rotameter

The pressure could be measured by strain gage pressure transducers (Model 3P91 Senso-Metrics) or calibrated bourdon gages. An accuracy of 1% full scale was the manufacturer's supplied information on the transducers.

Eighteen probing holes are provided at the top and bottom of the test section in intervals of 10 mm downstream of the step. The holes are located alternately at 4.8 mm on the sides of the vertical plane of symmetry. The first and last holes are on the axis of symmetry. The combustor could also be probed from the sides provided the quartz windows were replaced by similar steel plates.

A picture of the experimental appartus is shown in Figure 2.4. Important factors in the design of this system are:

1. - Thorough mixing of air and propane before entering the test section.
2. - A uniform velocity flow field at the entrance to the test section.
3. - Safety.

Adequate mixing was insured by choice of venturies and a long premixing chamber (about 1 m). For selection of the length of the premixing chamber the experience of the previous researchers, Schefer (1976), Roffe and Ferri (1976), Anderson (1975), and Spadaccini and Szetela (1975) was of great help. The physical dimension of the laboratory was another factor in the design, limiting the length of the premixing section.

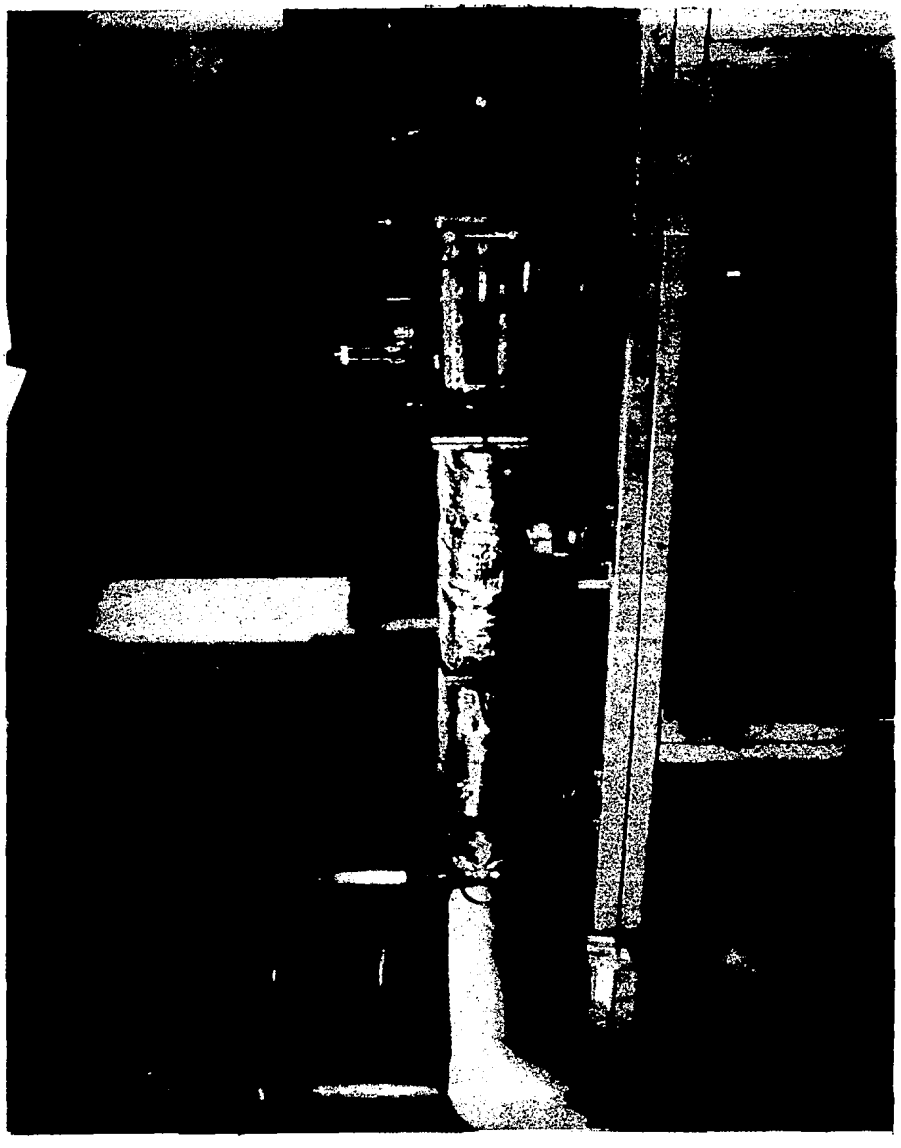

Fig. 2.4 Experimental apparatus. Flow from left to right.

The extent of mixing was tested by mixing CO_2 with air at the mixing venturies and measuring the composition of CO_2 by a Beckman Model 315 nondispersive infrared analyser at the entrance to the test section. The measurement was done along the centerline in the transverse direction as well as along three vertical lines (centerline and two lines 51 mm to the sides) for two carbon dioxide flow rates. The results are shown in Figure 2.5. The deviation between maximum and minimum CO_2 concentration is less than 2% for all cases. Carbon dioxide was chosen in this test for two reasons: firstly to avoid dumping explosive propane air mixture in the exhaust and secondly because carbon dioxide has the same molecular weight as propane.

To test flow uniformity, flow velocity was measured in horizontal and vertical transverse directions at the entrance to the test section. The measurements were done by using a pitot static tube and a water micromanometer. Figure 2.6 shows the velocity profile in the horizontal transverse direction. The deviation between the maximum and minimum value of the data points is less than 3%. Figure 2.7 shows the velocity profile in the plane of symmetry at the entrance to the test section. The maximum deviation from the average is less than 8%. This value has been calculated ignoring the velocity data just at the edge of the step, within the boundary layer.

Because of the premixing of the fuel and air long before burning, the system is potentially susceptible to explosion, especially at high temperatures. Pre-ignition and flashback are the cause of this concern. As mentioned before the flow straightener acts also as an effective flame arrester. To minimize the chance of pre-ignition, disturbances to the flow which might increase the residence time of a combustible mixture in the premixing section were avoided.

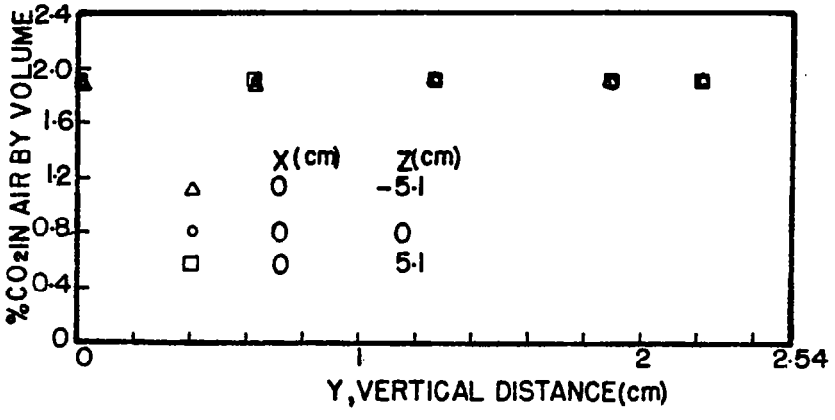

(a)

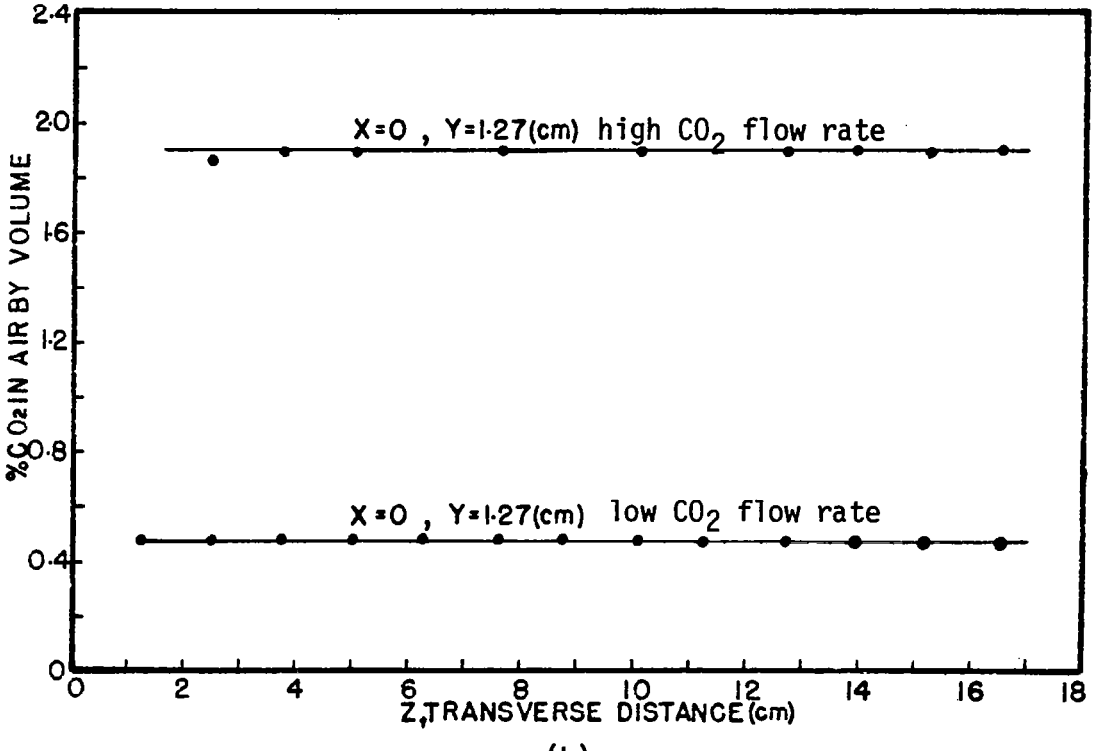

(b)

Fig. 2.5 CO_2 composition profiles at the entrance to the test section. CO_2 was mixed with air at the venturi nozzles, $V_o \cong 9.3$ m/sec.

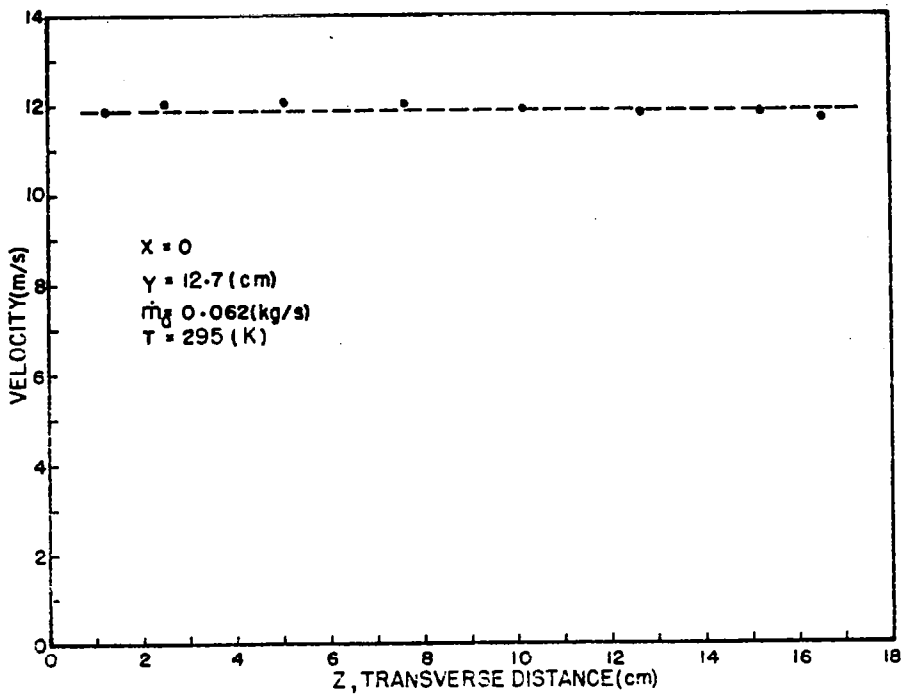

Fig. 2.6 Velocity profile in the horizontal transverse direction.

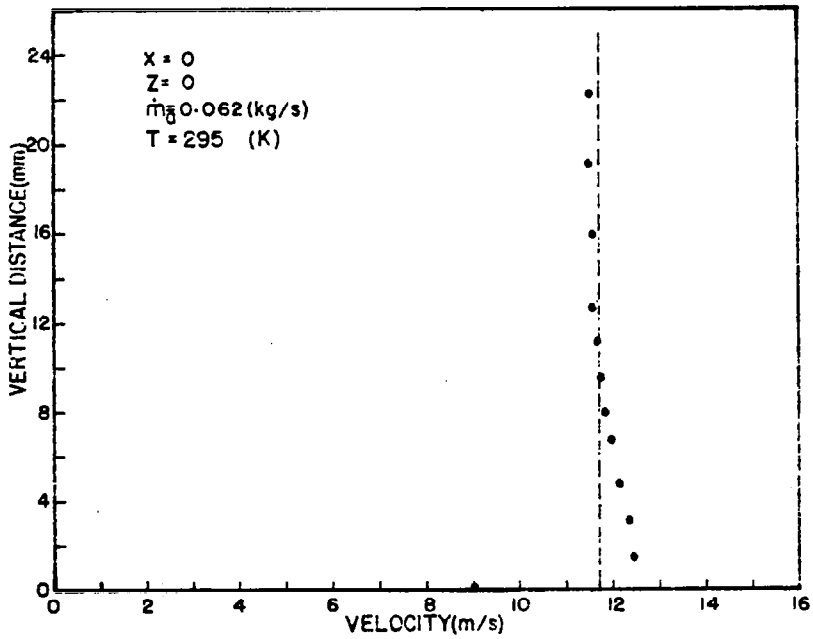

Fig. 2.7 Velocity profile in the vertical transverse direction.

In addition to the above considerations, the following safety detectors are installed and connected to a central control panel. If any of the detectors senses a default, through the safety circuit it will shut off the automatic solonoid valve in the propane line and the corresponding red light on the control panel will light up to show the reason for shut off. The detectors as shown in Figure 2.1 are:

1. - Flame detector: Described before.
2. - Over pressure control: Described before.
3. - Over temperature control: This is installed on the outer plate of the combustor and is set at about 500 K. In case the chamber is overheated it will shut the fuel off.
4. - Water pressure control: This is installed in the water line which cools the exhaust block and products of combustion. If for any reason water pressure falls below the set point (2×10^5 N/m^2) it will shut the fuel off.
5. - Under temperature control: This is a Fen-well Thermoswitch installed in the exhaust manifold downstream of the water sprays, set at about 400K. If for any reason the flame is extinguished, this detector will shut off the fuel. This detector prevents dumping of explosive mixtures into the exhaust trench.
6. - Air flow control: This is a pressure differential switch which detects the drop in the pressure difference across one of the critical flow nozzles. It is set at $.4 \times 10^5$ N/m^2 pressure differential. If for any reason (line rupture, compressor defect, etc.) air pressure difference drops below the preset value, the fuel will be shut off by this detector.
7. - Fuel leak detectors: There are two fuel leak detectors (Davis Instruments Combustible Gas Monitor, Model 3800) which are installed next to the propane tanks and under the mixing venturies. The instrument is factory calibrated for 0% - 100% lower flamability limit of propane. They detect any fuel leak through a heated platinum wire and shut the

fuel off if the local concentration of propane is above 25% of the flammability limit.

All above safety devices were calibrated and checked before the start of the operation of the system and have been checked regularly during the course of the experiments.

2.2 Velocity Measurements

Velocity was measured with a stainless steel pitot-static tube and a water micromanometer. The pitot-static tube used is shown in Figure 2.8. It was mounted on a probe traversing mechanism described in Section 2.4. The velocity measured in this experiment was the time averaged value in the direction of the mean flow. At later stages of this experiment, an LDV system became available and was used to measure the velocity throughout the flow field, Houser (1979).

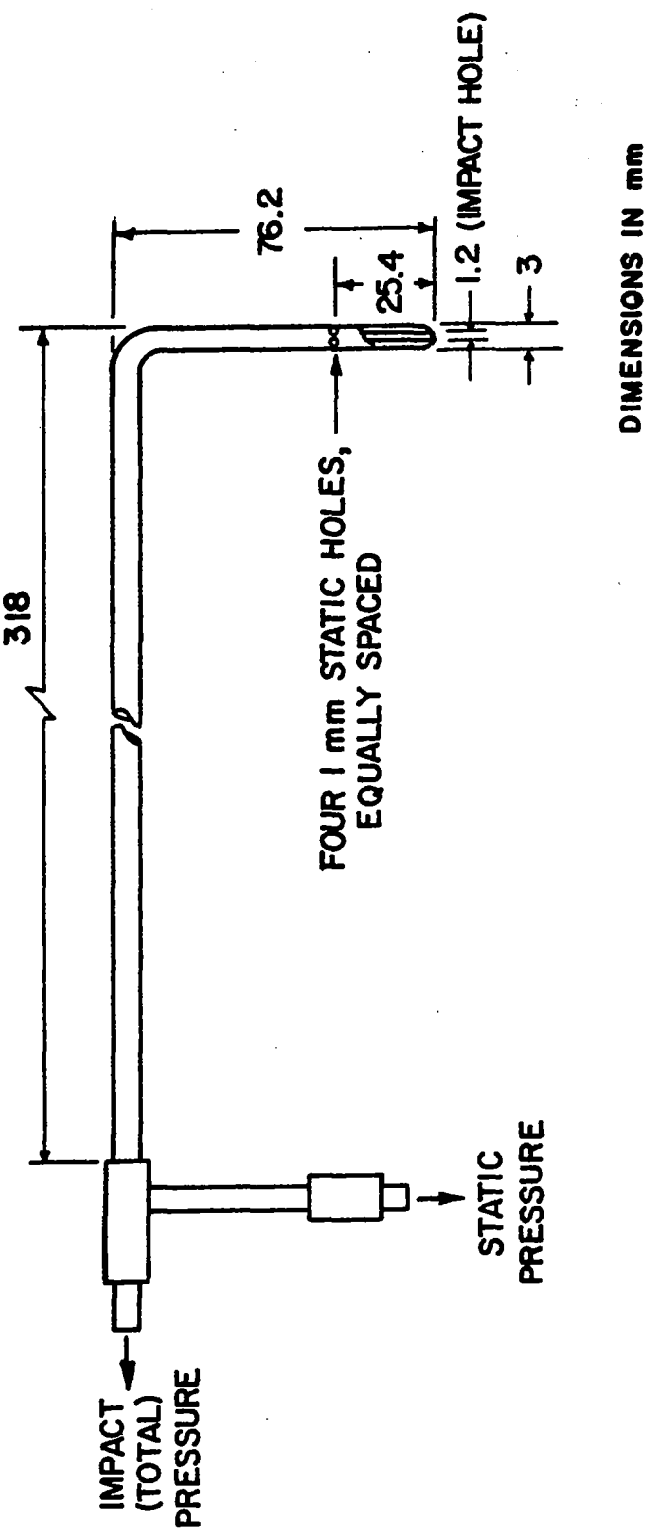

Fig. 2.8 Pitot static tube. Dimensions in mm.

2.3 Temperature Measurements

Inside the flame, temperature was measured using a 76 μm diameter Pt versus Pt - 13% Rh thermocouple. A diagram of the thermocouple is shown in Figure 2.9. Pt and Pt - 13% Rh wires were butt welded together, following the recommendations of Fristrom and Westenberg (1965). The size of the bead is slightly larger than the diameter of the wires. The 76 μm thermocouple wires are in turn supported by 254 μm wires of the same material. The junction between the 76 μm and 250 μm wires is also butt welded. The thermocouple bead was then silica coated (using silicon oil) to reduce the problem of catalyzation, Fristrom and Westenberg (1965). According to Kent (1970) a mixture of beryllium oxide in yttrium chloride for coating has some advantages over the silicon oil. But because of the carcinogenicity of this material, silicon oil was preferred.

The thermocouple could be inserted either from the side or from the bottom of the combustor. For probing the combustor from the side the thermocouple wires were supported by a 4 mm double bore quartz tube which was bent 90^{o} for a length of 65 mm. The purpose of bending the support tube was to minimize the flow disturbance at the measurement point. But even with the bent section, the disturbing effect of the probe could be readily seen in changing the shape of flame, especially when measurements were made close to the edge of the step. This problem is discussed in more detail in Section 2.4. Temperature measurements from the side were made to check burning uniformity across the combustor. Once the two dimensionality of the combustor was established, it was recognized that probe measurements from the bottom of the combustor through the probing holes (Section 2.1) is much faster and less disturbing to the flow. The measurements were made at intervals of 1.6 mm in the vertical direction

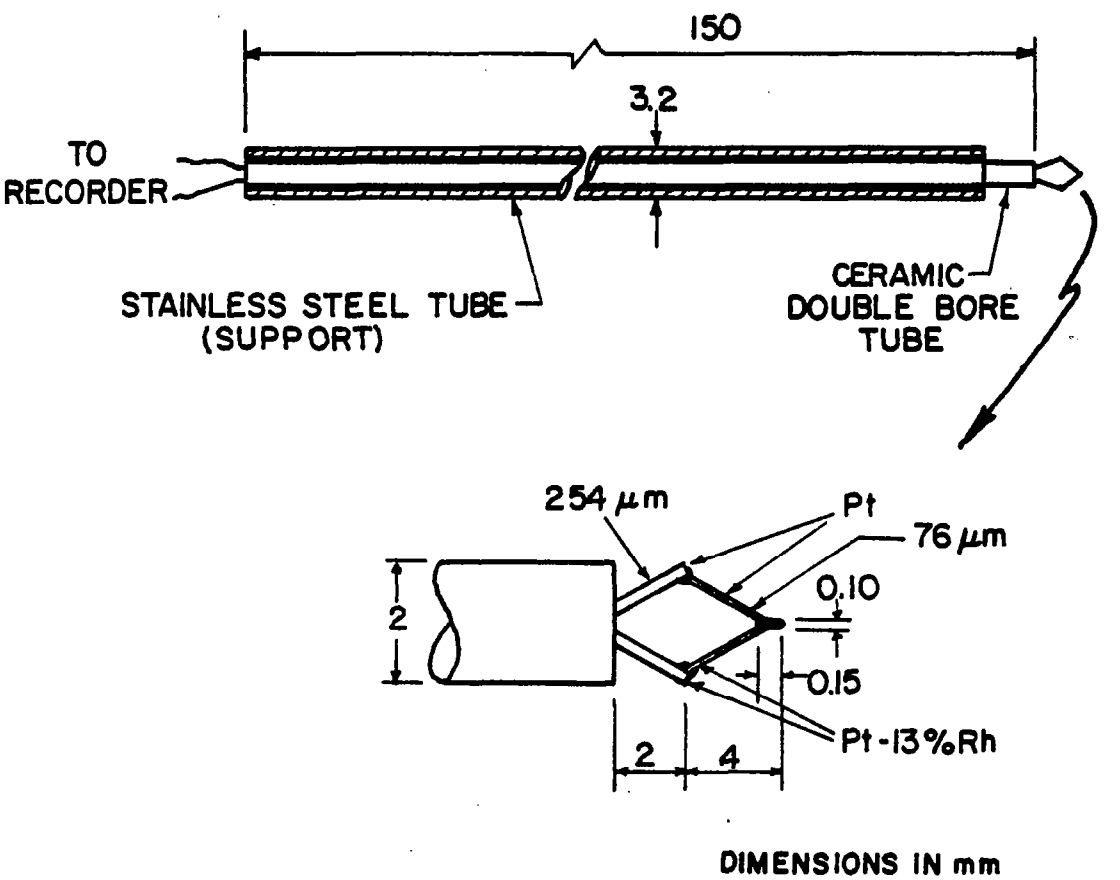

Fig. 2.9 Thermocouple probe.

and at intervals of 10 mm downstream of the step. In either case, probing from the side or the bottom, the probes were mounted on a probe transversing mechanism described in the next section. Reported temperatures have not been corrected for radiation losses.

2.4 Composition Measurements

Space resolved but time averaged composition measurements of CO, CO_2, NO, NO_2 and unburned hydrocarbons were made by probe sampling of the flame. As discussed in Section 2.1, the system is considered to be reasonably two dimensional, so it was concluded that the compositions measured on a vertical plane are representative of the entire combustor. Samples of the composition were taken along a plane 4.8 mm to the side of the plane of symmetry.

Two primary considerations must be dealt with in composition measurements inside the combustion system. Any disturbance (thermal or fluid mechanical) of the flow field due to sampling must be minimized and an accurate or representative sample must be transferred to the gas analysis equipment. Three commonly used gas sampling probes for this type of system are cooled stainless steel probes and cooled and uncooled quartz microprobes. Because of the catalytic effect of metal surfaces on the reaction of both radical species and stable combustion products, Bowman (1977), stainless steel probes were rejected although in terms of durability and physical strength they are superior to quartz probes chosen for this experiment. In his composition measurements in the recirculating flow of an opposed reacting jet, Schefer (1976) found that a partially cooled quartz microprobe was best suited for species measurement.

In the present two experiments two different methods for probing the flame were considered. The first method was probing the combustor from the side by a partially water cooled quartz probe (3.2 mm outside diameter) with the probe bent by 90°, Figure 2.10, to minimize the flow disturbance at the sampling position. Because of the presence of the probe, the temperature downstream of the probe decreased considerably (10-15%), and the flame stability was affected. It was also observed that the flame stabilized behind the cooling jacket. Because of these disturbances to the flow field a second method was applied. An uncooled quartz probe was inserted through holes at the bottom of the combustor. The quartz probe (1.5 mm outside diameter) used, was designed according to the recommendations of Fristrom and Westenberg (1965) and partially shilded by a stainless steel tube for mechanical strength, Figure 2.11. Since the probe insertion into the flame is at most 50 mm, the period that the sample is in contact with the hot walls is very short (normally about 2 msec). The temperature at the probe exit was measured by a fine Chromel-Alumel thermocouple and was found to be less than 320 K for all cases including the high inlet temperature experiments. This temperature is considerably less than the maximum 530 K measured by Schefer (1976) at the exit of his partially cooled probe.

Probes were mounted on a probe positioner with the three degrees of freedom. This device was specifically designed and manufactured for use on the two dimensional combustor, Figures 2.12 and 2.13. Samples were taken at 3.2 mm intervals in the vertical direction and at intervals of 20 mm downstream of the step.

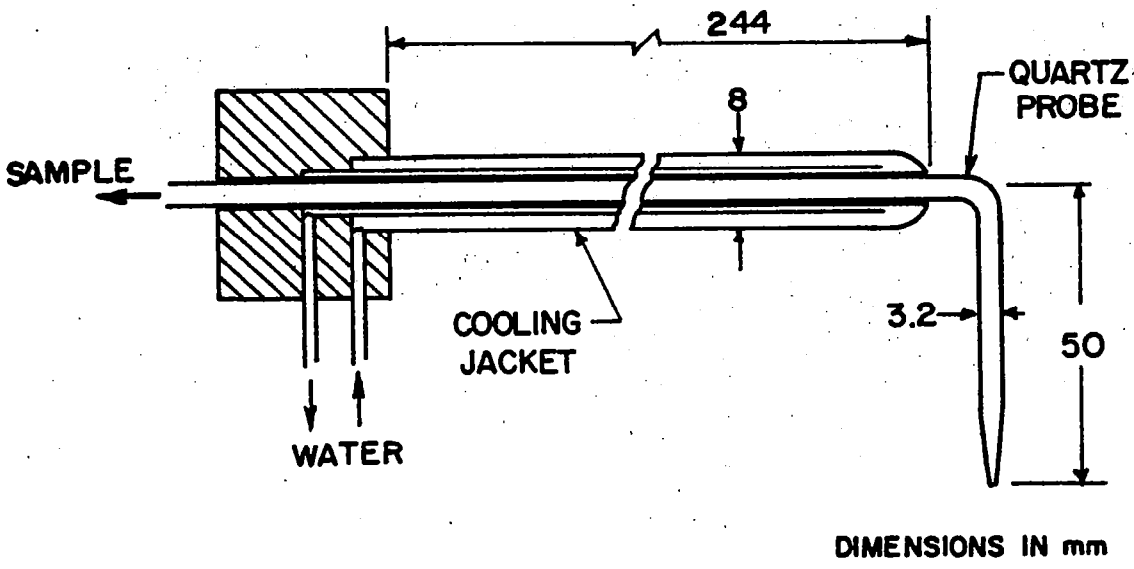

Fig. 2.10 Partially cooled quartz sampling probe. Probe tip is .2 mm ID.

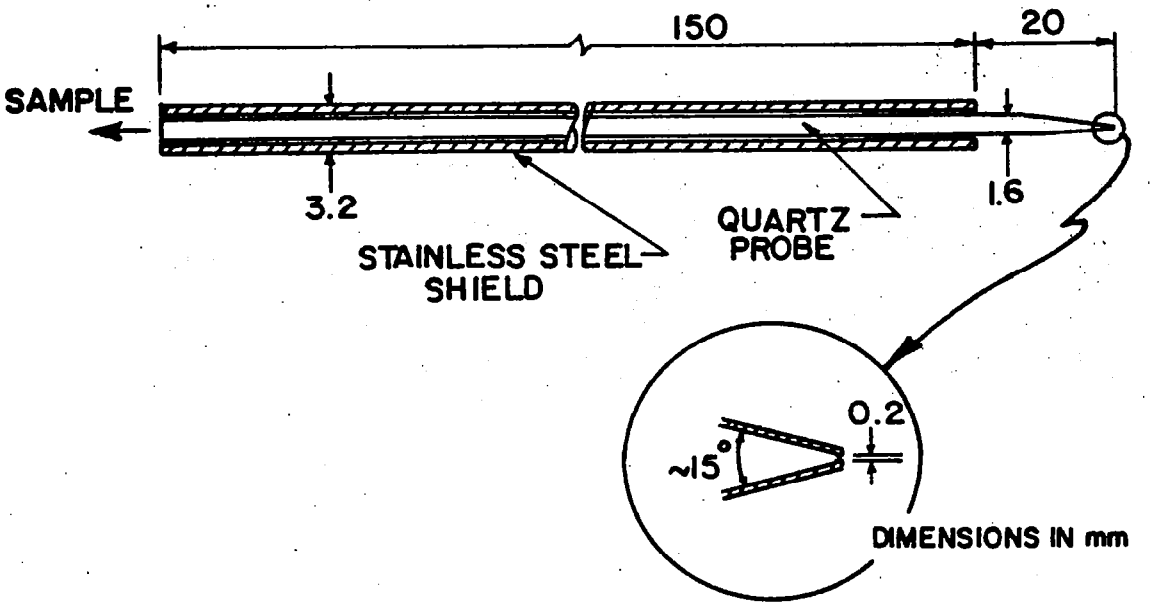

Fig. 2.11 Uncooled quartz sampling probe used for probing the combustor from the bottom. Inner diameter of the probe is 1 mm.

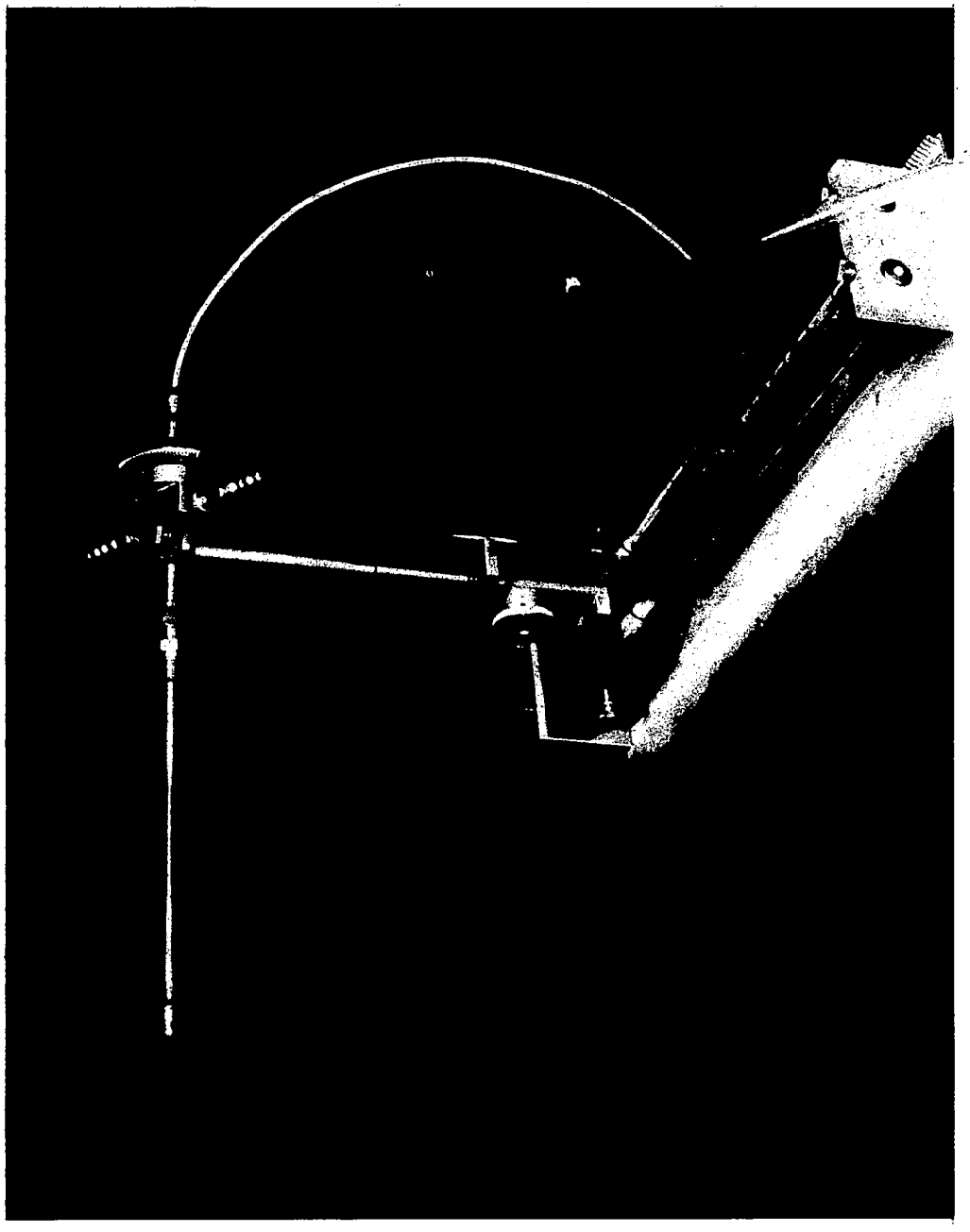

Fig. 2.12 Probe traversing mechanism.

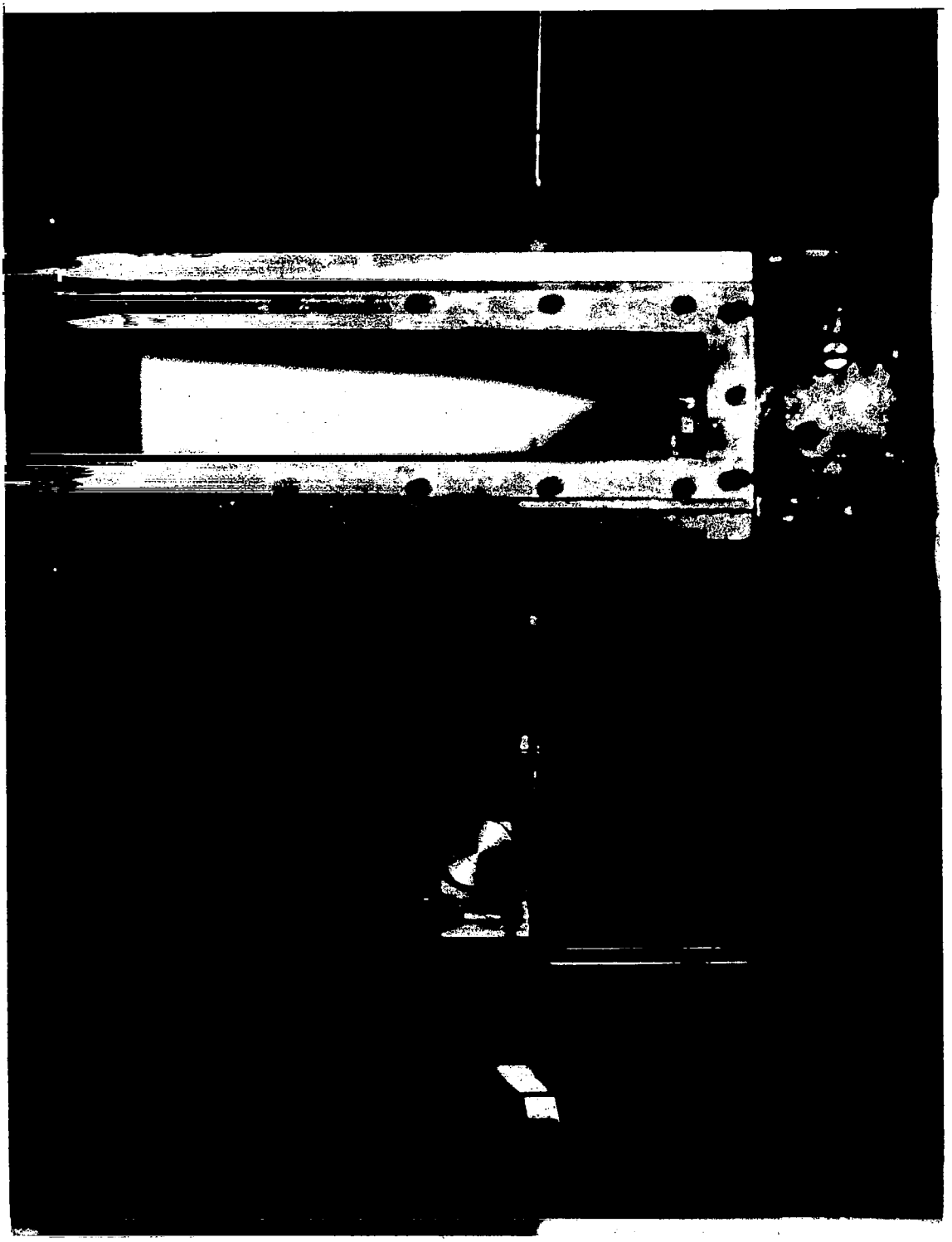

Fig. 2.13 Probe traversing mechanism used for probing the combustor from the bottom.

After leaving the probe the sample passes through a 3.2 mm diameter teflon line to the gas analysis equipment, Figure 2.14. Carbon monoxide was measured using a Beckman Model 315A nondispersive infrared analyser. CO_2 was measured using a Beckman Model 315 nondispersive CO_2 analyser. It is known that the presence of water in sample interferes with CO and CO_2 measurements in infrared analysers. To minimize this effect an ice bath water trap was used for water condensation before the sample enters CO and CO_2 analysers. Unburned hydrocarbons were measured in the form of total carbon atoms by a Beckman Model 412 flame ionization detector. Since the hydrocarbons are of low molecular weight, sample line heating was not required. NO and NO_2 were measured using a Thermoelectron Model 12A chemiluminescent analyser.

Due to the small orifice at the tip of the probe the pump could not supply an adequate sample flow for all analyzers to be operated simultaneously. The pressure in the line was always kept below 280 mm Hg absolute to promote aerodynamic quenching of the sample in the probe, reduce probe reactions, and prevent water condensation. The pressure varied according to the position of the probe in the flame. This is because of the variation of average stagnation temperature and density with position, which in turn affects the mass flow rate passing through the probe tip, Figure 2.14. The line pressure corresponding to the use of each analyser is given in Table 2.2. This pressure was measured at the entrance to the main sample pump (about 1 m from the probe exit).

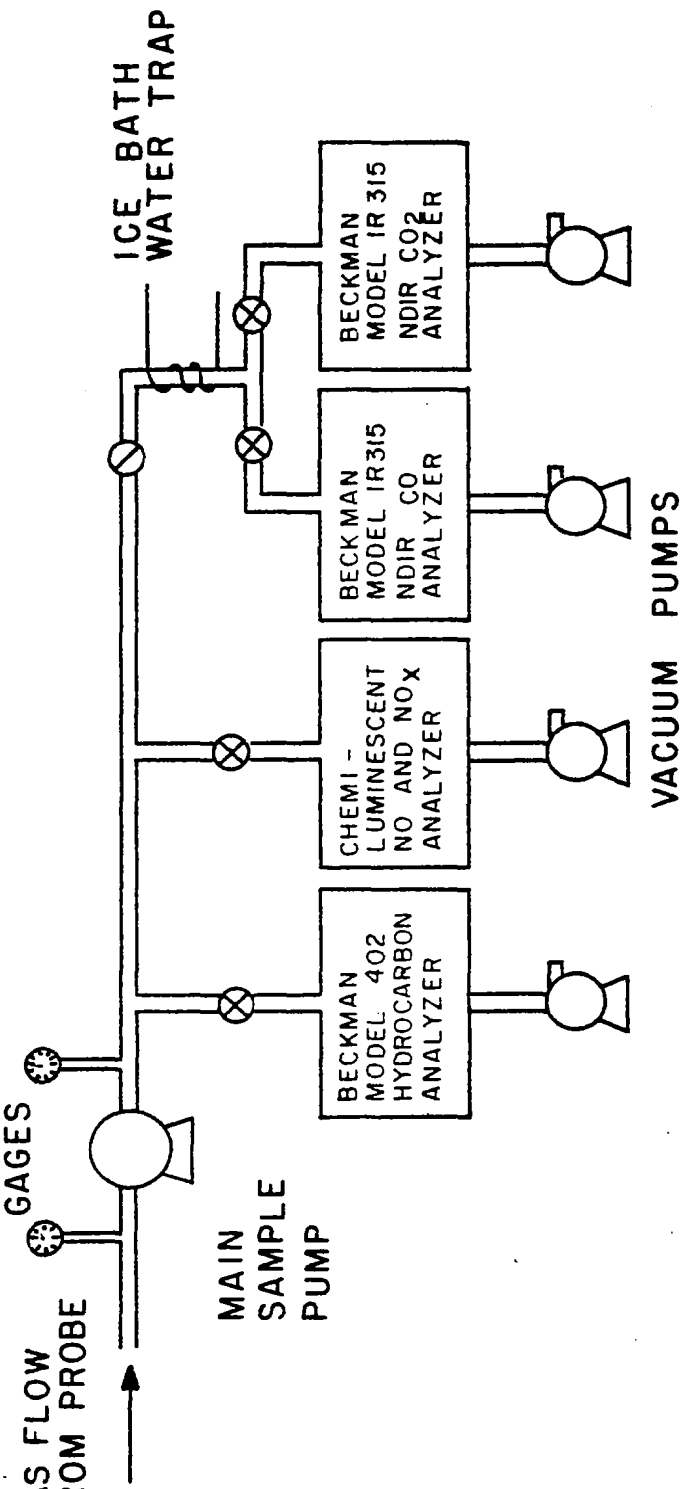

Fig. 2.14 Gas analysis equipment.

Table 2.2

Line Pressure for Different Analysers.
Sample Withdrawn from Recirculation Zone

Analyzer	NDIR, CO	NDIR, CO_2	FID, HC	CLA, NO_x
Pressure mm Hg (abs.)	160	240	247	222

The quenching of chemical reactions is one of the most important functions of a sampling probe if a representative measurement of gas composition is to be made. Since the rates of gas phase chemical reactions in combustion gases are sensitive to temperature, quenching can be obtained by a rapid reduction in gas temperature. In aerodynamically quenched probes, such as the present, this rapid reduction in temperature is obtained by attaining supersonic expansion behind the nozzle. Often a shock wave is formed not far downstream behind the nozzle that brings up the temperature of the sample, but at that position usually convective quenching becomes important, Bowman (1977).

Several difficulties are encountered when measuring oxides of nitrogen, Cernansky (1977). Tuttle, et al. (1973) have pointed out that water condensation in the sample line is associated with significant NO_2 losses. This problem was solved by keeping the pressure in the sample line significantly below atmospheric pressure, Table 2.2. The lines were checked after about four hours of operation and no water condensation could be observed. Carbon particulates have been shown to result in absorption of NO_2 and reduction of NO_2 to NO, Tuttle, et al. (1973).

Schefer (1976) checked the sample for carbon particulates in a LPP combustor with similar operational conditions and found out that because of lean conditions very little carbon particulate was produced. His conclusion was assumed to apply to this system. H_2O, CO_2 and O_2 present in the sample are known to affect the quenching of excited NO_2 in the reaction chamber of a chemiluminescent analyzer calibrated with a mixture of NO and N_2, Matthews, et al. (1977). Corresponding corrections have been applied to measured values of NO_x and NO_2. It is suspected that hydrocarbon, mostly C_3H_8 must have an appreciable effect on quenching of excited NO_2 but no reliable data are available for applying the corresponding corrections.

2.5 Optical System

Schlieren and shadowgraph optical systems were used for flow visualization experiments on the two dimensional combustor. These systems, their theoretical basis and their application to this burner are discussed in this section.

2.5.1 Principles of Flow Visualization Techniques

The above mentioned flow visualization techniques use the principle of deflection of a light beam upon passing through a field of refractive index in a transparent medium. The refractive index is given by $n = \frac{c_o}{c}$, where c_o and c are the speeds of light in vacuum and in the medium. If the deflection of light is recorded, as on a film, the record will show the refractive index field, which can be directly related to the examined flow field. In a flow field, this field of refractive index can be created by a density or composition field or both.

According to the Lorenz-Lorentz relation for a homogeneous transparent medium, the density and refractive index are related through

$$\frac{1}{\rho}\frac{n^2 - 1}{n^2 + 2} = \text{constant} \qquad (2.1)$$

For gases $n = 1 + \delta$ where δ is on the order of 10^{-4} (for air $\delta = .000292$), Weinberg (1963). This relation reduces to

$$\frac{1}{\rho}(n - 1) = C = \text{constant} \qquad (2.2)$$

which is known as the Gladstone-Dale relation for refractive index, where the constant C depends on the nature of the gas. Table 2.3 shows some values of $C\rho_s$ for typical species present in combustion systems. ρ_s is the density of the gas at standard conditions.

Table 2.3

Values of $\rho_s C$ for some species present in combustion systems. ρ_s at 273K, 760 mm Hg, λ = 5893A, Liepmann and Roshko (1957)

Gas	$\rho_s C$
Air	0.000292
Nitrogen	0.000297
Oxygen	0.000271
Carbon Dioxide	0.000451
Water Vapor	0.000254

Consider a beam of light passing through a medium with a density gradient and for simplicity assume that the variation of density is only along the y direction, Figure 2.15. The time for the wave to travel from w_1 to w_2 is

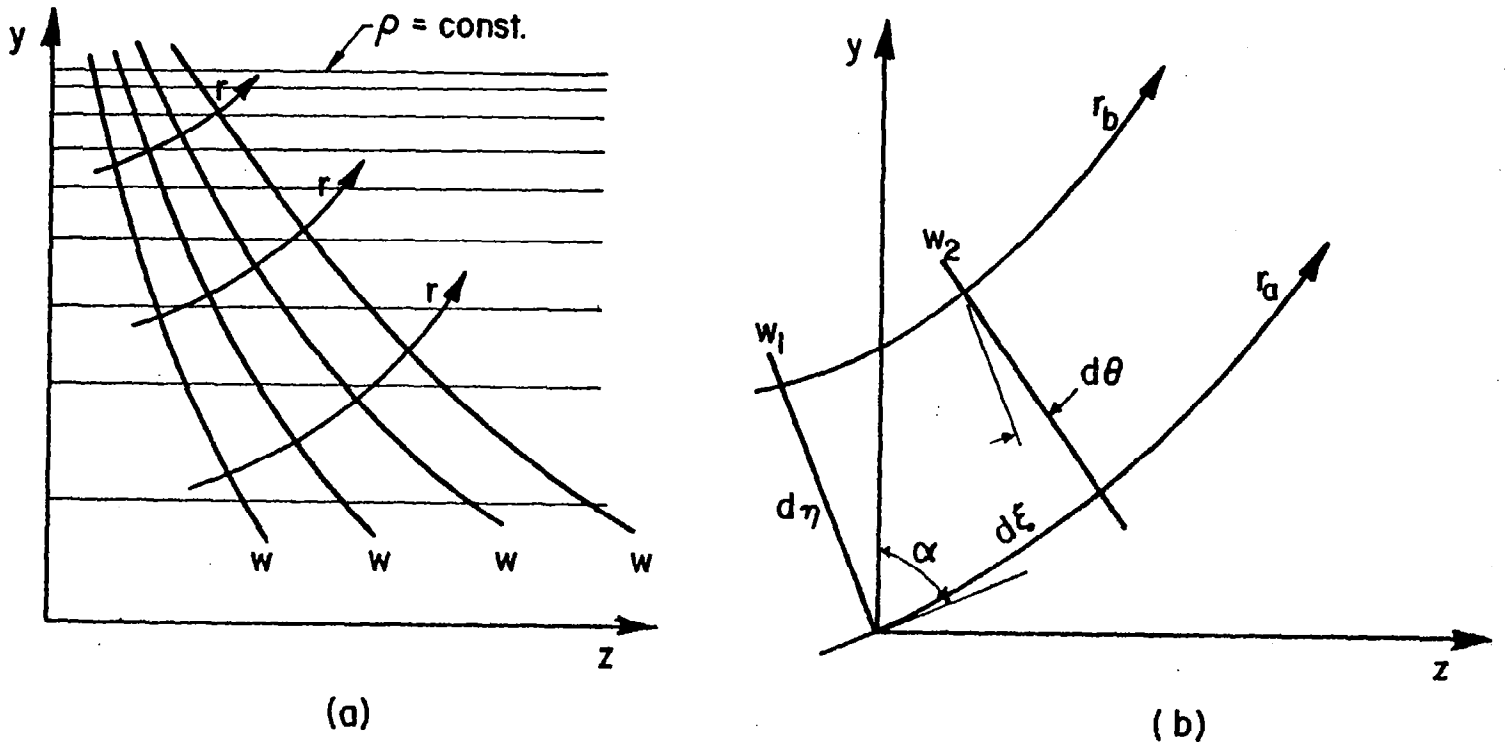

Fig. 2.15 (a) Refraction of light in a density field, r and w represent rays and wave fronts respectively.
(b) Orthogonal mesh element formed by rays and wave fronts.

$$\tau = \frac{d\xi}{c} \tag{2.3}$$

If density is increasing in the y direction the rays will bend toward the positive y (as shown in Figure 2.15). So the wave front will turn

$$d\theta = \frac{\tau dc}{d\eta} \tag{2.4}$$

and the curvature of the ray will be

$$\frac{1}{R} = \frac{d\theta}{d\xi} \tag{2.5}$$

Substituting for $d\theta$, τ and $d\eta = \frac{dy}{\sin \alpha}$ in Equation 2.5:

$$\frac{1}{R} = \frac{\sin \alpha}{c} \frac{dc}{dy}$$

where c is the speed of light in the medium. Using the definition of refractive index the above equation results in:

$$\frac{1}{R} = \frac{\sin \alpha}{n} \frac{dn}{dy} \tag{2.6}$$

In a general three dimensional density field the above result generalizes into

$$\frac{1}{R} = \frac{\sin \alpha}{n} \cdot \left|\text{grad } n\right|$$

where the curvatuve is in the direction of increasing density. The radius of curvature in the z-y plane is:

$$\frac{1}{R} = \frac{d^2y/dz^2}{\left[1 + (\frac{dy}{dz})^2\right]^{3/2}}$$

As $(\frac{dy}{dz})^2 << 1$

$$\frac{1}{R} = \frac{d^2y}{dz^2} \tag{2.7}$$

Equations 2.6 and 2.7 result in:

$$\frac{d^2y}{dz^2} = \frac{1}{n}\frac{dn}{dy} \tag{2.8}$$

In order to find the deflection of the ray after passing through the test section, Equation 2.8 should be integrated as:

$$\frac{dy}{dz}\Big|_L - \frac{dy}{dz}\Big|_o = \int_o^L \frac{1}{n}\frac{dn}{dy}\,dz$$

where L is the point that the ray leaves the field. Usually the rays enter the test section at right angles to the test section wall (refer to the note at the end of this section) so that $\frac{dy}{dz}\Big|_o = 0$. Thus

$$\frac{dy}{dz}\Big|_L = \int_o^L \frac{1}{n}\frac{dn}{dy}\,dz \tag{2.9}$$

The angle of deflection of the ray after leaving the test section will be:

$$\alpha \approx \tan\alpha = \int_o^L \frac{1}{n}\frac{dn}{dy}\,dz$$

as $n \approx 1$

$$\alpha = \int_o^L \frac{dn}{dy}\,dz \tag{2.10}$$

Equation 2.10 shows the ray deflection in the y direction in a two dimensional field. Having reduced the formula to this form for a two dimensional field, the generalization to a three dimensional field follows at once. Since both the angle and refractive index gradient can be resolved into two independent components, thus

$$\alpha = \sqrt{\alpha^2_x + \alpha^2_y}$$

which is the angle of the ray with respect to the z axis.

For the case where the refractive index gradient is normal to the incident ray, as is the case in the present investigation, $\frac{\partial n}{\partial y}$ and $\frac{\partial n}{\partial x}$ will not be a function of the transverse distance, thus:

$$\alpha_y = L \frac{\partial n}{\partial y}$$

$$\alpha_x = L \frac{\partial n}{\partial x}$$

As the ray deflection is very small, the above derivatives do not change appreciably along the ray path and as a result they can be calculated at the point the ray enters the test section.

The rest of the formulation in this section will be only for a single deflection angle or simply:

$$\alpha = L \frac{dn}{dy} \tag{2.11}$$

According to the Gladstone-Dale Expression, Equation 2.2, the angle of deflection will be:

$$\alpha = L \frac{d(\rho C)}{dy}$$

where C is a constant for each component. Expanding the right hand side of the above equation:

$$\alpha = L\rho \frac{dC}{dy} + C \frac{d\rho}{dy} \tag{2.12}$$

In turn, change in density can be disintegrated into change in temperature and composition (at constant pressure as is the case in this experiment).

The result is:

$$\frac{d\rho\ (x_i,T)}{dy} = \sum \frac{\partial \rho}{\partial x_i} \frac{dx_i}{dy} + \frac{\partial \rho}{\partial T} \frac{dT}{dy} \qquad (2.13)$$

where ρ is the density of the gas and x_i is the mass fraction of the individual components.

Perfect Gas Law:

$$\rho = \frac{P}{RT}$$

$$= \frac{P}{(\Sigma x_i R_i)T}$$

where P, T are pressure and temperature of the mixture and R_i is the gas constant for each component. Substutition of ρ in Equation 2.13 and of $\frac{d\rho}{dy}$ in Equation 2.12 subsequently results in:

$$\alpha = \underbrace{L \frac{P}{T \Sigma x_i R_i} \frac{dC}{dy}}_{I} - LC \left[\underbrace{\frac{1}{T^2} \cdot \frac{P}{\Sigma x_i R_i} \cdot \frac{\partial T}{\partial y}}_{II} + \underbrace{\frac{P}{T(\Sigma x_i R_i)^2} \cdot R_i \frac{x_i}{\partial y}}_{III} \right] \qquad (2.14)$$

Equation 2.15 shows that in a reacting system the light refraction might be due to:

a) Composition gradient, Terms I and III in Equation 2.15.
b) Temperature gradient, Term II in Equation 2.15.

The relative importance of the above effects has been discussed by Weinberg (1963). The conclusion is that at constant pressure combustion processes, most of the refractive index variation is caused by temperature rather than by composition changes.

The first effect has been used by Roshko (1976) for flow visualization

of a free-shear layer with no variation in density across the layer, and the refractive effect is quite pronounced.

Based on the principles explained in this section, two different refractive index techniques, schlieren and shadowgraph, have been used for visualization of the flow field in the two dimensional combustor. The techniques and their application are discussed in the next three sections of this chapter.

Note

In application of the refractive index methods to systems such as the present two dimensional combustor, the rays usually enter at a right angle to the side walls which are normally glass windows, Figure 2.16.

For a ray going through a discontinous refractive index field:

$$\begin{aligned} n \sin\alpha &= n_w \sin\alpha_w \\ n_a \sin\alpha_a &= n_w \sin\alpha_w \end{aligned} \qquad (2.16)$$

where n, n_w and n_a are refractive indices of the test section gas, windows and air respectively. α, α_w and α_a are the angles shown in Figure 2.16.

From Equation 2.16

$$n \sin\alpha = n_a \sin\alpha_a \quad .$$

Since $\sin\alpha \ll 1$, $\sin\alpha \approx \alpha$

$$\alpha_a = \frac{n}{n_a}\alpha \quad . \qquad (2.17)$$

Therefore the deflection angle changes by a small (usually negligible) factor due to passage of the ray through air and does not change due to presence of the windows.

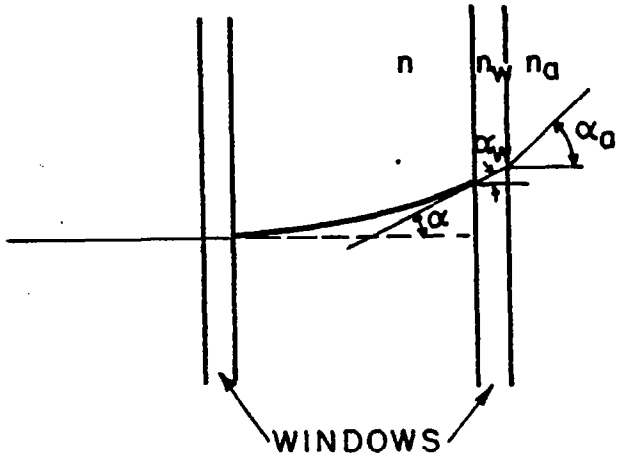

Fig. 2.16 Ray deflection through a test section with window walls.

2.5.2 Schlieren Technique

The basic idea behind the schlieren system is that part of the deflected light is intercepted by a physical obstacle such as a knife edge or a color filter before it reaches the viewing screen or photographic plate, so that the parts of the field which it has traversed appear darker or colored. A schematic of a ray deflection diagram for a schlieren system as used here is shown in Figure 2.17. In this system the rays emanating from the source are collimated by the concave mirror M_1 and directed into the test section and focussed again at the focal plane of mirror M_2. At point A the light is deflected by an angle α as a result of passing through the refractive index gradient $(\frac{\partial n}{\partial y})$. Upon refocussing the light by mirror M_2, the refracted light beam R_r, will be deflected by a distance Δ, from the focal point. This distance can be calculated as follows:

According to Figure 2.17

$$\Delta = f_2 \tan\alpha = f_2\alpha \tag{2.18}$$

(α is usually very small, in the present system $\alpha_{max} \approx .6$ degree).

By substituting for α from Equation 2.15 in Equation 2.18:

$$\Delta = fL \left\{ C\left[-\frac{1}{T^2}\frac{P}{\Sigma x_i R_i}\frac{\partial T}{\partial y} - \frac{P\Sigma R_i \frac{\partial x_i}{\partial y}}{T(\Sigma x_i R_i)^2}\right] + \frac{P}{T\Sigma x_i R_i}\frac{\partial C}{\partial y}\right\} . \tag{2.19}$$

Neglecting the effect of composition variation and change in C, Equation 2.19 reduces to:

$$\Delta = fLC\left(-\frac{\rho}{T}\cdot\frac{\partial T}{\partial y}\right)$$

$$= -fL\cdot C\frac{\rho}{T}\cdot\frac{\partial T}{\partial y}$$

$$= -fL\cdot\frac{n_o-1}{\rho_o}\cdot\frac{P}{RT^2}\cdot\frac{\partial T}{\partial y}$$

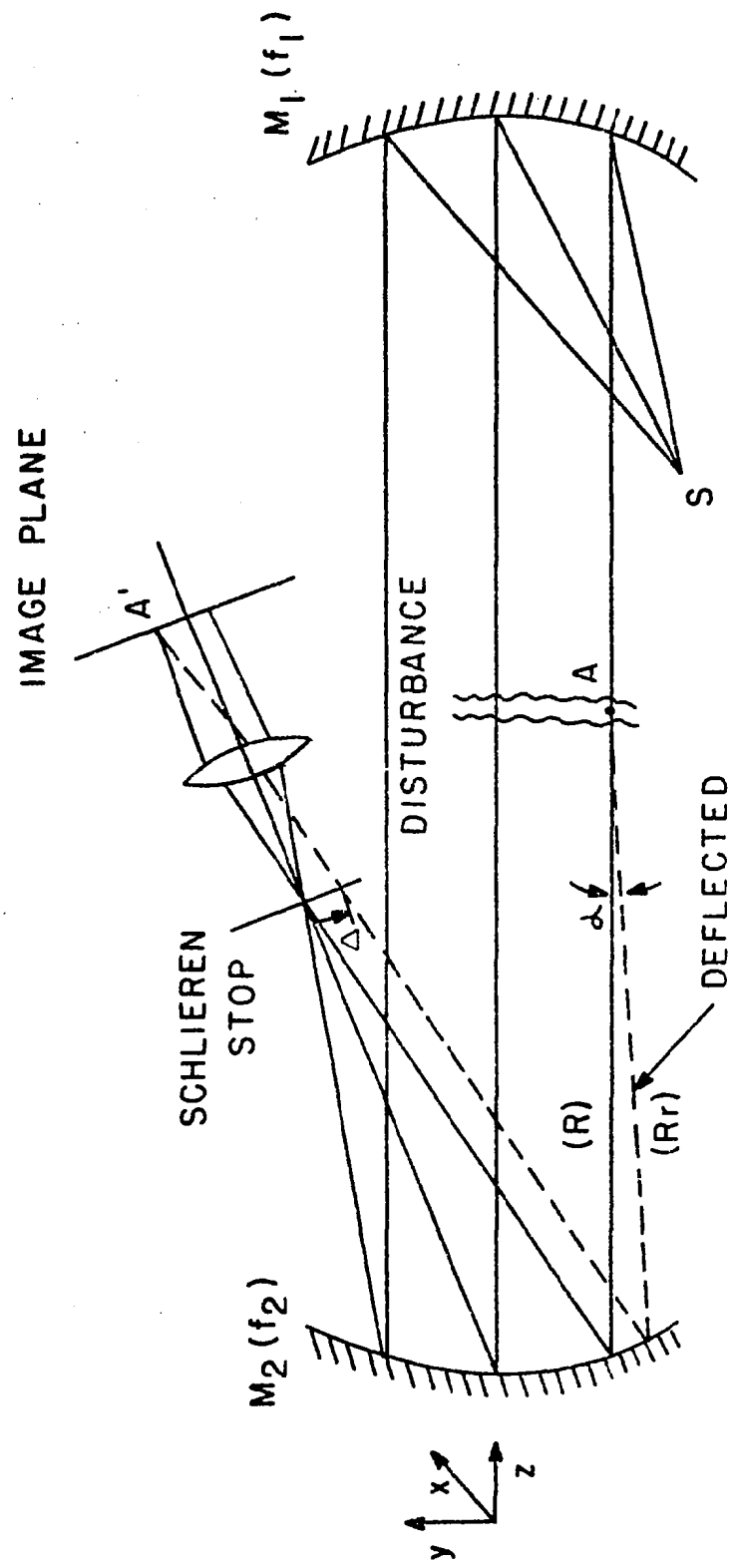

Fig. 2.17 Schematic of ray deflection diagram, illustrating the effect of refractive index at point A on the light ray originated at S.

Thus:
$$\Delta = fL \frac{n-1}{\rho} \cdot \frac{P}{R} \frac{\partial(\frac{1}{T})}{\partial y} \qquad (2.20)$$

where n and ρ are the refractive index and density of the reactants and $C = \frac{n-1}{\rho}$. Equation 2.20 provides a relationship between the temperature gradient (or actually $\frac{\partial(\frac{1}{T})}{\partial y}$) and the deflection distance at the schlieren stop. The function of the schlieren stop is to label the deflected ray so that it may be identified as having passed through a specified temperature (or generally refractive index gradient) when returned to the image plane at A'. Depending on the type of stop used in the optical system the rays are cut off or passed through a neutral density filter for black and white recording (photography or cinematography) or by a frequency selective color filter for color recording. Types of stops used in this system will be discussed later.

2.5.3 Shadowgraph Technique

In a shadowgraph system the linear displacement of the perturbed light beam is measured rather than the angular deflection as in a schlieren system. Figure 2.18 shows a schematic of a ray deflection diagram.

If the initial intensity of light is I_o (non-refracted) the intensity on the screen is:
$$I_{sc} = \frac{\Delta y}{\Delta y_{sc}} I_o \qquad (2.21)$$

If z is the distance from the test section to the screen we have:
$$\Delta y_{sc} = \Delta y + z d\alpha \qquad (2.22)$$

so the contrast on the screen will be:
$$\frac{\Delta I}{I_o} = \frac{I_{sc} - I_o}{I_o}$$

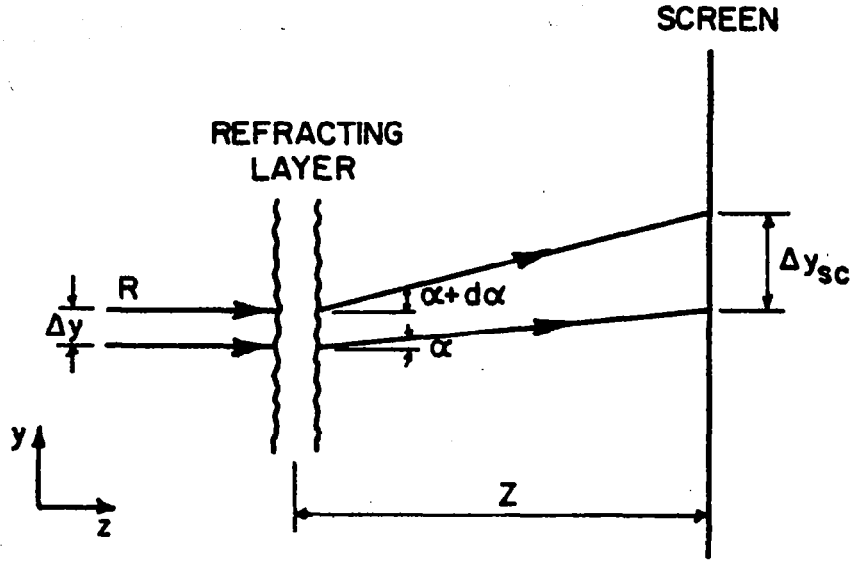

Fig. 2.18 Schematic of a ray deflection diagram for a shadowgraph system.

or
$$\frac{\Delta I}{I_o} = \frac{\Delta y}{\Delta y_{sc}} - 1$$

$$= -z \frac{\partial \alpha}{\partial y} \qquad (2.23)$$

In order to derive the contrast in terms of properties of the gas under examination, the value for α from Equation 2.15 can be substituted in Equation 2.23. It is concluded that the contrast (relative darkness and brightness) of a shadow image is a function of second order derivatives of temperature, composition, and C. Again in a system such as the present, the effect of temperature gradients dominates, so that it can be assumed that the shadowgraph represents the second order derivative of the temperature field. The shadowgraph system is much simpler than the schlieren. It is not essential to have additional optical components after the test section, but they are sometimes used (as in the present) for proper magnification and increased freedom in component location. The essential feature of shadowgraphy in distinction from schlieren, is that the receptor is not optically conjugate with the test section. Actually a shadow system is a defocussed schlieren system where the stop has been removed.

Principles of refractive index methods and also schlieren and shadowgraph systems have been discussed in detail by many authors. The interested reader is referred to Landenburg, et al. (1954), Liepmann and Roshko (1957), Weinberg (1963) and Eckert, et al. (1976).

2.5.4 Application of Schlieren and Shadowgraph Techniques to the Two Dimensional Combustor

In principle the schlieren and shadow techniques can be used for temperature measurements of composition. Because of limited accuracy, Weinberg (1963), they have been used mostly as flow visualization techniques. Because of the complexity of our flow, no attempt was made to reduce any quantitative temperature or composition data from the schlieren or shadowgraph records.

The schlieren system used in the present experiments is shown in Figure 2.19. The light originating from the light source (high intensity xenon arc lamp, Oriel model C-60-50 or an electric discharge lamp) is collimated by the concave mirror M_1 (focal length 394 cm) and directed through the test section to the second concave mirror, M_2, (focal length 394 cm) and refocused at the focal plane of mirror M_2, where the schlieren stop is located. Lens L (focal length 135 mm) focuses the test section on the film in the camera. A Wollensac Fastax Model WF-17, 16 mm camera capable of framing rates up to 7500 frames/sec was used for filming the flow field. A 4 x 5 Polaroid camera was used to take still pictures of the flow field.

The following schlieren stops were tested for visualization of the flow field in the combustor:

1 - Aperature, 1.6 mm to 14.4 mm in intervals of 1.6 mm.

2 - Concentric rings.

3 - Horizontal double knife edge (slit), 1.6 mm to 14.4 mm in intervals of 1.6 mm.

4- Vertical double knife edge (slit), 1.6 mm to 14.4 mm in intervals of 1.6 mm.

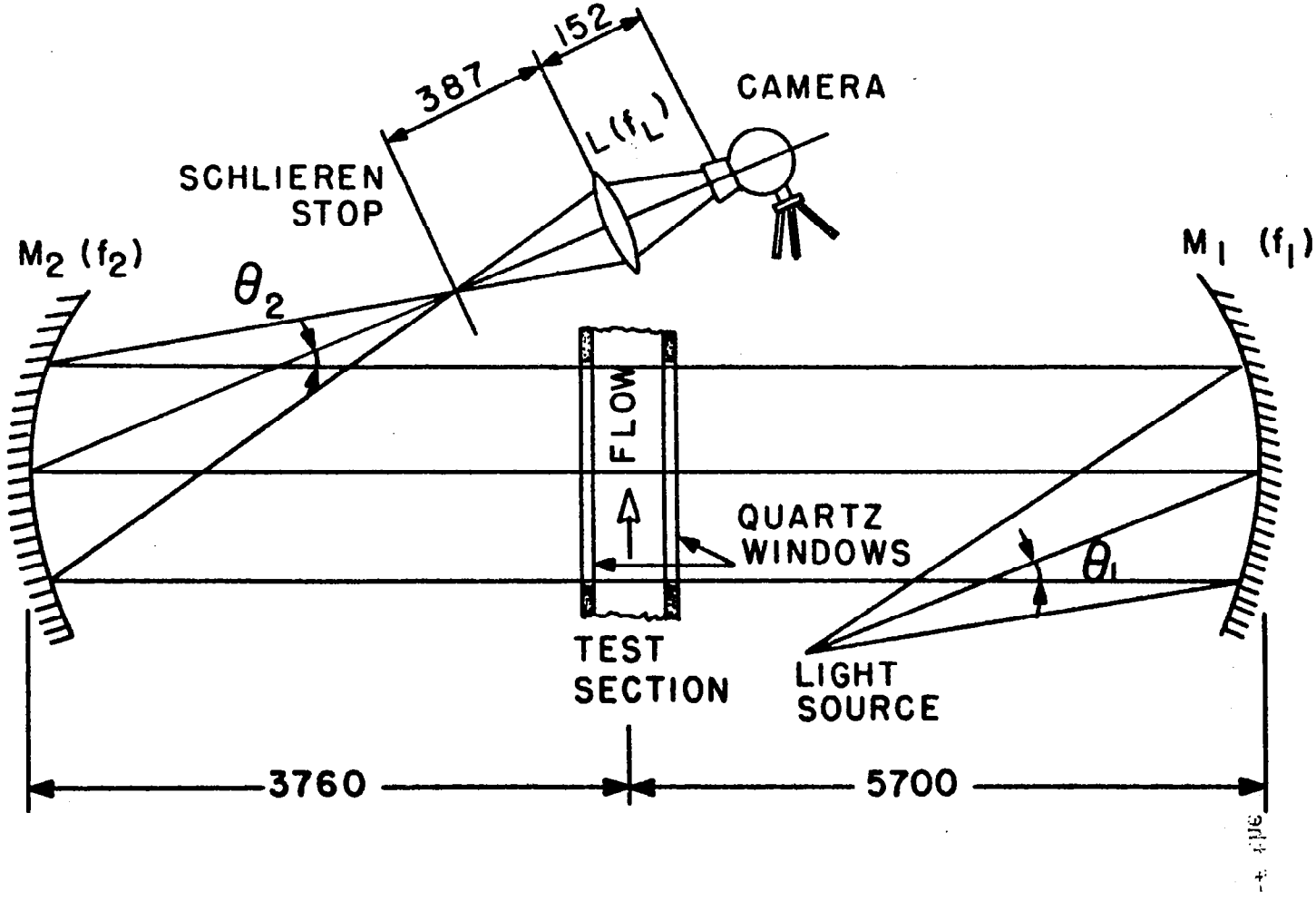

Fig. 2.19 Schematic of the schlieren cinematographic system used for flow visualization of the two dimensional combustor. Distances in mm.

5 - Concentric color ring filters
6 - Horizontal color strip filters
7 - Vertical color strip filters

All of the stops that cut or colored a substantial amount of the light refracted from the gas near the lower plate of the combustor generated a dark or uniformly colored region on the photograph corresponding to the lower part of the combustor (depending on the cut off, this region was up to 10 mm thick). This phenomenon presents a difficulty in the visualization of the flow process for a substantial part of the mixing layer downstream of the step. This observation excluded the aperture, concentric rings (both colored and black and white), and horizontal colored strips for this investigaiton. A horizontal double knife edge was used to take a time exposure photograph of the flame which is described in Chapter 3 .A vertical double knife edge and vertical color strips were found to be the most appropriate schlieren stops for photography of this system. Their form and size is shown in Figure 2.20.

The schlieren system described above was used to take the following records of the flow field.

1 - Long exposure polar diagram of the deflected light
2 - Long exposure schlieren pictures
3 - Spark schlieren pictures
4 - High speed schlieren movies

The polar diagram shows the pattern of deflection of light due to the refractive index field in the test section. It is produced by positioning the photographic plate of the camera at the focal plane of mirror M_2. Figure 2.21 shows long exposure photographs of non-refracted and refracted light at this point.

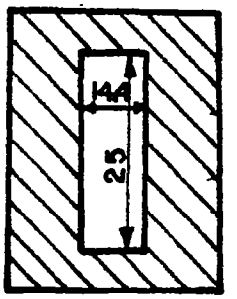

(A)

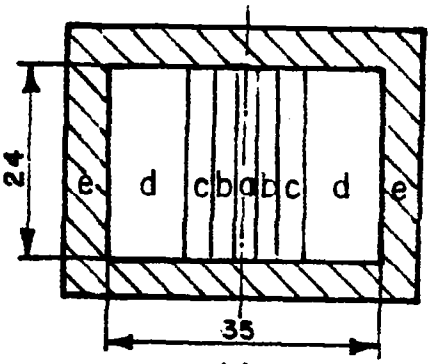

(B)

Fig. 2.20 (A) Double knife edge (slit) used for black and white cinematography of the reacting and nonreacting flow fields.
(B) Color stop used for color schlieren cinematography of the flow field in the two dimensional combustor. The stripes are: (a) blue, 2.6 mm, (b) red, 2.6 mm, (c) yellow, 2.6 mm, (d) blue, 11 mm, and (e) frame.

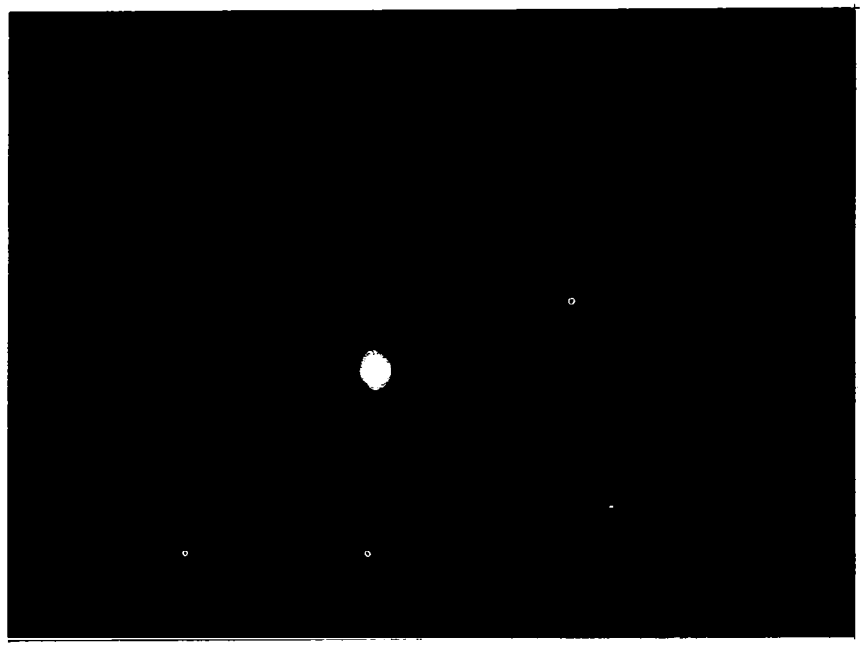

a

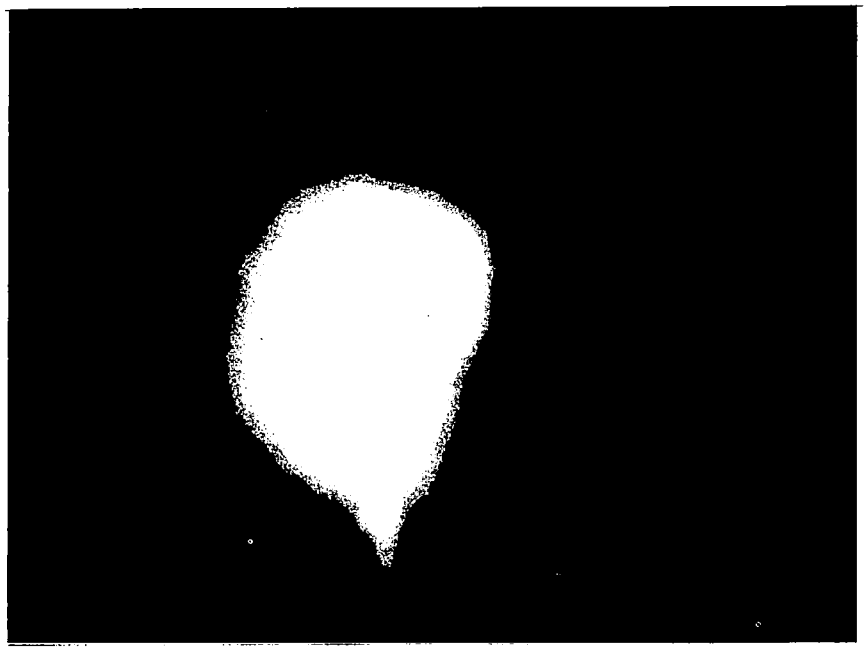

b

Fig. 2.21 Polar diagrams of nonrefracted (a) and refracted (b) light in the test section. Both photographs have been taken in the focal plane of mirror M_2 .

Comparison of the two photographs in Figure 2.21 reveals that the refraction is in both the y and x directions. As there are high rates of heat transfer to the lower plate of the combustor which results in sharp temperature gradients in this region, the polar diagram has a tail at the bottom, which represents the light refracted towards the lower plate (higher density). This observation is also a justification for using vertical stops in schlieren photography of this flame.

In the present investigation the shadow system was used to take spark photographs of the reacting flow field. As was mentioned in Section 2.5.3 the shadow system is a defocussed schlieren system where the stop has been removed. In this experiment the above fact was used to change the schlieren system to a shadowgraph system.

The light source for spark photography (both schlieren and shadow) was a laboratory constructed electric discharge lamp with a duration of less than 1 μsec which also determines the exposure time of the photograph (but the film was exposed for a much longer time, on the order of a tenth of a second). Because of this, at high equivalence ratios the combustor became hot and the film was exposed to the radiation from the test section. This phenomenon resulted in over exposure of some parts of the photographs. To eliminate this effect, filters were put in the light path (before the lens L), and as a result the corresponding pictures are darker.

Kodak Tri-X reversal and High Speed Ecktachrome-EF films were used for black and white and color schlieren cinematography of the flow field, respectively. Polaroid Type 52 film was used for taking the still photographs.

CHAPTER 3

CINEMATOGRAPHY OF THE QUASI-STEADY FLOW FIELD

Conventional Eulerian type measurements in shear layers have obscured some basic features of these flows which are Lagrangian in nature. While measurement of flow properties in the Lagrangian frame of reference is a formidable task, a Lagrangian viewpoint of the flow processes is of great help in understanding these phenomena. Flow visualization techniques can serve as such tools, providing considerable insight into the flow processes in shear flows.

Schlieren and shadowgraph flow visualization techniques described in Chapter 2 have been found to be particularly useful and informative in investigation of two dimensional shear layers, Brown and Roshko (1974), and two dimensional flames, Nicholson and Field (1949). The drawback of these methods is that they mostly provide qualitative information about the developments in the flow, without providing substantial information on the details of the structure of the flow field (especially in the turbulent case). Finally, because of the averaging nature of these techniques in the third dimension, the three dimensionalities of the system cannot be separated from the real variations in the other two dimensions which are usually of primary interest.

In the present investigation, these techniques were used to study the structure of the reacting and nonreacting free shear layers downstream of the rearward facing step, and the transient processes of

flashback and blowout of the flame. A schlieren photograph of the flame is shown in Figure 3.1. It is a single frame taken from a high-speed color schlieren movie of the flame in the combustor. The features of the flow in Figure 3.1 are typical of the free shear layer which will be discussed in this chapter. Figure 3.2 contains three schlieren photographs, the first two of the flame (reacting shear layer behind the step) and the last of the corresponding nonreacting shear layer. Figure 3.2.a is a long exposure time (20 msec) photograph of the flame which shows the extent of the spread of the flame in a time averaged manner similar to what is observed by the eye. The well-defined region behind the step is conventionally called the "recirculation zone" and the bright region is conventionally called the "flame mixing zone," Zukoski and Marble (1955). Figure 3.2.b shows a spark schlieren (exposure time < 1 μsec) of the flame with the same conditions as in 3.2.a, but with strikingly different features now visible. As in Figure 3.2.a, the flow field consists of three distinct regions:

1. The region at the top (clear zone) consisting of fresh reactants.
2. The region behind the step which is fairly clear, implying little or no refraction of light. This is the hot recirculation zone, which is responsible for self-ignition of the flame and actually is the source that starts the propagation of the flame into the shear layer.
3. The striated region which is dominated by large vortices and is bound by the recirculation zone, the bottom of the combustor and the fresh reactants. This is the mixing/reacting zone.

Figure 3.2.c shows a flow at the same conditions but without combustion.

Fig. 3.1 Color schlieren photograph of the flame.

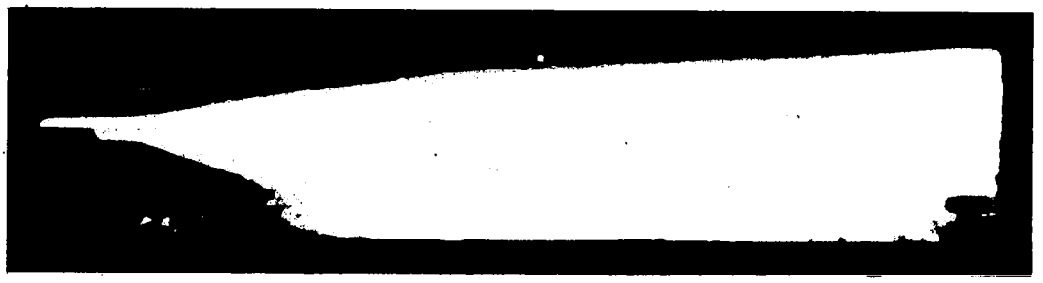

a. Flame, long exposure time (20 msec), ϕ = 0.52.

b. Flame, short exposure time (< 1 μsec), ϕ = 0.57.

c. Nonreacting flow, short exposure time (< 1 μsec), ϕ = 0.00.

Fig. 3.2 Schlieren photographs of the flow field inside the combustor test section. V_o = 13.5 m/sec, N_{Re} = 8800 cm^{-1}, T_o = 295 K.

In this chapter some details of the reacting and nonreacting flows behind the step as revealed from the schlieren and shadowgraph movies and photographs are discussed. These details include a description of the sequence of events as the shear layer leaves the edge of the step, formation of vortices, formation position, formation period, interaction of vortices, their coherence, coalescence, survival rate, velocity as they move downstream, and the effect of boundary layer trip on the vortices. Finally, the difference between reacting and nonreacting layers and the effect of combustion on the layer is discussed.

3.1 Reacting Mixing Layer

Figure 3.2.b shows that the mixing layer starts with a laminar shear layer at the trailing edge of the step. The layer at this stage is almost horizontal, indicating little or no flame propagation into the fresh reactants. Based on laminar flame propagation, the flame inclination should be 1.7°. This is the inclination of the flame front with respect to the laminar mixing surface which is in turn oscillatory. The laminar layer leaving the edge shows the appearance of small waves which result from the linear instability of the shear layer between the two flows at two different velocities, in this case, between the nearly stagnant recirculation zone and the nearly uniform velocity fresh reactants. This region of concentrated vorticity is characterized by linear instability and has been studied in detail in nonreacting mixing layers. Small waves created by the flow disturbances in this zone result in higher vorticity concentrations in downward segments of the travelling waves and lower vorticity concentrations in the upward segments. This difference in vorticity concentration in the

two segments of the wave results in growth of the ripple which in turn develops into vortical eddies. The instability of the parallel streams for nonreacting, uniform density flows in this regime has been discussed in detail by (Betchov and Criminale) (1967). The instabilities (due to creation of wave-like disturbances) in the layer described above can be mechanically driven or occur due to the most unstable wave of the system as is the case in Winnant and Browand (1974). In the case of mechanically driven instabilities (like instabilities driven by a loud speaker), the frequency of vortices is fixed by the frequency at which the forcing mechanism is driven. In this system the entrance flow has been examined by a hot wire probe, Pitz (1978). Frequency spectra of the flow are shown in Figure 3.3. The figure shows a series of peaks in the entrance flow which are attributed to the acoustic frequencies of the mixing section. We believe that these frequencies, the effect of recirculation of the products in the recirculation zone, and the magnitude of entrance velocity (which determines the thickness of the initial laminar layer) are the driving force behind the instability of the layer leaving the step. Needless to say, this velocity field is unconditionally unstable and the layer develops into discrete vortices for any value of entrance velocity. In any case, the result of instability of the initial layer is the generation of wave-like disturbances which grow into discrete vortices.

Transformation of wave-like disturbances into discrete vortices is due to the nonlinearity effect between disturbances and the flow (Kelvin Helmoltz instability). The Kelvin Helmoltz instability, vortex formation and interaction, and entrainment in uniform density or gravitationally stable stratified flows have been reviewed by

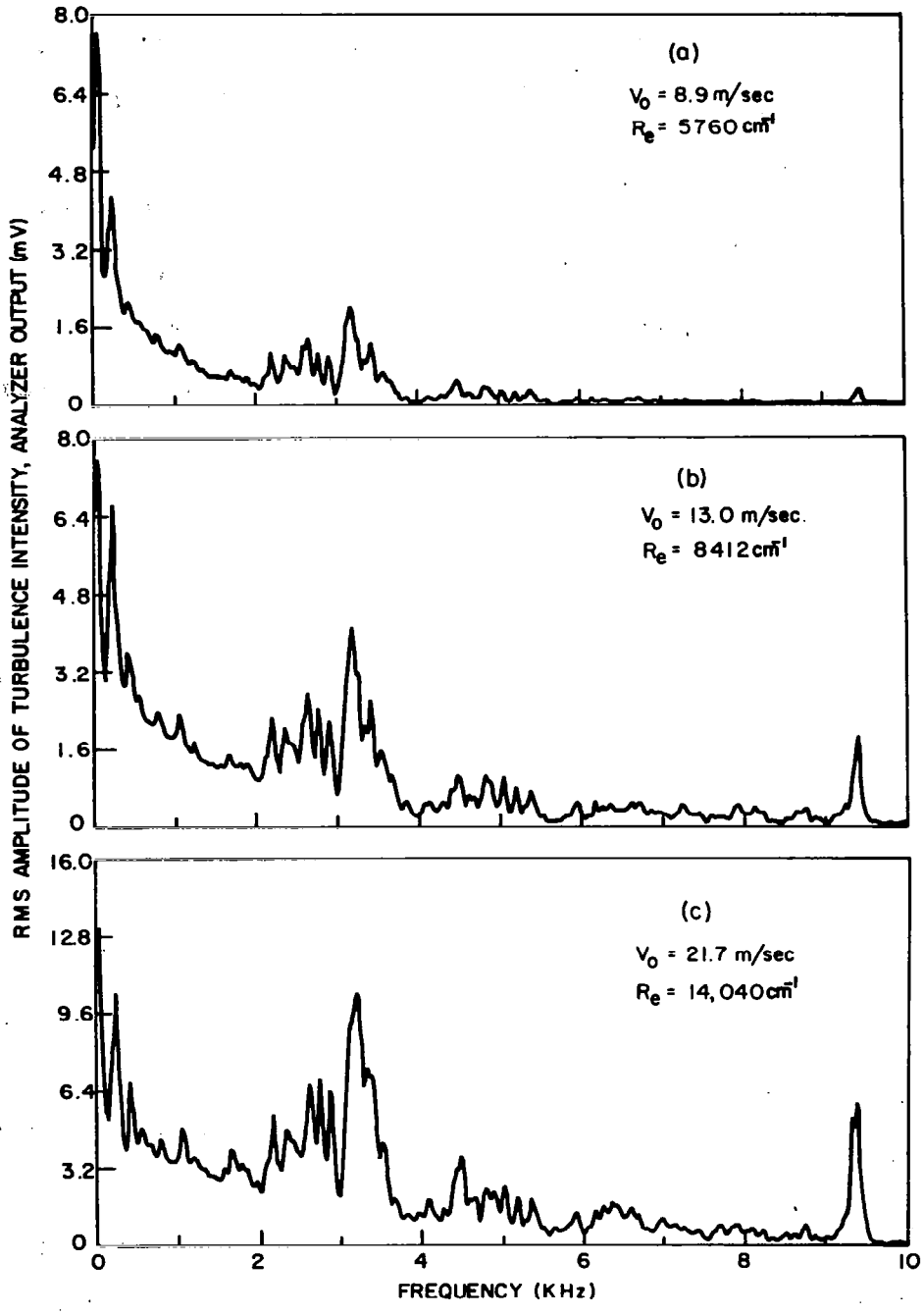

Fig. 3.3 Frequency spectra of the entrance flow at the center of the entrance plane to the test section for different values of reference velocity, T_0 = 295 K.

Sherman (1977). It is of interest to note that heat release does not change the basic features of the development of the discrete vortices which can be explained by the same concepts known for the nonreacting flows discussed by Winnant and Browand (1974) and Sherman (1977). Figure 3.2.b explicity shows that the propagation of the flame into the fresh reactants corresponds to the growth of large discrete vortices in the free shear layer and apparently reaction occurs mostly in the contact surface of these large eddies with the fresh mixture. The effect of combustion intensity on the shear layer was investigated by varying equivalence ratio at constant reference velocity. Figure 3.4 and 3.5 show shadowgraphs and schlieren photographs of the flame at three different values of equivalence ratios. All photographs have been taken with the combustor running in the stable mode of operation and the reactants at the same reference velocity and essentially the same Reynolds number. The increase in equivalence ratio is less than 10% from one flow to the next, but considering the narrow range of stability of the burner (Chapter 4), this should be sufficient to change the structure of the flame. The existence and extension of the laminar layer, the formation of small waves in this layer, and finally transition to discrete large vortices is evident.

The effect of Reynolds number on the flow field and large vortices is shown in Figures 3.6 and 3.7. Reynolds numbers are based on entrance velocities, viscosity of air at entrance conditions, and one centimeter characteristic distance. The equivalence ratio has been kept nearly constant so that variations in chemistry of the flames are minimal. The Reynolds number has been increased only by a factor of 2.44 which is

a. Equivalence ratio, ϕ = 0.56.

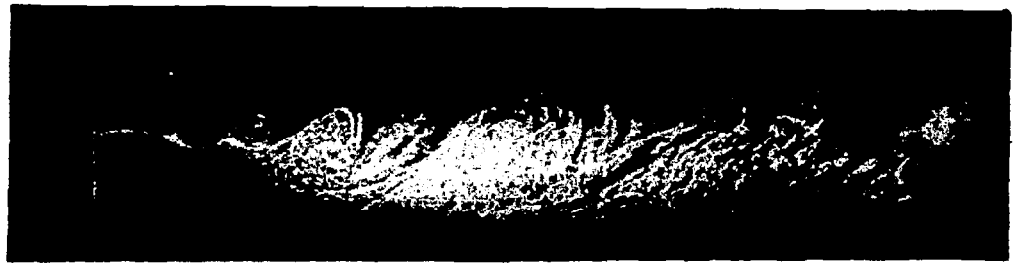

b. Equivalence ratio, ϕ = 0.60.

c. Equivalence ratio, ϕ = 0.64.

Fig. 3.4 Spark shadowgraphs of the flame behind the step for different reactant equivalence ratios. V_o = 13.3 m/sec, N_{Re} = 8600 cm^{-1}, T_o = 295 K, exposure time < 1 μsec.

a. Equivalence ratio, ϕ = .55.

b. Equivalence ratio, ϕ = .60.

c. Equivalence ratio, ϕ = .64.

Fig. 3.5 Spark schlieren of the flame behind the step for different reactant equivalence ratios. V_o = 13.3 m/sec, N_{Re} = 8600 cm^{-1}, T_o = 295 K, exposure time < 1 μsec.

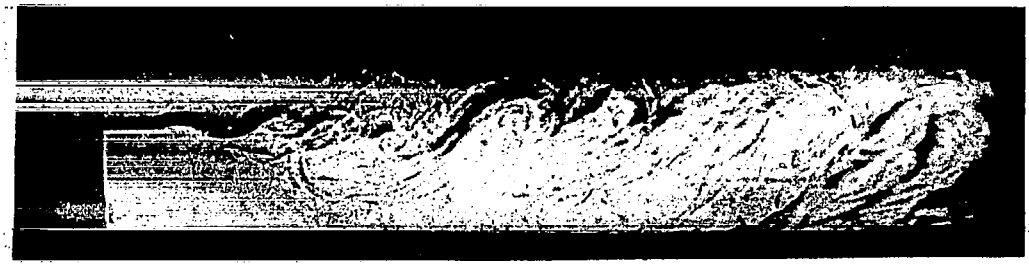

a. Velocity 9.1 m/sec, N_{Re} = 5900 cm^{-1}, ϕ = 0.60.

b. Velocity 13.3 m/sec, N_{Re} = 8600 cm^{-1}, ϕ = 0.60.

c. Velocity 22.2 m/sec, N_{Re} = 14400 cm^{-1}, ϕ = 0.58.

Fig. 3.6 Spark shadowgraphs of the flame behind the step for different reactant inlet velocities and Reynolds numbers. T_o = 295 K, exposure time < 1 μsec.

a. Velocity 9.1 m/sec, N_{Re} = 5900 cm^{-1}, ϕ = 0.60.

b. Velocity 13.3 m/sec, N_{Re} = 8600 cm^{-1}, ϕ = 0.64.

c. Velocity 22.2 m/sec, N_{Re} = 14400 cm^{-1}, ϕ = 0.60.

Fig. 3.7 Spark schlieren photographs of the flame behind the step for different reactant inlet velocities and Reynolds numbers. T_o = 295 K, exposure time < 1 μsec.

not large enough to show any drastic effect on the flame or flow structure. Over the range examined, the effect of the increase in Reynolds number seems to be reduction in the stability of the initial laminar layer, shortening the distance of the formation of discrete vortices with respect to the step edge, and an increase in the small scale turbulence inside the large eddies. For a similar case in a nonreacting free shear layer, see Figure 20 of Brown and Roshko (1974). The main features do not change with increase in Reynolds number: the laminar layer breaks into discrete vortices (large scale structures), the structures are coherent and they grow downstream.

What is clearly seen in all of these spark schlieren and shadowgraph pictures of the flame is that large eddies contain the reaction zone of the flame and that roll-up of each eddy corresponds to engulfment of hot products from the recirculation zone into a layer of fresh reactants in which reaction front propagates, see Figures 3.4 through 3.7.

To investigate the transition to turbulence, Konrad (1976) took plan view shadowgraphs of a two dimensional nonreacting free shear layer between two streams of gases (N_2 and He). He observed that the formation of Taylor type vortices (their vorticity is in the direction of the flow) appear in certain portions of the large structures. For details about this type of instability, refer to Rosenhead (1966). These vortices become unstable as they roll up into the large structures. Thus, the large structure itself has its own instability and, above critical Reynolds numbers, this instability generates strong local three-dimensionality and a cascade to high wave numbers within the basically two-dimensional large

structure. This cellular structure instability propagates into the braids connecting the large structures, thus producing small scale three-dimensionality throughout much of the layer. Konrad further discusses the interaction between Taylor vortices and large two dimensional vortex structures. He also offers an explanation for the mechanism of vortex stretching, a characteristic feature of turbulent flows, whose apparent absence in two dimensional vortical structures has been one of the main objections to the notion of "coherent large scale structures" in turbulent flows. Konrad concludes that transition to turbulence occurs at Reynolds numbers of about 0.4×10^4 ($N_{Re} = \frac{\Delta u \delta \omega}{\nu}$, where Δu, $\delta\omega$ and ν are the velocity difference between the two flows, vorticity thickness of the boundary layer, and kinematic viscosity of the higher velocity layer, respectively). By probe measurements inside the flow, he also shows that above the critical Reynolds number, the amount of small scale mixing in the shear layer is substantially increased. The entrainment rates into the turbulence are also shown to be larger above the critical Reynolds number.

Because of technical difficulties in the present investigation, the form of the vortices in the third dimension was not checked. It is anticipated that a similar mechanism will distort the large scale vortices in the third dimension and will probably be responsible for creation of small scale turbulence besides the Reynolds stress.

To estimate variation of Reynolds number downstream of the step, we calculated an approximate Reynolds number based on velocity, viscosity and shear layer thickness through the equation:

$$N_{Re} = \frac{\Delta U \cdot \delta\omega}{\nu} \tag{3.1}$$

where $\Delta U = U_1 - U_2$ was calculated as the difference between free stream and mid-step level measured velocities, Figure 5.1. Results of Brown and Roshko (1974) show that for the density ratios investigated ($\frac{\rho_o}{\rho_1} = \frac{1}{7}$, 1 and 7), the ratio of

$$\delta w/\delta_{vis} = .48 \tag{3.2}$$

where δ_{vis} is the visual thickness of the free shear layer. The same relation (Equation 3.2) was used to calculate the δw from δ_{vis} in the present investigations. Kinematic viscosity of gases is very temperature sensitive and even though there are no accurate measurements of viscosity at flame temperatures, kinematic viscosity varies approximately as $T^{3/2}$. So it is assumed that

$$\nu = \nu_o \left(\frac{T}{T_o}\right)^{3/2} \tag{3.3}$$

where ν_o has been assumed to be the viscosity of air at a temperature of 300 K. Values of δw were calculated based on shear layer thickness of Figure 3.30. Temperature measurements inside the flame at the step level were used to calculate the viscosity of burning gases.

Table 3.1 shows the values of Reynolds numbers calculated at reference velocities of 13.0 m/sec for nonreacting and 13.3 m/sec for reacting flows. These are the two values of velocities for which the measurements were available. The equivalence ratio for the reacting case is 0.57. The Reynolds number calculation in Konrad's work was based on the viscosity of the higher velocity side (N_2) which happens to be about an order of magnitude lower than the low velocity side (He). Table 3.1b shows that the Reynolds numbers based on the viscosity of hot products are considerably lower than the critical Reynolds number observed by Konrad, while those based on the viscosity of fresh reactants predict that the critical Reynolds number is attained very close to the trailing edge of the step. Which Reynolds number should be used to check for the critical value for transition to turbulence is controversial. Other evidence, such as the rate of propagation of flame and an apparent breakdown of the two dimensional structures suggests that the layer does reach a turbulent stage. Table 3.1 also shows that the layer might become laminar due to increase in viscosity, reduction of velocity difference, and lower spreading rate of the flame. However, according to the standards discussed above, the nonreacting flow will definitely become turbulent in the very early stages of the development of the shear layer.

For a better understanding of the development of these large scale structures and their role in the development of the flame mixing/reacting layer, a series of schlieren movies of the flame were taken. Figure 3.8 shows a sequence of frames from one of the high speed schlieren movies of the reacting flow behind the step. The flow

Table 3.1

Shear layer Reynolds numbers for reacting and nonreacting shear layers (a) V_o = 13.3 m/sec, N_{Re} = 8606 cm^{-1}, ϕ = .57, T_o = 295 K. (b) V_o = 13.0 m/sec, N_{Re} = 8411 cm^{-1}, ϕ = 0.0, T_o = 295 K.

FLOW	x(cm)	Δu(m/sec)	T(K)	$\nu_{\text{step level}}$ (cm^2/sec)	$Re = \frac{\Delta u \cdot \delta\omega}{\nu_{comb}}$	$Re = \frac{\Delta u \cdot \delta\omega}{\nu_{air}}$
(a) NONREACTING	1	13.0	295	.1568	-	1824
	4	14.1	295	.1568	-	7193
	8	12.5	295	.1568	-	11846
	12	10.4	295	.1568	-	13862
(b) REACTING	1	13.2	552	.316	1066	2148
	4	14.5	821	.710	1220	5524
	8	13.3	961	.898	1451	8309
	12	7.1	1053	1.031	884	5812
	16	2.8	1024	1.26	358	2876

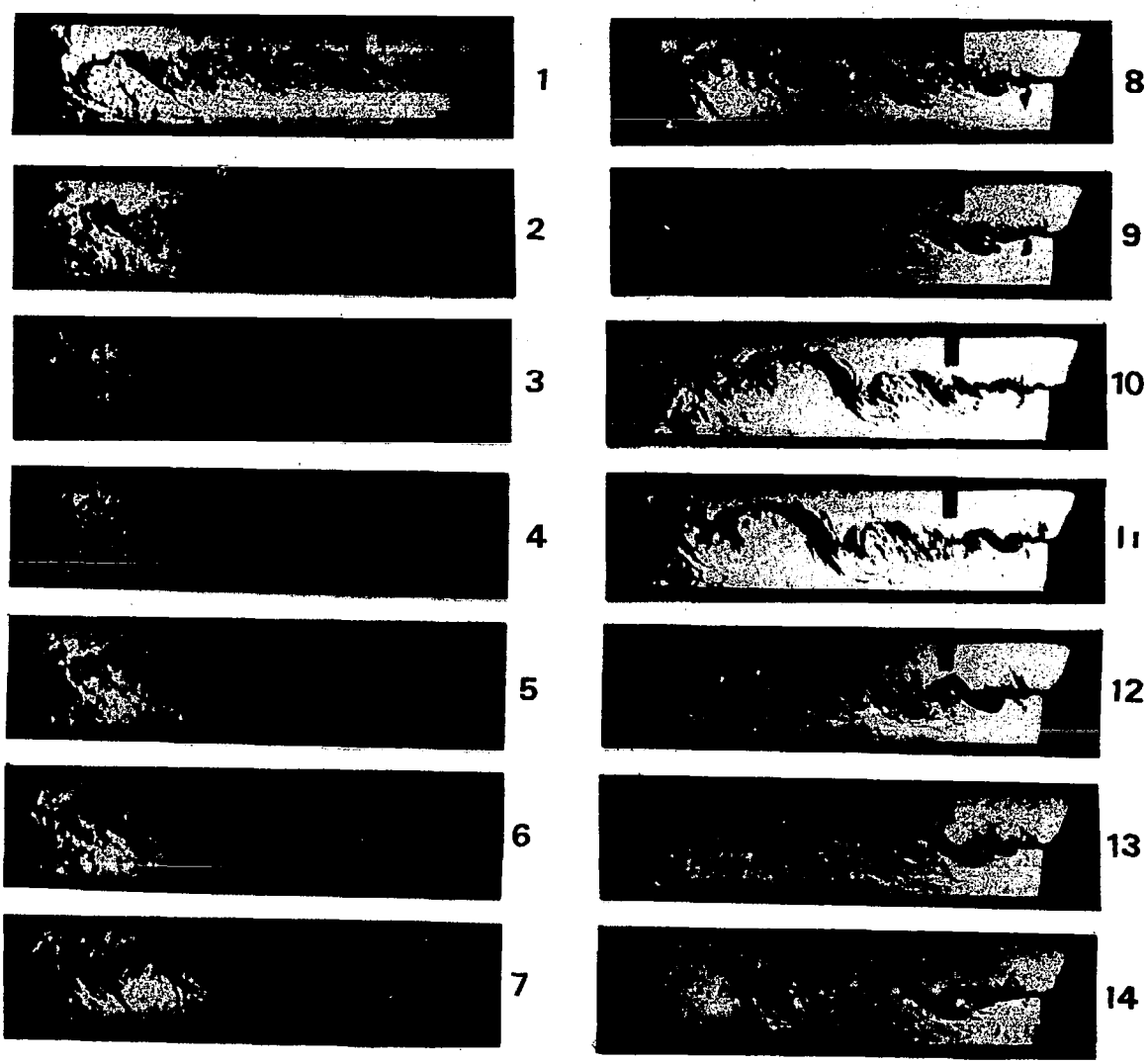

Fig. 3.8 Sequential series of the frames from a high speed schlieren movie of the flame. The time interval between the frames is 1.16 msec. V_o = 13.6 m/sec, N_{Re} = 8800 m/sec, ϕ = 0.57, T_o = 295 K.

conditions were at reference velocity of 13.6 m/sec, equivalence ratio of 0.57, ambient inlet temperature, and entrance Reynolds number of 8800 cm^{-1}. The time interval between the frames is 1.16 msec. Although these prints do not show the features of the eddies as elaborately as can be seen on the films, they have enough details to represent the basic features. The sequence in Figure 3.8 has been shot at a maximum framing rate of 7500 frames per second. The dark layer behind the step is the laminar mixing layer previously discussed. As this layer extends downstream, due to disturbances in the flow and concentrated vorticity in the layer, it ripples (frame 1) and, as the layer moves downstream, by the action of vorticity this ripple develops into a roll up vortex (bulging of the layer - frame 3), entraining fresh and burning mixtures as it moves downstream (frames 3 and 4).

The occurrence of the bulge, its position and period are two of the determining factors in the later development of vortices in the flow field. Spark shadow and schlieren records of the flame show that the mixing/reaction layer starts to grow when the initial laminar layer starts bulging or a new vortex is formed. The bulging is a fluid-mechanical rather than chemical phenomena. This fact is confirmed by the observation that, by increasing the reference velocity, this point (the vortex formation position) moves upstream. If chemistry were the dominant factor, the bulging should have been delayed, because of the longer induction distance for higher values of velocity at the same equivalence ratio.

The position of occurrence of the bulge, which is identified as the eddy formation position (x_o), has been reduced from the schlieren movies. They are presented in the form of a histogram that shows the

population distribution of the measured quantity. The histogram of the eddy formation position for the conditions close to those of Figure 3-8 is shown in Figure 3.9, and is observed to be nearly Gaussian. With the knowledge of the framing rate of the camera (which can be directly reduced from the timing marks on the film, the vortex formation period can also be reduced from the schlieren movies. The histogram of vortex formation period, for flow conditions close to those of Figure 3.8, is clearly skewed, Figure 3.10. The skewness of the shedding histograms represents the effect of driving frequencies on this phenomenon. The corresponding mean values for eddy formation position and period are also given in Figures 3.9 and 3.10. Similar histograms were constructed for different values of reference velocities, equivalence ratios and inlet temperatures The results for mean values of eddy shedding position ($\overline{x}_0$) and shedding period ($\overline{\tau}$) are summarized in Tables 3.2 and 3.3. The eddy formation position moves towards the step with increasing flow velocity (essentially the Reynolds number of the entrance flow), does not change with equivalence ratio, and moves away from the step with increase in temperature. These results show that, by increasing the entrance Reynolds number, the laminar layer behind the step destablizes (the layer breaks down) closer to the edge of the step. This view also explains the variation of the vortex formation position with temperature, that is, by increasing temperature for the same reference velocity, the vortex formation position moves away from the step. Table 3.2 shows that in the range examined, equivalence ratio does not have a pronounced effect on the position of eddy formation. The exact equality of values for $\overline{x}_0$ in this case (Table 3.2.b) may

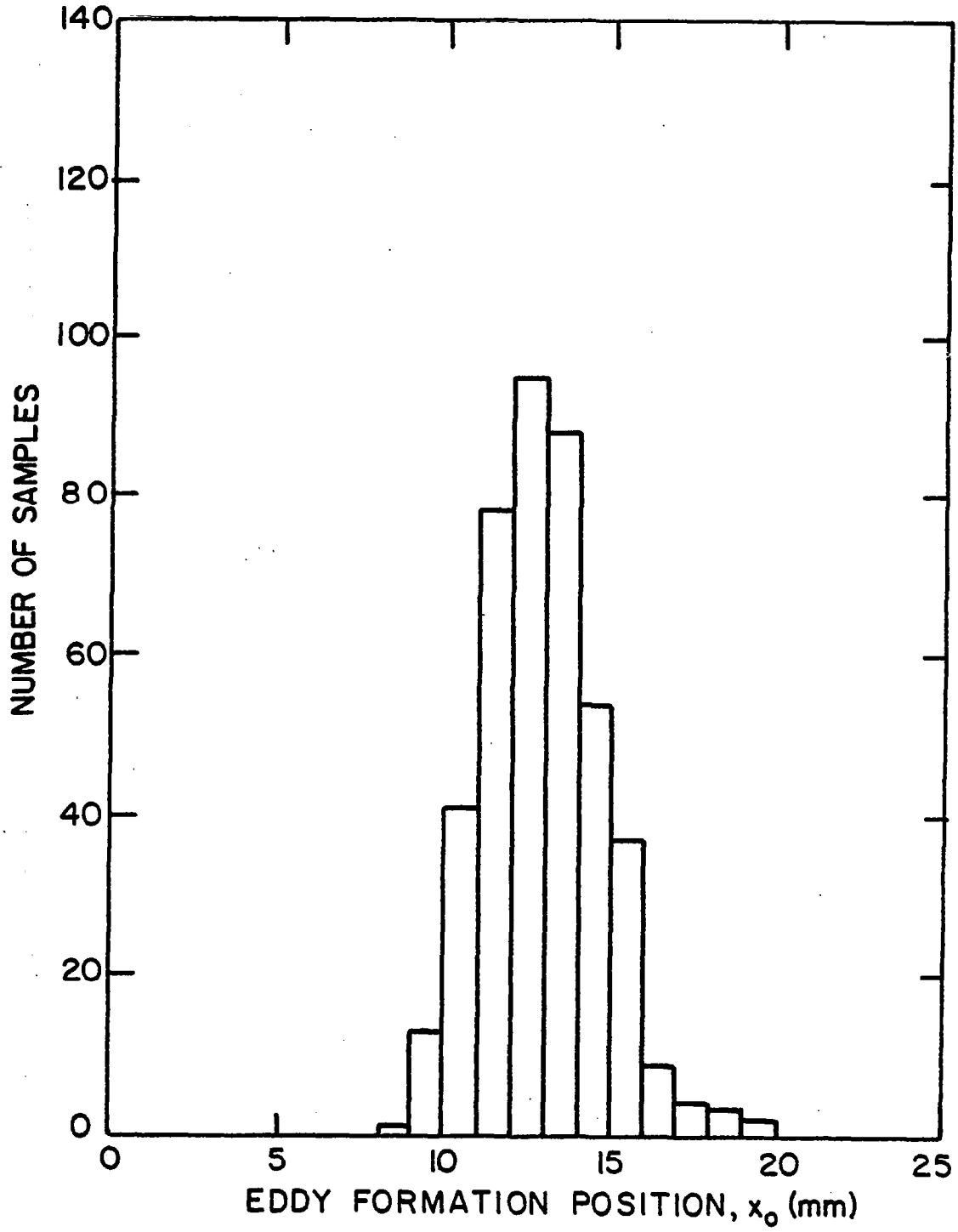

Fig. 3.9 Histogram of eddy formation position, x_o. V_o = 13.4 m/sec, N_{Re} = 8670 cm^{-1}, ϕ = 0.60, T_o = 295 K, $\bar{x}_o$ = 1.3 cm. Total number of samples = 426.

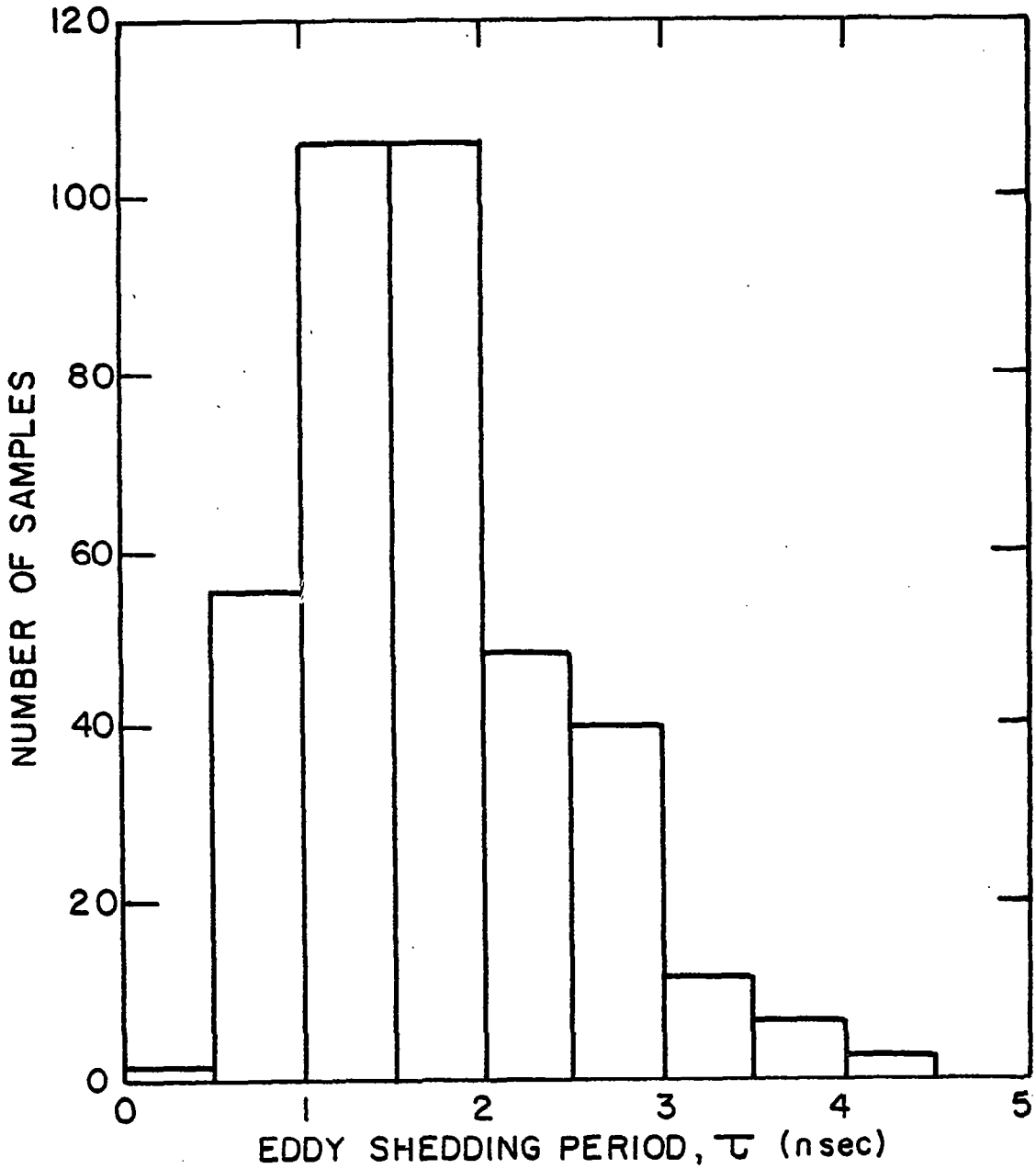

Fig. 3.10 Histogram of eddy shedding period. V_0 = 13.4 m/sec, N_{Re} = 8670 cm^{-1}, ϕ = 0.60, T_0 = 295 K, $\bar{\tau}$ = 1.70 msec. Total number of samples, 375.

Table 3.2

Effect of velocity (V_o), equivalence ratio (ϕ), and inlet temperature (T_o) on eddy formation position.

a. T_o = 295 K, ϕ = .60

V_o (m/sec)	9.2	13.4	22.5
N_{Re} (cm^{-1})	5953	8670	14559
$\bar{x}_o$ (cm)	1.7	1.3	0.9

b. T_o = 295 K, V_o = 9.2 m/sec, N_{Re} = 5953 cm^{-1}

ϕ	0.52	0.59	0.63
$\bar{x}_o$ (cm)	1.7	1.7	1.7

c. V_o = 13.3 m/sec

T_o (K)	295	454
N_{Re} (cm^{-1})	8606	3900
ϕ	0.55	0.53
$\bar{x}_o$ (cm)	1.3	1.6

d. T_o = 295 K, ϕ = 0.0 (nonreacting flow)

V_o (m/sec)	8.8	13.0	18.8
N_{Re} (cm^{-1})	5694	8412	12164
$\bar{x}_o$ (cm)	1.6	1.4	1.2

Table 3.3

Effect of velocity (V_o), equivalence ratio (ϕ), and inlet temperature (T_o) on eddy shedding period.

a. T_o = 295 K, ϕ = 0.6

V_o (m/sec)	9.2	13.4	22.5
N_{Re} (cm^{-1})	5953	8670	14559
$\bar{\tau}$ (msec)	2.9	1.7	1.2

b. T_o = 295 K, V_o = 9.2 m/sec, N_{Re} = 5953 (cm^{-1})

ϕ	0.52	0.59	0.63
$\bar{\tau}$ (msec)	2.8	2.9	2.5

c. V_o = 13.3 m/sec

T_o (K)	295	454
N_{Re} (cm^{-1})	8606	3900
$\bar{\tau}$ (msec)	1.9	0.8

d. T_o = 295 K, ϕ = 0.0 (nonreacting flow)

V_o (m/sec)	8.8	13.0	18.8
N_{Re} (cm^{-1})	5694	8412	12165
$\bar{\tau}$	2.5	1.9	1.5

be just a matter of coincidence. Table 3.3 shows that the shedding period decreases with increasing flow velocity and does not show any definite trend with equivalence ratio. Increase in temperature reduces the formation period of eddies. This is attributed to the increase in frequency of acoustic waves with temperature in the mixing section, Parker, et al. (1979). Increase in frequency of formation of eddies with velocity is attributed to the thickness of the boundary layer at the edge of the step. Higher velocities result in thinner boundary layers at the edge of the step ($\delta \sim \frac{1}{\sqrt{Re}}$) which results in a steeper velocity gradient in the laminar mixing layer. Because of the steeper velocity gradient, there is a higher concentration of vorticity in the layer, which makes the layer more susceptible to flow disturbances. It is important to bear in mind that whatever the mechanism of introduction of the disturbance is, the effect of velocity will be reduction in eddy formation position and increase in frequency of vortex formation. Parker, et al. (1979) have developed a modified laser schlieren method for measurement of frequency of large vortices in a two dimensional flame. This method was not used in the present investigation.

The vortex thus formed revolves as a result of bulk vorticity of the layer (the vorticity, $\omega_z = \frac{\Delta u}{\delta}$, where Δu is the velocity difference and δ is the shear layer thickness), which spreads across the flow as the vortex moves downstream. As the vortex revolves and is convected downstream, it entrains fresh and burned mixtures. Due to this entrainment, merging with other vortices (to be discussed later), and exothermic chemical reaction inside the eddies grow downstream. Vortical motion

of vortices is reduced as the vortices move downstream (this can be clearly observed in the schlieren movies.) In this system, we believe that heat release and wall constaints control expansion of the gases inside the shear layer. Expansion of the fluid in the shear layer results in reduction of the rate of rotation (conservation of angular momentum) of vortices so that their growth and expansion is mostly confined to the horizontal direction, Figure 3.8. Figure 3.8 also shows that burning takes place mostly during the process of engulfment into the layer at the boundaries of large scale eddies.

An interesting phenomenon first observed by Winnant and Browand (1974) to be the cause of the growth of the free shear layer in a water tunnel and later confirmed by Brown and Roshko (1974) in their high Reynolds number experiment of a free shear layer between two gas flows, is amalgamation or coalescence of eddies. This phenomenon is simply the take-over of an eddy by the one following it. The result of this process is the formation of a larger eddy. This process has also been called "pairing of vortices." This phenomenon has been observed to be partially responsible for the growth of the large eddies and consequently the shear layer. The phenomenon of eddy coalescence was also observed in the present flow field and was observed to be partly responsible for the growth of the reacting shear layer. A clear picture of coalescence of eddies in the reacting shear layer is shown in Figure 3.11. The first two eddies "A" and "B" in the first frame are followed in the subsequent frames. It can be seen that, as the eddy ahead moves downstream, it is pushed down and the following eddy moves forward and up. At the same time, they rotate around each other and finally become one identity (at least optically) as shown in frame number 7.

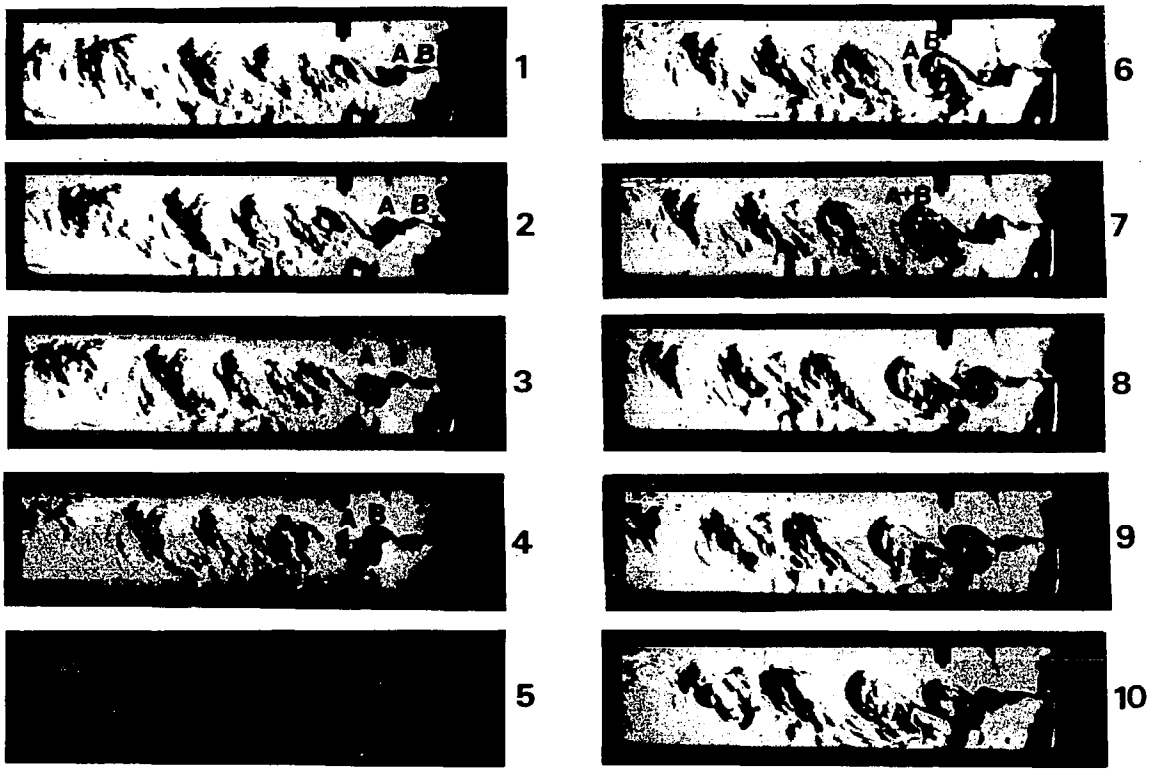

Fig. 3.11 Sequential series of frames from a high speed schlieren movie of the flame. The time interval between the frames is 0.67 msec. V_o = 13.3 m/sec, N_{Re} = 3900 cm^{-1}, ϕ = 0.53, T_o = 454.

The coalescence of eddies is more clearly shown in the work of Winnant and Browand (1974) where the camera has followed the eddies at the average speed of the two flows. This phenomenon can be characterized by calculating the percent of the eddies which survive as they move downstream. This will be discussed in the "Eddy Coherence and Coalescence" section. The coalescence of eddies observed on the schlieren movies may be by the action of fluid dynamics, observed by Winnant and Browand (1974) or by chemical reaction. By the latter, it is meant that, because of chemical reaction, the observable interface between two eddies might disappear and the two be identified as one, while fluid-dynamically, they might be two different structures. This problem cannot be resolved for data reduced from the schlieren or shadowgraph movies.

3.2 Nonreacting Mixing Layer

Visualization of the nonreacting flow field was made possible by using the residual temperature gradient existing in the thermal boundary layer on the surface of the step and the temperature difference between the incoming flow and the air in the recirculation zone immediately following the fuel shut off and flame extinction. The effect would persist for only a few seconds following the fuel shut off. The sensitivity of the system was also increased to make the detection of smaller refractive indices possible. Two spark schlieren photographs of the flow field at two values of reference velocity are shown in Figure 3.12. The basic features of the nonreacting shear layer seem to be very similar to the reacting shear layer. The layer immediately behind the step is laminar. It rolls up into discrete vortices which

a. Velocity 9.1 m/sec, N_{Re} = 5900 cm^{-1}, ϕ = 0.0.

b. Velocity 13.5 m/sec, N_{Re} ≈ 8800 cm^{-1}, ϕ = 0.0.

Fig. 3.12 Spark schlieren photographs of the nonreacting flow field behind the step for different air reference velocities and Reynolds numbers. T_o = 295 K, exposure time < 1 μsec.

are coherent and persist to some distance downstream. They lose their identity about midway downstream in the test section. We believe that this is due to the weaker refractive index at the periphery of the eddies as they move downstream and cool due to entrainment of fresh air. The cooling of eddies results in their optical disappearance. A sequence of frames from a high speed schlieren movie of the nonreacting flow field is shown in Figure 3.13. The figure shows that the sequence of events explained in the previous section also applies to the formation and growth of the layer for nonreacting flow. The mixing layer seems to have a higher spreading rate. The latter will be discussed later in this chapter. Histograms of the eddy formation position and period corresponding to Figure 3.13 are shown in Figures 3.14 and 3.15. As in the reacting flow, the histogram of eddy formation position is nearly Gaussian with an average close to the corresponding reacting flow. The histogram of the eddy shedding period is skewed towards higher frequency shedding rate with an average close to the average value of the shedding period for the corresponding reacting flow. Variation of mean values of eddy shedding position and period with velocity are shown in Tables 3.2 and 3.3. The trend is the same as in the reacting flows. As in the reacting flows, the process of coalescence of large eddies also occurs in nonreacting flows behind the step see Figure 3.13, frames 4 to 6. The disappearance of eddies here is purely a fluid mechanical process.

This observation suggests that heat release which results in expansion and increase in kinematic viscosity of the gas mixture in the layer does not considerably affect the vortex shedding in the layer behind the step. The similarities and differences of the two layers

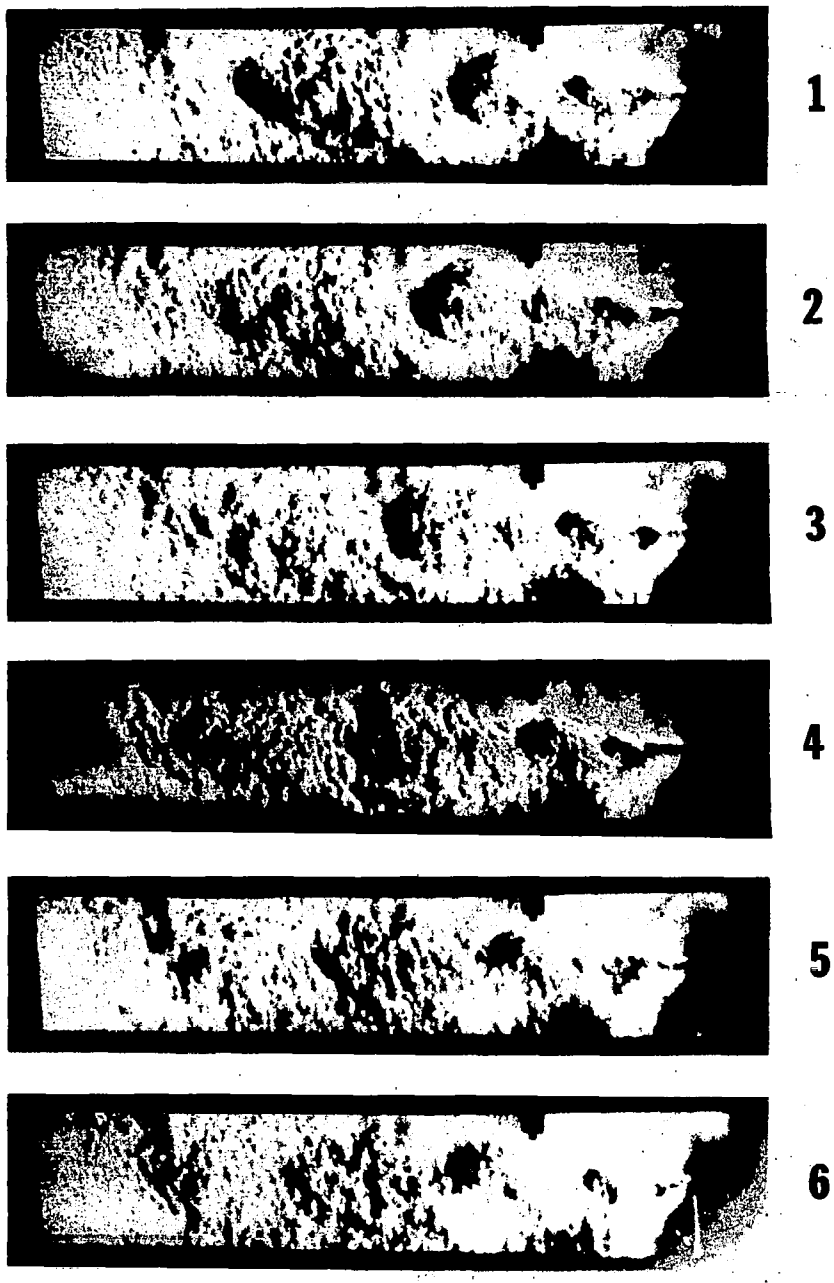

Fig. 3.13 Sequential series of the frames from a high speed schlieren movie of the nonreacting flow in the test section. The time interval between the frames is 1.13 msec. V_o = 13.0 m/sec, N_{Re} = 8474, T_o = 295 K. Flow is from right to left.

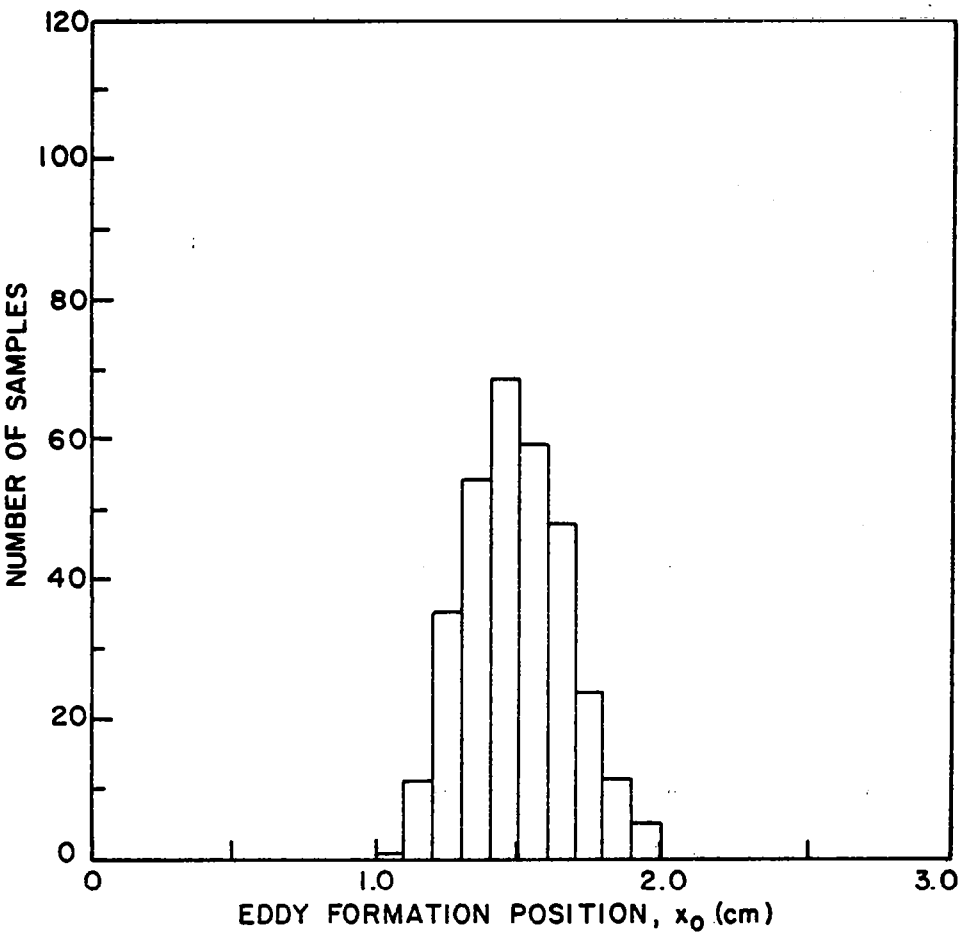

Fig. 3.14 Histogram of eddy formation position, x_0 for nonreacting flow. V_0 = 13.0 m/sec, N_{Re} = 8474 cm^{-1}, T_0 = 295 K, $\bar{x}_0$ = 1.5 cm. Total number of samples, 315.

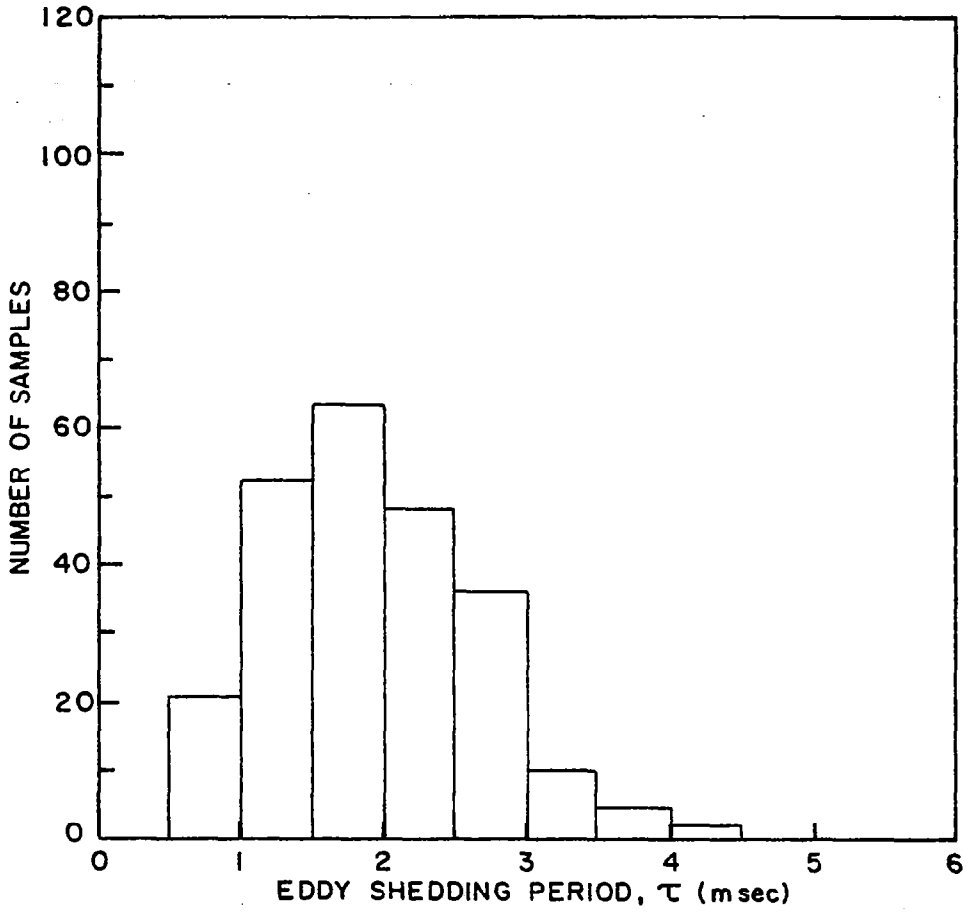

Fig. 3.15 Histogram of eddy shedding period for nonreacting flow. V_o = 13.0 m/sec, N_{Re} = 8474 cm^{-1}, T_o = 295 K, $\bar{\tau}$ = 1.8 msec. Total number of samples = 310.

will be discussed further later in this chapter. The schlieren observations do not allow the determination of whether the greater apparent persistence of the vortices in the reacting flow is due to stabilization by increased viscosity, or is simply a matter of increased schlieren visibility.

3.3 Coherence and Coalescence of Large Vortices in the Reacting and Nonreacting Mixing Layers

The quality of coherence is to be logically or aesthetically consistent, Webster (1973). In the present context, it is meant to describe the order and consistency in shape and development of the large scale structures in the shear layers. The term has been used in a somewhat different context in some turbulent literature, Spalding (1978a).

The quasi-orderly formation of large scale structures (see Sections 3.1 and 3.2) is the first sign of coherence of these structures in this system. A schematic of the development of eddies inside the layer is shown in Figure 3.16. x, Δx, and y represent distance of an eddy from the trailing edge, eddy spacing, and growth into the free stream respectively. A histogram of the ratio of spacing to growth of the eddies is shown in Figure 3.17, where $\Delta x = x_{i+1} - x_i$, $y = y_{i+1}$ and i is the sequence number of the eddy in the test section in the direction of the flow. The figure clearly shows the coherence in growth and spacing of the eddies. The distribution is nearly normal with an average of 2.6. On the average, spacing and growth increase downstream of the origin, but their ratio stays nearly constant (with a small standard deviation).

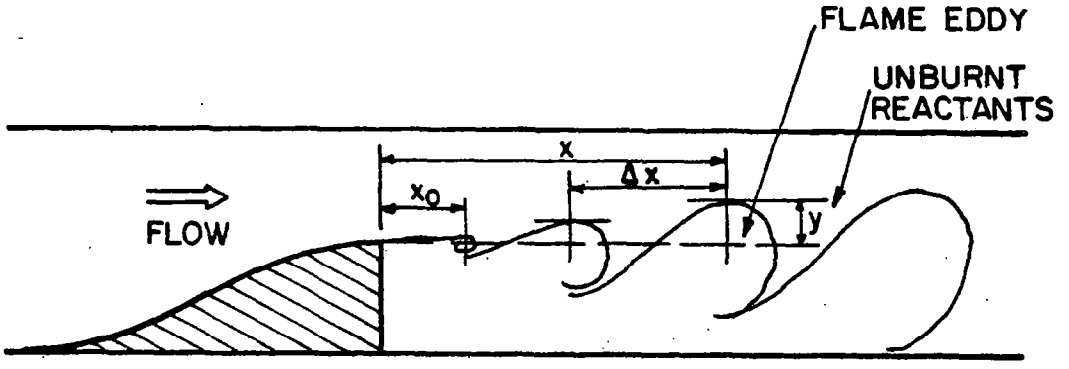

Fig. 3.16 Schematic of eddy development inside the two dimensional combustor.

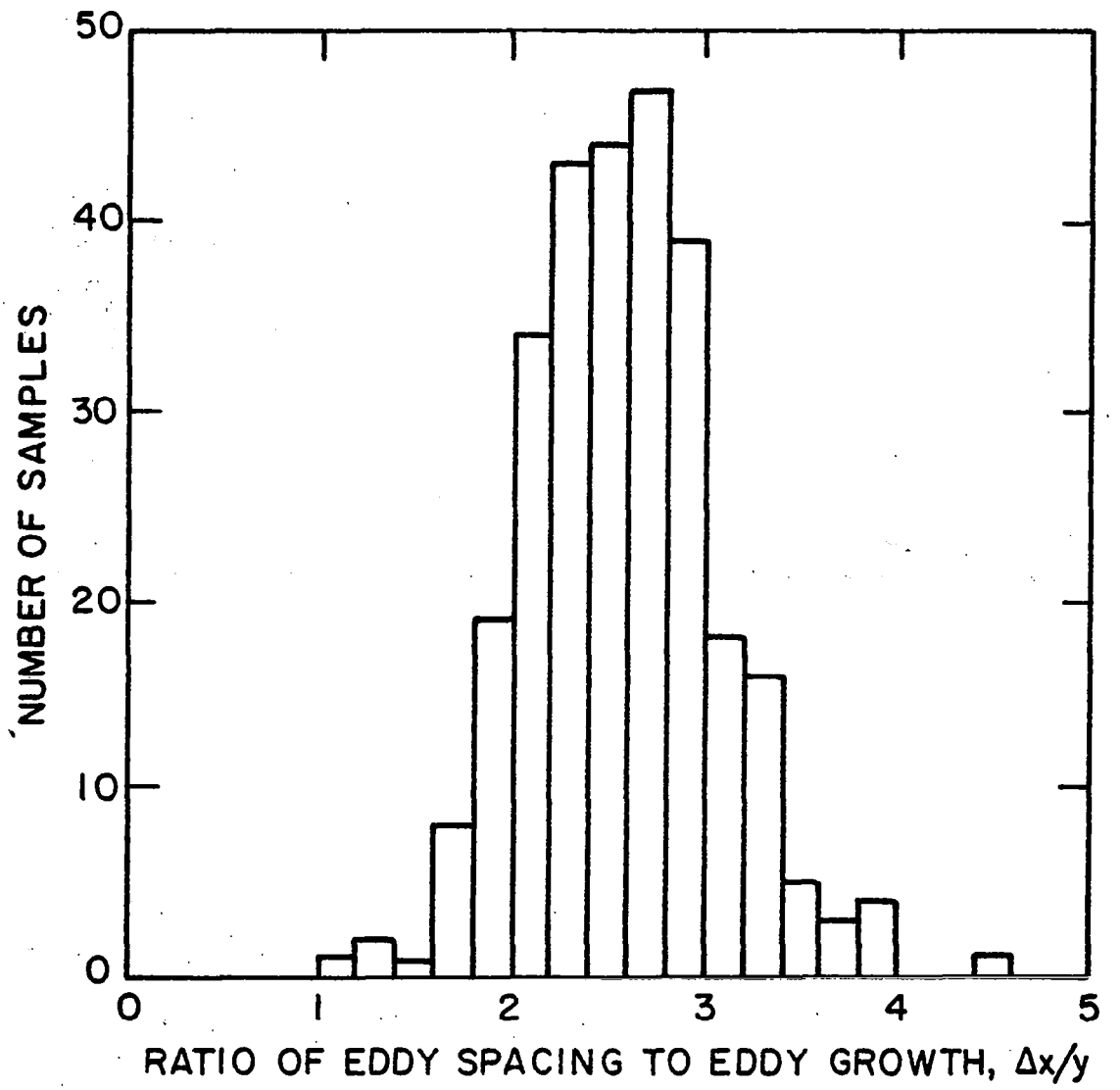

Fig. 3.17 Histogram of the ratio of eddy spacing to eddy growth in a reacting mixing layer behind the step. V_o = 13.4 m/sec, N_{Re} = 8735 cm^{-1}, ϕ = 0.57, T_o = 295 K, $(\overline{\frac{\Delta x}{y}})$ = 2.6. Total number of samples - 285.

The vortices shown in Figure 3.8 can be followed frame by frame on a high speed schlieren movie and the movement of these eddies in the mixing layer plotted against time on an x-t diagram. Such a diagram was first introduced by Brown and Roshko (1974) to show the coherence and the lifetime of eddies in their free mixing layer experiment. Trajectories of 100 consecutive eddies in the present reacting mixing layer are shown in Figure 3.18. x represents distance of the eddy from the edge of the step, Figure 3.16. Time has been calculated starting from an arbitrary frame of the film of the motion picture, knowing how the framing rate is changing with frame number, since the framing rate is not constant. Second order polynomial curve fits to the data of Figure 3.18 are plotted in Figure 3.19. Each corresponds approximately to the trajectory of the vortex in the shear layer. The trajectories are nearly parallel to each other, showing that the vortices nearly move with the same convective velocity in space and a general trend of increasing velocities as they move downstream. The latter can be shown by taking the derivative of the above curves. Average values of the longitudinal velocities at which the eddies are convected along the combustor have been calculated from the trajectory data (curve fit diagrams of Figure 3.19) and are presented in Figure 3.20. Because this is a confined reacting flow with energy release and expansion, the observed acceleration is expected. Histograms of reduced values of velocity from the x-t diagram of Figure 3.19 are shown in Figure 3.21. The calculated standard deviation for these three cases is at most 17% of the mean value. Results of velocity measurement by laser Doppler anemometry at the step level along the combustor, Houser (1979), are also shown in Figure 3.20. The measured values of velocity are

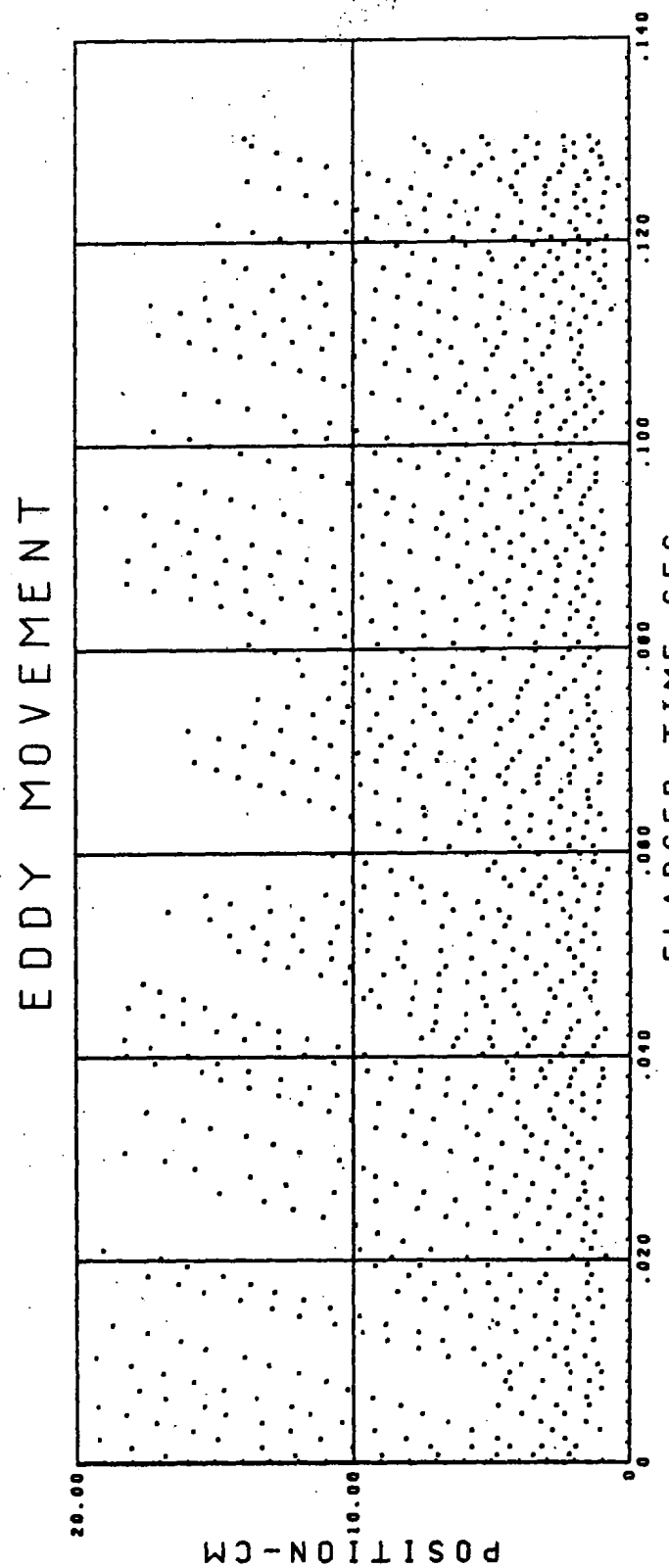

Fig. 3.18 Eddy trajectories of reacting flow behind the step. V_o = 13.6 m/sec, N_{Re} = 8800 cm^{-1}, ϕ = 0.57, T_o = 295 K.

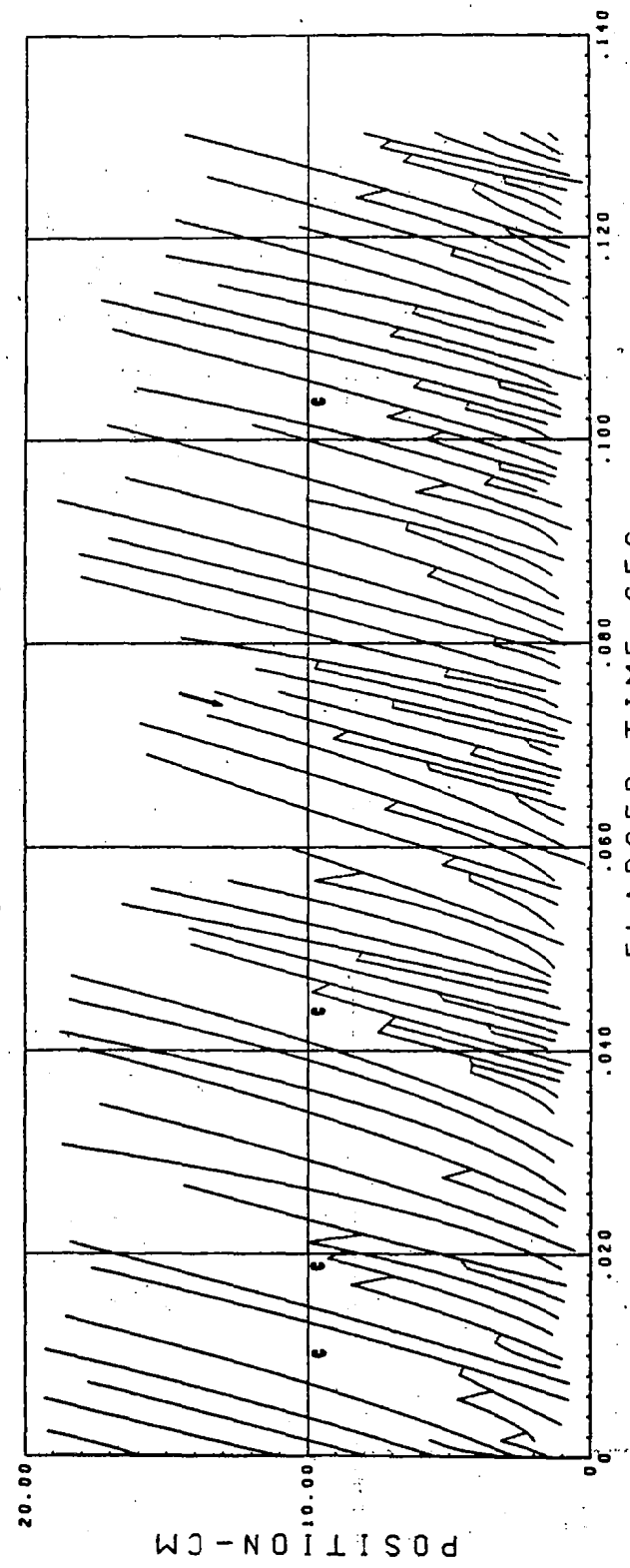

Fig. 3.19 Eddy trajectories of reacting flow behind the step. Second order polynomial curve fit to the data of Figure 3.18. V_o = 13.6 m/sec, N_{Re} = 8800 cm^{-1}, ϕ = 0.57, T_o = 295 K. Multiple coalescence is noted by the letter, c.

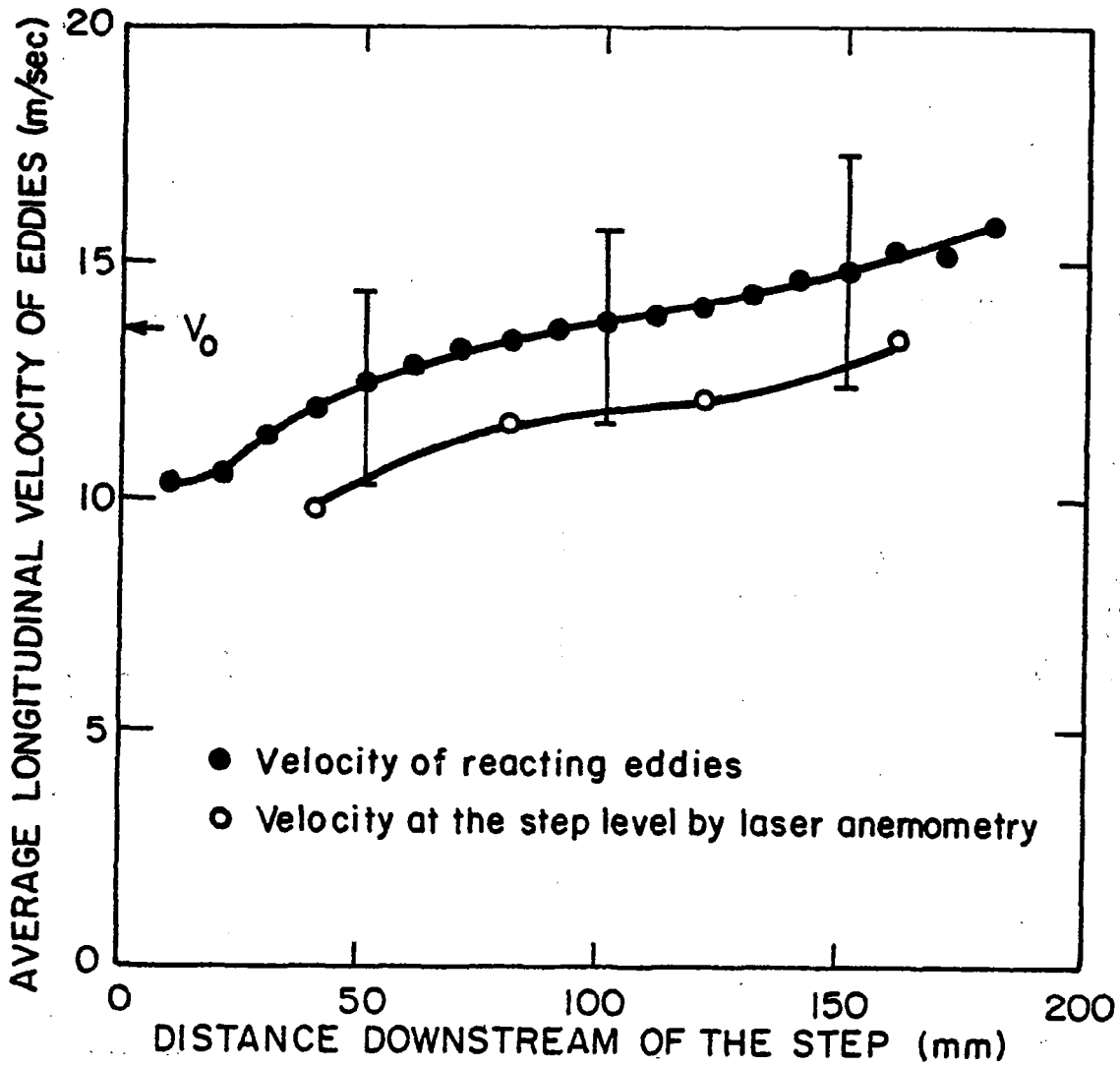

Fig. 3.20 Variation of longitudinal velocity of reacting eddies along the test section. Data reduced from Figure 3.19. V_o = 13.6 m/sec, N_{Re} = 8800 cm^{-1}, ϕ = 0.57, T_o = 295 K.

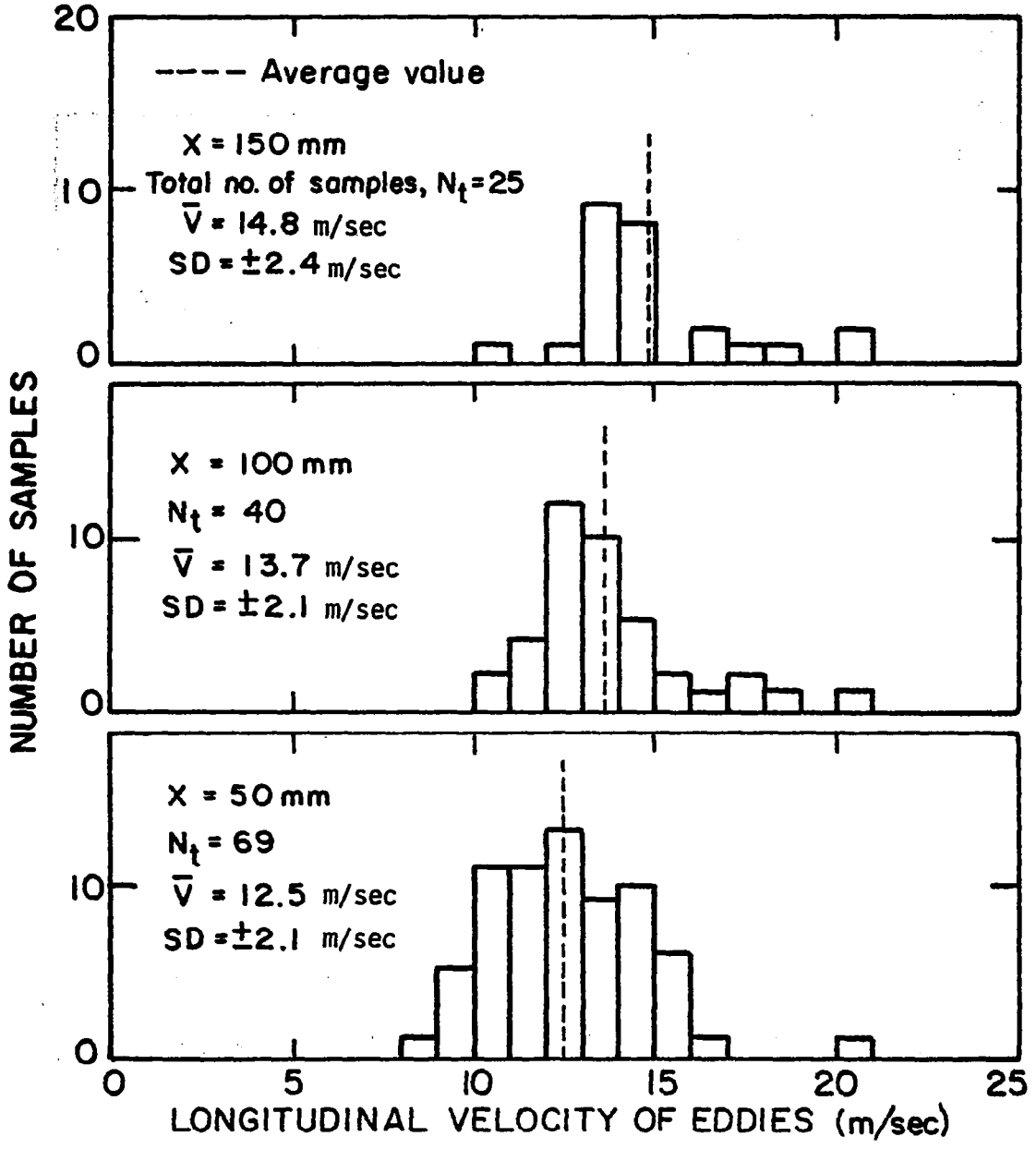

Fig. 3.21 Histograms of three values of velocities reduced from x-t diagram of Figure 3.19. V_θ = 13.6 m/sec, N_{Re} = 8800 cm^{-1}, ϕ = 0.57, T_0 = 295 K.

systematically lower than the eddy velocities reduced from the x-t diagram of Figure 3.19, but they show the same trend. The difference is considered to be within the uncertainty of the measurements, and is attributed to the nature of the curve fit, reduction of the data for the filming rate, numerical integration of the related curve, effect of flame propagation with respect to the flow, and the possibility that the eddies travel faster than the flow at the step height.

Eddy trajectories for 40 eddies in a corresponding nonreacting flow are shown in Figure 3.22. The second order polynomial curve fit of the data in Figure 3.22 is shown in Figure 3.23. Longitudinal velocity of eddies derived from the trajectories of Figure 3.23 is given in Figure 3.24. This figure also shows an acceleration in the longitudinal velocity of the eddies. It will be shown in the next section that the eddies in the nonreacting shear layer have a higher growth rate into the free stream which will naturally increase the velocity of the eddies towards the free stream velocity. Brown and Roshko (1974) argue that the instability theory shows there is a tendency to pull the wave speed towards the velocity on the high density side. This effect might be partially responsible for the differences in velocities in Figure 3.24.

The resemblance of the forms of vortices observed in spark photographs and high speed movies, their quasi-orderly formation downstream of the step, and their motion in the mixing layer with fairly consistent velocity in space suggests that, in both reacting and non-reacting flows, the large structures formed as a result of the instability of the original laminar separated layer are coherent. They grow and increase their spacing as they move in the shear layer down-

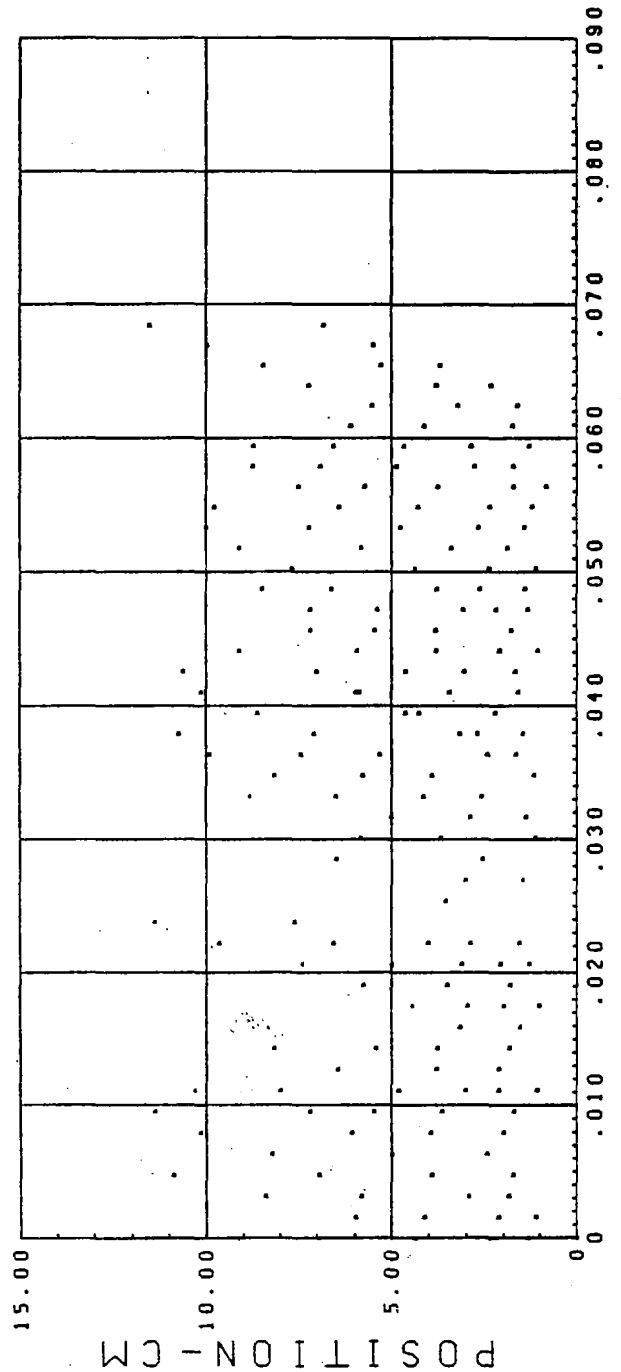

Fig. 3.22 Eddy trajectories of nonreacting flow behind the step. V_o = 13.0 m/sec, N_{Re} = 8412 cm^{-1}, ϕ = 0.0, T_o = 295 K.

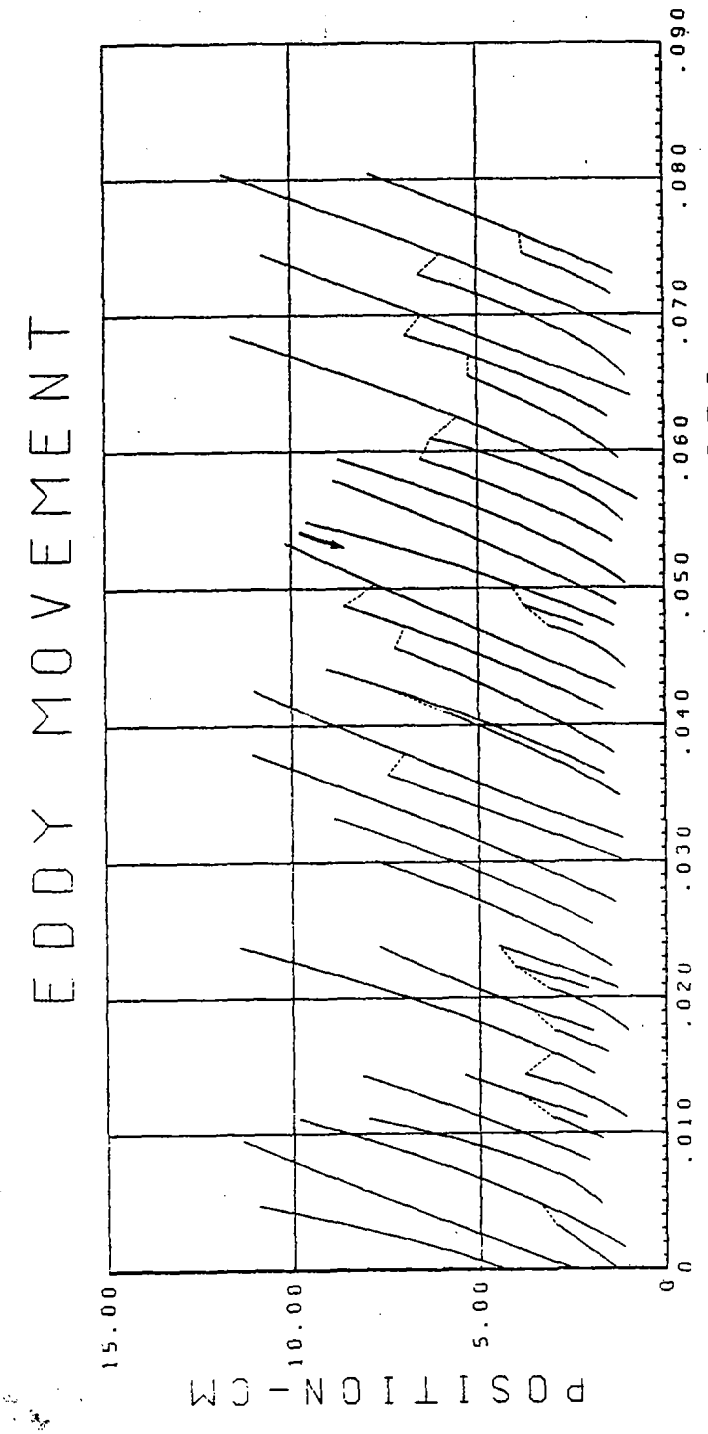

Fig. 3.23 Eddy trajectories of nonreacting flow behind the step. Second order polynomial curve fit to the data of Figure 3.22. V_o = 13.0 m/sec, N_{Re} = 8412 cm^{-1}, ϕ = 0.0, T_o = 295 K.

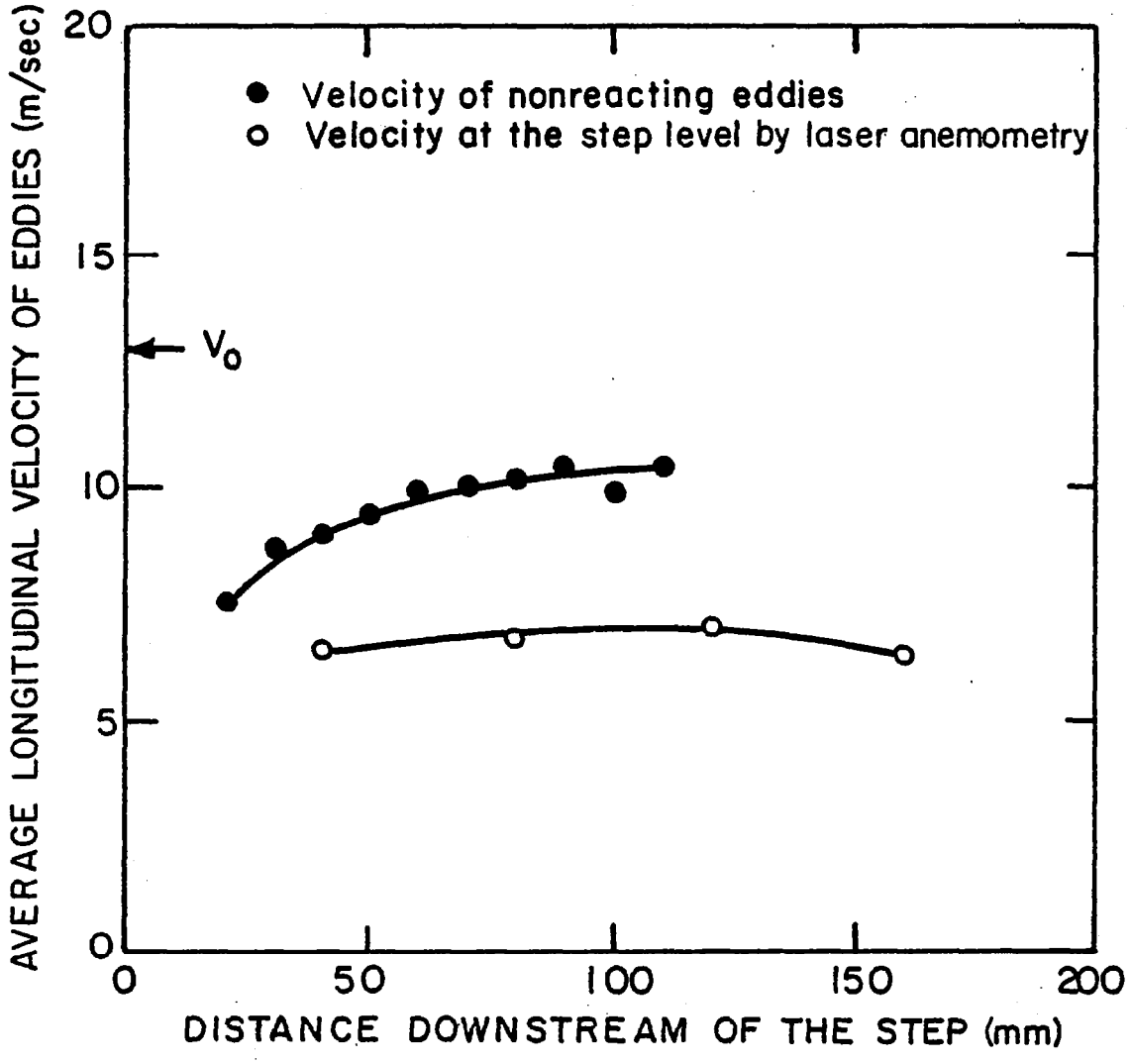

Fig. 3.24 Variation of longitudinal velocity of nonreacting eddies along the test section. Data reduced from Figure 3.23. V_o = 13.0 m/sec, N_{Re} = 8474 cm^{-1}, ϕ = 0.0, T_o = 295 K.

stream of the step.

Coalescence or vortex pairing is shown by dashed lines in Figures 3.19 and 3.23. After each pairing, a new vortex is formed which arbitrarily has been assumed to be the continuation of the second vortex. This assumption is based on the observation of this process on schlieren and shadowgraph movies, see Figures 3.8, 3.9 and 3.13. As was briefly described in the previous section, a pair of coalescing eddies rotate around each other as they are convected downstream, Figure 3.11. One is pushed down while the following is pushed upward and, at the same time, they elongate to form one larger eddy. Movement of coalescing eddies in the x-y coordinate of motion is shown in Figure 3.25. The figure corresponds to the coalescing eddies in reacting and nonreacting cases, shown by arrows in Figures 3.19 and 3.23. The time interval for the motion of each eddy between two points is also given. Since two series of coalescing eddies in reacting and nonreacting flow fields have arbitrarily selected, their behavior cannot be exactly compared. The general observation, also shown in Figure 3.25, is that the nonreacting eddies could grow or coalesce at a faster rate in the initial stages of the development of the layer, so that their growth and interaction are limited further downstream.

Figures 3.10, 3.11, 3.14 and 3.15 show that, for both reacting and nonreacting shear layers, the formation of eddies is distributed in space and time. According to Winnant and Browand (1974), pairing is a result of instability of the row of finite amplitude vortical structures. Because pairing is promoted by small variations in the strength and

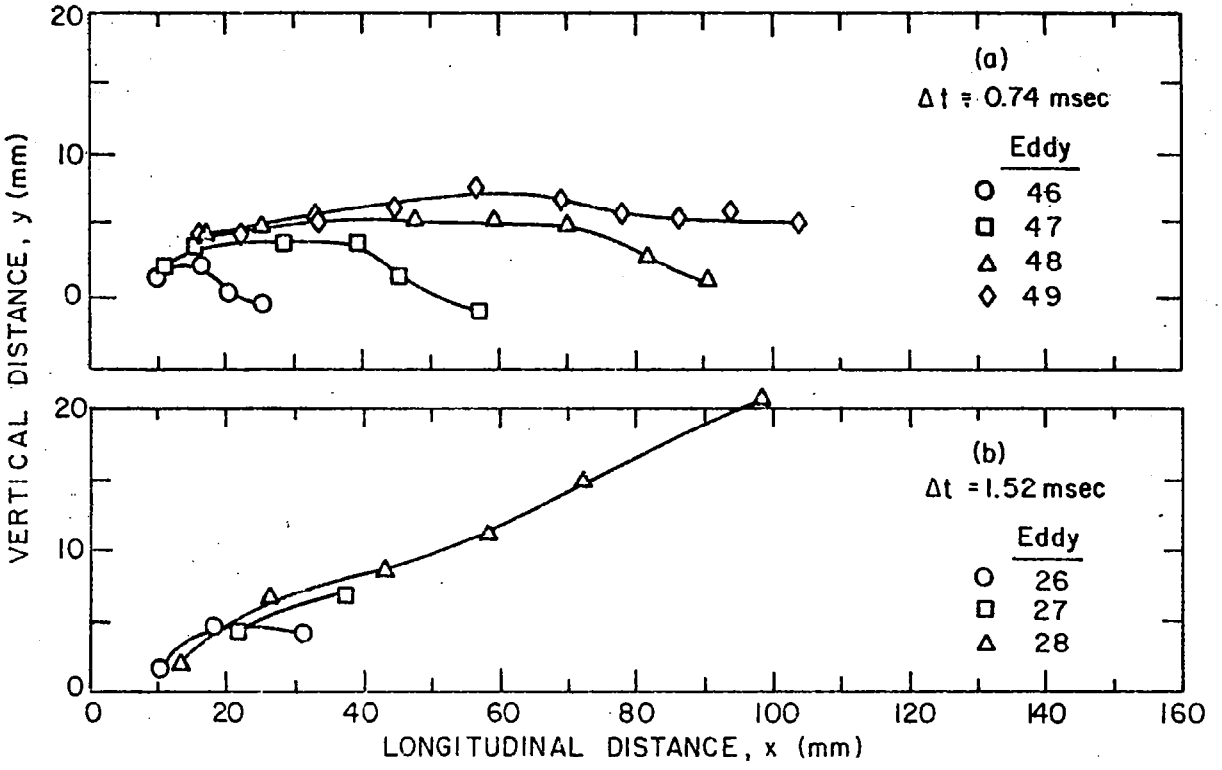

Fig. 3.25 Motion of coalescing large scale eddies in the test section. (a) reacting flow, V_o = 13.6 m/sec, N_{Re} = 8800 cm^{-1}, ϕ = 0.57, T_o = 295 K, time interval between the data points is .74 msec. (b) nonreacting flow, V_o = 13.0 m/sec, N_{Re} = 8474 cm^{-1}, T_o = 295 K, time interval between the data points is 1.52 msec.

spacing of the original row of vortical structures, its initiation does not always occur at the same point in space. Spatial and temporal irregularities in the vortex structure are amplified by the progression of pairing. During the process of pairing or coalescence, as the eddies rotate around one another they entangle the irrotational fluid from both sides of the mixing layer, and mix them together. Because of the process of coalescence of eddies in the mixing layer, the number of eddies decreases downstream of the step. Using the x-t diagram of Figure 3.19, the percent of reacting eddies which survive as they move downstream can be determined. Survival of eddies versus distance downstream of the step is shown in Figure 3.26. The figure shows an exponential decay in the number of eddies as they move downstream which is qualitatively in agreement with the finding of Roshko (1976).

In high speed schlieren and shadowgraph movies of the flame, a periodic intrusion of large eddies into the recirculation zone was observed. In reducing the data for Figure 3.19, it was noted that each of these intrusions corresponds to coalescence of a series of vortices close to the edge of the step. Four of these intrusions are identified by "C" on Figure 3.19. A picture of this intrusion is presented in Figure 3.27, which shows two portions of the same schlieren high-speed movie. Part (a) shows a normal mode of formation of vortices behind the step with occurrence of one pairing, while part (b) shows the amalgamation of a series of consecutive vortices leading to a gross mass flow into the recirculation zone. It was observed that the intrusion was more frequent in leaner flames, while in nonreacting flows it could not be identified.

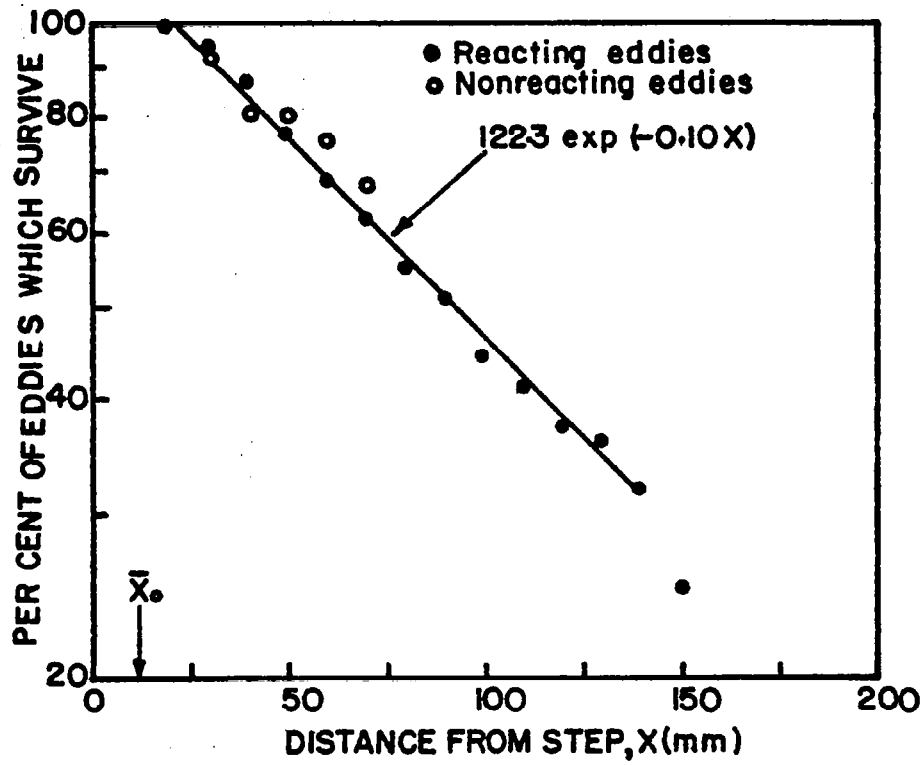

Fig. 3.26 Eddy survival, ● reacting mixing layer, V_o = 13.6 m/sec, N_{Re} = 8800 cm^{-1}, ϕ = 0.57, T_o = 295 K; o nonreacting mixing layer, V_o = 13.0 m/sec, N_{Re} = 8411 cm^{-1}, ϕ = 0.0, T_o = 295 K.

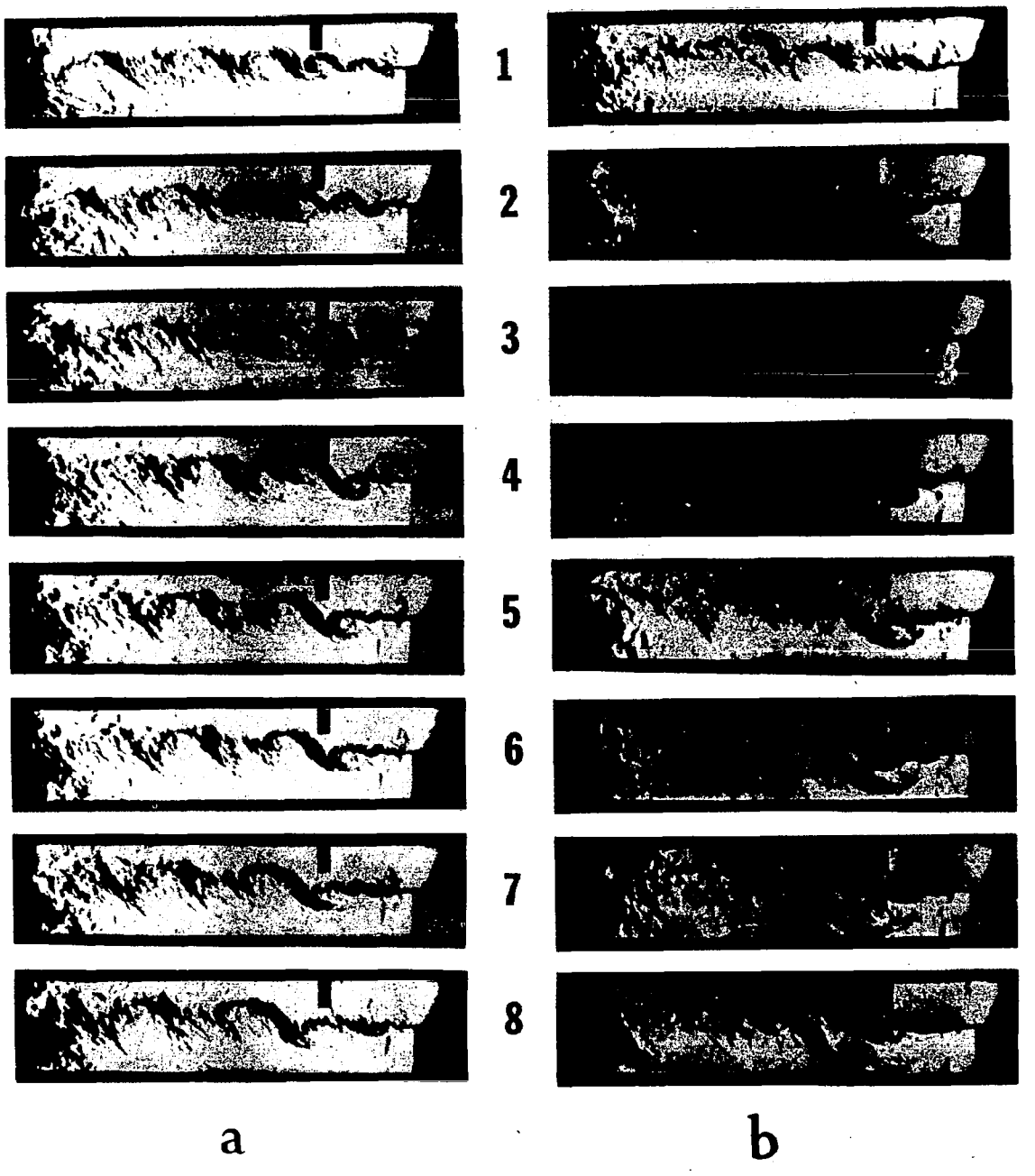

Fig. 3.27 Two sequential series of the same high speed schlieren movies of a flame behind the step. V_o = 13.6 m/sec, N_{Re} = 8800 cm^{-1}, ϕ = 0.57, T_o = 295 K.
(a) Normal formation and development of eddies in the mixing layer. Time interval between the frames is 1.16 msec.
(b) Coalescence of a sequence of eddies and process of intrusion into the recirculation zone. Time interval between the frames is 1.22 msec.

For nonreacting flow, the survival of eddies versus distance downstream was calculated from the data presented in Figure 3.23. Corresponding results are also shown in Figure 3.26.

3.4 Effect of Combustion on the Mixing Layer

From previous discussions in this chapter, it becomes clear that there is a close resemblance in the development of eddies in the reacting and nonreacting shear layers under investigation. In both cases, the eddies are formed downstream of the step and carried through the layer, they grow through coalescence and engulfment and increase their spacing as they move downstream.

Effect of combustion on the local Reynolds number was discussed in Section 3.1. It was concluded that, because of the increase in viscosity, dilation, and, consequently, in lower shear layer growth, there is an order of magnitude reduction in the Reynolds number. Another effect of combustion-created dilation is the reduction of small scale turbulence. The rate of turbulent energy exchange inside a turbulent shear layer directly depends on the strain rate in the layer, Tennekes and Lumley (1972). Reduction in the rate of energy exchange in the layer results in a lower turbulent energy, which corresponds to a lower turbulent intensity. As the rate of energy transfer is directly related to the wavelength of turbulent scales, reduction in the rate of energy transfer from the main flow to the shear layer will reduce the rate of production of small scale turbulence inside the layer.

Variation of the position of eddy formation with respect to velocity for both reacting and nonreacting shear layers is shown in Figure 3.28.

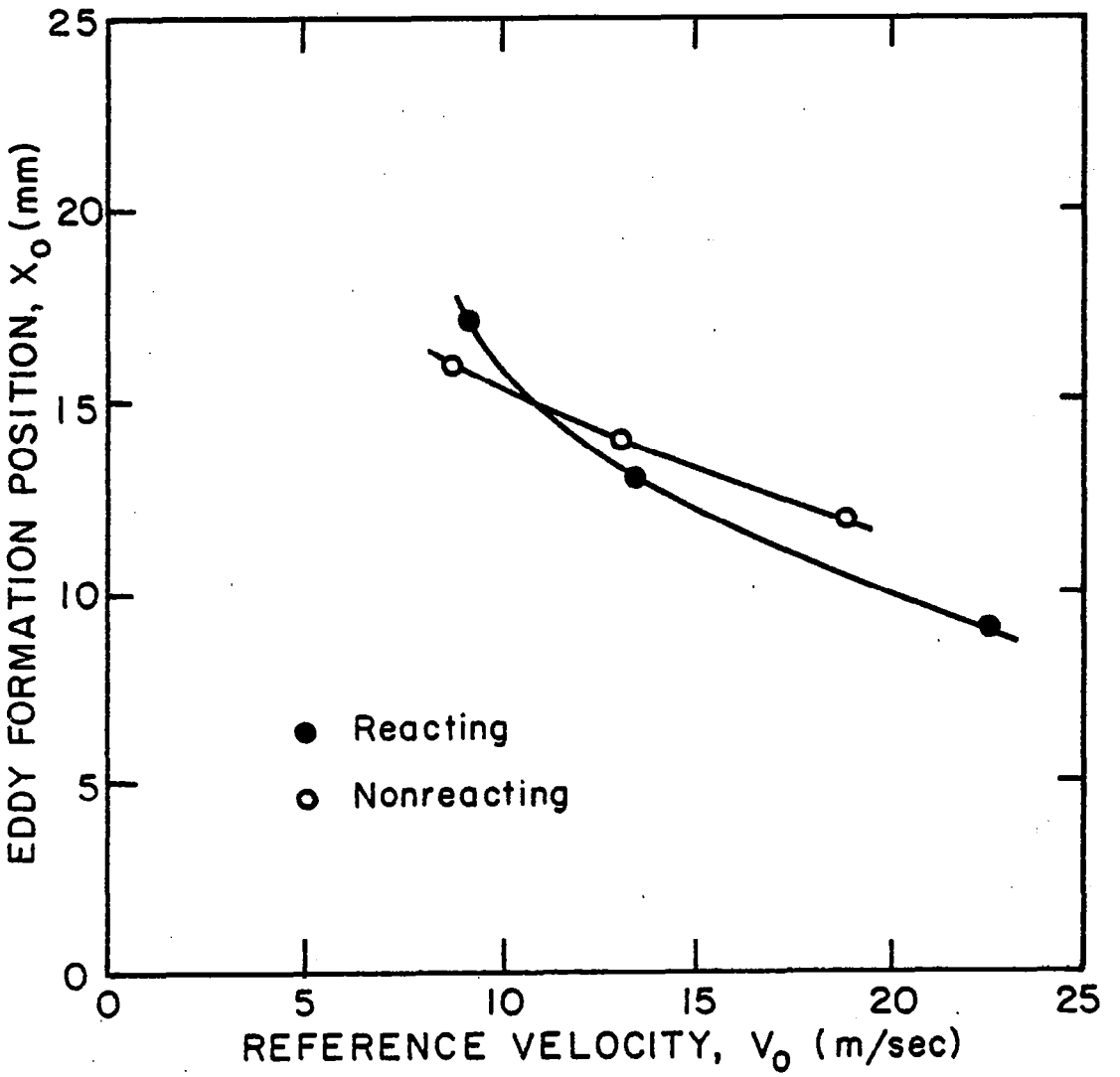

Fig. 3.28 Variation of eddy shedding position versus reference velocity, ● reacting flow, ϕ = 0.6, T_o = 295 K; o nonreacting flow, ϕ = 0.0, T_o = 295 K.

In the range examined, the laminar layers seem to roll up at comparable distances for comparable velocities in both cases. This result is in sharp contrast with the observation by Chigier and Yule (1979) for unconfined jet diffusion flames. They found that the transition from the laminar layer to unstable vortex rings extends from 3D to 20D (D is the nozzle diameter) from nonreacting to reacting jets. They attribute this phenomenon to an increase in the kinematic viscosity of the gases which is a result of heat release in the shear layer.

Among many factors which may influence the transition of a separated layer, the following are the most important: the thickness of the layer, Reynolds number, turbulence of the mainstream and flow disturbances. The flow disturbances can be due to acoustic feedbacks, adjacent flow fields, etc. It is suggested that breakdown of the layer in Chigier and Yule's jet is controlled by the Reynolds number as they argue (thickness of the layer and turbulence are presumably the same for both reacting and nonreacting cases), while in the present system it is believed that breakdown of the layer is influenced by disturbances due to reverse flow in the recirculation zone and also by the acoustics of the combustion chamber or upstream flow channel. These effects were not quantified in this experiment.

Variation of eddy shedding period versus velocity for reacting and nonreacting layers is plotted in Figure 3.29. A simple dimensional reasoning might make the trends more clear. The frequency of formation of eddies, f, might be expressed by $f = \text{const} \cdot \frac{V}{\theta}$, where V is the reference velocity and θ is the momentum thickness. For a laminar layer on a flat plate, $\theta = \text{const}\, V^{-\frac{1}{2}}$, thus $f = \text{const} \cdot V^{3/2}$. This

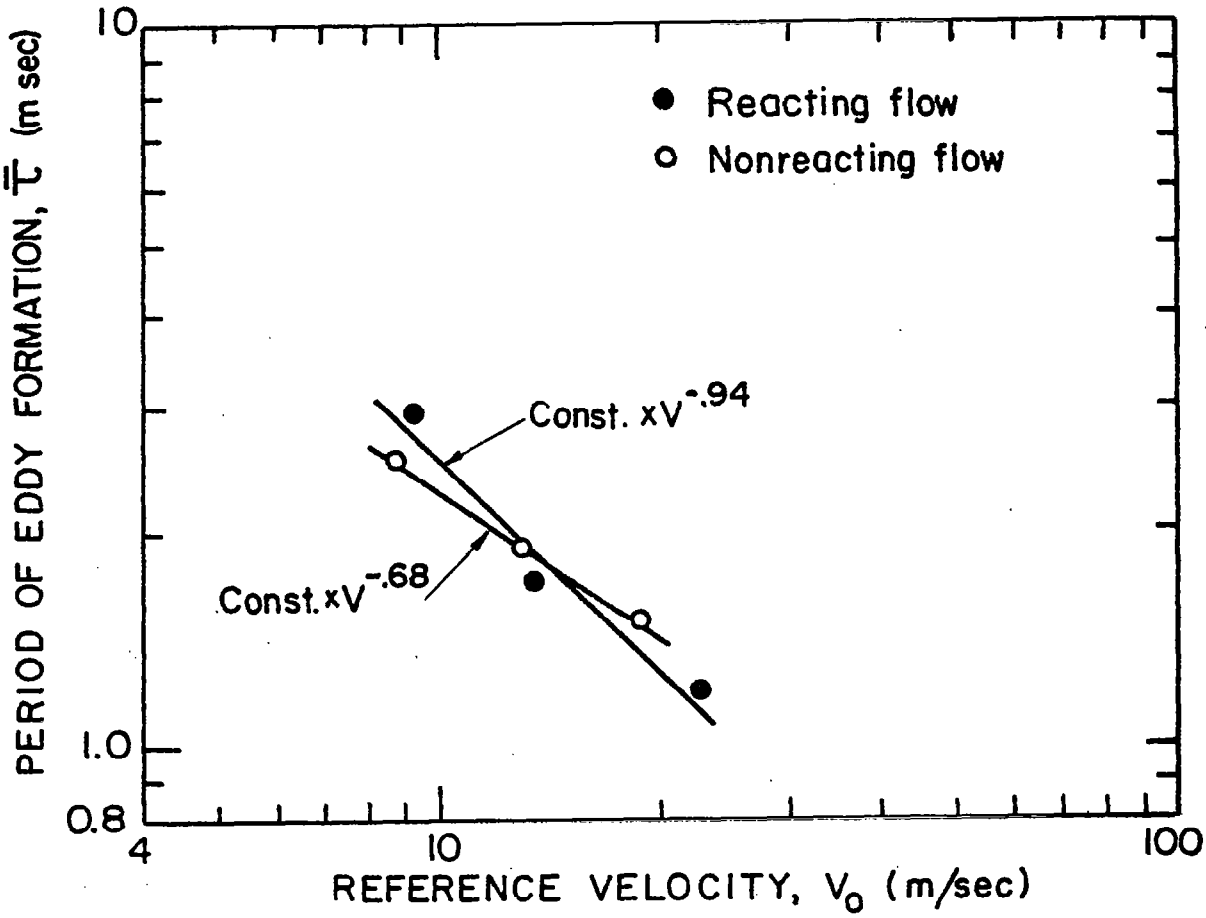

Fig. 3.29 Variation of eddy shedding period versus reference velocity, ● reacting flow, ϕ = 0.6, T_o = 295 K; o nonreacting flow, ϕ = 0.0, T_o = 295 K.

relation correlates Sato's (1956) data with high accuracy, but it does not fit the data in the present experiment. The difference in power dependence of period on velocity for cold and hot flows can be attributed to the acceleration of the gases due to heat release in the layer. Actually, the apparent velocity profile between the free stream and stagnant recirculation zone will be similar to the nonreacting case, with higher reference velocity. As a result, this effect appears in the form of an increase in power dependence of velocity for the reacting case.

Another aspect of the large scale structures that has been of interest is the spacing between the eddies as they move downstream. Figures 3.19 and 3.23 show that, on average, the eddies increase their spacing through coalescence as they move downstream. Histograms of spacing between eddies normalized by the distance from the average point of formation of eddies is shown in Figure 3.30. The data for construction of these histograms were reduced by a computer program from data of Figures 3.19 and 3.23 by calculating the spacing between the eddies at 2 msec time intervals. The choice of time was arbitrary. The histograms have a very close resemblance in shape, and are both skewed towards the lower values of $\frac{\Delta x}{x-x_o}$. This is because $\Delta x \approx \bar{u} \cdot \tau$, where $\bar{u}$ is the average velocity of the two eddies, and τ is the period between these two eddies. So generally, Δx will follow the same trends as the period of eddy formation. The same effect is also consistently seen in the shedding period histograms. The average value of $\frac{\Delta x}{x-x_o}$ for nonreacting flow is close to

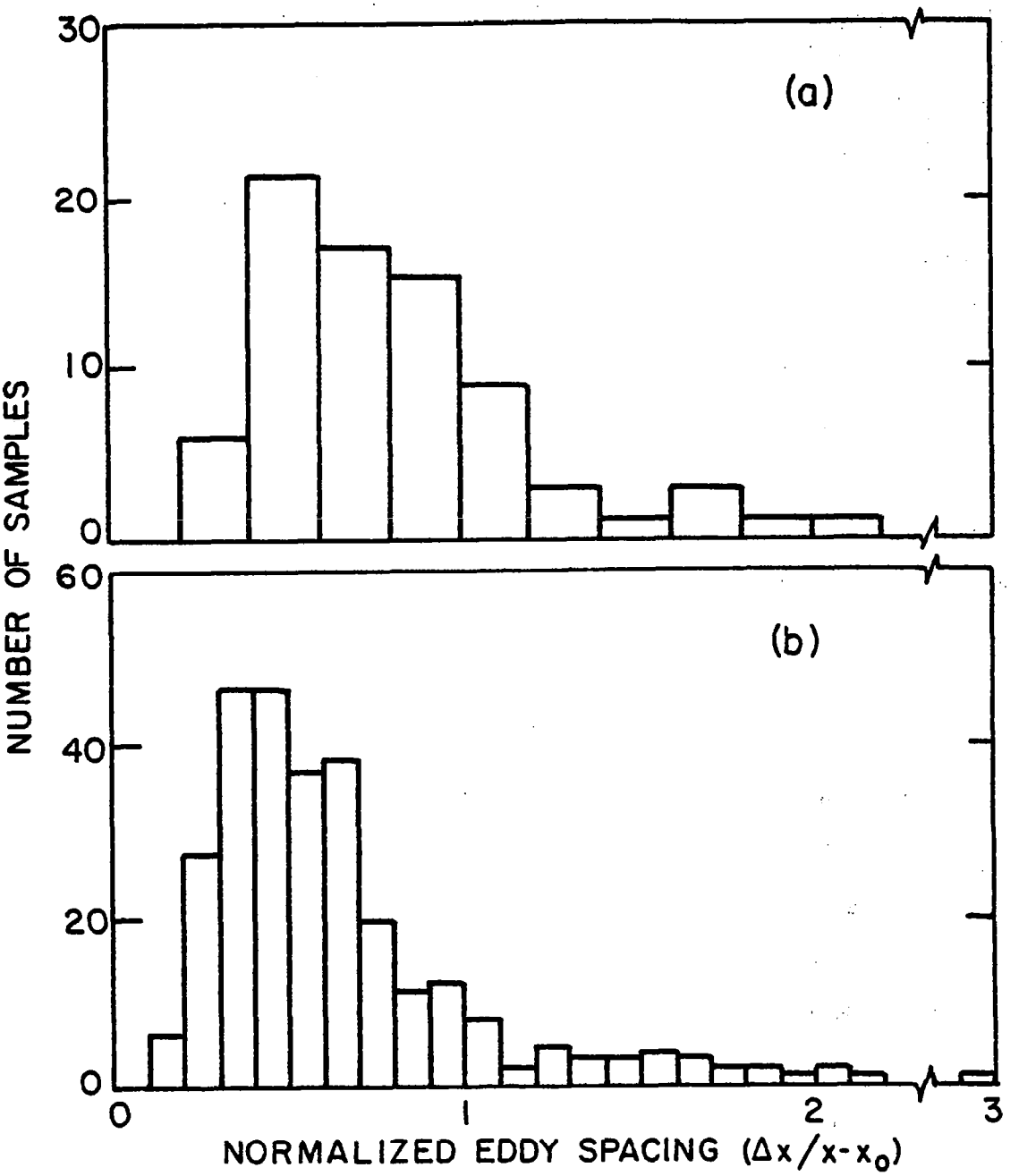

Fig. 3.30 Histogram of normalized eddy spacing.
(a) Nonreacting flow, V_o = 13.0 m/sec, N_{Re} = 8474 cm^{-1}, T_o = 295 K, $(\frac{\overline{\Delta x}}{x-x_o})$ = 0.85. Total number of samples, 78.
(b) Reacting flow, V_o = 13.6 m/sec, N_{Re} = 8800 cm^{-1}. T_o = 295 K, $(\frac{\overline{\Delta x}}{x-x_o})$ = 0.66. Total number of samples, 278.

30% higher than the reacting flow. In both cases, the average value is considerably higher than the $\frac{\overline{\Delta x}}{x-x_o} = 0.31$ obtained by Brown and Roshko (1974). By a similarity argument, Roshko (1979) concluded that $\overline{(\frac{\Delta x}{x-x_o})} = \frac{\overline{\Delta x}}{x-x_o}$ for their mixing layer between two streams of gases. Inspection of the spreading rate of the shear layers in this system shows that they lack the essential features of self-similarity. In any case, if we use the above relation as an approximation for the present layers, the conclusion is that the average spacing between the eddies is higher in the nonreacting shear layer than in the reacting shear layer.

Growth of the shear layer was calculated for reacting and non-reacting cases employing the data from the high speed schlieren movies of the flowfield in the test section. The method used was as follows: starting from an arbitrary frame of the film, the y coordinates of eddies (see Figure 3.16) were measured in intervals of 10 frames. For each eddy, the coordinates were measured from the incipience to the disappearance location. The disappearance of an eddy could happen because of its merging with another eddy, entering the exhaust, or blurring so that it could not be identified any more (see Figures 3.19 and 3.23). The measurement was also discontinued when the eddy grew to the size of the combustor, reaching the top plate of the combustor. The latter case was very rare. The path of the apex of each individual eddy was calculated by interpolation of the discrete experimental data through cubic spline functions. Finally, at intervals of one centimeter downstream of the step, the path for different eddies was averaged considering a unit weight for each eddy path.

The averaging was done for 40 nonreacting and 100 reacting eddies. The results for spread of both reacting and nonreacting layers are shown in Figure 3.31. In the case of nonreacting shear layers, the eddies became indistinct midway in the combustor. Because of this difficulty, the growth of the layer was calculated only up to 11 cm downstream of the step. Because of the coalescence or disappearance of eddies, the averaging could not be performed on equal numbers of eddies at different locations downstream of the step. Tables 3.4 and 3.5 show the location and number of eddies for which data were averaged for reacting and nonreacting flows. Wright and Zukoski (1962) have shown

Table 3.4

Average growth of the nonreacting mixing layer versus distance from the edge of the step. Number of eddies for which data were averaged is also given. V_o = 13.0 m/sec, N_{RE} = 8412 cm^{-1}, ϕ = 0.0, T_o = 295.

Distance From Step x (cm)	Growth of Layer y (cm)	Number of eddies
2	.41	35
3	.64	37
4	.83	32
5	.99	32
6	1.16	30
7	1.36	27
8	1.55	21
9	1.71	15
10	1.74	11
11	1.9	5

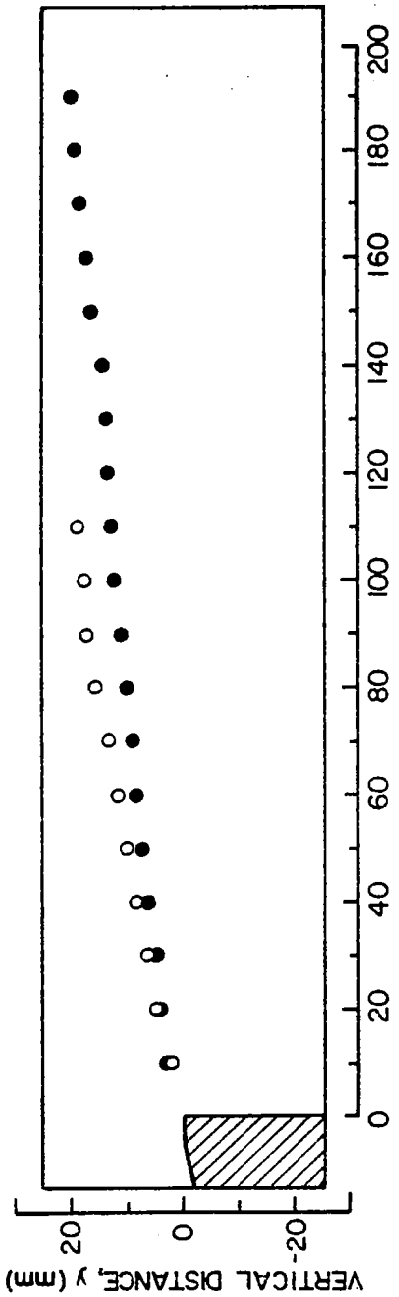

Fig. 3.31 Mixing layer spread in the test section, ● reacting layer, V_{o_0} = 13.6 m/sec, N_{Re} = 8800 cm^{-1}, ϕ = 0.57, T_o = 295 K; o nonreacting layer, V_o = 13.0 m/sec, N_{Re} = 8474 cm^{-1}, T_o = 295 K.

Table 3.5

Average growth of the reacting mixing layer versus distance from the edge of the step. Number of eddies for which data were averaged is also given. V_o = 13.6 m/sec, N_{RE} = 8800 cm^{-1}, ϕ = 0.57, T_o = 295 K.

Distance From Step x (cm)	Growth of Layer y (cm)	Number of Eddies
1	.33	18
2	.42	93
3	.53	91
4	.62	82
5	.74	73
6	.82	65
7	.90	58
8	1.02	52
9	1.10	47
10	1.25	42
11	1.29	41
12	1.34	41
13	1.38	38
14	1.46	33
15	1.65	25
16	1.71	22
17	1.84	18
18	1.91	10
19	2.01	4

that the equivalence ratio does not considerably change the spreading rate of premixed turbulent flames stabilized behind two dimensional bluff bodies. Based on their results and the observations here, it

was assumed that the equivalence ratio will not considerably influence the spreading rate of the flame in this system. Consequently, the spreading rate for only one equivalence ratio was calculated.

Figure 3.31 shows that, on the average, the growth of the reacting shear layer is about 30% less than that of the nonreacting shear layer. The main factors that should be considered in explaining the above phenomenon are: increase in viscosity, dilation effect of the combustion, and increase in average velocity of the gas flow in the layer. The above effects are discussed separately in the following paragraphs.

According to Liepman and Laufer (1947), the average rate of growth of a nonreacting free turbulent shear layer (self similar) is linear with respect to the distance from the trailing edge of the layer and evidently independent of viscosity ($\bar{y}$ = const X), while in the laminar case, the growth is proportional to the square root of viscosity ($\bar{y}$ = const $X/\sqrt{Re_x}$). Combustion would decrease the Reynolds number and increase the spreading rate of a laminar shear layer. As this contradicts the present experimental results, it is concluded that viscosity is not a dominant factor controlling the growth of the shear layer in this system.

The effect of density variation on the spreading rate of the free shear layers has been experimentally investigated by Brown and Roshko (1974). They conclude that reducing the density of the lower

velocity side reduces the spreading rate of the layer. This reduction depends on the density and velocity ratios of the two mixing streams. For the case of a density ratio of 1/7 in a half jet (similar to the present experiment), the spreading rate is reduced by close to 30%. Considering the dilation effect of combustion in this sytem, and neglecting the effect of increase in velocity, about a 20% reduction in the spreading rate should be expected, less than what is observed in this experiment. The additional reduction in the spreading rate due to combustion should be attributed to acceleration of products of combustion in the free shear layer in the confined flow of these experiments.

The problem of the growth of a turbulent mixing layer is basically the kinematic problem of the unstable motion induced by vorticity. The growth corresponds to diffusion of vorticity into the free stream and the drive behind this diffusion is the average vorticity of the layer. Because of heat release in the layer, the velocity gradient diminishes more rapidly in a reacting layer than in a nonreacting shear layer, and this results in reduction of the average vorticity in the layer (see Figure 5.2). As a result, on the average the reacting shear layer will spread with a lower rate.

Despite the first impression that flame propagation might increase the visible spread of the shear layer, the results presented here show that the fluid mechanical effects of the heat release (dilation and resulting acceleration) supercede the propagation effect of the flame and reduce the visible growth of the free shear layer behind the step.

3.5 Boundary Layer Effect on Formation of Vortices

In this section, the effect of the upstream step boundary layer on the formation and persistence of vortices in the test section is described. It is suspected that the boundary layer just upstream of the free shear layer may have an effect on the growth of the free shear layer. Batt (1975) has checked the results of Wygnanski and Fiedler (1970) for growth of a nonreacting shear layer. He concluded that tripping the boundary layer upstream of the free shear layer, even if it does not trigger transition to turbulence (which is the case for both above experiments), thickens the boundary layer and thereby increases the spreading rate and turbulent intensity of the free shear layer. Recently, Browand and Latigo (1978) have carried out an experimental study of the effect of the upstream boundary layer on the free shear layer. From their hot wire anemometry results, but without direct visual observation, they conclude that the introduction of small scale turbulence obstructs the large scale interactions in the initial stages of the mixing layer. This results in a lower initial growth rate, but eventually the shear layer relaxes towards the higher growth rate which is observed for a shear layer with a laminar initial layer. By this argument, they conclude that at this stage the important role of the large scale structures is reestablished.

To establish the effect of the upstream boundary layer on the large scale structures in the present reacting and nonreacting shear layers, the boundary layer was tripped by laying a wire on the top of the step as shown in Figure 3.32. Wire sizes and their positions

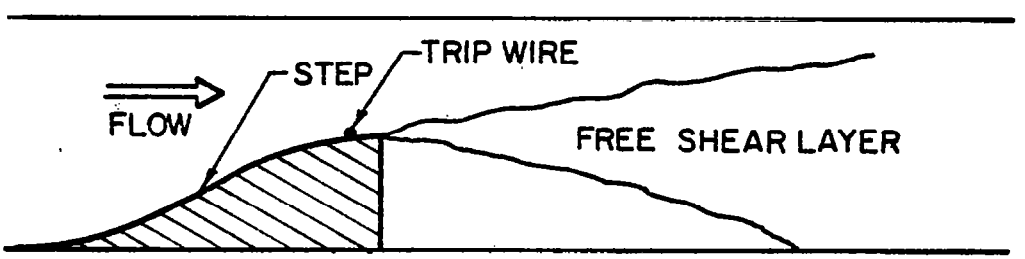

Fig. 3.32 Schematic of the test section with trip wire.

with respect to the edge of the step are shown in Table 3.6. Approximate values for the size of the wire and its position to ensure the transition before the trailing edge can be estimated following

Table 3.6

Wire size and location for boundary layer trip tests.

Case	Wire Diameter (d), mm	Wire Location (ℓ), mm
1	0.5	11
2	0.5	2
3	1.1	11
4	1.1	2

Schlichting (1960). The furthest upstream position of the wire in this experiment was restricted by physical constraints for mounting the wire on the surface of the step. The diameter of both wires was larger than the critical diameter for tripping the boundary layer. Calculations were based on a flat plate and a uniform converging nozzle. The larger wire is close to the value of .93 mm predicted by equation: $\frac{Ud}{V} > 900$ for full effectiveness of the trip wire, Schlichting (1960). The distance $x_{tr} - x_w$ downstream of the wire derived from $\frac{u(x_{tr} - x_w)}{\nu} = 2 \times 10^4$ ensures the transition to turbulence in the boundary layer. In the above two equations, u is the free stream velocity, d, the diameter of the wire, x_{tr} and x_w, the

transitional distance and wire distance from the leading edge, and ν is the viscosity of the fluid. The above equations are all empirical relations for flat plates, but they were used to test the conditions in this experiment. The upper bound of the transitional distance to turbulence predicted by the above equation for 13.5 m/sec reference velocity is 2.1 cm. The boundary layer thickness at the edge of the step, based on the flat plate and uniformly converging nozzle for reference velocity of 13.5 m/sec, is 2 mm and 1.2 mm respectively. Based on the above explanations, it is predicted that the 0.5 mm wire will just disturb the boundary layer without any serious change in the layer the 1.1 mm wire at 11 mm upstream will trip the boundary layer in the sense that it causes transition to turbulence in the boundary layer.

Schlieren movies of reacting and nonreacting flow fields in the test section with the various trip wires of Table 3.6 were taken. Figure 3.33 shows two series of still pictures from two schlieren movies of the flame with 0.5 mm boundary layer trips. Figure 3.33.a shows the flow field with a 0.5 mm wire trip located 11 mm upstream of the edge while in Figure 3.33.b, the trip wire is located 2 mm upstream. The entrance conditions, except for the laminar boundary layer upstream of the edge of the step, are the same as in Figure 3.8, that is, reference velocity of 13.6 m/sec, equivalence ratio of 0.57, and inlet temperature of 295 K. It is evident that the basic features of large scale structures remain unchanged. In both cases, large scale vortices clearly dominate the reaction zone. In Figure 3.33.a, the eddies almost lose their identity far downstream in the test

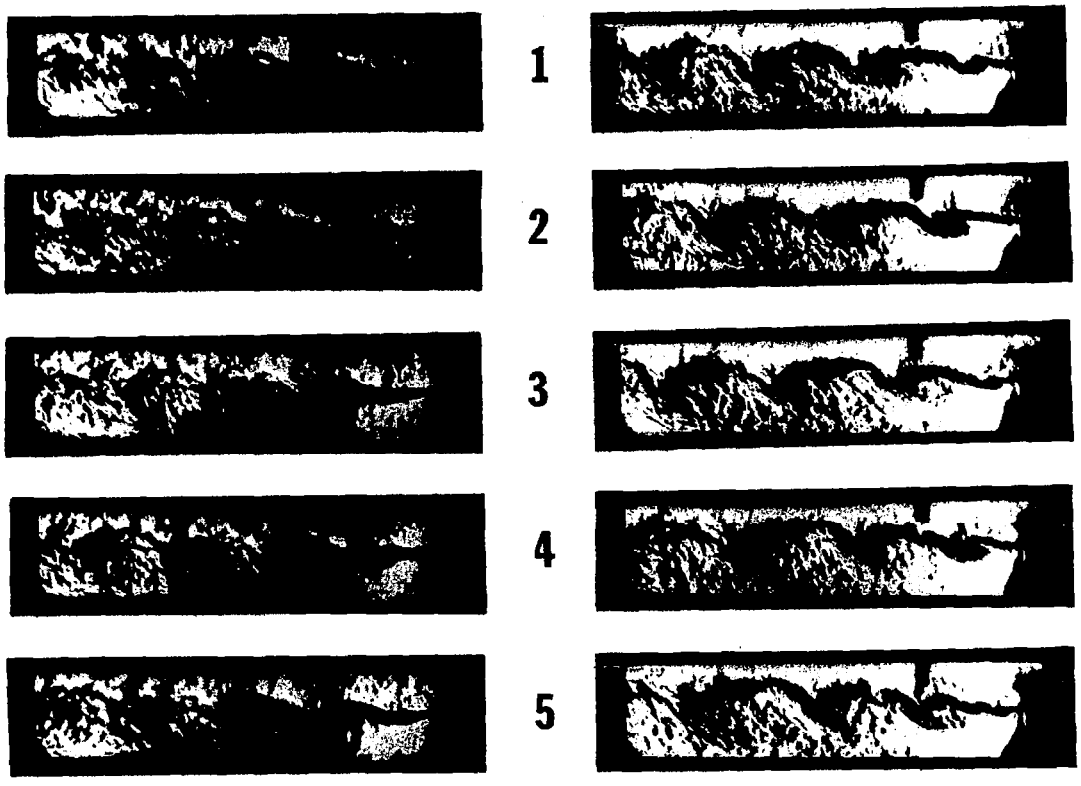

Fig. 3.33 Sequential series of frames from high speed schlieren movies of the flame with tripped upstream boundary layers. V_o = 13.6 m/sec, N_{Re} = 8800 cm^{-1}, ϕ = 0.57, T_o = 295 K.

(a) 0.5 mm trip wire located 11 mm upstream of the edge. Time interval between frames is 1.6 mm.

(b) 0.5 mm trip wire located 2 mm upstream of the edge. Time interval between frames is 1.8 msec.

section, while in Figure 3.33.b, the eddies clearly retain their identity all the way through the test section. Figure 3.34 shows the effect of 1.1 mm trip wire on the flow field inside the test section. Figure 3.34.a (trip wire 11 mm upstream of step edges) shows almost no organized structures in the layer, while in Figure 3.34b (trip wire 2 mm upstream of the step edge), the large coherent structures are clearly formed in the form of distinct vortices and preserve their identity all the way through the test section. Comparison of these figures shows the effect of the position of the trip wire. As was described before, it is believed that the boundary layer has become turbulent in the case of Figure 3.34.a (1.1 mm trip wire, 11 mm upstream of the edge), while in the other three cases the wire is buried in the laminar boundary layer and just acts as a distrubance to the layer. Figure 3.34.a shows that the large scale structures are not completely absent from the flow, but regular and identifiable structures with distinct braids and eyes (as Corcos and Sherman (1975) call them) are definitely not very visible. Close examination of the schlieren movies corresponding to Figure 3.34.a reveals that the appearance of large eddies are more frequent far downstream in the combustor rather than close to the edge of the step. The recirculation zone seems to be lengthened in this case. An increased graininess in the schlieren records suggests a higher level of mixedness and a smaller scale turbulence in the flow.

In the three cases in which the layer is dominated by large scale structures, compared to the untripped case of Figure 3.8, the initial

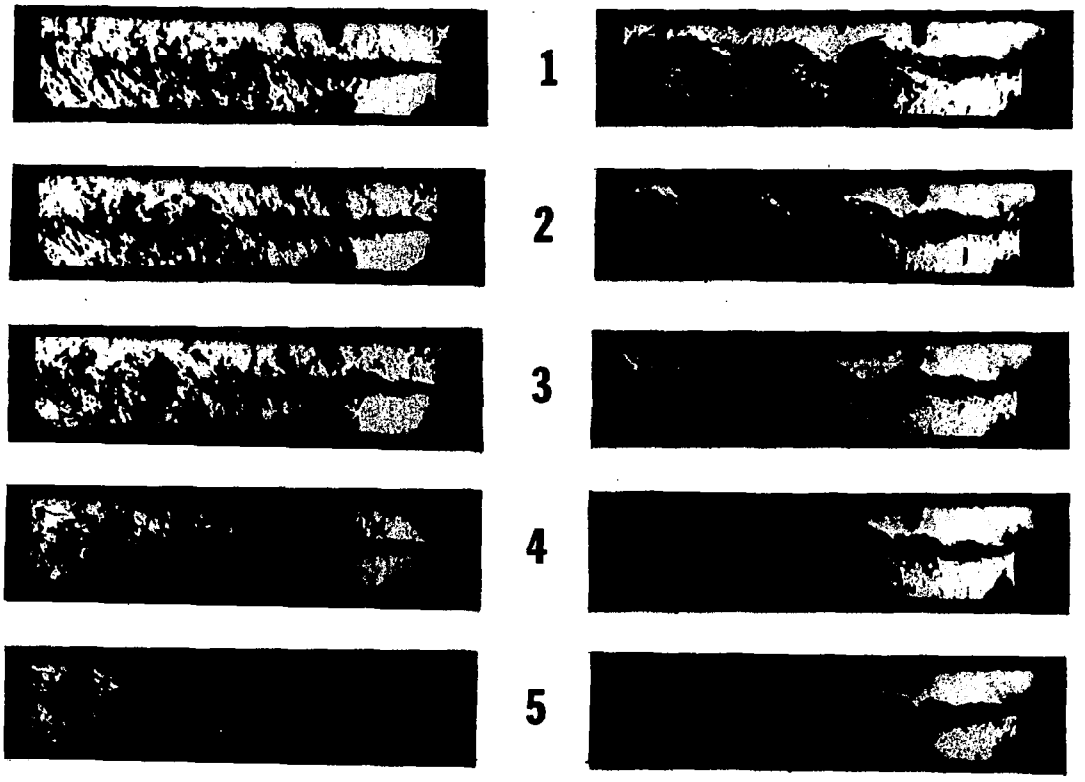

Fig. 3.34 Sequential series of frames form high speed schlieren movies of the flame with a tripped upstream boundary layer. V_o = 13.6 m/sec, N_{Re} = 8800 cm^{-1}, ϕ = 0.57, T_o = 295 °K.

(a) 1.1 mm trip wire located 11 mm upstream of the edge. Time interval between frames is 1.46 msec.

(b) 1.1 mm trip wire located 2 mm upstream of the edge. Time interval between frames is 1.32 msec.

layer has a higher growth rate, the eddies are further separated (large eddy distances) and there is more distinct small scale turbulence inside the large vortices. Finally, the reaction fronts on the edge of the eddies are thicker and clearer. The coalescence of vortices was clearly observed in all of the above three cases. In similar nonreacting flows, the same trends explained above were observed. The results of these experiments explain the difference between the observations of Brown and Roshko (1974) and the conclusions of Browand and Latigo (1978).

Brown and Roshko (1974) observed that placing wire trips just upstream of the trailing edge of the splitter did not disrupt the visible large structures a few boundary-layer thicknesses downstream, while Browand and Latigo (1978) placed the wire trips further upstream to insure transition in the layer and concluded that the effect of the trips was to obstruct the interaction of large scale structures in the early stages of the formation of the mixing layer. From the observations in our experiments, it is concluded that formation and interaction of eddies and the resulting shear layer growth depends on the size and location of the disturbances in the upstream boundary layer.

Analysis of the schlieren movies for average eddy formation, position and period is shown in Tables 3.7 and 3.8. Upstream disturbance of the boundary layer delays the formation of the vortices in the layer. This is due to the thickening of the initial vorticity layer which makes it less susceptible to flow disturbances.

Table 3.7

Position of eddy formation for laminar and tripped upstream boundary layers. V_o = 13.6 m/sec, N_{Re} = 8800 cm^{-1}, ϕ = 0.57, T_o = 295 K.

Wire Size (d), mm	Wire Location (ℓ), mm	$\overline{X}_o$ (cm)
0.0	-	1.3
0.5	11	2.6
0.5	2	2.7
1.1	2	2.2

Table 3.8

Period of eddy formation for laminar and tripped upstream boundary layers. V_o = 13.6 m/sec, N_{Re} = 8800 cm^{-1}, ϕ = 0.57, T_o = 295 K.

Wire Size (d), mm	Wire Location (ℓ), mm	$\overline{\tau}$ (msec)
0.0	-	1.7
0.5	11	3.45
0.5	2	3.05
1.1	2	2.71

From the results of the experiment described in this section, it is concluded that large coherent structures can form and play the major role in the development of the free shear layer if the initial layer is laminar, otherwise, the formation and interaction of the large coherent structures in not observed.

CHAPTER 4

STABILITY OF THE FLAME

Stability is certain to be a major problem for lean premixed prevaporized combustors. The two extremes of stability of a premixed flame are blowout and flashback. Blowout is the extinction of the flame due to failure of self ignition of the reaction zone. Some investigators have also observed that in blowout the flame fails to propagate into the reactants, but a residual flame remains in the recirculation zone. Flashback in the present context is upstream propagation of the flame into the premixing section of the combustor. These two limits of stability for the present burner, transition from stable combustion to these limits, and the effect of tripping the upstream boundary layer from laminar to turbulent flow are discussed in the following sections of this chapter.

4.1 Blowout Limit and Blowout Process

In this system blowout could be produced by reducing the equivalence ratio while maintaining the reference velocity nearly constant or by increasing the reference velocity while maintaining the equivalence ratio constant. For operational convenience the first procedure was adopted. The blowout limit was determined by keeping the air flow rate constant and reducing the fuel flow rate, that is, leaning the mixture, until the flame blew out. It was found that the rate of reduction of the fuel flow rate had some effect on the observed limit so that a slow reduction was required to obtain reproduceable results.

Blowout limits of the flame for two values of reactant temperature are shown in Figure 4.1. The data points in this figure are the average of at least five measurements. Increasing the incoming reactant temperature shifts the lean blowout limit toward lower equivalence ratios. That is, increasing reactant temperature improves the lean stability of the combustor.

The blowout in laminar flames is controlled by the laminar flame speed and the velocity gradient at the rim of a burner. The stability of turbulent flames is controlled by turbulent heat and mass exchange between the fresh reactants and the ignition source which can be a pilot flame, or, more often, a recirculation zone. It is the mechanism of this exchange process which has been a contraversial subject for over two decades. The limits and mechanism of blowout have been experimentally investigated in great detail, see for example: Nicholson and Field (1949), Williams, et al. (1949), Wright and Zukoski (1962), and Ballal and Lefebvre (1978). Although some empirical relations describe the experimental blowout data fairly accurately, Zukoski and Marble (1955), Ballal and Lefebvre (1978), Plee and Mellor (1978a), more fundamental approaches to the problem have always been of interest. It is an accepted model that flame stabilization involved a competition between fluid mechanical and chemical processes. There have been efforts to separate these two effects and thereby to obtain a correlation that explains the observed experimental data.

Zukoski and Marble (1955) proposed a minimum ignition delay time, τ_m, defined by $\tau_m \sim L/V_{B.O.}$, where L is the length of the recirculation zone and $V_{B.O.}$ is the reference velocity at blowout conditions. In their model L is fluid dynamically controlled and τ_m depends only on

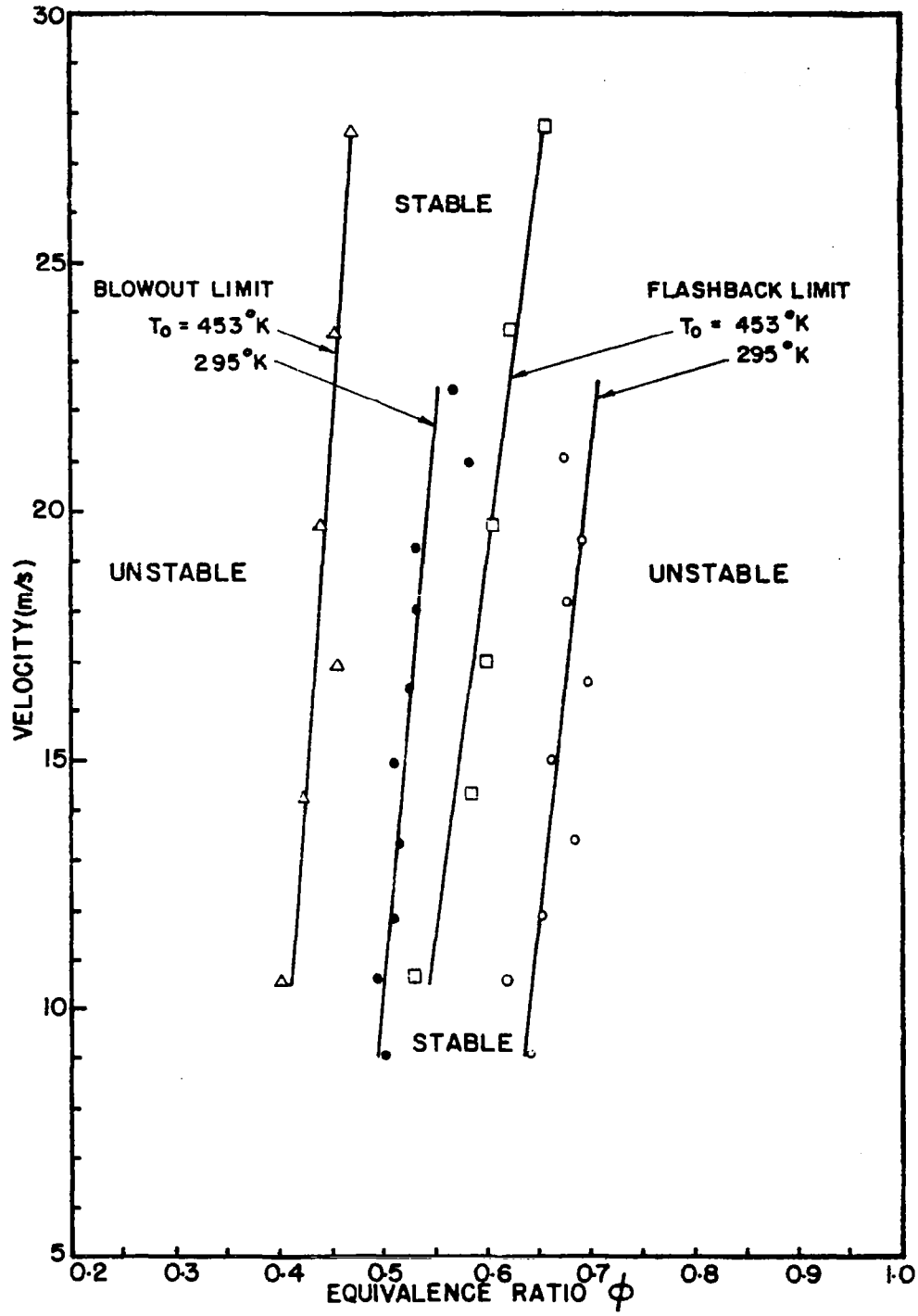

Fig. 4.1 Stability limits of the flame for two values of initial temperature.

chemical rate process which are determined primarily by equivalence ratio and temperature. This model is considered too simple to be applied to a flow which is highly intermittent.

A refinement of the Zukoski and Marble model has been introduced by Plee and Mellor (1978a). They assume the correlation of a mixing time ($\tau_m = \frac{D}{V}$, where D and V are characteristic length and velocity in the combustor) with a characteristic homogeneous chemical reaction time ($\tau_r \sim \frac{T}{T_0} \frac{e^{E/RT}}{\phi}$, where T, T_0, E, R and ϕ are adiabatic flame temperature, reactants temperature, activation energy, universal gas constant and equivalence ratio respectively). They present a correlation of τ_m and τ_r for experimental data of Ballal and Lefebvre (1978) for stability of a premixed propane/air flame stabilized behind a cone as $\tau_m = 2.11\ \tau_r - 0.46$. In terms of the variables in the present combustor, this equation translates into

$$\phi_{B.O.} = \frac{2.11 \times 10^{-4} \frac{T}{T_{in}} \exp\ (21000/RT)}{D/V + .46} \qquad (4.1)$$

where R, T, D and V are universal gas constant in $\frac{Cal}{mole\ K}$, adiabatic flame temperature K, height of the entrance to the test section in m and reference velocity in m/sec. In Figure 4.2 this correlation is compared with the experimental data of the present experiment.

Ballal and Lefebvre (1978) used a different and more fundamental approach to correlate their experimental data. Based on global rate of reaction for hydrocarbons from the stirred reactor experiments of Longwell and Weiss (1955), they derived an expression for reaction rate as a function of the fraction of burned fuel, with the equivalence ratio as a parameter. They assumed that the maximum of reaction rate

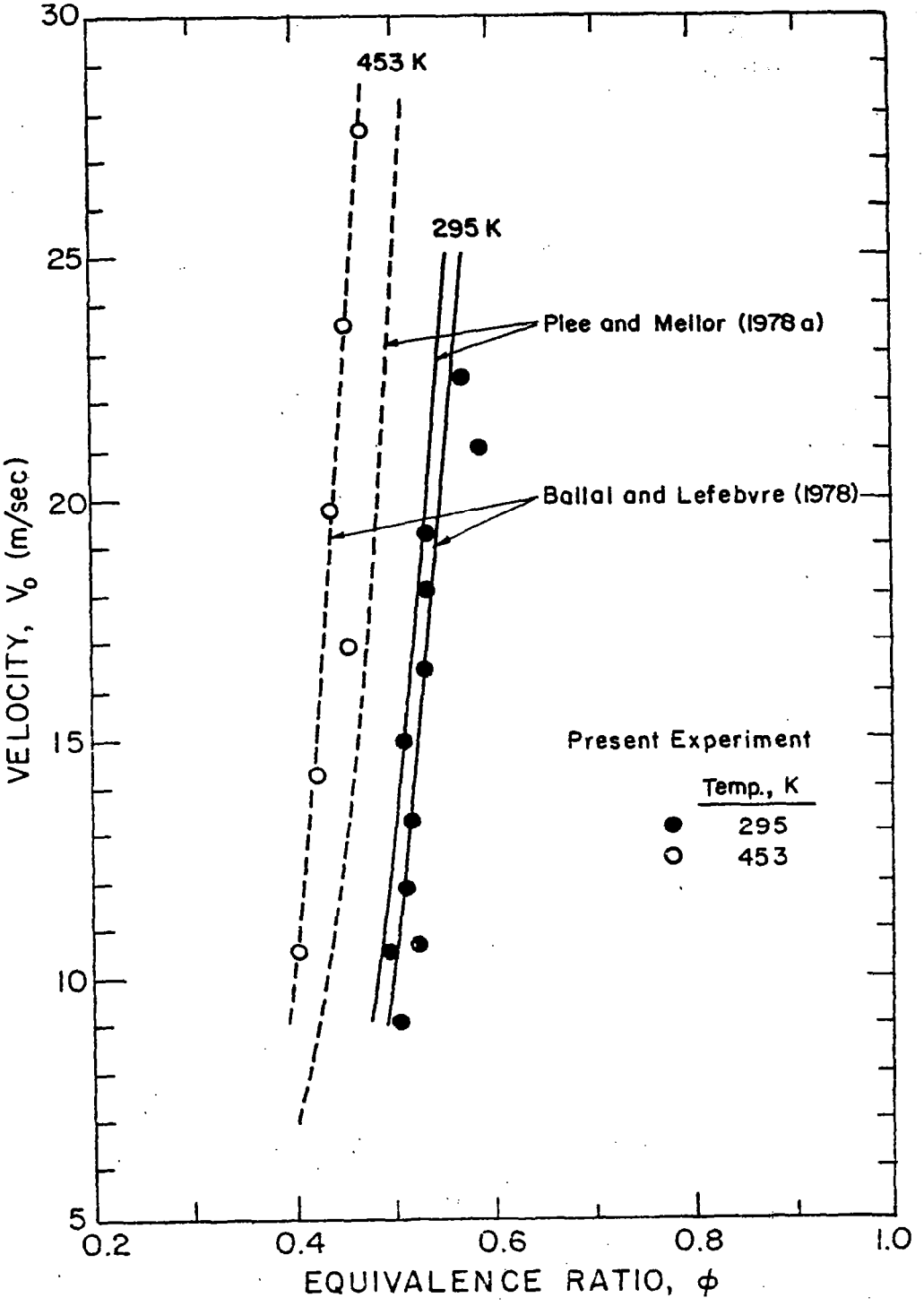

Fig. 4.2 Comparison of the lean blowout limits of the present flame with those of Ballal and Lefebvre (1978) and Plee and Mellor (1978a).

with respect to the fraction of burned fuel corresponds to the maximum air flow rate the combustion zone can tolerate before extinction. Finally they concluded that the variation of this maximum air flow rate with equivalence ratio corresponds to the blowout limit of a lean premixed prevaporized combustor. They incorporated the entrance flow turbulent intensity by modifying the reference velocity using the fact that increase in entrance flow turbulence adversely affects the stability of the flame. Their final result is in the form of:

$$\phi_{B.O.} = \left[\frac{2.25\ (1 + 0.4\ V\ [1 + 0.1\ Tu])}{p^{0.25}\ T_0\ \exp\ (T_0/150)\ D\ (1-B)}\right] \qquad (4.2)$$

where V, Tu, P, T_0, D and B are mainstream velocity, percent turbulent intensity, reactant pressure and temperature, characteristic flame holder dimension and flame holder blockage. To compare this correlation with the present experimental data, $\frac{V}{1-B}$ was assumed to be the reference velocity and D the step height. The results are shown in Figure 4.2. The present data are in surprisingly good agreement with the Ballal and Lefebvre (1978) proposed empirical correlation of their experimental data. The Plee and Mellor (1978a) model of the Ballal and Lefebvre data provides a poorer agreement with the present experiment, especially at high temperature.

The present experiments suggest that the chemical and physical processes controlling blowout are complex and not adequately described by a two parameter model based on a single reaction and residence times. In these vortex dominated flows the mixing of reactants and products occurs through a process of engulfment and coalescence of eddies and, to a less extent, through eddy nibbling. Thus flame propagation must happen

on the contact surfaces of the entrained layers of reactants and products. Flame speed will depend on the level of small scale turbulence (diffusion) in these layers. As the equivalence ratio is reduced at constant entrance velocity, the rate of reaction is reduced and, consequently, more entrainment occurs before reaction. Movement of eddies downstream and their vortical motion result in higher levels of reactant species in the downstream eddies. It is postulated that the increased entrainment of cold reactants quenches the reaction fronts in the downstream eddies. The feedback of this effect through the recirculation zone causes the quenching to propagate upstream towards the flame holder.

In the course of the present experiments it was attempted to observe the blowout process with the objective of investigating the interaction between large eddy structures and the process of blowout. Several schlieren movies of the transient process of blowout were taken. A sequence of stills of one of these movies is shown in Figure 4.3. This series covers the transition from a normal flame to a totally nonreacting mixing layer behind the step. It can be seen that the process of blowout appears to be a gradual process with no abrupt change observable between the reacting and nonreacting states. What can be deduced from Figure 4.3 is that the schlieren effect fades first downstream and than propagates upstream. The extinction time appears to be an order of magnitude larger than the main flow passage time which is consistent with a process which first occurs downstream and gradually propagates upstream as the temperature in the recirculation zone falls.

This view is also shared by Nicholson and Field (1949), Fillippi and Fabbrovich (1962) and Williams and Shipman (1953). Demotakis and Brown (1975) have also shown that the mixing layer dynamics at any

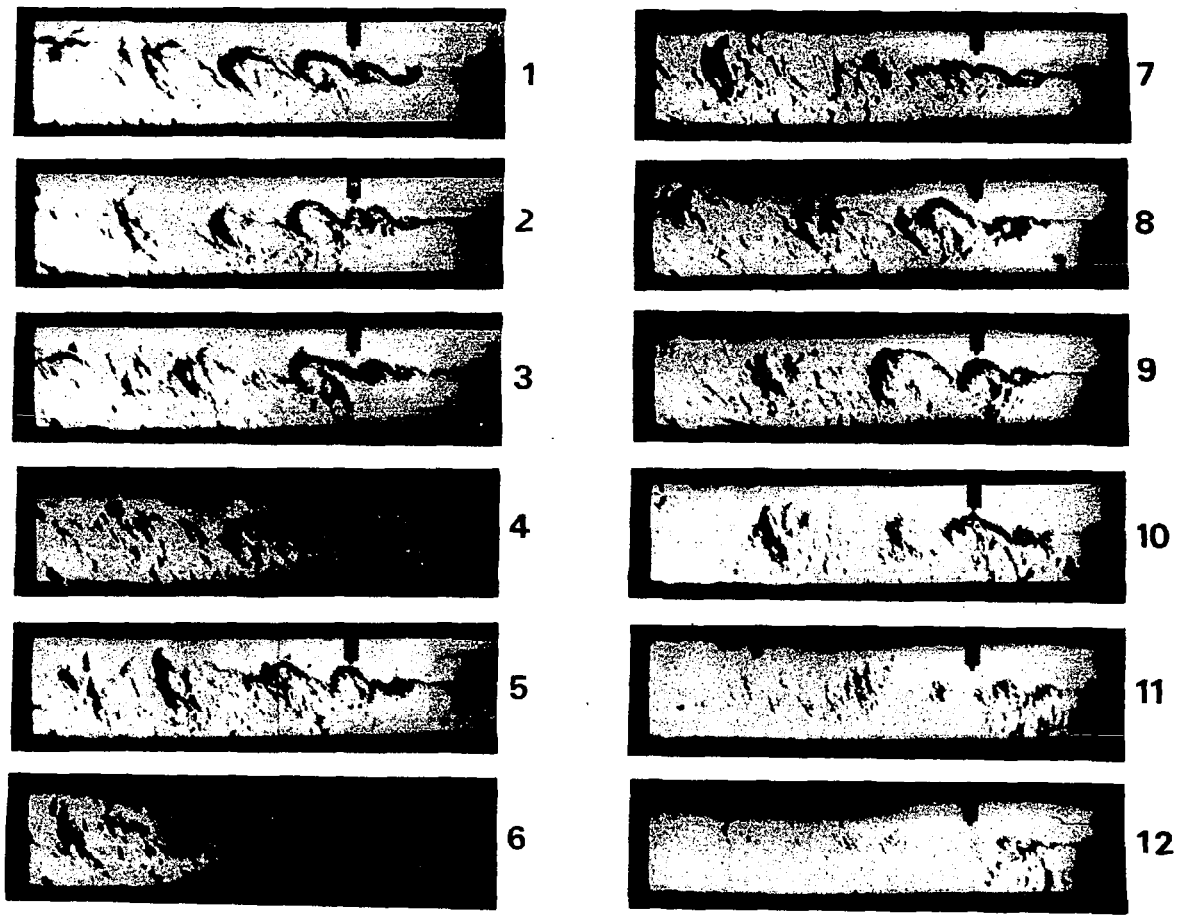

Fig. 4.3 Sequential series of frames from a high speed schlieren movie of the transition to blowout of the flame. The time interval between the frames is 24 msec. V_o = 9.2 m/sec, N_{Re} = 5950 cm^{-1}, T_o = 295 K.

point is coupled to the large structures further downstream. As was discussed in the previous chapter, Konrad (1976) has shown that breakdown of Taylor vortices formed in the large scale structures results in increasing the entrainment rate into the layer. These phenomena might be partly responsible for the start of the blowout from a downstream location in the shear layer.

Stability data were taken when the combustor had reached steady state conditions, i.e. the step was at its equilibrium conditions. No attempt was made to find the effect of step temperature on the stability of the flame. It is known that at high velocities, increase in flame holder temperature improves the stability of the flame, Russi, et al. (1953), while the improvement in stability depends on the characteristic dimension of the flame holder, being insignificant in some cases, Williams and Shipman (1953). In dealing with the effect of flame holder temperature on stability of the flames, two different aspects, namely heating the upstream boundary layer and heat transfer from the recirculation zone to the stabilizer should be considered. Russi, et al. (1953) explain their results in terms of the second mechanism rather than the boundary layer heating. As a result of addition of heat to the stabilizing cylinder, the temperature of burned gases in the recirculation zone increases, and subsequently the flame can withhold higher flow velocities (higher heat and mass transfer) for a given equivalence ratio. In extended flame holders such as the present in which the boundary layer upstream of the flame has a long history of contact with the flame holder surface, the first mechanism might seem to be important. As was discussed previously, the blowout in bluff body stabilized premixed flames is believed to be a phenomenon associated with the

turbulent reacting/mixing layer downstream of the flame holder, rather than being controlled by the initial contact layer that is influenced by the boundary layer upstream of the recirculation zone. If the argument holds to be true, then the effect of preheating the boundary layer should not be significant while heat transfer from the recirculation zone will dominate because the recirculation zone combustion products are the ignition source for the bulk of the flow in the shear layer. Table 4.1 shows temperature measurements inside the boundary layer 1 mm downstream of the edge of the step. Any increase in boundary layer temperature due to heat transfer from the step will have little effect on the preheating of the bulk of the flow but may still affect flow stability. Unfortunately boundary layer heating through step heat transfer was not controlled in our experiments.

Table 4.1

Temperature measurements in the boundary layer 1 mm from the edge of the step. V_o = 13.3 m/sec, ϕ = .56, T_o = 295 K.

Vertical Distance from the Step (mm)	0	.8	1.6	3.2
Temperature K	638	418	366	302

At high inlet temperatures, cooling of the flame holder has been used to prevent flashback and also damage to the flame holder, see for example Roffe and Venkataramani (1978).

4.2 Flashback Limit and Flashback Process

Flashback in the classical sense is propagation of the flame front into the premixing section in the boundary layer, Lewis and Von Elbe (1961). This propagation against the gas stream occurs when the gas velocity at some point, usually in the boundary layer, becomes smaller than the burning velocity. Plee and Mellor (1978b) have reviewed the subject of flashback in premixed prevaporized combustors in detail. They conclude that to date classical flashback has not been observed in noncatalytic, premixed, gas turbine-type combustors burning liquid fuels or propane. Instead, they propose that upstream combustion resulting from autoignition, flame propagation through reverse flow fields, or preignition of the separated reactant flow is responsible for the so-called flashback observed in these systems.

A different type of upstream flame propagation and burning is reported here. Flashback is taken to be the transient condition of the system which leads to an oscillatory mode of operation of the combustor which will be called "chugging." "Chugging" is a combustion instability common for liquid rocket motors. The underlying cause of this instability is a delay between injection and propellant combustion, which can lead to a coupling between combustion and propellant fuel injection, Barrère and Williams (1969). Although the phenomenon to be discussed is quite different from chugging in liquid rocket motors, it has been suggested that the above term seems appropriate, Oppenheim (1979). Since the phenomenon to be discussed is an upstream flame propagation, it is "flashback," although not the classical flashback described by Lewis and Von Elbe (1961).

In this system flashback conditions could be obtained by increasing

the equivalence ratio (maintaining the reference velocity and inlet temperature constant), by reducing the reference velocity (maintaining the equivalence ratio and inlet temperature constant), or by increasing the inlet temperature (maintaining the equivalence ratio and reference velocity constant). For ease of operation and reproducibility, the first procedure was adopted in these experiments. By increasing the fuel flow rate while holding the air flow rate constant, it was possible to get the flame to propagate into the flow upstream of the edge of the step. The ceramic flow straightener was effective in preventing the flame from propagating into the premixing chamber (see Figure 2.2). The flashback limits of this combustor for two values of inlet temperature are shown in the stability map of Figure 4.1. Increasing the reference velocity shifts the flashback to higher equivalence ratios. Increasing the inlet temperature moves the flashback limit to lower equivalence ratios (leaner mixtures).

Figure 4.4 shows a sequence of prints from a high speed schlieren movie of a flashback. The process begins with a vertical oscillation of the shear layer at the edge of the step which leads to increased coalescence of eddies and transport of the resulting large eddy into the recirculation zone. The eddy thus formed overexpands as it moves downstream and in turn augments the entrainment of reactants into the recirculation zone behind the step. This, in turn, is postulated to cause the lifting of the flame from the edge of the step and a subsequent increase in eddy growth. This process repeats until pressure pulsations occur which are sufficient to stagnate or possibly reverse the flow into the combustor, allowing the flame to move into the inlet section upstream of the step. After the flame moves into the throat of

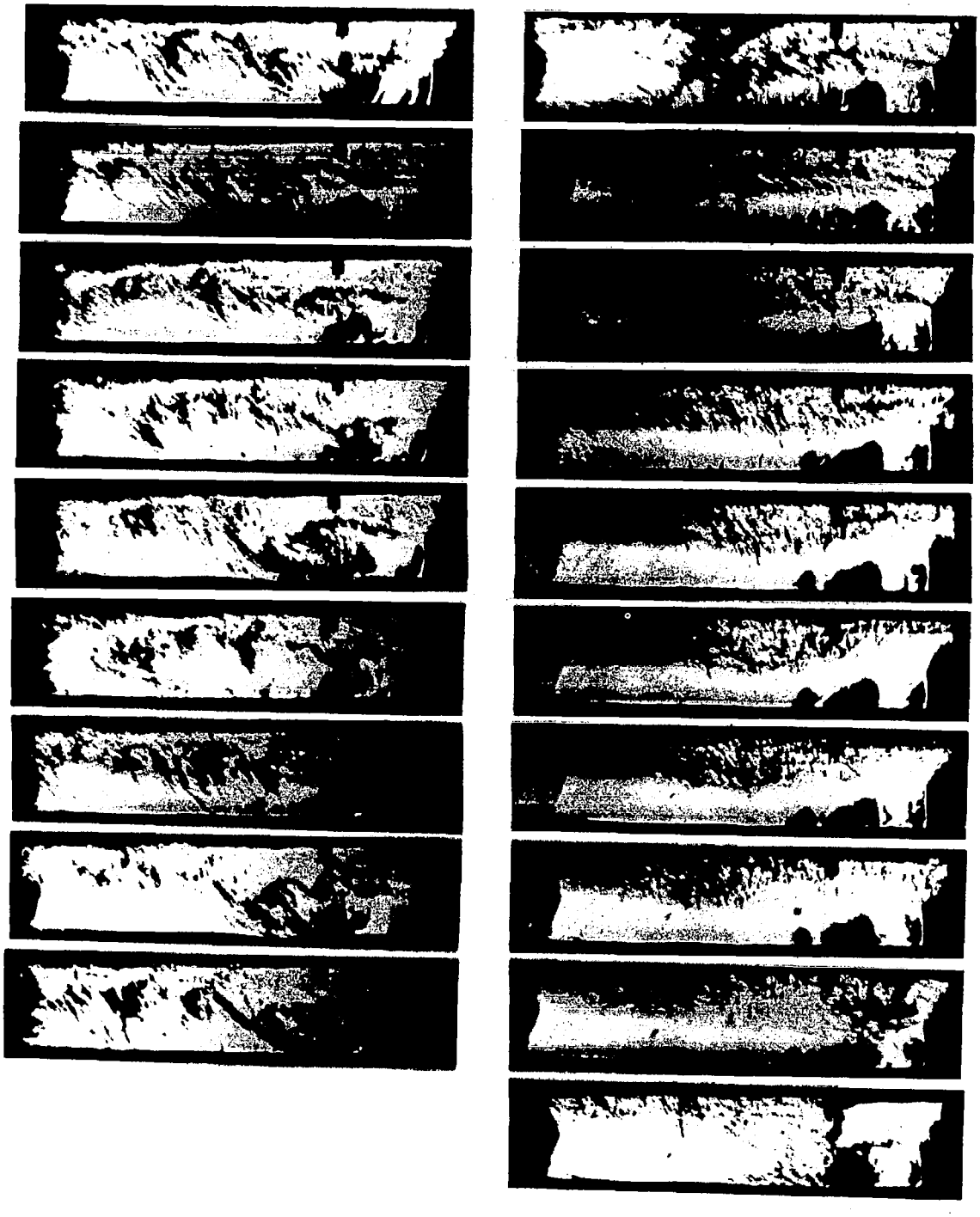

Fig. 4.4 Sequential series of frames from a high speed schlieren movie of the flashback of the flame. The time interval between the frames is 6.6 msec. V_o = 13.2 m/sec, N_{Re} = 8530 cm^{-1}, ϕ = 0.57 to 0.68, T_o = 295 K.

the combustor (see Figure 2.2), it cannot pass through the honeycomb flow straightener and also there is no means of stabilization for the flame, so it is blown downstream. It is after this first disgorging of the flame from the throat that the chugging starts. Figure 4.5 shows a sequence of prints from a highspeed schlieren movie of this chugging process which is a continuation of the previous figure. Chugging involves the periodic propagation of the flame into the region upstream of the edge of the step, disgorging of the flame from the throat followed by unreacted mixture, formation of a single large vortex behind the step which fills the entire combustor, convective propagation of the flame through the recirculation zone and once again upstream. The period at which this occurs is approximately 20 msec as observed from the motion pictures and corresponds to the flow time through the combustor test section. A variable reluctance pressure transducer mounted midway on the side of the test section measured pressure oscillations at this same frequency, Figure 4.6. The pressure oscillations are much higher than the dynamic pressure of the flow at the step, indicating that the flame may not simply propagate upstream but may be convected upstream by a flow reversal. This is also consistent with the discrepancy between an estimated flame velocity of certainly less than 1 m/sec and the average incoming flow of 13.2 m/sec. The chugging mode of operation appears to the eye to be a steady attachment of the flame at some location upstream of the step, while in reality, as it is shown in Figure 4.5, this is not the case at all. Operation of the combustor at an intermediate state, between the normal and chugging conditions, was possible for some high reference velocities. At this intermediate stage the flame would oscillate on the edge of

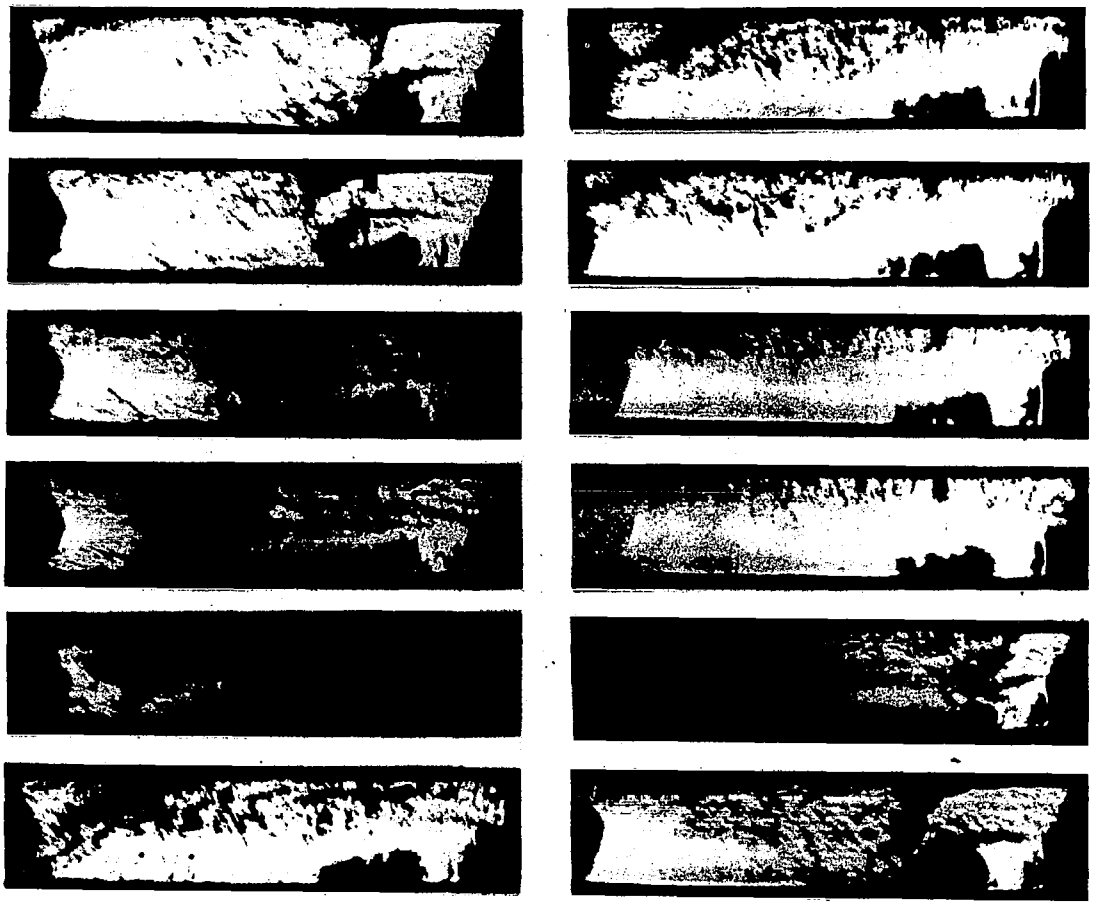

Fig. 4.5 Sequential series of frames from a high speed schlieren movie of the chugging mode of the flame. Time interval between the frames is 1.6 msec. V_o = 13.2 m/sec, N_{Re} = 8530 cm^{-1}, ϕ = 0.68, T_o = 295 K.

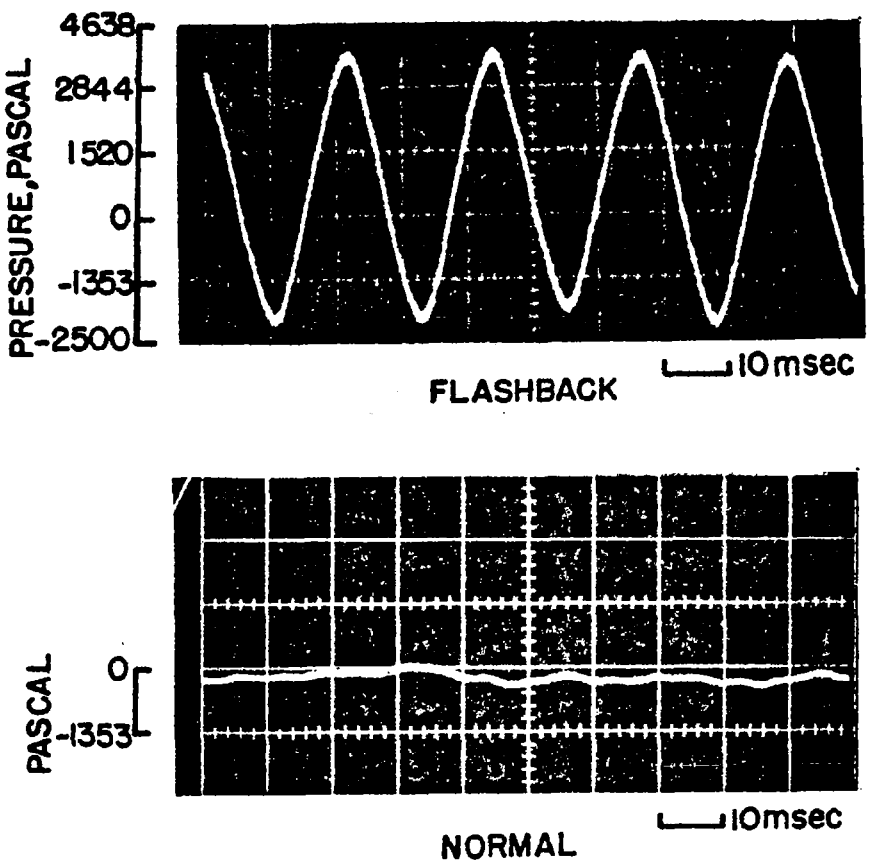

Fig. 4.6 Traces of the pressure inside the combustor at the chugging mode (V_o = 13.2 m/sec, N_{Re} = 8530 cm^{-1}, ϕ = 0.63, T_o = 295 K) and the normal mode (V_o = 13.2 m/sec, N_{Re} = 8530 cm^{-1}, ϕ = 0.63, T_o = 295 K).

the step in the vertical direction, but would not propagate upstream of the edge. This oscillatory mode of operation of the burner is attributed to the pressure pulsations which are not strong enough to allow flame propagation into the premixing section. The mechanism of flashback discussed in this section was observed for the whole range of velocities and temperatures of our experiment. The details of the flashback mechanism and the chugging phenomena described above remain to be investigated the present study reveals a new mechanism of upstream flame propagation in this type of flow system. While the type of flashback (transition from steady to chugging combustion) observed may be peculiar to this experimental apparatus, it would seem prudent to look for similar processes in other premixed combustors.

4.3 Effect of Upstream Boundary Layer Trips on Blowout and Flashback Limits

It was suspected that tripping the boundary layer might alter the stability characteristics of the combustor. Following the procedures outlined in the first section of this chapter, blowout and flashback limits of the burner with a trip wire in the upstream boundary layer were determined. The results, including stability data for the combustor without the boundary layer trip, are shown in Figure 4.7. There appear to be two major differences between the stability limits of flames with and without trip wires in the upstream boundary layer.

The first is the shift of the lean blowout limit to higher equivalence ratios. At constant reference velocity this shift seems to be as high as 8%. All the trip wires appear to have a similar effect on the lean stability limit with the size and location of the trip wire

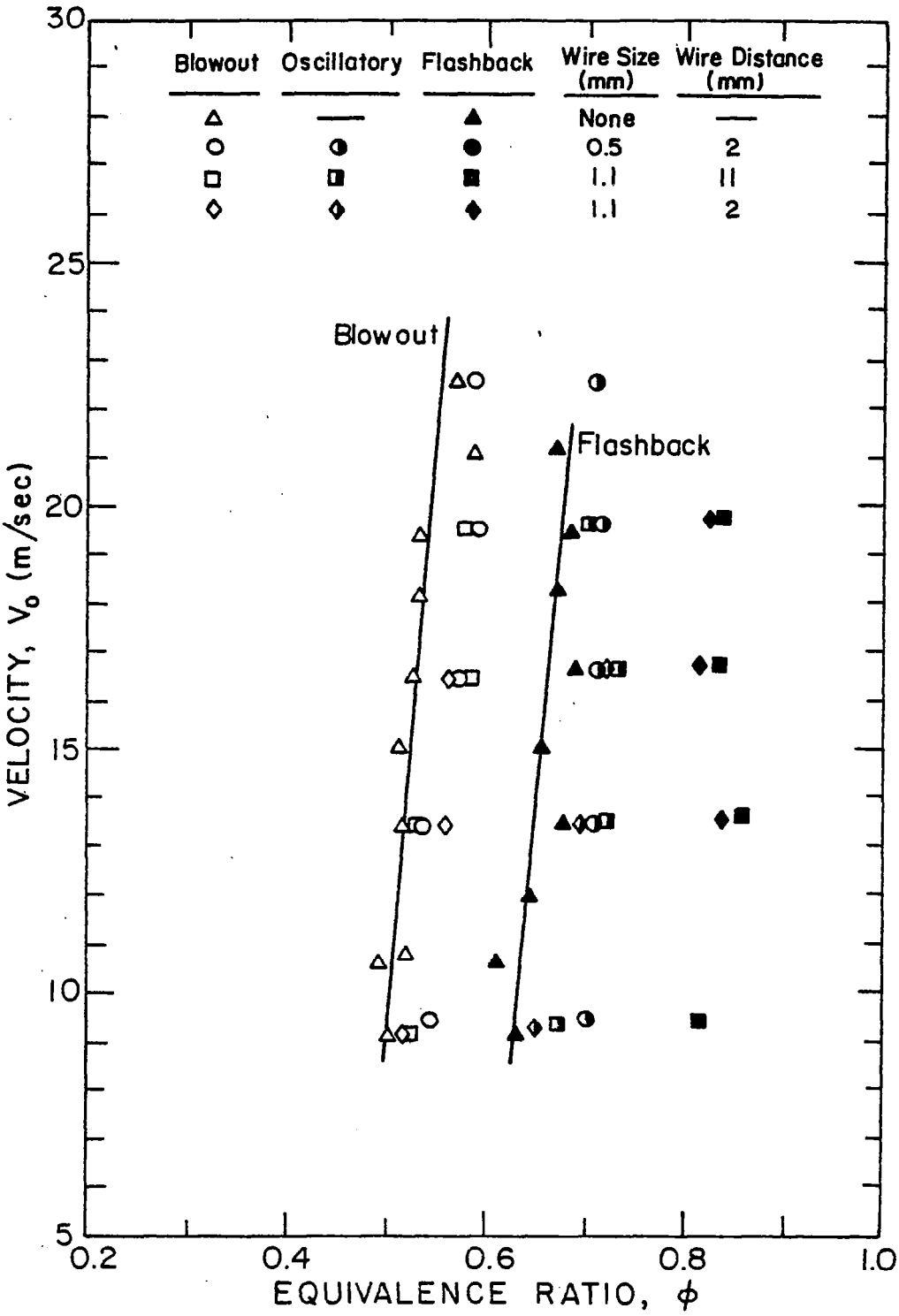

Fig. 4.7 Stability limits of the flame with and without upstream boundary layer trips. T_o = 295 K.

apparently not playing a major role. It has been known that the initial zone of contact between the free stream and recirculation zone has considerable effect on the stability of the turbulent flames. Williams, et al. (1957) showed that the suction of the boundary layer upstream of the edge of a half ellipse bluff body stabilizer shifted the lean blowout limit to higher equivalence ratios.

According to the discussion of Section 3.5, the effect of a trip wire on the large scale structures in the free shear layer depends on the size and location of the wire. It was also pointed out that, depending on the location of the trip wire, the growth rate can be higher, Batt (1975), or lower (at least in the initial stages of the development of the layer, Browand and Latigo (1978), than the case without trip wire in the upstream laminar boundary layer. But Figure 4.7 shows that all trip wires have a similar effect on the blowout limit.

In all the above cases the initial layer probably has a higher free stream turbulent intensity which results in the shift of the lean blowout limit to richer mixtures. This is consistent with the observations of Ballal and Lefebvre (1978). In the cases where transition to turbulence does not occur in the boundary layer, according to Batt (1975), the mixing layer still has a higher spreading rate, implying that the downstream entrainment rate is higher. This phenomenon might in turn destabilize the combustion at near blowout conditions. So it seems that effect of trip wires on the initial layer and resulting downstream entrainment of reactants into the hsear layer serve to destabilize the flame near the blowout limit. Effects of trips on the structure of the turbulent shear layers is not completely

understood. Full explanation of the effect of tripping the upstream boundary layer on lean blowout limits of burners such as the present one depends on further understanding of the tripping phenomenon.

The other effect of tripping the upstream boundary layer is on the flashback limit which is more pronounced than its effect on the lean blowout limit. Apparently, the trip wires shift the flashback (transition to chugging) to much higher equivalence ratios (up to 30%) while creating a wide region of oscillatory mode of burning (transition between normal mode of operation and chugging). This region could not be identified as clearly in the case of nontripped boundary layer flames. Again, like the blowout case, the trip wires seem to have a consistent effect on shifting the flashback limit to higher equivalence ratios, with no evident effect of wire size or location on this limit (for the few data points available). Fundamental understanding of this type of flashback and the upstream boundary layer effects on it awaits further investigation of the subject. It is suspected that the delay of gross mass entrainment into the recirculation zone delays the overgrowth of the large eddies in the recirculation zone, and as a result, widens the oscillatory mode of combustion in the burner.

CHAPTER 5

PROBE MEASUREMENT RESULTS

In extracting a representative sample of species from a point in a reacting flow, it is important to minimize flow disturbances (chemical, thermal, and fluid mechanical) due to the presence of the probe. To reduce the fluid mechanical disturbances, the probe was chosen to be as small as possible. It was inserted from the bottom of the test section, so that the stabilizing effect of the probe was negligible. The uncooled inserted section of the probe and its small surface area minimizes the heat transfer to the probe. To check the effect of the probe on the large structures, schlieren movies of the flow with the probe inside the test section were taken. Figure 5.1 shows the motion of vortices past a sampling probe with two different probe insertion lengths. The probe does not have any visible effect on the structure of the vortices in the test section.

Results of time averaged but space resolved velocity, temperature, and gas composition measurements inside the test section are reported in this chapter. After preliminary measurements of the velocity by the pitot-static probe, measurements by the method of laser doppler velocimetry (LDV) became available, Houser (1979). In the first section of this chapter, LDV velocity measurements in reacting and nonreacting flow fields are reported. Results of thermocouple measurement of

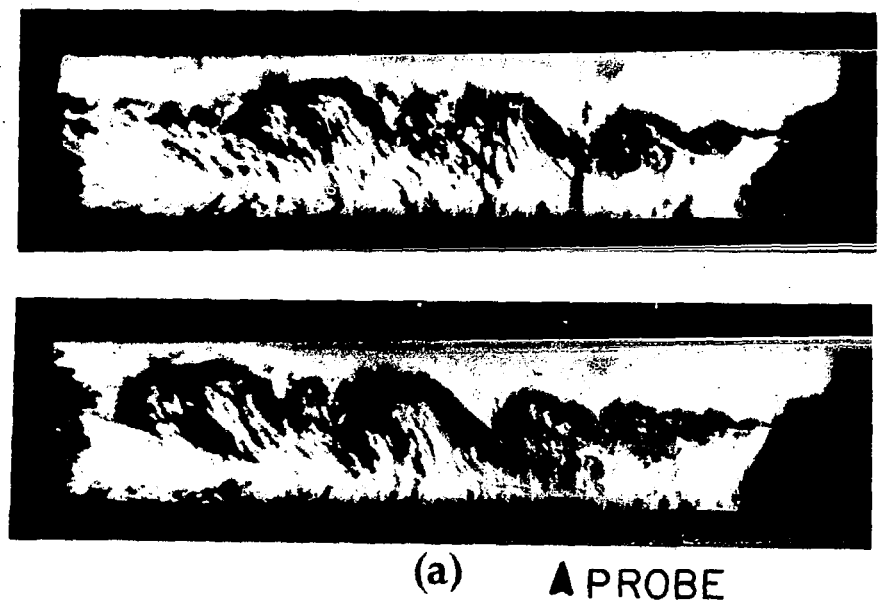

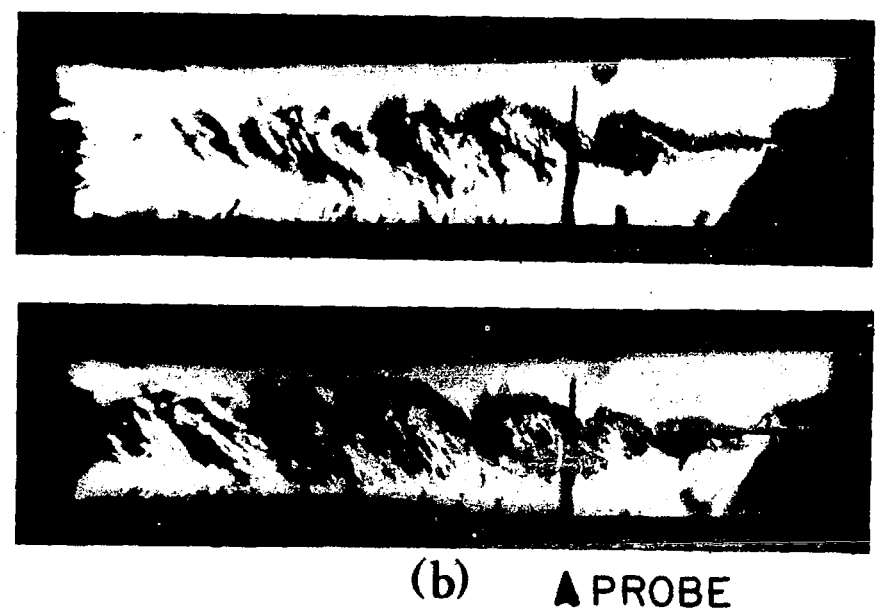

Fig. 5.1 Passage of large scale eddies over a probe in the flame zone. V_o = 13.6 m/sec, N_{Re} = 8800 cm^{-1}, ϕ = 0.57, T_o = 295 K.

(a) Time interval 2.1 msec, probe insertion 24 mm.
(b) Time interval 2.3 msec, probe insertion 40 mm.

average temperature for different values of reference velocities and inlet temperatures are reported in the second section. Section 5.3 describes the results of probe measurements of average concentrations of CO, CO_2, NO_x, NO_2, and unburned hydrocarbons. Table 5.1 presents the four cases selected for temperature and composition measurements.

Table 5.1

Experimental operating conditions for composition and temperature measurements.

Case	Equivalence Ratio	Inlet Temperature (K)	Reference Velocity (m/sec)
1	0.56	295	13.3
2	0.58	456	13.1
3	0.56	558	22.2
4	0.55	460	23.4

The selection of the experimental conditions of Table 5.1 was made to investigate the effect of reference velocity (holding temperature and equivalence ratio constant) and inlet temperature (holding equivalence ratio and velocity constant) on the flame. Because of the narrow range of stability of this flame, the effect of equivalence ratio (holding velocity and inlet temperature constant) was not studied. The slight variation of the approximately constant terms ϕ, T_o or V_o results from the difficulty of precisely setting the reference velocity and inlet temperature at predetermined conditions.

5.1 Velocity Measurement Results

The mean longitudinal velocity in reacting and nonreacting flow fields was measured by an LDV system. Details of this system are reported by Houser (1979). The results reported here were taken from his work. The velocities were measured in the vertical plane of symmetry of the test section. The profiles of velocity in nonreacting and reacting flow fields are shown in Figures 5.2 and 5.3. Initially, the profiles are very similar. Both have jet-type profiles close to the entrance plane and both have a secondary recirculation zone downstream of the step. Further downstream the effect of combustion becomes more evident as an increase in the velocity in the shear layer, especially in the lower part of the layer (below the step level). Comparison of Figures 5.2 and 5.3 shows that the average length of the recirculation zone for the reacting flow field is less than for the nonreacting flow field. This is attributed to the dilation effect of combustion. It is expected that the ratio of recirculation zone length to step height would change with blockage ratio in both reacting and nonreacting cases. The other difference between the two sets of profiles is the lower spreading rate of reacting shear layer with respect to nonreacting shear layer. If the shear layer spread is defined as the vertical position at which the longitudinal velocity reaches a certain percentage of the free stream (or reference) velocity, then obviously the nonreacting layer has a higher spreading rate. This result confirms the previous similar conclusion in Chapter 3. Because of the lack of additional experimental data (e.g., on the intensity of turbulence or local flow direction), no further conclusions are

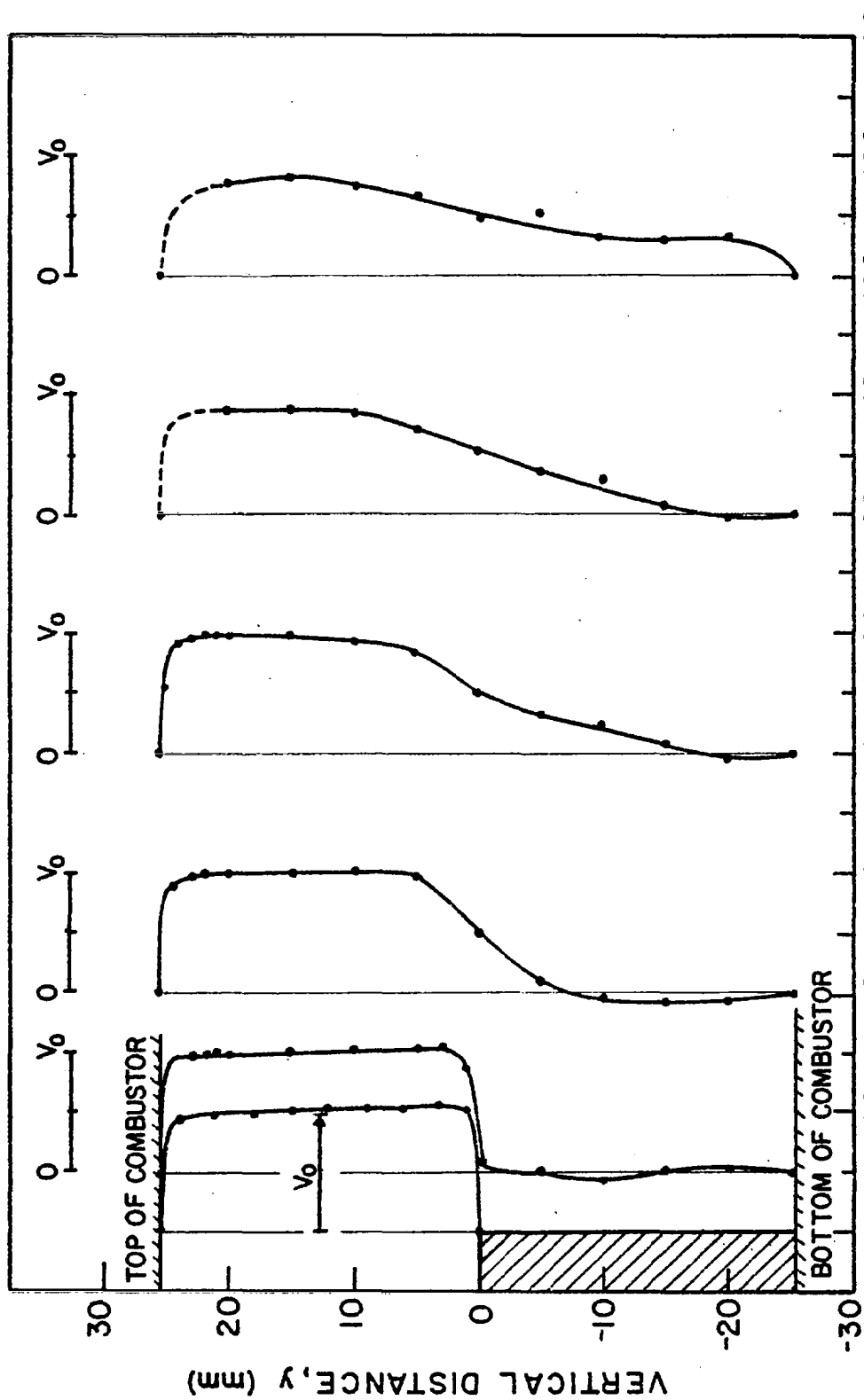

Fig. 5.2 Velocity profiles along the combustor for nonreacting flow. V_o = 13.0 m/sec, N_{Re} = 8474 cm^{-1}, T_o = 295 K.

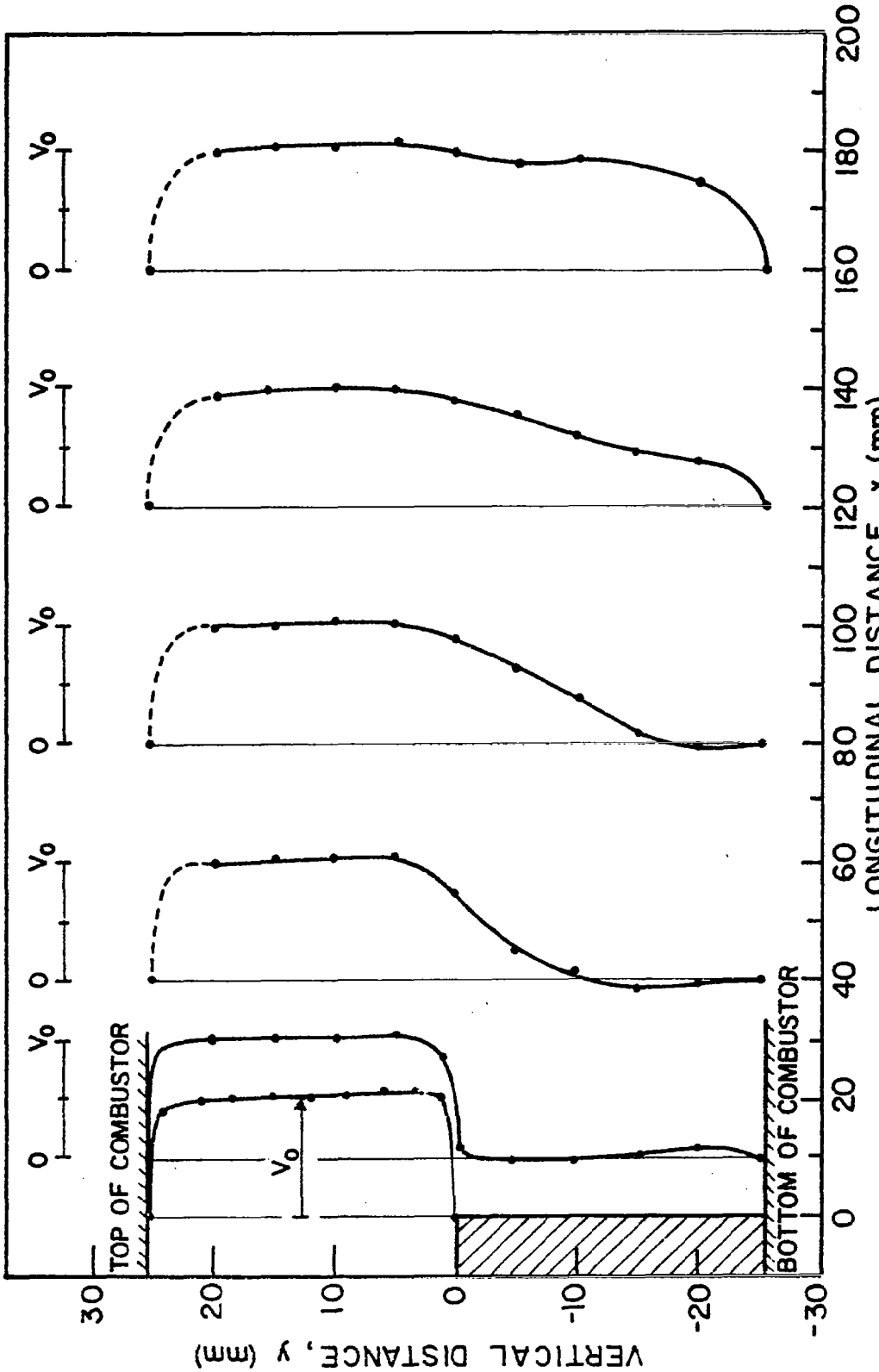

Fig. 5.3 Velocity profiles along the combustor for reacting flow. V_o = 13.3 m/sec, N_{Re} = 8670 cm^{-1}, T_o = 295 K.

drawn from the present velocity measurements. A nonreacting flow field behind a backward facing step has recently been studied in detail by Kim, et al. (1978). Further details of the velocity field in the present system will be reported later, Pitz (1979).

5.2 Temperature Measurement Results

Measured values of temperature in the flame for the four cases of Table 5.1 have been reported by Ganji (1979). Figure 5.4 shows typical temperature profiles along the combustor. The temperature gradient and relatively low temperature of the products in the recirculaton zone is due to heat transfer to the bottom of the combustor. The pattern is common for all inlet conditions. The sharp temperature gradient at 10 mm downstream close to step level corresponds to the thin laminar shear layer just behind the step. The profile shows that this layer is only a few mm thick. It is the sharp gradients in this region that cause the diffusion of heat and species into the fresh reactants and initiate the combustion in the shear layer. Further downstream, the layer grows and becomes turbulent (see Chapter 3). Decrease of the temperature gradient downstream of the step shows the lack of a stationary turbulent flame front, and signifies the effect of the intermittency of the flame front (mostly at the edges of the eddies) in this type of vortex dominated flame. The temperature presented here is an average of the temperature of reacting, product, and reactant gases which intermittently pass the thermocouple bead. For the type of averaging introduced by a thermocouple, refer to Bilger (1977). Similar temperature profiles for the other conditions of Table 5.1 are presented in Figures 5.5 and 5.6. Figure 5.5 compares the

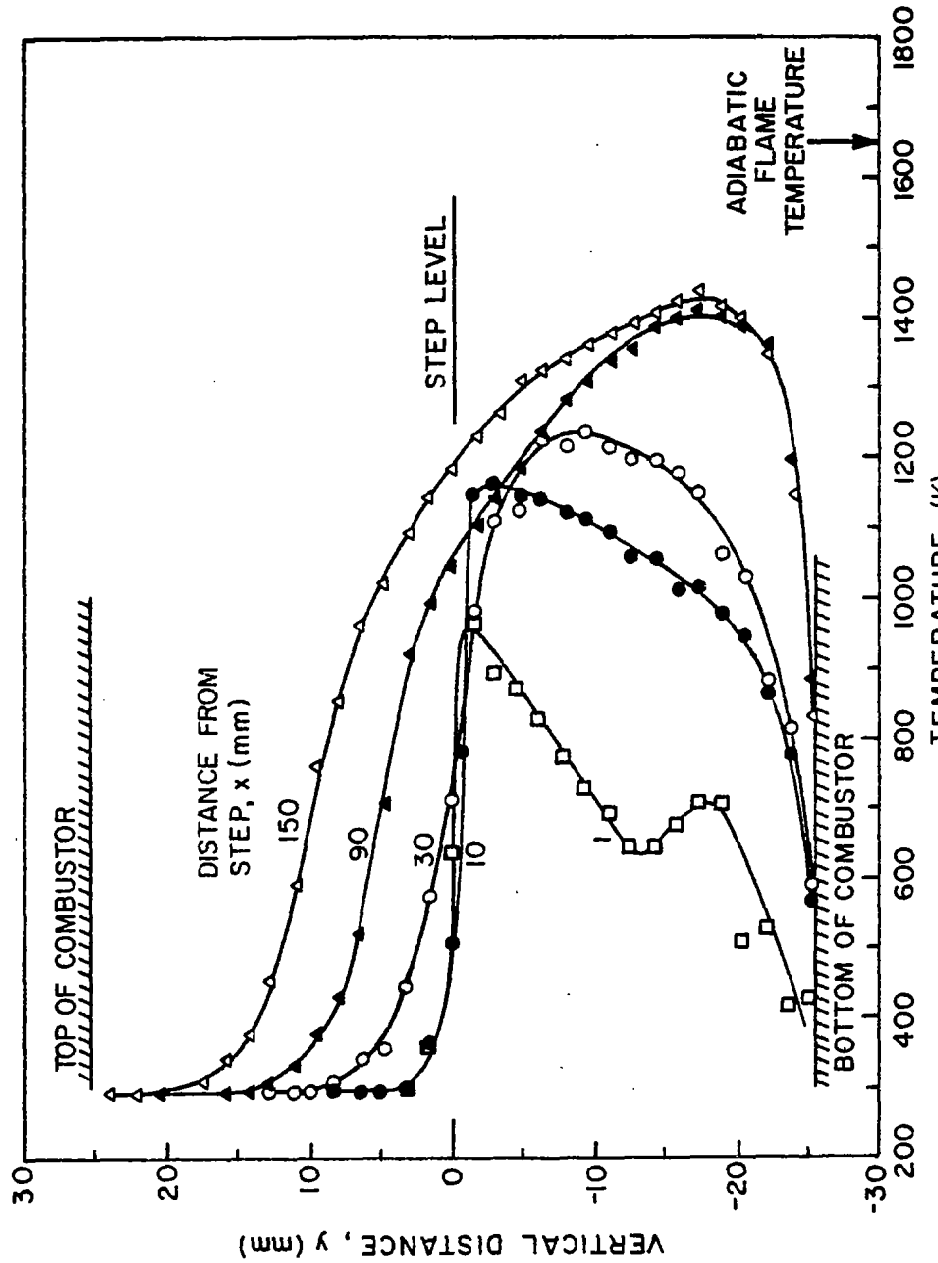

Fig. 5.4 Five temperature profiles inside the flame. V_o = 13.2 m/sec, ϕ = 0.57, T_o = 295 K.

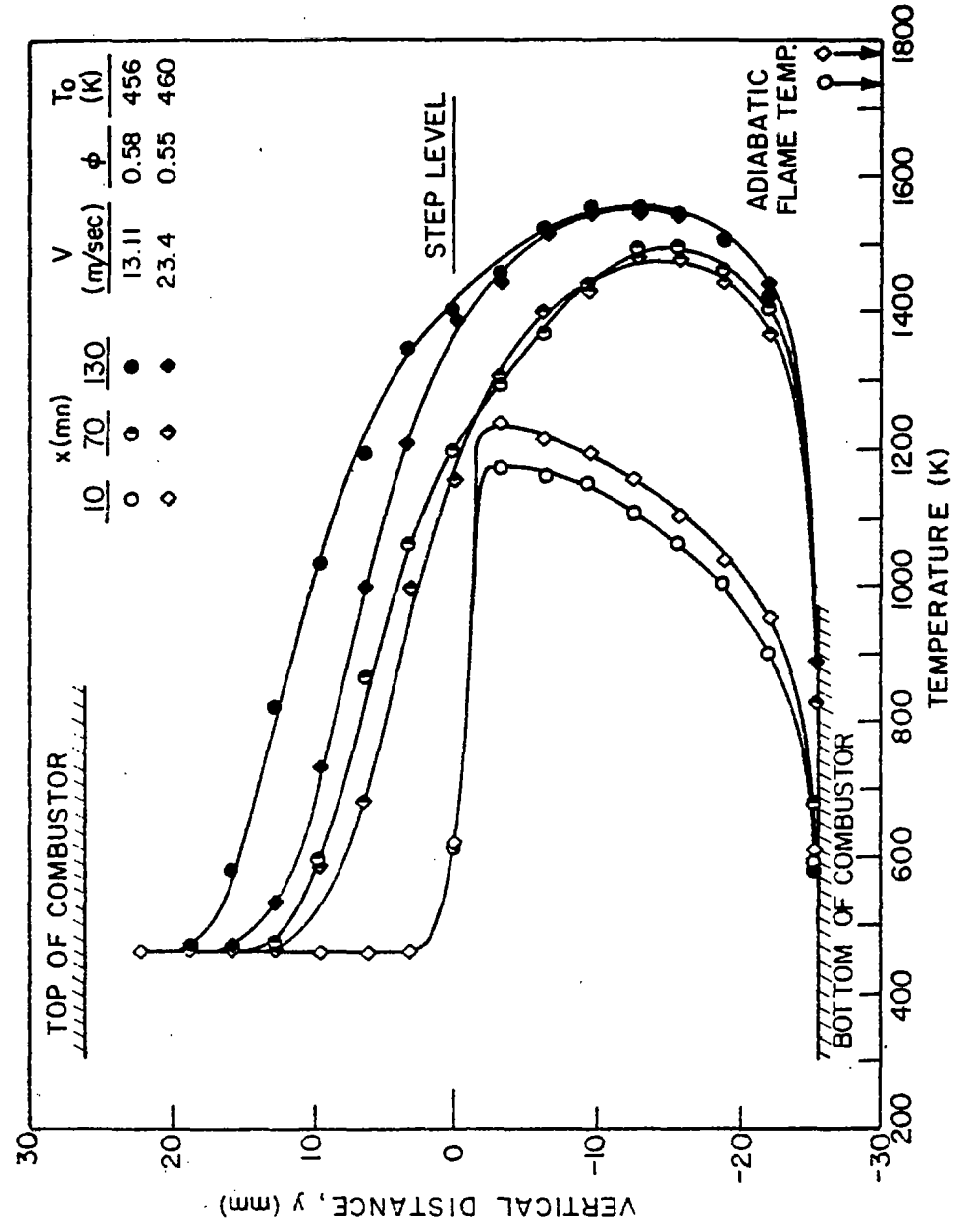

Fig. 5.5 Temperature profiles inside the flame for two different reference velocities.

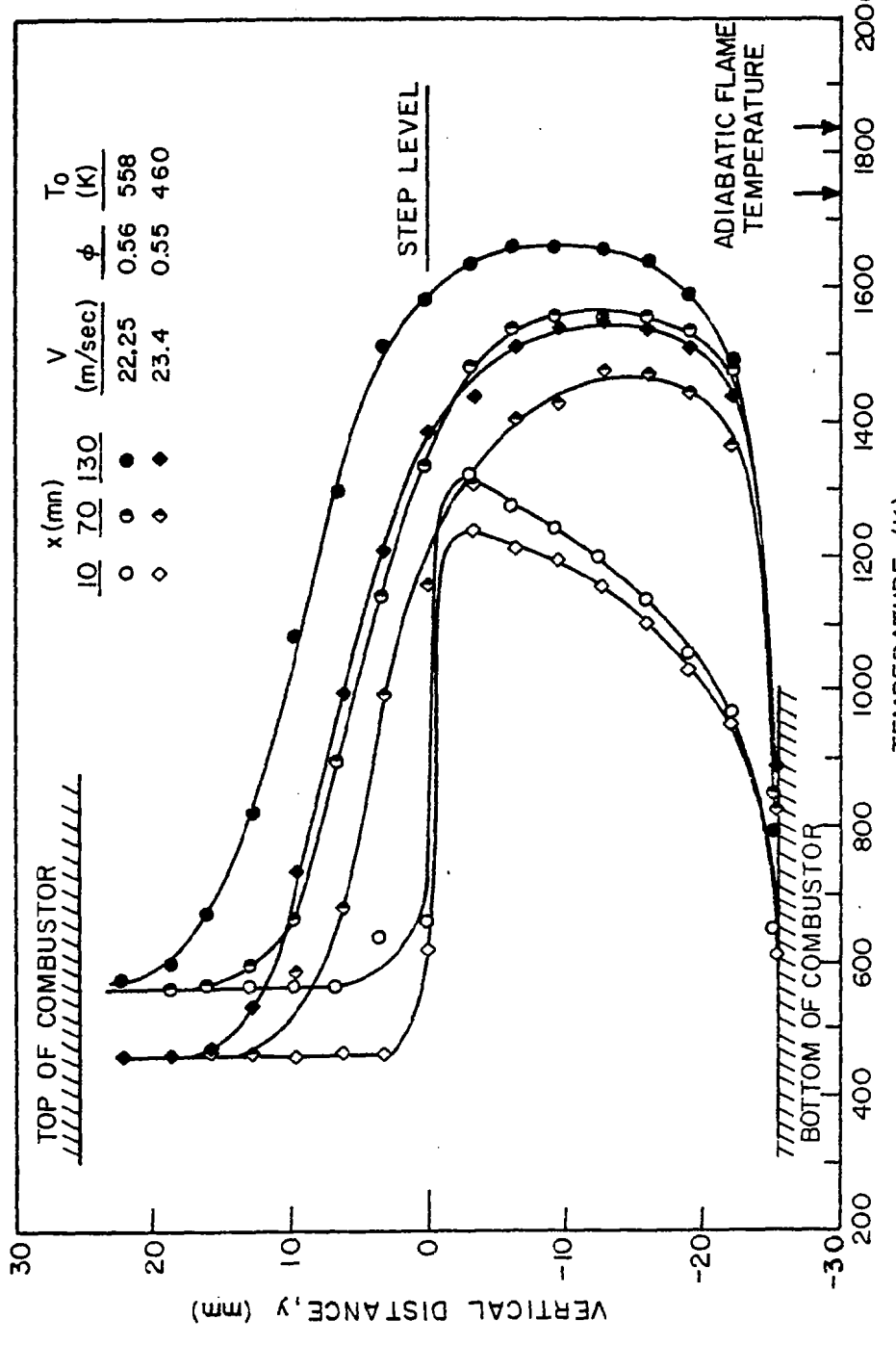

Fig. 5.6 Temperature profiles inside the flame for two different inlet temperatures.

temperature profiles for two flows with essentially the same equivalence ratio and inlet temperature, but with different reference velocities. For the lower reference velocity, the effect of higher residence time is shown in the lower temperature of the recirculation zone. If the shear layer spread is defined as the position where $T_s-T_{in} = K(T_{ad}-T_{in})$, in which K is a constant and T_s is the temperature at the given point, Figure 5.4 shows that in the lower velocity case, the flame has clearly higher spreading rate. Figure 5.6 compares the temperature profiles for the two flows with essentially the same equivalence ratio and reference velocity, but with different initial temperatures. Figure 5.7 shows the nondimensionalized temperature profiles for the last three cases of Table 5.1. Actually, Figure 5.7 represents the progression (and roughly the efficiency) of reaction in the free shear layer. The recirculation zone and lower part of the shear layer is strongly influenced by the heat transfer to the step and bottom plate of the combustor. So actually, the section of the shear layer above the step (rather than that below the step) represents the thermal growth of the layer. Figure 5.7 shows that, on average, an increase in inlet temperature increases the rate of flame spread while an increase in reference velocity reduces the spreading rate. This is basically the effect of flame speed with respect to the free stream velocity. The inconsistency in the spreading rate of the flame of Case 3 with respect to the other two cases at 170 mm location is attributed to the thermocouple error (most probably reduced radiation to hot surfaces).

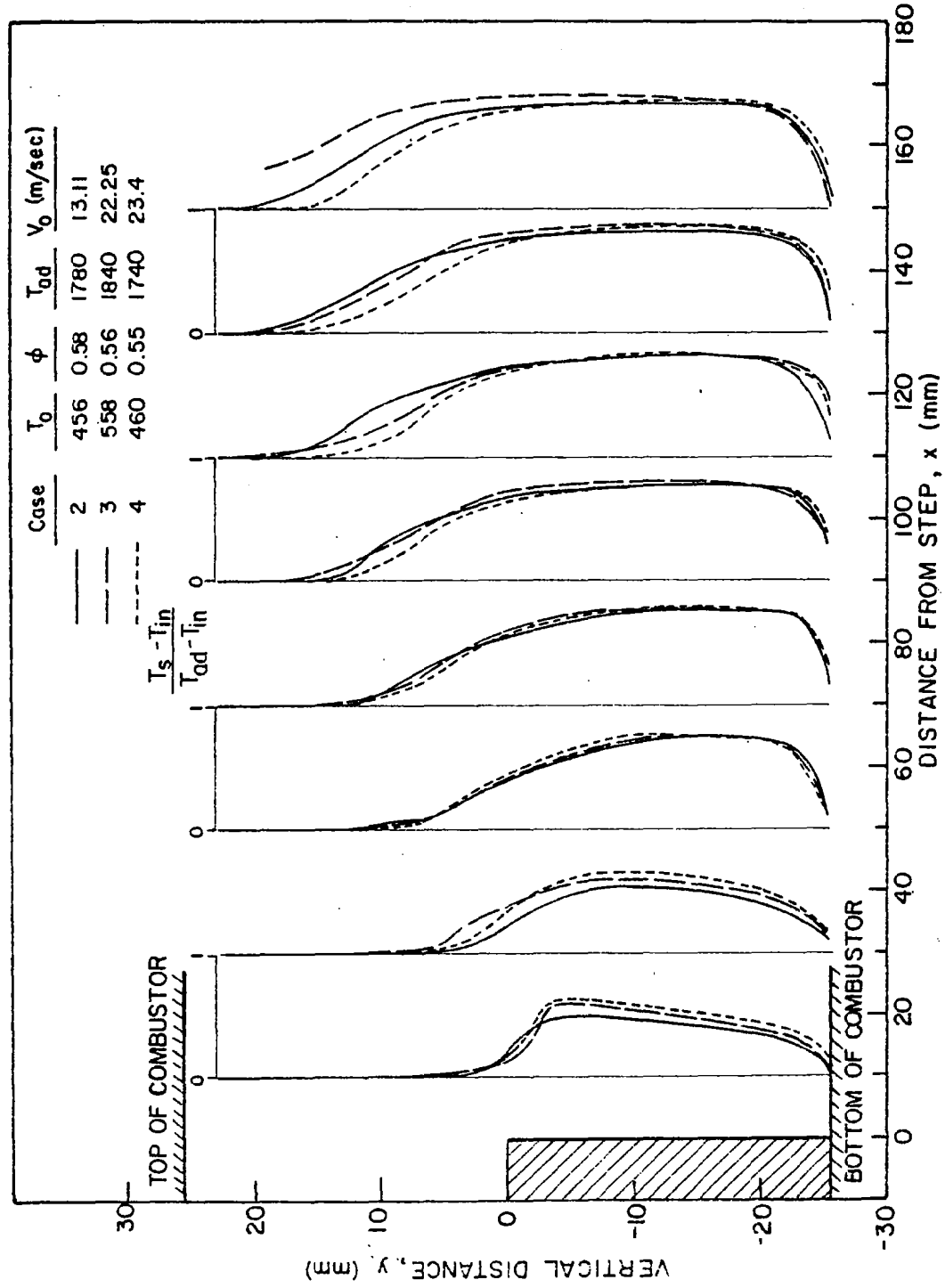

Fig. 5.7 Nondimensionalized temperature profiles for cases 2, 3, and 4.

5.3 Composition Measurement Results Inside the Flame Zone

In this section the concentration measurements of CO, CO_2, NO_x, NO_2 and unburned hydrocarbons are reported. The influence of mixing on the burning of the mixture and also on the formation and destruction of pollutants is described. The above species were measured for the four cases given in Table 5.1.

5.3.1 Experimental Observations

Figures 5.8 through 5.11 show the concentration porfiles of CO, CO_2, NO_x, NO_2, and the temperature across the combustor at three different positions along the combustor for the four cases of Table 5.1. Measured values of the species concentrations at 20 mm intervals were reported by Ganji (1979). Species profiles in the recirculation zone, 10 mm downstream of the step, show that the concentration of these species remains virtually constant, Figures 5.8 through 5.11. In some cases, the value of the concentrations at the bottom is an exception. At these locations, the probe tip is leveled with the bottom surface and is surrounded by colder gases of the hole through which the probe is inserted into the test section. Interchange of these cold pockets of gas with the flow and also the low temperature at these locations are possible causes of these nonuniformities. This justification is confirmed by the fact that, in all cases, at the bottom surface NO_x has a lower and CO a higher concentration than average corresponding values in the recirculation zone. The fact that, despite the variation of temperature in the recirculation zone, the composition does not follow the same trends, implies that little

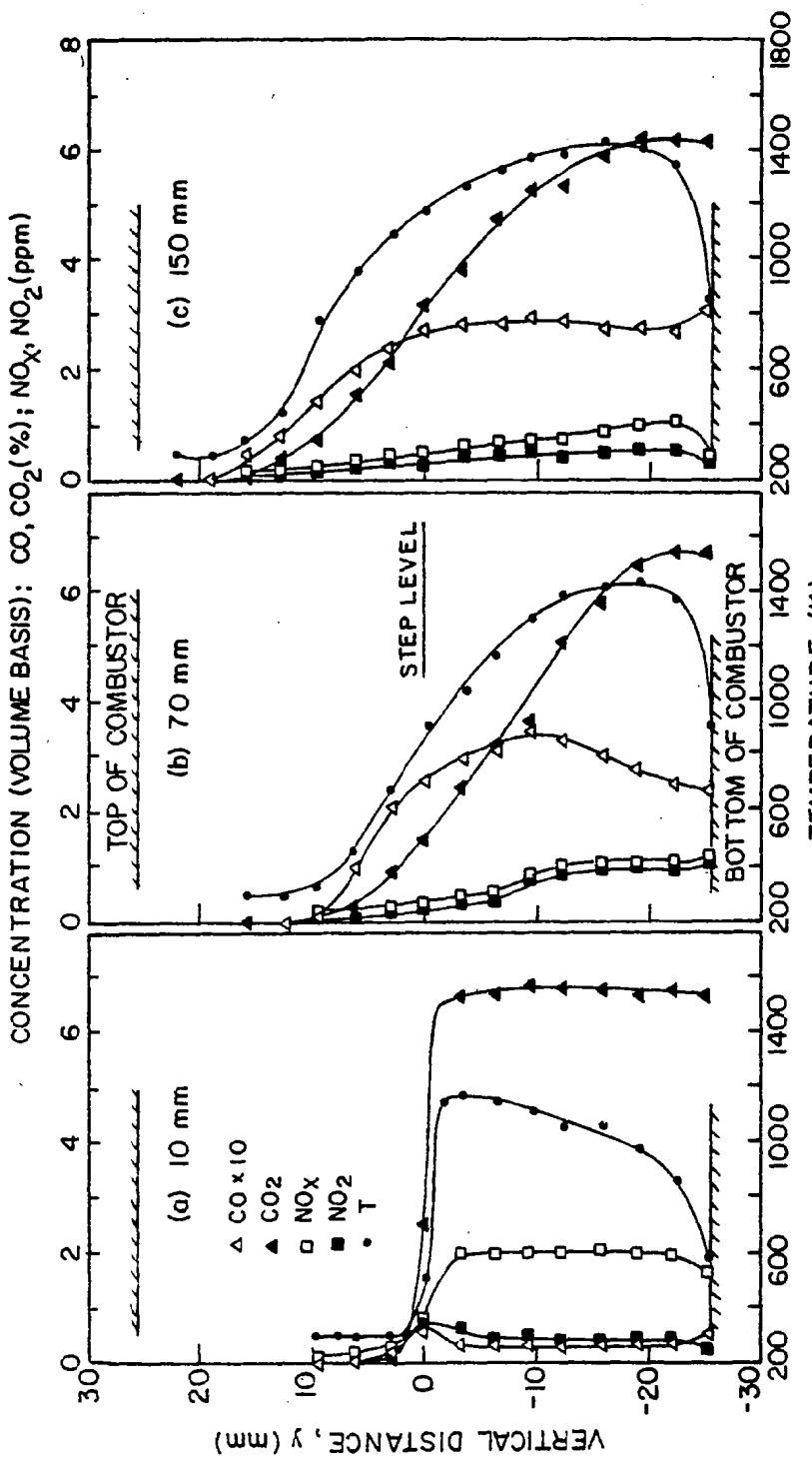

Fig. 5.8 Selected temperature and species profiles for Case 1: V_o = 13.3 m/sec, N_{Re} = 8670 cm^{-1}, ϕ = 0.56, T_o = 295 K.

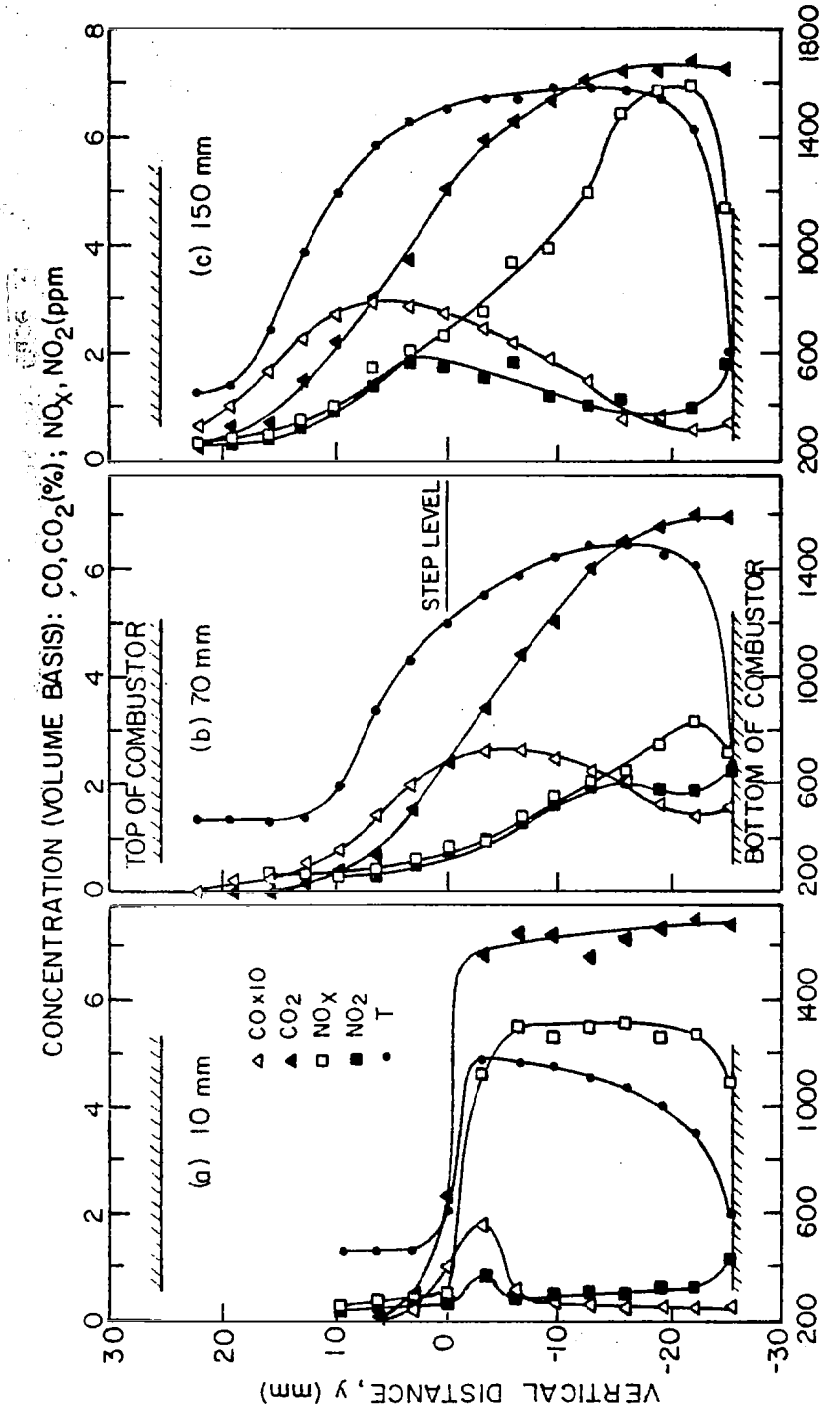

Fig. 5.9 Selected temperature and species profiles for Case 2: V_o = 13.1 m/sec, N_{Re} = 3850 cm^{-1}, ϕ = 0.58, T_o = 456 K.

reaction occurs in the recirculation zone, and that the concentrations in this region depend primarily on the stoichiometry and inlet temperature.

Equilibrium concentrations for the above four cases were calculated using the computer programs of Gordon and McBride (1971), and the results are presented in Table 5.2.

Table 5.2

Equilibrium concentration of measured species for reactants of Table 5.1.

Case	ϕ	T_{in} (K)	T_{ad} (K)	HC (ppm)	CO volume %	CO_2 volume %	NO (ppm)	NO_2 (ppm)
1	0.56	295	1624	< 5	.001	6.723	1440	< 5
2	0.58	456	1784	< 5	.004	6.948	2560	< 5
3	0.56	558	1826	< 5	.006	6.717	3020	< 5
4	0.55	460	1731	< 5	.002	6.607	2210	< 5

Comparison of the measured concentration in the recirculation zone and equilibrium values of Table 5.2 shows that CO_2 is at its equilibrium level (within maximum deviation of 10% in case 2), CO is about one to two orders of magnitude above its equilibrium level, and NO_x is about two to three orders of magnitude below its equilibrium level. High rates of entrainment of cold reactants and partially reacted gases, heat transfer to the bottom plate, quenching of the reaction fronts and low residence time are the main reasons for the deviation of CO and NO_x from equilibrium levels predicted for a diabolic combustion. The

matter will be further discussed later in this section. Figures 5.8 through 5.11 also show that CO and NO_2 peak in the free shear layer at the lower temperature regions (compared to the maximum temperature locations). Further downstream, as the shear layer grows and turbulent mixing occurs, CO_2 holds its general shape of having a constant value close to the bottom (mostly reacted gases) and decreasing gradually upwards. The CO_2 concentration is an indicator of reaction progress and follows the same trends as does the temperature. Figure 5.12 compares the CO_2 concentration profiles of the last three cases in two different locations downstream of the step. Comparison of Figure 5.12 with Figure 5.7 shows, regarding the spreading rate of the layer, that the CO_2 profiles confirm the conclusions of the previous section.

The effect of reference velocity and inlet temperature on CO is shown in Figure 5.13, which reveals that the CO concentration is strongly influenced by residence time, but is less influenced by the inlet temperature. An increase in reference velocity (constant inlet temperature and equivalence ratio) increases the CO concentration.

The behavior of the oxides of nitrogen is particularly interesting. Figures 5.8 through 5.11 show that, in the recirculation zone, NO_2 is a negligible part of the oxides of nitrogen. Referring to Case 1 (Figure 5.8), at 70 mm downstream more than 80% of NO_x is in the form of NO_2 and, further downstream at 150 mm from the step, more than 50% is in the form of NO_2. Figure 5.9 shows that at 70 mm and 150 mm downstream colse to the bottom of the combustor, oxides of nitrogen are mostly in the form of NO, while at temperatures of about 1500 K and less (uncorrected for radiation), NO_2 comprises more than 80% of oxides of nitrogen. Figures 5.10 and 5.11 also show the same trends

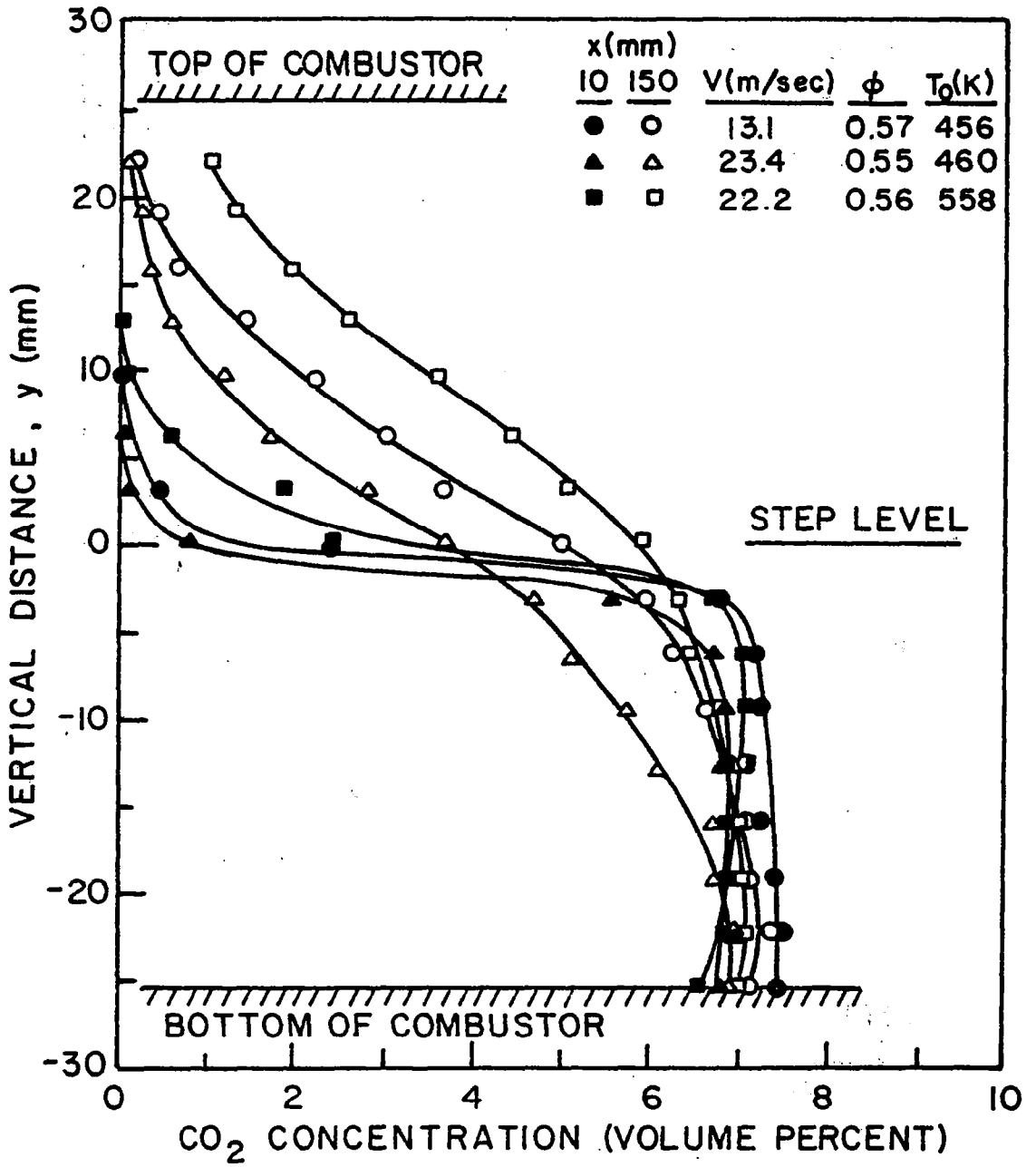

Fig. 5.12 Effect of velocity and temperature on CO_2 concentration profiles at 10 and 150 mm downstream of the step.

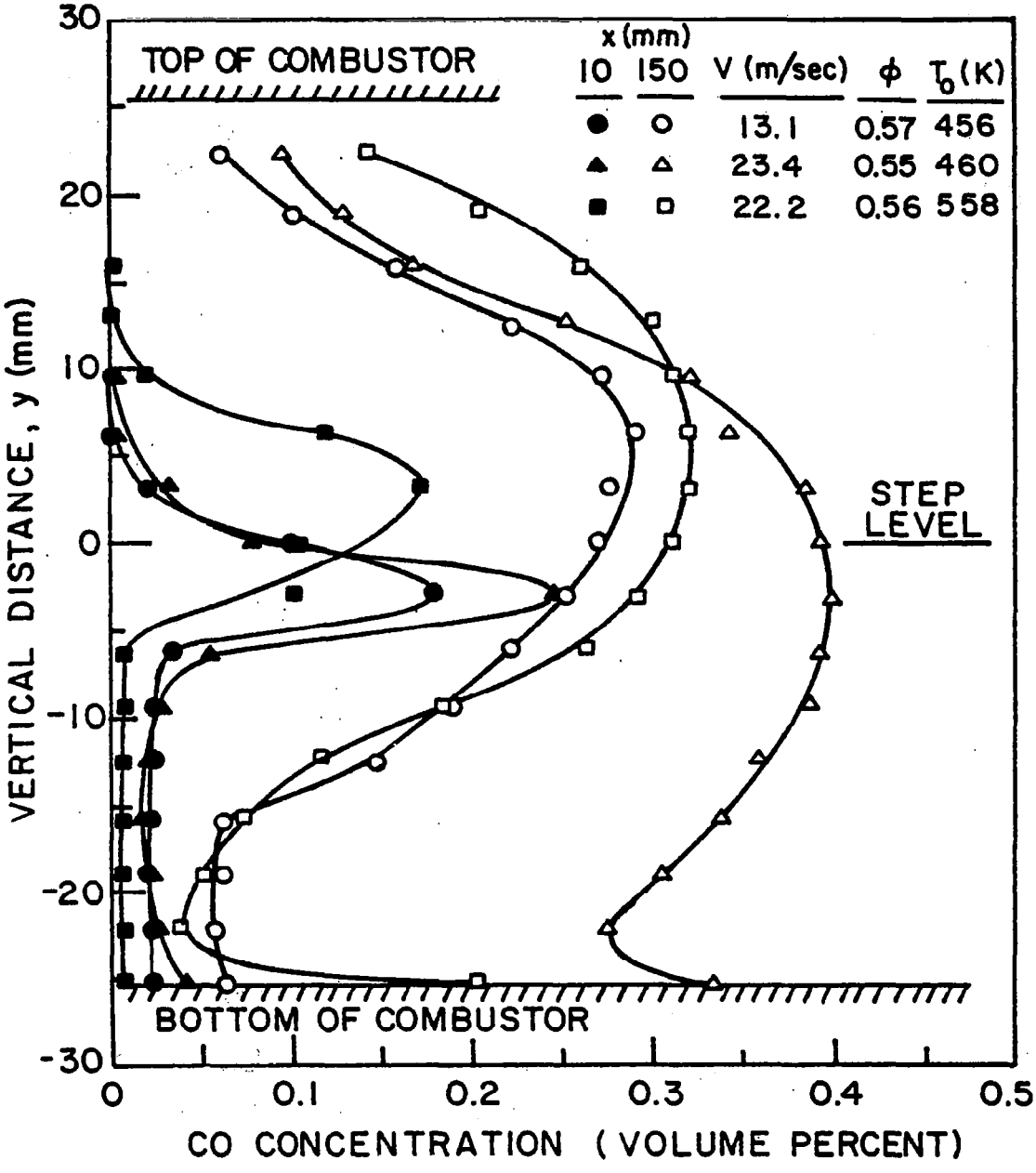

Fig. 5.13 Effect of velocity and temperature on CO concentration profiles at 10 and 150 mm downstream of the step.

observed for Case 2 in Figure 5.9. Finally, Figures 5.8 through 5.11 show that downstream of the recirculation zone the NO_x concentration peaks close to the bottom of the burner where the temperature is not necessarily at its peak and also falls rapidly upwards, while the average temperature is not necessarily declining. This effect is believed to result from the mixing characteristics of the flow. The effect of reference velocity and inlet temperature on NO_x and NO_2 profiles at two locations in the combustor is illustrated in Figures 5.14 and 5.15. As expected, by increasing the reference velocity (at constant inlet temperature), NO_x concentration is reduced while increase in inlet temperature clearly increases NO_x concentration. Figure 5.15 shows that changing reference velocity and inlet temperature creates similar trends on NO_2 as on NO_x. The shift in the peaks of NO_2 profiles is clearly influenced by temperature variation in the shear layer, see Figures 5.9 to 5.11.

5.3.2 Entrainment Considerations

Production and destruction of chemical species in combustion systems at a constant pressure depends on (1) the concentration of the involved species, (2) the kinetics of their chemical reactions, (3) the temperature of the reaction environment and, possibly, (4) catalytic effects. In a system such as the present, the variation of temperature in the reaction zone is controlled by the dynamics of the flow field and heat transfer to the containing surfaces of the combustor.

According to the observations and detailed discussions of Chapter 3 on the time scale of formation and convection of eddies (order of msec),

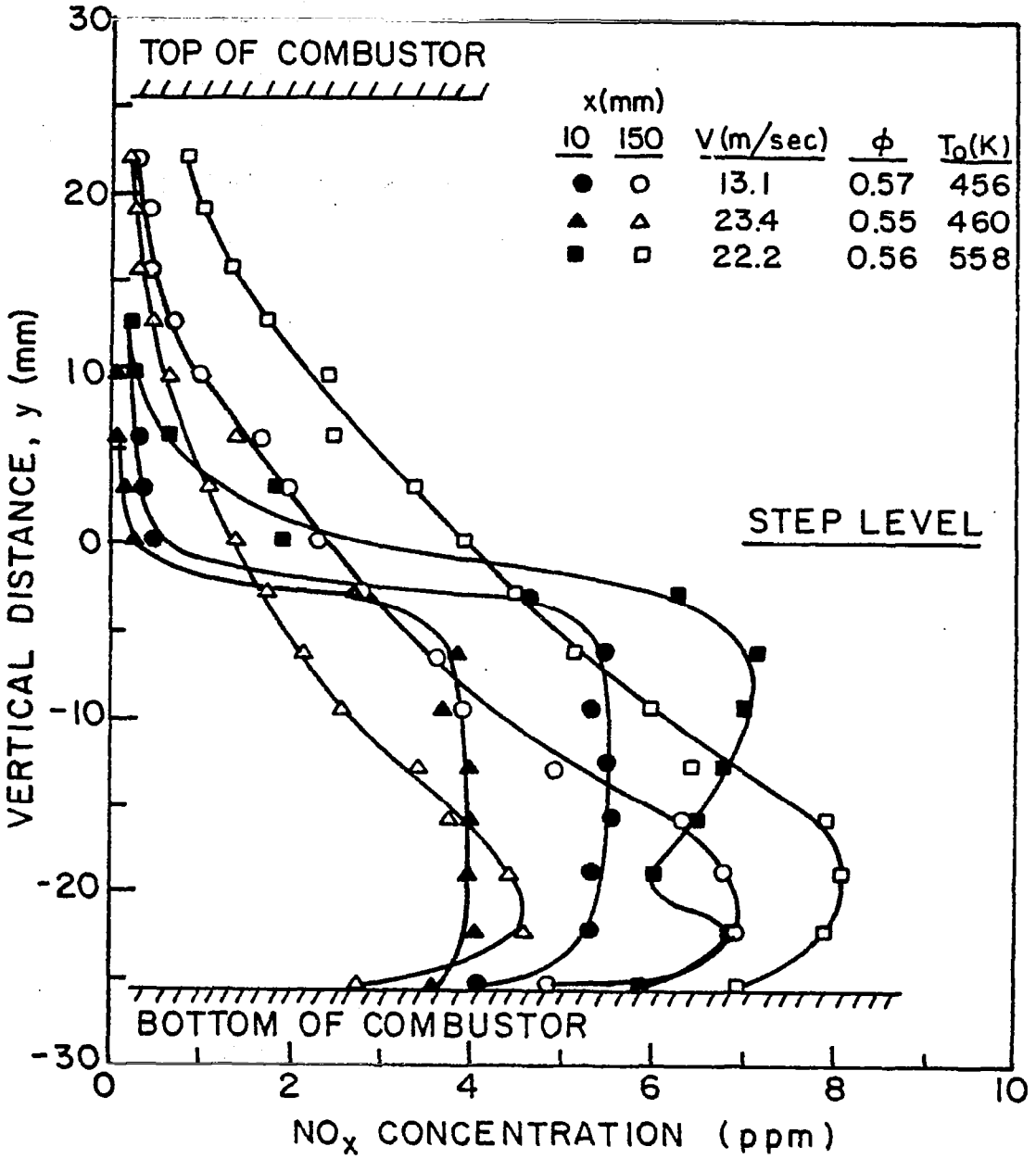

Fig. 5.14 Effect of velocity and temperature on NO_x concentration profiles at 10 and 150 mm downstream of the step.

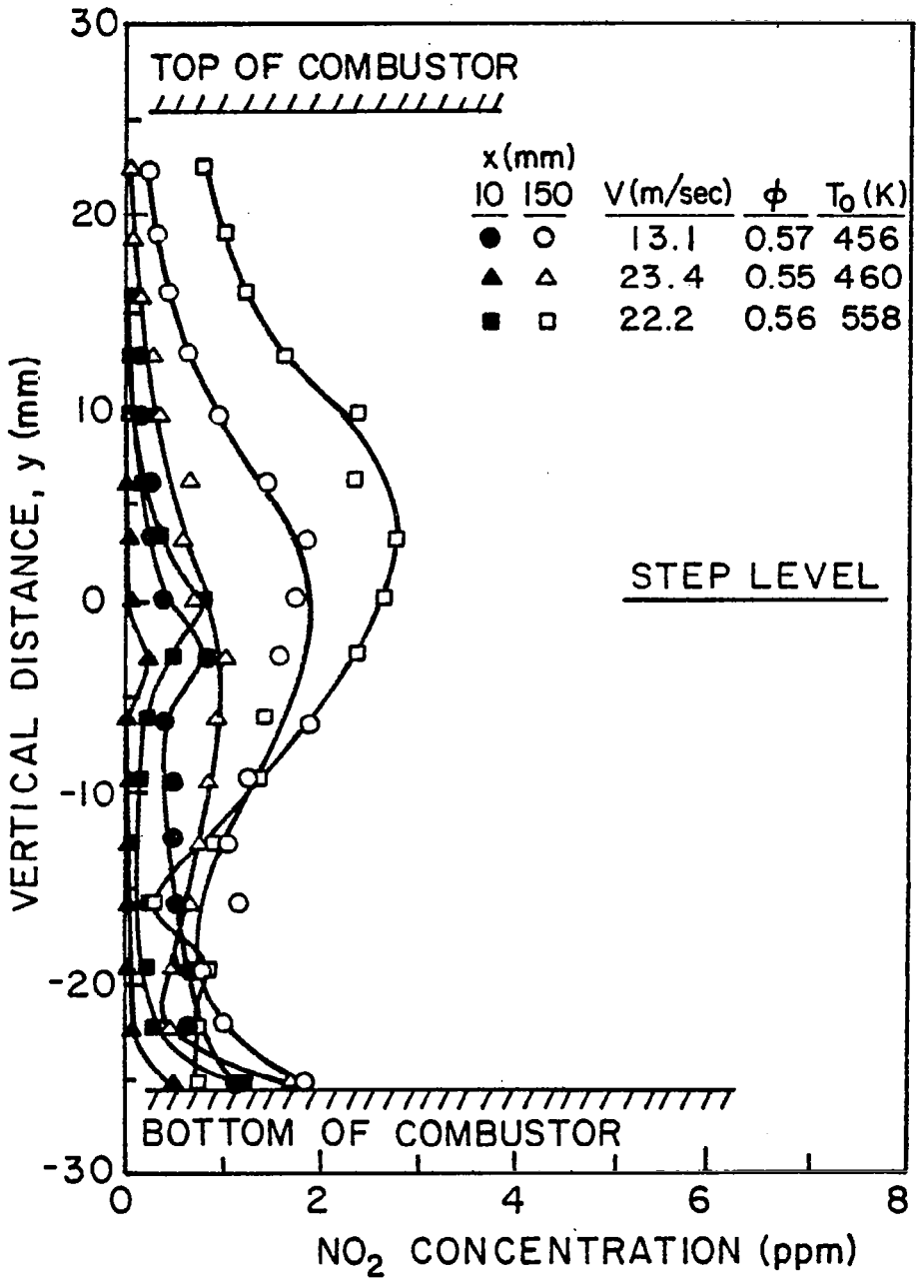

Fig. 5.15 Effect of velocity and temperature on NO_2 concentration profiles at 10 and 150 mm downstream of the step.

the whole flow field is highly unsteady and flow properties are highly intermittent. Figures 5.16 and 5.17 show the temperature records in the form of the output of the chart recorder without being averaged for 10 and 160 mm downstream of the step. Although, because of the thermal lag and slow response of the thermocouple to high frequency temperature variations, the fluctuations shown by no means show the actual fluctuations of temperature at the given position, the above two figures confirm high levels of temperature fluctuations in the flow field. Similar fluctuations, no doubt, occur in the concentrations. Konrad (1976) and Roshko (1976) have reported measured concentration fluctuations in similar but non-reacting flows.

According to the observations of the reacting flow field in this system (Chapter 3) and also the evidence from the previous experimental works in similar, but non-reacting flows, the entrainment of gases into the mixing/reacting layer can be idealized as shown in Figure 5.18. The figure illustrates that combusting gases and reactants are entrained into the reacting eddies and are interleaved as the eddy rotates and moves downstream. At the same time, reaction occurs on the surfaces of these flame sheets. As the reaction progresses, fresh reactants are continuously entrained into the eddy. Similar idealizations have been made by Spalding (1978b) and Marble and Broadwell (1977) in their theoretical studies of combustion in premixed and diffusion flames. The thickness and persistence of the sheets of reactants will depend on the rates of rotation, reactions, and diffusion. The reaction front is always in close contact with the cold reactants and because of this there is a potential for the quenching of species whose production or destruction is temperature sensitive, namely NO and CO.

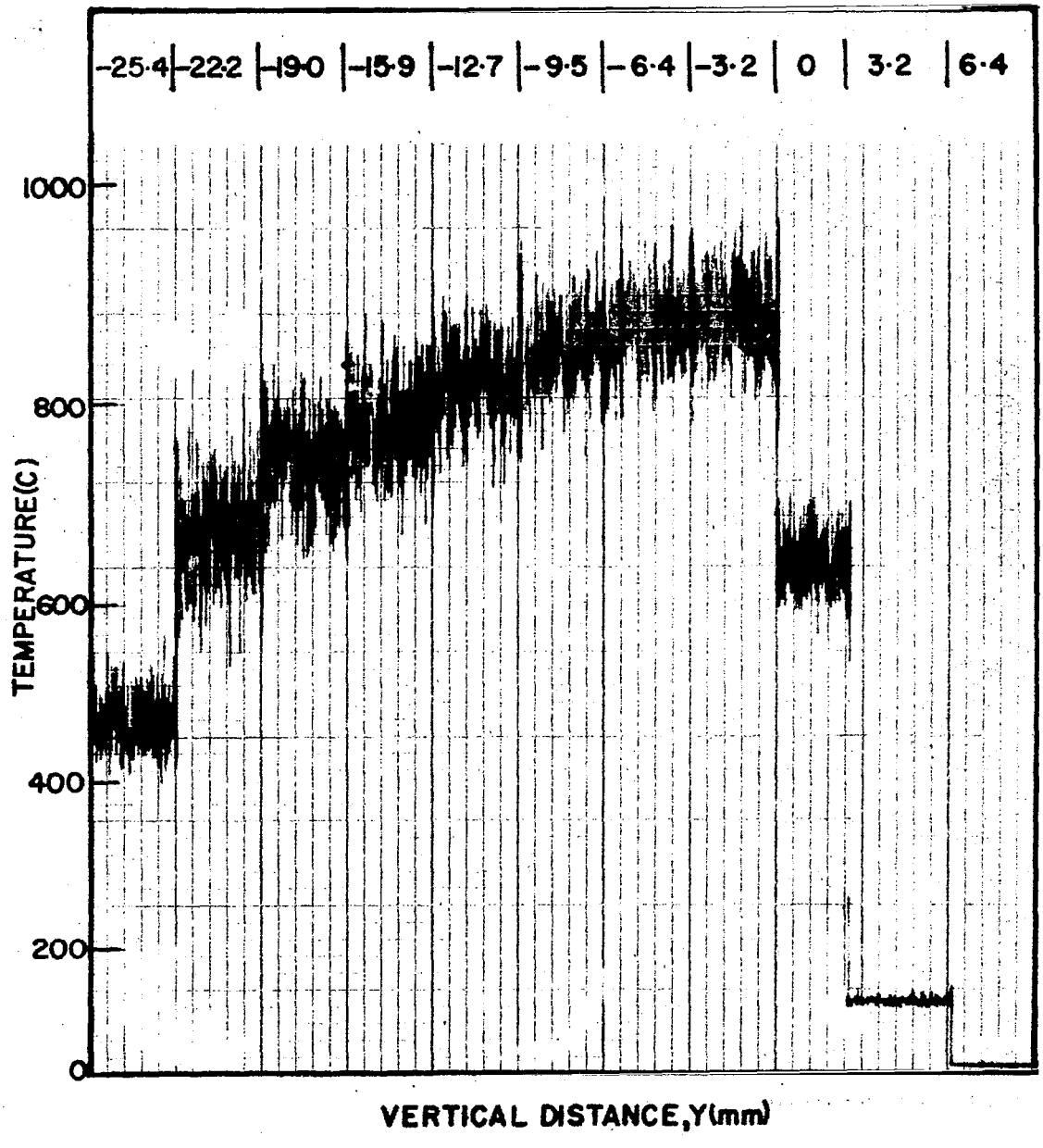

Fig. 5.16 Temperature record in the vertical transverse direction 10 mm downstream of the step. V_o = 13.3 m/sec, N_{Re} = 8670 cm^{-1}, ϕ = 0.56, T_o = 295 K (Case 1).

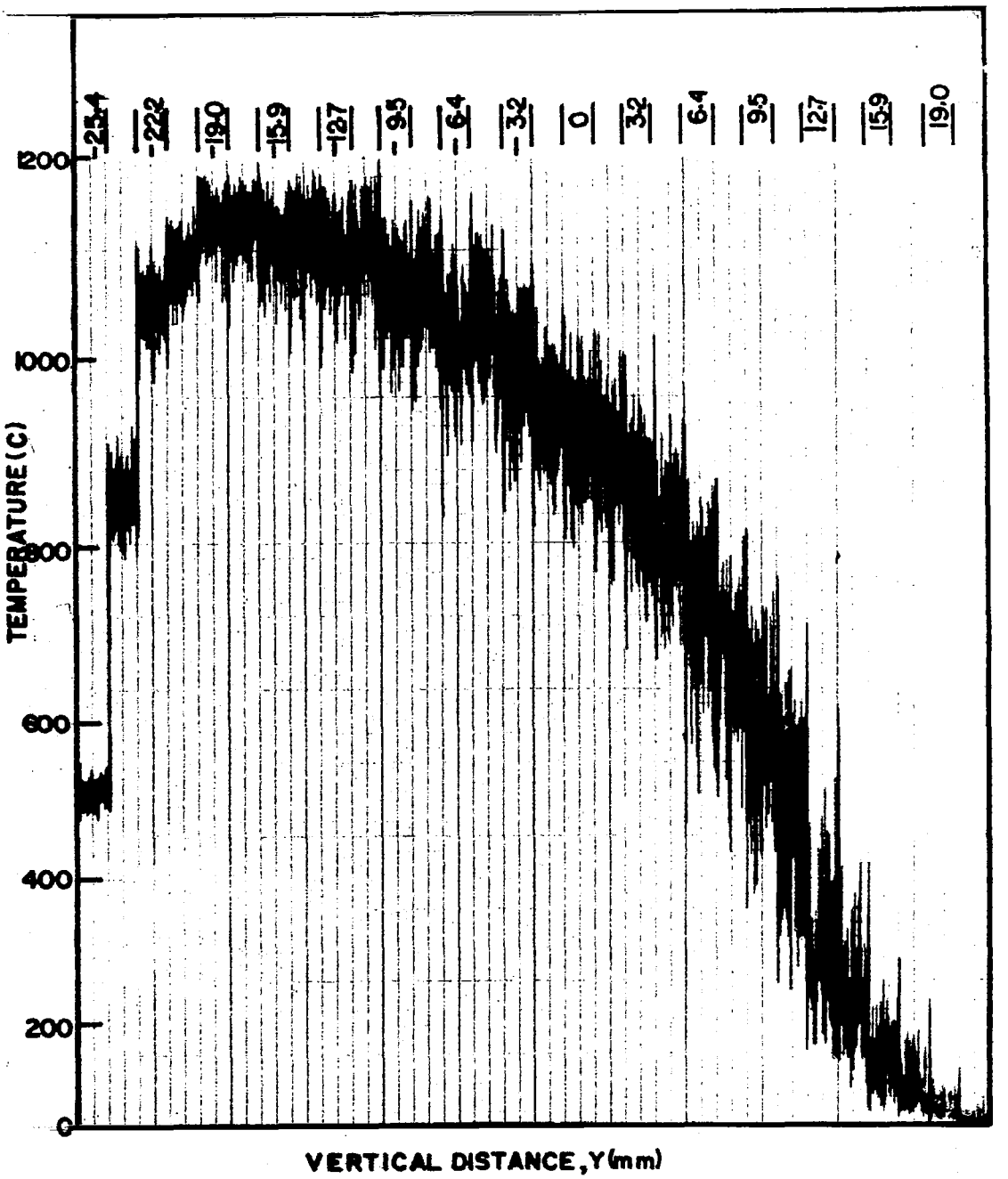

Fig. 5.17 Temperature record in the vertical transverse direction 160 mm downstream of the step. V_o = 13.3 m/sec, N_{Re} = 8670 cm^{-1}, ϕ = 0.56, T_o = 295 K (Case 1).

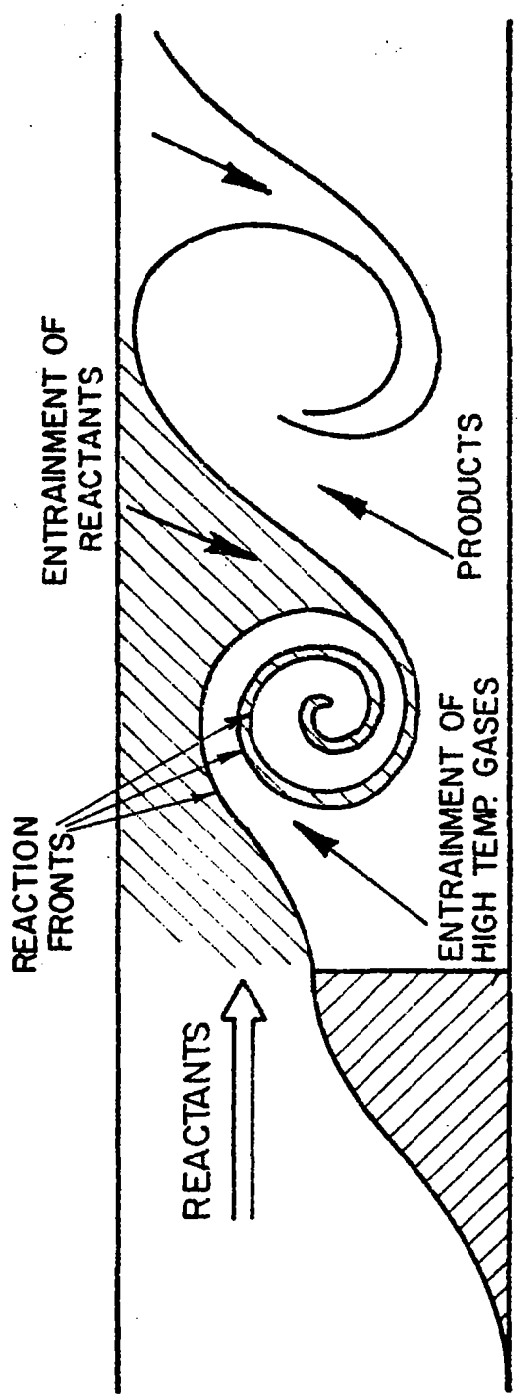

Fig. 5.18 Illustration of the entrainment process in a reacting free shear layer.

A characteristic entrainment time can be estimated by the time each eddy makes half a revolution and, as a result, engulfs fresh reactants deep into the mixing/reacting layer. Thus

$$\text{Characteristic entrainment time} \quad \tau_e \approx \frac{\pi}{\omega}$$

$$\text{Angular velocity} \quad \omega \approx \frac{V_o - V_b}{2h}$$

$$\text{Substituting for } \omega \quad \tau_e \approx \frac{2\pi h}{V_o - V_b} \tag{5.1}$$

h , V_o , and V_b are step height, reference velocity, and burned gas velocity below the step level. Residence time in the shear layer can be approximated by

$$\tau_{res} \approx \frac{L}{V_o} \tag{5.2}$$

where L is the length of the test section. Estimates of entrainment time and residence time for the cases considered are presented in Table 5.3. Values of mixing time proposed by Vranos (1974) and Tuttle, et al. (1976) are comparable to the above entrainment times.

Table 5.3

Characteristic times in the combustor for the conditions of Table 5.1

Case	ϕ	T_o (K)	V_o (msec)	τ_e (msec)	τ_{res} (msec)	τ_c (msec)	τ_{NO} (msec)
1	0.56	295	13.3	12.	16.5	14.0	772
2	0.58	456	13.1	12.2	16.8	8.1	40.6
3	0.56	558	22.2	7.2	10.0	1.6	14.3
4	0.55	460	23.4	6.8	9.4	7.8	83.0

Following Vranos (1974), combustion time, τ_c , is the time required for a well-mixed gaseous fuel-air mixture to release its chemical energy by molecular scale processes. τ_c is estimated by dividing laminar combustion wave thickness by laminar burning velocity:

$$\tau_c \approx \frac{\delta}{U_b} \tag{5.3}$$

where δ is the flame thickness, taken as defined by Fristrom and Westenberg (1965), and U_b is the laminar burning velocity, estimated from the work of Kaskan (1957). Estimated values of characteristic combustion times corresponding to the four cases of the present experiment are also given in Table 5.3. Table 5.3 shows that the estimated combustion times are one to two orders of magnitude higher than those predicted by Vranos (1974) and Tuttle, et al. (1977). This large difference is due to higher inlet temperatures (up to 200 to

300 C), higher pressures (up to an order of magnitude) and higher equivalence ratios (above 0.7) in the above two investigations.

Comparison of entrainment and combustion times in Table 5.3 reveals that in these types of flames, the combustion times are comparable to entrainment and also residence time, as is consistent with operation near the lean blowout limit. If the entrainment time is reduced (through increase in velocity) or combustion time is increased (through reduction in inlet temperature or equivalence ratio) and, as a result, entrainment time falls significantly below combustion time, blowout would occur.

On the other hand, small entrainment and residence times and relatively large combustion times is the main reason for high levels of unburnt hydrocarbons (see Figures 5.20 and 5.21) and carbon monoxide. In high intensity gas turbine combustors, combustion time is just a fraction of a millisecond and the residence time is one to two orders of magnitude higher, and combustion is nearly complete. Here both are of the same order of magnitude. For the same reason, because the production and destruction of chemical species have characteristic times of the same order as entrainment time, they become very susceptible to the quenching effect of the cold reactants entrained into the reaction layer.

5.3.3 CO Formation and Destruction

The details of the kinetics of oxidation of hydrocarbons are mostly unknown, Bowman (1975). It is often assumed that hydrocarbons in a series of fast chemical reactions are pyrolyzed and oxidized to CO and H_2O and then, through a much slower chemical reaction, CO is

oxidized to CO_2 by the reaction $CO + OH \rightarrow CO_2 + H$, Westenberg (1971) and Bowman (1975). As the temperature in the reaction zone is decreased CO is "frozen" which is consistent with experimental observations, Figures 5.8 through 5.11. Note that, except at the 10 mm location downstream, all peaks in CO profiles occur near a measured temperature of 1300 K. The high levels of CO in the shear layer are attributed to the low residence time (see Figure 5.13 for effect of residence time) and quenching of CO after formation. In their experiments of ethylene-air flame sheets interleaved with cooling air streams, Fenimore and Moore (1974) found that at mean temperatures below about 1250 K at atmospheric pressure, a few hundred to a few thousand ppm of CO were quenched at the boundaries of fuel lean flame and persisted unreacted for many miliseconds in the mixed gas. Incidentally, this value of temperature is very close to the 1300 K observed for the peak of the CO profiles in these experiments. It was speculated (Section 5.3.2, based on the observations of Chapter 3), that in the present mixing/reacting layer, combustion mostly occurs between layers of reacted and reactant gas mixtures which interleave as a result of vortical action of the large vortices, which is very similar to the laminar flame and cooling sheets of Fenimore and Moore.

Oxidation of CO can also occur in the sample probe. The problem has been briefly discussed by Kramlich and Malte (1978). Their kinetic

calculations show that substantial oxidation of CO (up to an order of magnitude) occurs in their free convection cooled probe (uncooled length of 7.5 cm and pressure of .5 to .9 atm). Their measured values of CO relative to theoretical predictions depend on pressure and volume flow rates, and are by a factor of 2 to 10 too low. Because of much lower pressure (see Table 2.2), high surface to volume ratio and smaller length of probe insertion in the test section, conversion of CO in the present probe is expected to be much less than the observed value in the above reference. Direct evidence of little or no probe reaction in this system is the constant value of CO concentration measured in the recirculation zone, with different insertion lengths of the probe, see Figures 5.8 through 5.11.

5.3.4 NO_x Formation

Usually NO_x is referred to as the sum of oxides of nitrogen, NO and NO_2, produced in a flame. Due to the absence of fuel nitrogen in this system, all oxides of nitrogen produced in this system are thermal NO_x. Thermal NO_x is formed primarily through the Zeldovich mechanism:

$$N_2 + O \rightleftharpoons NO + N \tag{5.4}$$

$$N + O_2 \rightleftharpoons NO + O \tag{5.5}$$

Lavoie, et al. (1970) suggest that the reaction:

$$N + OH \rightleftharpoons NO + H \tag{5.6}$$

also contributes to the formation of oxides of nitrogen. This reaction becomes important at near stoichiometric and fuel rich mixtures. So it will be of little importance in this system.

Based on steady state approximation of the reaction:

$$O + OH \overset{M}{\rightleftharpoons} O_2 + H \tag{5.7}$$

and equilibrium assumption for O through:

$$O + O \overset{M}{\rightleftharpoons} O_2 \tag{5.8}$$

several authors have derived reaction rates for NO production in terms of the concentration of main species in the system, see for example Westenberg (1971), Bowman (1975), and Schefer and Sawyer (1977). It is shown that production of NO is exponentially dependent on temperature and in temperatures typical of flames, a ten percent increase in flame temperatures results in approximately a five-fold increase in NO production. NO_x concentrations in the recirculation zone have been plotted in terms of the reciprocal of adiabatic flame temperatures, Figure 5.19. Figure 5.19 confirms the fact that production of oxides of nitrogen have an Arrhenius dependence on flame temperature. The theoretical calculations of Westenberg (1971) and numerous derived reaction rates show that NO concentration has a mild (linear) dependence on residence time. It is known that in fuel lean systems, NO formation is a much slower process than the combustion rate, i.e. it is a post

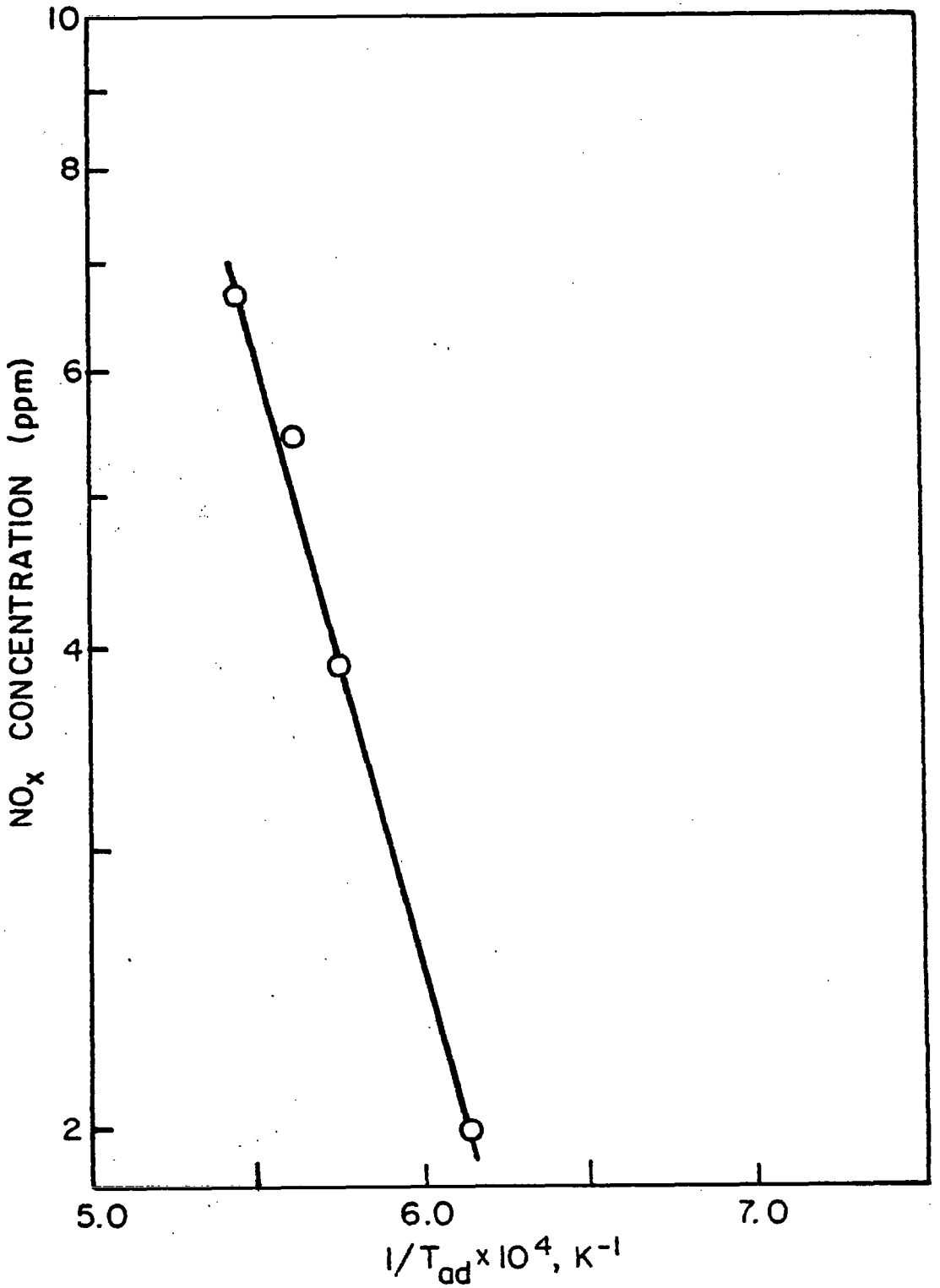

Fig. 5.19 Arrhenius plot of average oxides of nitrogen concentration at the recirculation zone.

flame process, Bowman (1975). To give an estimate of NO formation time, a characteristic time for formation of NO can be defined. Following Vranos (1974):

$$\tau_{NO} = \frac{[NO]_{eq}}{d[NO]/dt} \tag{5.9}$$

NO formation rate can be estimated according to Bowman (1975)

$$\frac{d[NO]}{dt} = 6 \times 10^{16} T_{eq}^{-\frac{1}{2}} \exp(-69090/T_{eq}) \cdot [O_2]_{eq}^{\frac{1}{2}} \cdot [N_2]_{eq} \frac{\text{moles}}{\text{cm}^3\text{sec}} \tag{5.10}$$

T_{eq} is the equilibrium temperature of the mixture. By substituting the data of Table 5.2 for $[NO]_{eq}$, T_{eq} and corresponding data for $[O_2]_{eq}$ and $[N_2]_{eq}$ in Equations 5.14 and 5.15, values of τ_{NO} can be calculated. These are also presented in Table 5.3. Values of τ_{NO} presented in Table 5.3 are several orders of magnitude higher than mixing and combustion times. Calculation of NO characteristic times from the formulation of Tuttle, et al. (1977) produced similar results. Increase in temperature or equivalence ratio drastically changes τ_{NO}. The conclusions form the above discussion are: (1) NO is produced in hot regions of the flame, (2) in a low temperature system such as the present, production of NO is slow, and (3) NO production is highly susceptible to thermal quenching

From the above consideration, it is speculated that oxides of nitrogen form primarily in the core of the large scale structures rather than reaction fronts which are mostly at the edge of the eddies. Also

for the same reasons, it is expected that augmentation of coalescence should reduce the rate of production of oxides of nitrogen. The speculations could not be directly confirmed in this experiment. With the help of above considerations, the behavior of NO_x in the test section can be better understood. High levels of NO_x in the recirculation zone is a result of transport from the reaction zone. This is confirmed by the fact that the temperature in the recirculation zone is considerably lower than further downstream of the step, see Figures 5.4 through 5.6, but NO_x concentration is comparable to NO_x levels at the reaction zone. Downstream of the recirculation zone, NO_x concentration peaks close to the bottom of the combustor, while at the same or higher levels of temperature in the shear layer, the NO_x concentration rapidly decreases. This is a combination of quenching, residence time, and mixing effects.

5.3.5 NO_2 Formation

Theoretical studies involving both chemical equilibrium considerations and chemical kinetic calculations have generally predicted that NO_2 should constitute a negligible fraction of the total oxides of nitrogen emitted from gas turbine combustors, Cernansky (1977). In their recent experiments of premixed combustion in an opposed reacting jet, Schefer and Sawyer (1977) found that, in the cooler regions of the flame, up to 100% of NO_x could be in the form of NO_2. Walsh (1975) has also measured substantial amounts of NO_2 at the exhaust of a gas turbine combustor. In the present experiment, NO_2 concentrations were calculated by the difference between measured values of NO_x and NO (by chemiluminescent analyzer). Sample profiles of NO_2 for the four

cases considered in these experiments are presented in Figures 5.8 through 5.11. The effect of inlet temperature and reference velocity on these profiles is shown in Figure 5.15.

A plausible kinetic mechanism proposed by Cernansky and Sawyer (1975) and Kramlich and Malte (1978) is:

$$\text{Flame cooling} \rightarrow HO_2$$

$$NO + HO_2 \overset{k_f}{\rightleftharpoons} NO_2 + OH$$

$$k_f = 10^{12.447 \cdot 5} T \exp\left(-\frac{2400}{RT}\right) \qquad (5.11)$$

The units are cm, gm-mole, k cal and sec. Formation of HO_2 is highly favored at lower temperatures. Possible reactions for formation of HO_2 are, Kramlich and Malte (1978):

$$H_2O_2 + H \overset{k_f}{\rightleftharpoons} HO_2 + OH \qquad k_f = 10^{13.447} \exp\left(-\frac{6400}{RT}\right) \qquad (5.12)$$

$$O_2 + H + M \overset{k_f}{\rightleftharpoons} HO_2 + M \qquad k_f = 10^{15.176} \exp\left(\frac{990}{RT}\right) \qquad (5.13)$$

For fuel lean mixtures, especially at low temperatures, Equation 5.13 becomes the main route to the formation of HO_2. The following reactions can destroy NO_2:

$$NO_2 + O \rightleftharpoons NO + O_2 \qquad k_f = 10^{13} \exp\left(-\frac{600}{RT}\right) \qquad (5.14)$$

$$NO_2 + H \rightleftharpoons NO + OH \qquad k_f = 10^{14.544} \exp\left(-\frac{1480}{RT}\right) \qquad (5.15)$$

Cernansky and Sawyer (1975) have shown that under fuel lean conditions, if the resulting cooling of hot combustion gases is rapid enough, radicals such as O, H and OH which favor NO_2 descruction fall to low levels and significant conversion of NO to NO_2 can occur via Equation 5.11. The present results, Figures 5.8 through 5.11, are consistent with the proposed mechanisms of NO_2 production. Figures 5.8 to 5.11 show that NO_2 is formed in cooler regions of flames at time average temperatures around and below 1500 K. Schefer (1976) also found that in the region where the temperature was in a range greater than 1400 to 1500 K (uncorrected for radiation), a measurable amount of NO could be detected.

Flow visualization in this system clearly shows the pattern of mixing and intermittency in this flame. Because of the form of the eddies, the intermittency increases towards the free stream, see Figure 5.17. Close to the bottom of the combustor the intermittency is minimum, implying that cold reactants and reacting mixtures seldom penetrate into this region. As a result of this and the high levels of temperature in this region, intermediate oxidizing species such as HO_2 will not be formed. Moving up towards the free stream, the chance of formation of HO_2 and subsequently NO_2 increases and this is exactly what is observed in the experimental results of NO_2.

Careful study of water-cooled and free-convection-cooled sample probe effects by Kramlich and Malte (1978) shows that the same reactions which can form NO_2 in combustion processes can convert NO to NO_2 in sampling probes. Their theoretical results are in fair agreement with the experimental results from a well-stirred reactor. Also, according to thier findings, the longer the uncooled portion of the probe that is

inserted into a hot region, the higher the possibility of conversion of NO_2 to NO. The argument does not seem to hold at least in the case of the present experiment, see Figure 5.10.b and 5.10.c. In the latter case, the insertion of the probe 25.4 mm into the flame corresponds to maximum NO_2. Johnson, et al. (1978) have used a laser resonance fluorescence technique to measure NO_2 *in situ* in a flame simultaneously with probe measurement techniques. They found that the true concentration of NO_2 in the flame was considerably less than the value recorded by the probing technique. Their measurements were performed on a CH_4 and H_2-O_2-N_2 flame on a circular schielded Meeks burner in the range of equivalence ratios of .83 to 1.05. The results of Johnson, et al. (1975) does not directly apply to turbulent flames (they themselves have noticed this fact).

Unfortunately, as many researchers have pointed out, Bowman (1975), Cernansky (1977), Kramlich and Malte (1978) and Schefer and Sawyer (1977), the mechanism that can cause the conversion of NO to NO_2 in the combustion system can equally alter NO to NO_2 in the probe, so a definite conclusion cannot be drawn with respect to the formation of NO_2. Overall results of the present experiments suggest that, because the pressure in this probe is much less than the cases considered by Kramlich and Malte (1978), the uncooled portion of the probe is much smaller, and $[NO_2]/[NO_x]$ levels are higher than their experimental and theoretical results; substantial amounts of NO_2 are formed in the shear layer rather than the probe. Direct confirmation of this speculation awaits further investigations and probably requires *in situ* measurement.

5.4 Unburned Hydrocarbons and Local Combustion Efficiency

Typical hydrocarbon concentration profiles (propane basis) are shown in Figure 5.20. Measured values of unburned hydrocarbons for the four cases of Table 5.1 were reported by Ganji (1979). Details of the oxidation of heavier hydrocarbons, including propane, is largely unknown and empirical reaction rates are usually obtained by curve fitting hydrocarbon consumption with respect to experimental variables, Schefer (1976). In their experiments of propane combustion in a flow reactor, Glassman, et al. (1975) measured hydrocarbons such as methane, ethane, ethene, etc. and partially oxidized hydrocarbons, such as accetaldehyde, which form after propane pyrolysis.

In the absence of detailed hydrocarbon species measurements, presenting the unburned hydrocarbon data in terms of equivalent propane is an approximation to the unreleased energy of combustion in the mixture. The effects of inlet temperature and reference velocity on hydrocarbon profiles 150 mm downstream of the step are shown in Figure 5.21. The figure shows the strong influence of temperature and residence time. An inlet temperature increase of 100 K could more than double the consumption rate of hydrocarbons. Despite high temperatures and long residence time of the flow in the lower part of the shear layer close to the bottom of the combustor, high levels of hydrocarbon (around 10% of free stream) were observed. This is attributed to the deep intrusion of fresh mixtures into the shear layer as has been discussed before.

Point efficiency of the flame was calculated by using the measured values of concentrations following the method introduced by Blazowski (1977).

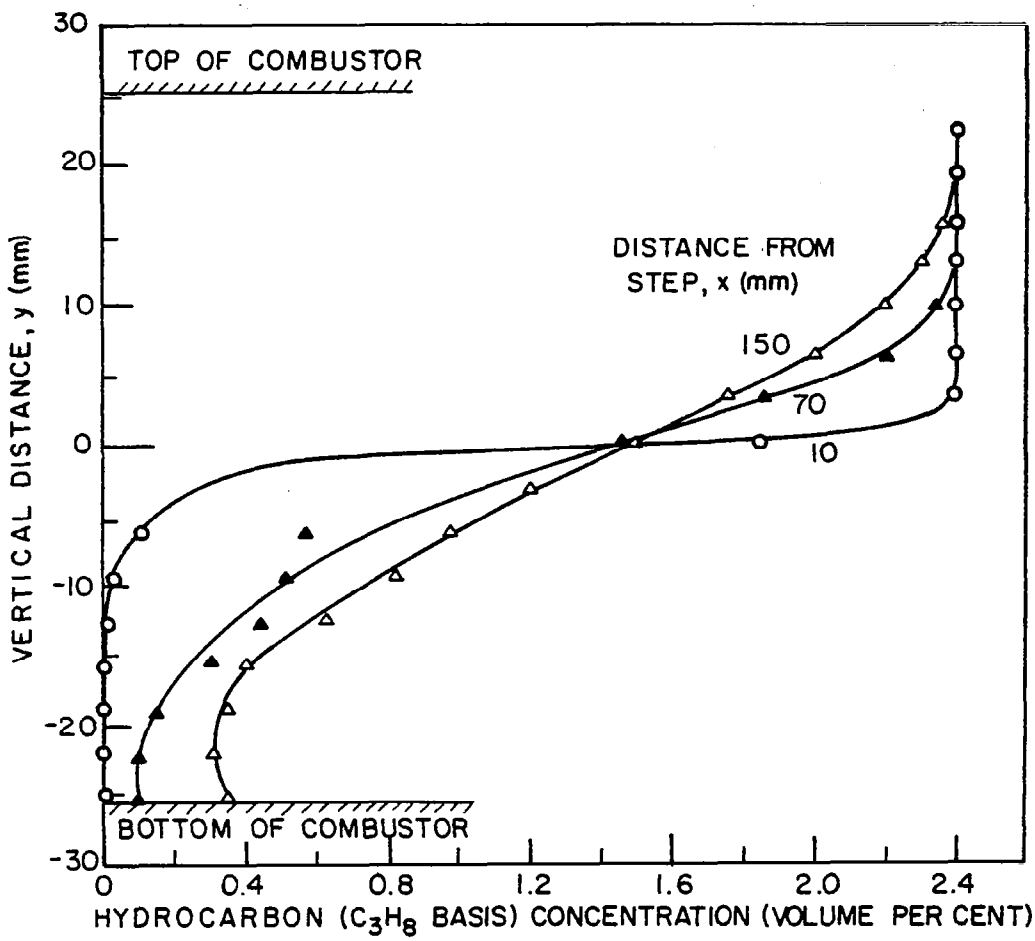

Fig. 5.20 Unburned hydrocarbon concentration inside the combustor. V_0 = 13.3 m/sec, N_{Re} = 8670 cm^{-1}, ϕ = 0.56, T_0 = 295 K (Case 1).

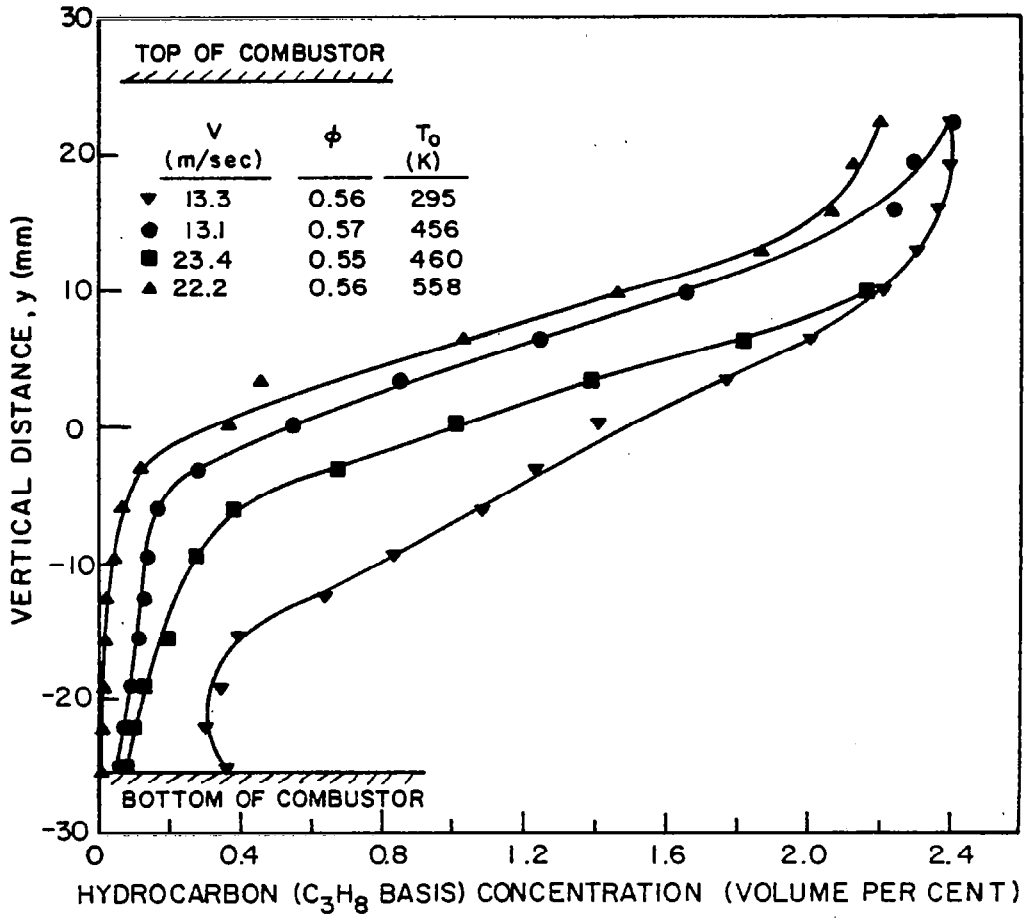

Fig. 5.21 Effect of velocity and inlet temperature on unburned hydrocarbon concentration at 150 mm downstream of the step.

In all efficiency calculations, the unburned hydrocarbons have been assumed to be in the form of propane (the fuel). While this method has proved to give good accuracy when applied to the exhaust emissions of gas turbine combustors, Moses and Stavinoha (1975), it will introduce some errors in the intermediate stages (where fuel hydrocarbons have been partially oxidized). Because of the lack of information about individual hydrocarbons and partially oxidized hydrocarbons, no attempt could be made to clarify this point. Figure 5.22 shows the local efficiency of the flame (case 1) at four different locations downstream of the step. The figure shows that the combustion is nearly complete in the recirculation zone, but the efficiency decreases sharply within the mixing/reacting zone. Downstream, as the mixing is increased, the drop in efficiency is more gradual. The flow at the top of the shear layer remains completely unreacted. The effects of inlet temperature and reference velocity are shown in Figure 5.23. Increases in temperature and residence time sharply increase the efficiency. Because the combustion in this system is entrainment controlled, even in the case in which residence time is close to an order to magnitude larger than combustion time (see Table 5.3), less than half of the combustion energy has been released at 150 mm downstream of the step.

5.5 Comparison of Pollutant Emissions and Efficiency

It was pointed out in the introduction (Chapter 1) that the main advantage of premixed prevaporized combustors over the conventional combustors is the low NO_x exhaust emissions while comparable overall efficiency in the combustor is maintained. The nautre of the present

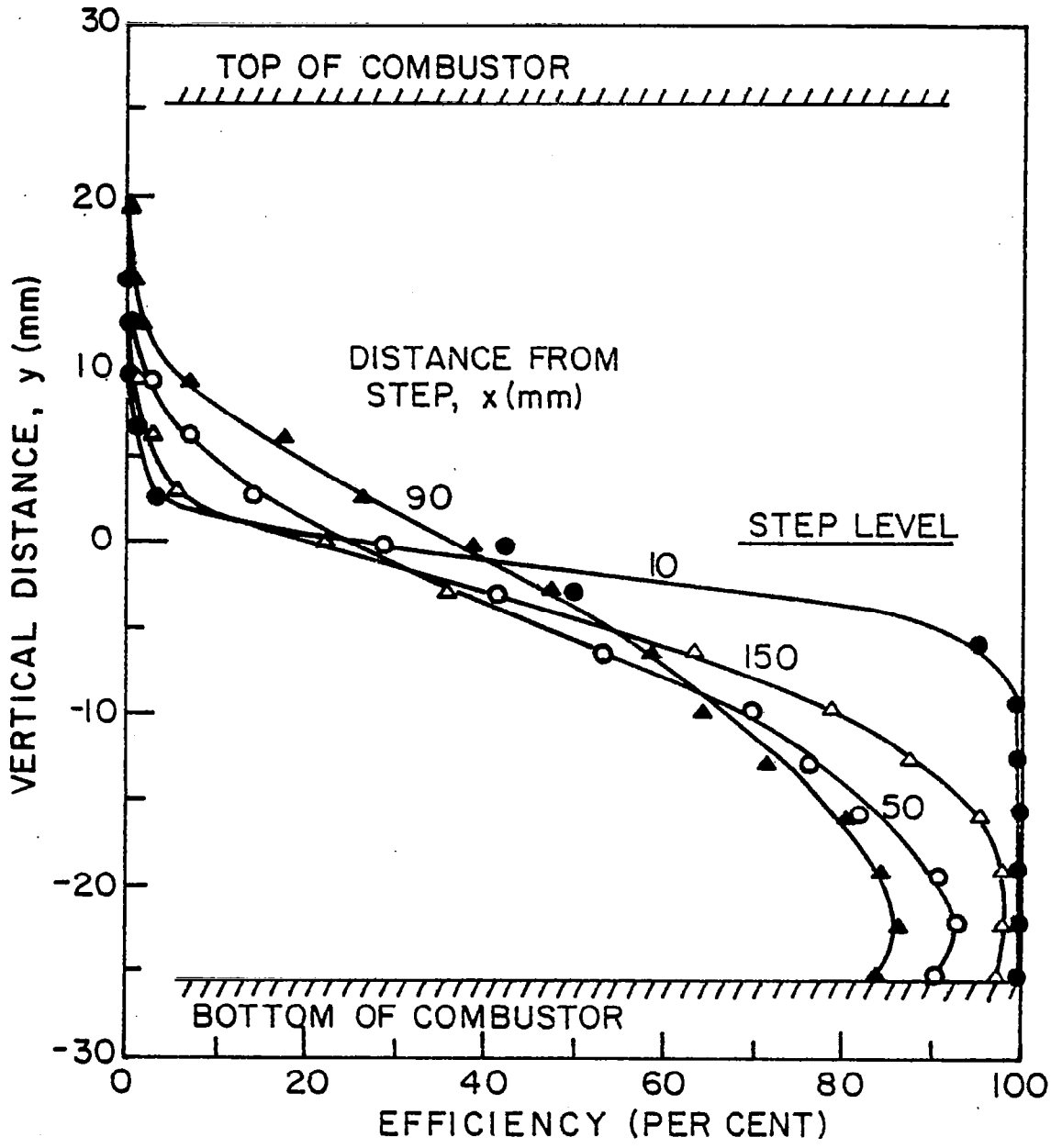

Fig. 5.22 Combustion efficiency along the combustor. V_o = 13.3 m/sec, N_{Re} = 8670 cm^{-1}, ϕ = 0.56, T_o =295 K (Case 1).

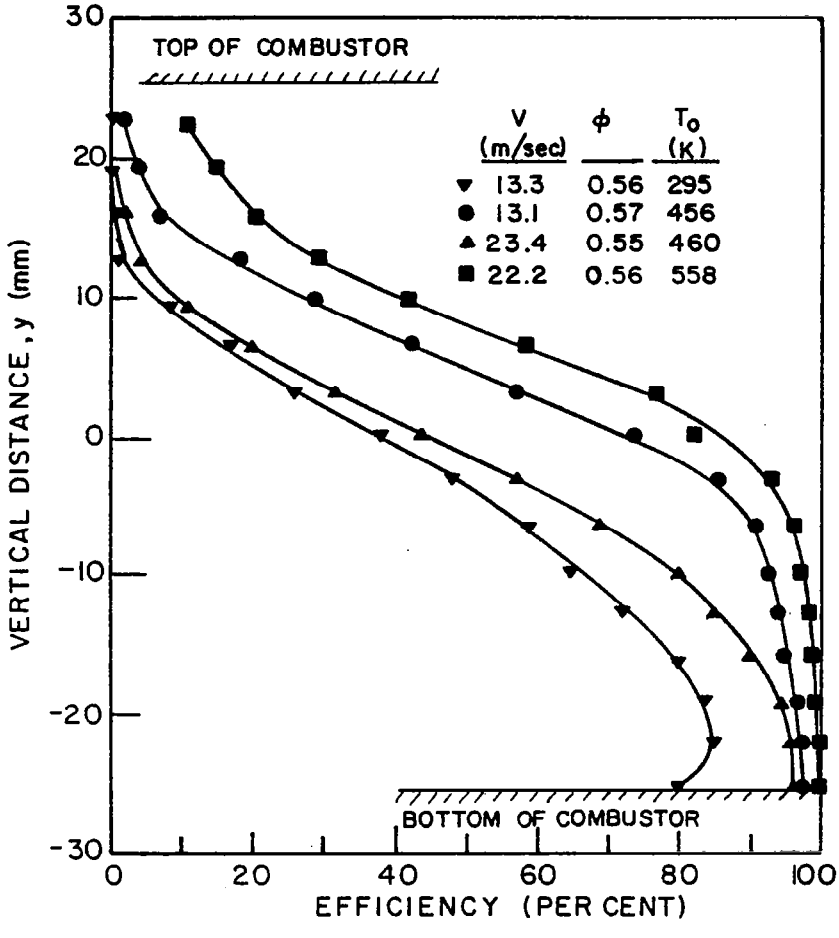

Fig. 5.23 Effect of velocity and temperature on combustion efficiency at 150 mm downstream of the step.

flame makes the direct comparison of the exhaust emissions rather irrelevant. This is because of the original design and purpose of the present experiment which was to study the propagation of the flame and subsequent pollution formation, rather than exhaust emission measurements. The combustor is too short to allow the reaction to approach completion. At the same time, it would be desirable to compare some emission levels obtained in the present investigation with those obtained in other premixed prevaporized combustors and also in some typical aircraft combustors. Emission levels are frequently presented in terms of an emission index (grams of pollutant per kilogram of fuel burned) to normalize emission on the basis of fuel flow. For the present combustor, emission indices were calculated for Case 3 at the point in the combustor downstream of the step where NO_x emission concentration is maximum (x = 150 mm, y = -16 mm). The results are compared in Table 5.4 with premixed prevaporized combustion emission levels of Schefer and Sawyer (1977) (T_{in} = 600 K, ϕ = 0.625, P_{in} = 1 atm), and Anderson (1975) (T_{in} = 600 K, ϕ = 0.56, P_{in} = 5.5 atm.); a conventional aircraft gas turbine engine, Pratt and Whitney JT9D (T_{in} = 710 K, P_{in} = 9.7 atm); and the supersonic aircraft gas turbine Olympius 593 (T_{in} = 824 K, P_{in} = 6.5 atm). Data for cruise conditions of the above two turbines were taken from Grobman and Ingebo (1975). Corresponding combustion efficiency is also shown for each case. A correlation equation developed by Niedzwiecki and Jones (1973) for application to swirl can and other lean combustors was used to correct the experimental data of the present investigation:

$$\frac{(EI_{NO_x})_1}{(EI_{NO_x})_2} = \frac{(P_{in}^{\frac{1}{2}})_1 (e^{T_{in}/288})_1}{(P_{in}^{\frac{1}{2}})_2 (e^{T_{in}/288})_2}$$

where P_{in} and T_{in} refer to combustor inlet pressure and temperature.

Table 5.4

Pollutant emission levels.

	EI_{UHC} (gCH_2/Kg fuel)	EI_{CO} (gCO/kg fuel)	EI_{NO_2} (gNO_2/kg fuel)	η_c (%)
Case 3	5.0	20.46	.38	99
Case 3 (corrected for JT9D)	-	-	1.99	-
Case 3 (corrected for Oly 593)	-	-	2.42	-
Schefer and Sawyer (1977)	6.8	5.2	.58	99
Anderson (1975)	-	-	1.0	> 99
JT9D, cruise	.1 - .3	.2 - .8	16 - 23	> 99
Olympus 593	< .1	1 - 5	18 - 1.9	> 99

Table 5.4 shows that the corrected maximum level of NO_x emission in this system is about an order of magnitude lower than those of conventional combustors. However, unacceptably high levels of unburned hydrocarbons and CO were obtained due to the nature of the

mixing in this system, the low flame temperature, and insufficient residence time. Slightly lower combustion efficiency is also due to the same effects. It was shown that inlet velocity and temperature have opposite effects on CO and unburned hydrocarbons on one hand and NO_x emissions on the other, see Figures 5.13, 5.14 and 5.21. Despite the shortcomings of this laboratory combustor as a practical gas turbine combustor (which it, of course, was never intended to be), lean premixed prevaporized combustion presents an attractive alternative to conventional combustion. For details of the subject, refer to the recent review by Jones (1978).

CHAPTER 6

CONCLUSIONS

6.1 Coherent Structures

The main objective of this work as stated in the introduction was to investigate the existence and importance of large coherent structures in the development of a reacting, and the corresponding nonreacting, two dimensional shear layer behind a backward facing step. Conclusions from these experiments are:

1. The large coherent structures previously observed to dominate the nonreacting free shear layers are also observed to dominate the reacting and nonreacting shear layers behind a backward facing step.
2. In the reacting case, the eddies persist all the way through the test section, but in the nonreacting flow they could not consistently be followed in the entire test section. The indistinguishibility of eddies in the nonreacting case is attributed to the inability of the schlieren system to resolve the vanishing temperature gradients.
3. Period and formation position of reacting and nonreacting eddies are found to be inversely affected by the Reynolds number, and negligibly affected by the equivalence ratio in the reacting case.
4. Combustion is confined to the eddies which develop as a result

of vortical action of the shear layer. The growth of vortices and the propagation of the flame are intimately linked. The dynamics of vortex pairing observed in the nonreacting flows is definitely one of the mechanisms for introduction of fresh reactants into the shear layer of a reacting flow.

5. On average the reacting eddies have a lower growth rate, are more closely distributed in space and have a slightly smaller rate of coalescence than nonreacting eddies with virtually the same reference velocity and initial Reynolds number.
6. Tripping the boundary layer changes the structure of the eddies both in reacting and nonreacting shear layers and, consequently, is expected to change the structure of the shear layer. Where the trip wire triggered the turbulent transition in the boundary layer, the coherent large scale structures could not be distinguished in the layer. Otherwise, the tripping just disturbs the boundary layer and delays the formation of coherent structures in the layer.

Just how truly two dimensional the flow is has not been fully established. The incoming flow is one dimensional, except at the walls which should not have an effect on the bulk of the flow in the combustion region. Time averaged probe measurements of compositions and temperature indicate that the flow is time-averaged two dimensional within ten percent over the transverse direction except at the walls. The schlieren visibility of the vortices argues that they are predominantly two dimensional structures and uniform along the optical path and that the mixing layer is uniform across the combustor. The decreased definition of the flow structures in the downstream region of the combustor could

be evidence of an increased three dimensionality of the flow or it could be the result of the fading of the optical density gradients in the other two dimensions.

6.2 Flame Stability

Regarding the stability of the flame, the main conclusions are:

1. Blowout is a gradual process, with the flame ceasing to propagate downstream of the recirculation zone in the mixing layer and then extinguishing in the recirculation zone.
2. A new type of upstream flame propagation (flashback) is observed in this system. It can be brought about by increasing the equivalence ratio. Upstream flame propagation is not a classical flashback, but a flame propagation in the bulk of the stagnant or reverse flow upstream of the flameholder edge. This stagnant or reverse flow field is created by pressure oscillations in the test section that can be about two orders of magnitude higher than the dynamic pressure of the flow.
3. Flashback is a transition process between the steady mode and the unsteady, "chugging" mode of operation of the system. "Chugging" is an oscillatory flow phenomenon.
4. Tripping the upstream boundary layer shifts the blowout limit to richer mixtures, creates a wide range of oscillatory mode of operation of the combustor which happens in the early stages of flashback and actually extends the range of operation of the combustor between blowout and flashback limits.

6.3 Time Average Flow Field Measurements

In the probe concentration measurements, it is observed that the region of maximum NO_x production does not necessarily coincide with the region of maximum temperature and that at regions of the flame with higher intermittency and cold reactant entrainment, almost all NO_x is in the form of NO_2.

6.4 Relation to Relevant Theoretical Models

The objective of the present experimental work was to clarify qualitatively some concepts dealing with flow fields that are academically and practically of great interest in the present stage of understanding of turbulent flows and flame propagation. It is hoped that eventually these concepts can be included in the theoretical considerations of turbulent reacting flows. Unfortunately, reasonable theoretical examination of a system such as the present one is beyond the contemporary state of the art of turbulence studies. Preliminary considerations of the concepts examined in this work have been employed in some resent theoretical investigations, the most relevant of which are briefly mentioned below.

Spalding (1978a) has proposed a theory called ESCIMO which separates the Lagrangian and Eulerian aspects of the turbulent reacting flows. The basic idea behind the theory concerns the formation of folds (layers) of the two different gases (reactants and partially or totally reacted products). The mixing/reaction starts propagating at the interface of the two layers and the rate of propagation corresponds to the rate of consumption of the reactants. In the theory, this rate is derived in terms of the age (time from the birth) of the layer. The

basic assumptions of this method when applied to a well-stirred reactor are: (a) knowledge of the thickness of the folds and their space distribution, (b) entrainment rates into the folds and (c) stretching rate of the folds. In this case, ESCIMO analysis proceeds by numerical integration of the one dimensional unsteady equations governing temperature and concentrations in the reacting layer and the results for different folds are summed with a suitable weighing for the whole population. The author suggests that the method is capable of handling complex chemical kinetic schemes with far less complexity than the Eulerian methods. The author has applied the method to the combustion of premixed reactants in a well-stirred reactor, Spalding (1978b), and obtained some qualitative results. The ability of the method to obtain quantitative results has not been established yet. The success of the method in application to more complex flows will depend on the possibility of incorporating fold formation statistics, fold transportation equations (details of the fluid mechanic aspects of the field), etc. into the theory, Spalding (1979).

Marble and Broadwell (1977) have used the same basic concept of interleaved gas folds, the contact surfaces of which are stretched in their plane under the diffusive character of turbulence. The flame propagation basically happens in the stretching surfaces. The effect of chemistry is separated from fluid mechanics and the only effect of the flame chemistry on turbulence is through heat release. Basically their method involves: a model for inhomogeneous turbulence, including closure conditions; a model for flame surface distribution over the turbulent region which leads to corresponding consumption and heat release rates; and, finally, calculation or measurement of the reactant

consumption rate for a laminar flame that is undergoing strain in its own plane.

Another promising method which so far has been applied only to nonreacting, uniform density, uniform viscosity shear layers is the vorticity generation and dispersal method developed by Chorin (1973). Ashurst (1977) has applied this method to the nonreacting free shear layers of Brown and Roshko (1974) and Winnant and Browand (1974). His results have quite similar visual appearance to those of the experimental work. The numerical simulation of aperiodic flow entrainment and vortex coalescence by this method is remarkable. The predicted shear layer spreading rates and other properties for the above two experiments are also acceptable. Ashurst (1978) has also applied the method to the present system for nonreacting flows. His computer-generated movies show a similar visual demonstration of the present experimental results. This method is being developed for application to reacting and non-reacting flows in this system, Ghoniem (1979).

REFERENCES

Anderson, D. (1975). Effects of Equivalence Ratio and Dwell Time on Exhaust Emissions from an Experimental Premixing Prevaporizing Burner. ASME Paper No. 75-GT-69.

Arnberg, B. T. (1962). Review of Critical Flow Meters for Gas Flow Measurement. Transactions of ASME, 84D, 447-460.

Ashurst, W. T. (1977). Numerical Simulation of Turbulent Mixing Layers Via Vortex Dynamics. Paper presented at the Symposium on Turbulent Shear Flows at Pennsylvania State University, University Park, Pennsylvania, April 18-20.

Ashurst, W. T. (1978). Private Communications. Sandia Laboratories, Livermore, California.

ASME (1959). Fluid Meters, Their Theory and Application.

Ballal, D. R. and Lefebvre, A. H. (1978). Weak Extinction Limits of Turbulent Flowing Mixtures. ASME Paper No. 78-GT-144.

Barrère, M. and Williams, F. A. (1969). Comparison of Combustion Instabilities Found in Various Types of Combustion Chambers. Twelveth Symposium (International) on Combustion, 169-181, The Combustion Institute, Pittsburgh.

Batt, R. G. (1975). Some Measurements of the Effect of Tripping the Two Dimensional Shear Layer. AIAA Journal, 13, 2, 245-246.

Baulch, D. L., Drysdale, D. D., Horne, D. G. and Lloyd, A. C. (1973). Evaluated Kinetic Data for High Temperature Reactions. Volumes 1 and 2. CRC Press, Cleveland, Ohio.

Betchov, R. and Criminale, Jr., W. O. (1967). Stability of Parallel Flows. Academic Press, New York.

Bilger, R. W. (1977). Probe Measurements in Turbulent Combustion. Progress in Astronautics and Aeronautics, 53, 49-69. (Zinn, B. T., Editor). American Institute of Aeronautics and Astronautics, New York.

Blazowski, W. S. (1977). Fundamentals of Combustion. Part I of AFAPL-TR-77-41.

Bowman, C. T. (1975). Kinetics of Pollutant Formation and Destruction in Combustion. Progress in Energy and Combustion Science, 1, 1, 33-45.

Bowman, C. T. (1977). Probe Measurements in Flames. Experimental Diagnostics in Gas Phase Combustion Systems. Progress in Astronautics and Aeronautics, 3, 3-24. (Zinn, B. T., Editor). American Institute of Aeronautics and Astronautics, New York.

Bowman, C. T. and Seery, D. J. (1972). Investigation of NO Formation Kinetics in Combustion Processes: The Methane-Oxygen-Nitrogen Reaction. Emissions from Continuous Combustion Systems, W. Cornelius and W. G. Agnew, Plenum, 123.

Browand, F. K. and Latigo, B. O. (1978). The Growth of the Two Dimensional Mixing Layer from Turbulent and Nonturbulent Boundary Layer. Project SQUID, Technical Report USC-1-PU.

Brown, G. L. and Roshko, A. (1974). On Density Effects and Large Structures in Turbulent Mixing Layers. Journal of Fluid Mechanics, 64, 775-816.

Cernansky, N. P. (1977). Sampling and Measuring for NO and NO_2 in Combustion Systems. Progress in Astronautics and Aeronautics, 53, 83-102. (Zinn, B. T., Editor). American Institute of Aeronautics and Astronautics, New York.

Cernansky, N. P. and Sawyer, R. F. (1975). NO and NO_2 Formation in a Turbulent Hydrocarbon/Air Diffusion Flame. Fifteenth Symposium (International) on Combustion, 1039-1050, The Combustion Institute, Pittsburgh.

Chigier, N. A. and Yule, A. J. (1979). The Physical Structure of Turbulent Flames. AIAA Paper No. 79-0217, 17th Aerospace Sciences Meeting, New Orleans, LA, January 15-17.

Chorin, A. L. (1973). Numerical Study of Slightly Viscous Flow. Journal of Fluid Mechanics, 57, 4, 785-796.

Corcos, G. M. and Sherman, F. S. (1976). Vorticity Concentration and the Dynamics of Unstable Free Shear Layers. Journal of Fluid Mechanics, 73, 2, 241-264.

Daily, J. W. (1978). Private Communications. Department of Mechanical Engineering, Berkeley.

Davies, P. O. A. L. and Yule, A. J. (1975). Coherent Structures in Turbulence. Journal of Fluid Mechanics, 69, 3, 513-537.

Dimotakis, P. E. and Brown, G. L. (1976). The Mixing Layer at High Reynolds Number: Large-Structure Dynamics and Entrainment. Journal of Fluid Mechanics, 78, 3, 535-560.

Eckert, E. R. G. and Goldstein, R. J. (1976). Measurements in Heat Transfer. 2nd Edition, Hemisphere Publishing Corporation, New York.

Environmental Protection Agency. (1976). Control of Air Pollution from Aircraft and Aircraft Engines - Supersonic Aircraft. Federal Register, 41, 34722-34725.

Fenimore, C. P. and Moore, J. (1974). Quenched Carbon Monoxide in Fuel Lean Flame Gas. Combustion and Flame, 22, 3, 343-351.

Fillipi, F. and Fabbrovich-Mazza, L. (1962). Control of Bluff Body Flameholder Stability Limits. Eighth Symposium (International) on Combustion, 956-963, The Combustion Institute, Pittsburgh.

Fristrom, R. M. and Westenberg, A. A. (1965). Flame Structure. McGraw-Hill Book Company, New York.

Ganji, A. R. (1979). Combustion and Stability Characteristics of a Premixed Vortex Dominated Two Dimensional Flow. Ph.D. Thesis, College of Engineering, University of California, Berkeley.

Ghoniem, A. (1979). Private Communications. Department of Mechanical Engineering, University of California, Berkeley.

Glassman, I., Dryer, F. L. and Cohen, R. (1975). Combustion of Hydrocarbons in an Adiabatic Flow Reactor; Some Considerations and Overall Correlations of Reaction Rate. Presented at Joint Meeting of the Central and Western States Sections of the Combustion Institute, The Combustion Institute, San Antonio, TX.

Gordon, S. and McBride, B. J. (1971). Computer Program for Calculation of Complex Chemical Equilibrium Compositions, Rocket Performance, Incident Shocks, and Chapman-Jouquet Detonations. NASA SP-273.

Grobman, J. and Ingebo, R. D. (1975). Forcast of Jet Engine Exhaust Emissions of High Altitude Commercial Aircraft Projected to 1990. Propulsion Effluents in Stratosphere, CIAP Monograph 2, Chapter 5.

Johnson, G. M., Smith, M. Y. and Mulcahy, M. F. R. (1978). The Presence of NO_2 in Premixed Flames. Presented at the Seventeenth Symposium (International) on Combustion, Leeds, England.

Jones, R. E. (1978). Gas Turbine Engine Emissions, Problems, Progress and Future. Progress in Energy and Combustion Science, 4, 2, 73-113.

Kaskan, W. E. (1957). The Dependence of Flame Temperature on Mass Burning Velocity. Sixth Symposium (International) on Combustion. The Combustion Institute, Pittsburgh.

Kent, J. A. (1970). A Noncatalytic Coating for Platinum Rhodium Thermocouples. Combustion and Flame, 14, 279-281.

Kim, J., Klines, S. J. and Johnston, J. P. (1978). Investigation of Separation and Reattachment of a Turbulent Shear Layer: Flow Over a Backward-Facing Step. Report MD-37, Thermoscience Division, Department of Mechanical Engineering, Stanford University.

Konrad, J. H. (1976). An Experimental Investigation of Mixing in Two Dimensional Turbulent Shear Flows with Application to Diffusion Limitted Chemical Reactions. Project SQUID, Technical Report CIT-8-PU, Purdue University.

Kramlich, J. C. and Malte, P. C. (1978). Modelling and Measurement of Sample Probe Effects on Pollutant Gases Drawn from Flame Zones. Combustion Science and Technology, 18, 91-104.

Landenburg, R. W., Lewis, B., Pease, R. N., Taylor, H. S. (1954). Physical Measurements in Gas Dynamics and Combustion. Princeton University Press.

Laufer, J. (1975). New Trends in Experimental Turbulent Research. Annual Review of Fluid Mechanics, 7, 307-326.

Lavoie, G. A., Heywood, J. B. and Keck, J. C. (1970). Experimental and Theoretical Study of Nitric Oxide Formation in Internal Combustion Engines. Combustion Science and Technology, 1, 313-326.

Lefebvre, A. H. (1966). CoA Note Aero. Report No. 163. The College of Aeronautics, Department of Propulsion, Cranfield Institute of Technology, Bedford, England.

Lefebvre, A. H. (Editor). (1977). Lean Premixed/Prevaporized Combustion. NASA CP-2016.

Lewis, B. and Von Elbe, G. (1961). Combustion, Flame and Explosions of Gases. 2nd Edition, Academic Press.

Libby, P. A. and Reiss, H. R. (1951). The Design of Two Dimensional Contraction Sections. Quarterly of Applied Mathematics, 10, 95-98.

Liepman, H. W. and Laufer, J. (1947). Investigation of Free Turbulent Mixing. NACA-TN-1257.

Liepman, H. W. and Roshko, A. (1957). Elements of Gas Dynamics. John Wiley and Sons, Inc.

Longwell, J. P. and Weiss, M. A. (1955). High Temperature Reaction Rates in Hydrocarbon Combustion. Industrial & Engineering Chemistry, 47, 8, 1634-1643.

Marble, F. G. and Broadwell, J. G. (1977). The Coherent Flame Model for Turbulent Chemical Reactions. Project SQUID, Report 29314-6001-RU-00, Purdue University.

Matthews, R. D., Sawyer, R. F., and Schefer, R. W. (1977). Interferences in Chemiluminescent Measurement of NO and NO_2 Emissions from Combustion Systems. Environmental Science and Technology, 11, 1092-1096.

Moses, C. A. and Stavinoha, L. L. (1975). Gas Chromatographic Analysis of Exhaust Hydrocarbons from a Gas Turbine Combustor. Paper No. 75-17, Presented at Western States Section, The Combustion Institute, Stanford Research Institute, Palo Alto, CA.

Niedzwieki, R. W. and Jones, R. (1973). Parametric Test Results of a Swirl Can Combustor. NASA TMX-68247.

Nicholson, H. M., and Field, J. P. (1949). Some Experimental Techniques for the Investigation of the Mechanism of Flame Stabilization in the Wakes of Bluff Bodies. Third Symposium (International) on Combustion, 44-68, Williams and Wilkins Co., Baltimore.

Offen, G. R. and Kline, S. J. (1974). Combined Dye-Streak and Hydrogen-Bubble Visual Observations of a Turbuelnt Boundary Layer. Journal of Fluid Mechanics, 62, 223-239.

Oppenheim, A. K. (1979). Private Communications. Department of Mechanical Engineering, University of California, Berkeley.

Papailiou, D. D. and Lykoudis, P. S. (1974). Turbulent Vortex Sheets and the Entrainment Mechanism of the Turbulent Wake. Journal of Fluid Mechanics, 62, 1, 11-31.

Parker, L. J., Sawyer, R. F. and Ganji, A. R. (1979). Measurement of Vortex Frequencies in a Lean, Premixed Prevaporized Combustor. Presented at Spring Meeting of the Western States Section of the Combustion Institute, Provo, Utah.

Pitz, R. W. (1978). Private Communications. Department of Mechanical Engineering, University of California, Berkeley.

Pitz, R. W. (1979). Ph.D. Dissertation, Department of Mechanical Engineering, University of California, Berkeley, California.

Plee, S. L. and Mellor, A. M. (1978a). Characteristic Time Correlation for Lean Blowoff of Bluff Body Stabilized Flames. Fall Meeting of Western States Section of Combustion Institute, October 16-17, Laguna Beach, California.

Plee, S. L. and Mellor, A. M. (1978b). Review of Flashback Reported in Prevaporizing/Premixing Combustors. Combustion and Flame, 32, 193-203.

Roffe, G. and Ferri, A. (1976). Effect of Premixing Quality on Oxides of Nitrogen in Gas Trubine Combustors. NASA CR-2657.

Roffe, G. and Venkataramani, K. S. (1978). Emission Measurements for a Lean Premixed Propane/Air System at Pressures up to 30 Atmospheres. NASA CR-159421.

Rosenhead, L. (1966). Laminar Boundary Layers, 465-506. Oxford University Press, Oxford, England.

Roshko, A. (1976). Structure of Turbulent Shear Flows; A New Look. AIAA Journal, 14, 10, 1349-1357.

Roshko, A. (1979). Private Communications. California Institute of Technology.

Russi, M. J., Cornet, I. and Cornog, R. (1953). The Influence of Flame Holder Temperature on Flame Stabilization. Fourth Symposium (International) on Combustion, 743-748. Williams & Wilkins Company, Baltimore.

Sato, H. (1956). Experimental Investigation on the Transition of Laminar-Separated Layer. Journal of the Physical Society of Japan, 11, 6, 702-709.

Sawyer, R. F., Cernansky, N. P. and Oppenheim, A. K. (1973). Factors Controlling Pollutant Emissions from Gas Turbine Engines. AGARD Conference Proceedings, No. 125 on Atmospheric Pollution by Aircraft Engines, Section 22-1-11.

Schefer, R. W. (1976). Pollutant Formation in Fuel Lean Recirculating Flows. Ph.D. Dissertation, Department of Mechanical Engineering, University of California, Berkeley.

Schefer, R. W. and Sawyer, R. F. (1977). Lean Premixed Recirculating Flow Combustion for Control of Oxides of Nitrogen. Sixteenth Symposium (International) on Combustion, The Combustion Institute, Pittsburgh.

Schlichting, H. (1968). Boundary Layer Theory. McGraw Hill Book Company, New York.

Sherman, F. S. (1976). The Dynamics of Unstable Free Shear Layers - Effects of Buoyancy and Nonlinear Interactions. Fluid Dynamics Transactions, 8, 141-193.

Spadaccini, L. J. (1977). Development of an Experiment for Determining the Autoignition Characteristics of Aircraft-Type Fuels. NASA CR-135329.

Spadaccini, L. J. and Szetela, E. J. (1975). Approaches to the Prevaporized Premixed Combustor Concept for Gas Turbines. ASME Paper No. 75-GT-85.

Spalding, D. B. (1978a). A General Theory of Turbulent Combustion. Journal of Energy, 2, 1, 16-23.

Spalding, D. B. (1978b). The Influences of Laminar Transport and Chemical Kinetics on the Time-Mean Reaction Rate in a Turbulent Flame. Seventeenth Symposium (International) on Combustion, to be published.

Spalding, D. B. (1979). The Theory of Turbulent Reacting Flows - A Review. AIAA Paper No. 79-0213. Presented at the 17th Aerospace Sciences Meeting, New Orleans, LA, January 15-17.

Stull, D. R. and Prophet, H. (1971). JANAF Thermochemical Tables, Second Edition. National Bureau of Standards, U. S. Department of Commerce.

Tennekes, H. and Lumley, J. L. (1972). A First Course in Turbulence. The MIT Press, Cambridge, MA.

Tuttle, J. H., Shisler, R. A., and Mellor, A. M. (1973). Nitrogen Dioxide Formation in Gas Turbine Engines: Measurements and Measurement Methods. Report No. PURDUE-CL-73-06, Purdue University.

Tuttle, J. H., Colket, M. B., Bilger, R. W., and Mellor, A. M. (1977). Characteristic Times for Combustion and Pollutant Formation in Spray Combustion. Sixteenth Symposium (International) on Combustion, 209-219, The Combustion Institute, Pittsburgh.

Vranos, A. (1974). Turbulent Mixing and NO_x Formation in Gas Turbine Combustors. Combustion and Flame, 22, 253-258.

Walsh, D. E. (1975). NO_2 Combustor Emissions Investigation. Technical Report AFAPL-TR-46.

Webster's New College Dictionary (1973). G. W. C. Merriam Company, Springfield, MA.

Weinberg, F. J. (1963). Optics of Flames. Butterworth & Company, London.

Westenberg, A. A. (1971). Kinetics of NO and CO in Lean Premixed Hydrocarbon-Air Flames. Combustion Science and Technology, 4, 59-64.

Williams, G. C., Hottel, H. C. and Scurlock, A. C. (1949). Flame Stabilization and Propagation in High Velocity Gas Streams. Third Symposium (International) on Combustion, 21-40, Williams and Wilkins Company.

Williams, G. C. and Shipman, C. W. (1953). Some Properties of Rod Stabilized Flames of Homogeneous Gas Mixtures. Fourth Symposium (International) on Combustion, Williams and Wilkins Company.

Williams, G. C., Woo, R. T., Shipman, C. W. (1957). Boundary Layer Effects on Stability Characteristics of Bluff Body Flame-Holders. Sixth Symposium (International) on Combustion, 427-438, The Combustion Institute, Pittsburgh.

Winnant, C. D. and Browand, F. K. (1974). Vortex Pairing: The Mechanism of Turbulent Mixing Layer Growth at Moderate Reynolds Numbers. Journal of Fluid Mechanics, 63, 2, 237-255.

Wright, F. A., and Zukoski, E. E. (1962). Flame Spreading from Bluff Body Flame Holders. Eighth Symposium (International) on Combustion, 933-943, The Combustion Institute, Pittsburgh.

Wygnanski, E. and Fiedler, H. E. (1970). The Two Dimensional Mixing Regions. Journal of Fluid Mechanics, 41, 2, 327-361.

Yule, A. J. (1978). Large Scale Structure in the Mixing Layer of a Round Jet. Journal of Fluid Mechanics, 89, 3, 413-432.

Zukoski, E. E. and Marble, R. E. (1956). Experiments Concerning the Mechanism of Flame Blow Off from Bluff Bodies. Proceedings of Gas Dynamics Symposium on Aerothermochemistry, 205-210, Northwestern University.

1. Report No.	2. Government Accession No.	3. Recipient's Catalog No.
NASA CR-3230		

4. Title and Subtitle	5. Report Date
TURBULENCE, COMBUSTION, POLLUTANT, AND STABILITY CHARACTERIZATION OF A PREMIXED, STEP COMBUSTOR	January 1980
	6. Performing Organization Code

7. Author(s)	8. Performing Organization Report No.
A. T. Ganji and R. F. Sawyer	None
	10. Work Unit No.

9. Performing Organization Name and Address	11. Contract or Grant No.
University of California Berkeley, California 94720	NSG-3028
	13. Type of Report and Period Covered
12. Sponsoring Agency Name and Address	Contractor Report
National Aeronautics and Space Administration Washington, D.C. 20546	14. Sponsoring Agency Code

15. Supplementary Notes

Final report. Project Manager, Cecil J. Marek, Airbreathing Engines Division, NASA Lewis Research Center, Cleveland, Ohio 44135.

16. Abstract

A two dimensional combustion tunnel was constructed to study a lean premixed turbulent propane/air flame stabilized behind a rearward facing step. Studied were: 1) the existence and importance of large coherent structures in turbulent reacting and nonreacting free shear layers behind the steps; 2) the effect of inlet temperature and reference velocity on combustion efficiency; 3) CO, NO_2 and NO_x production in the flame; and 4) the blowout and upstream propagation of the flame. In the ranges studied (reference velocity, 9.0 to 22.2 m/sec; inlet temperature, 295 to 560 K; equivalence ratio, 0.4 to 0.67; entrance Reynolds number, 0.39×10^4 to 1.5×10^4 cm^{-1}), the large coherent structures dominated both the reacting and the nonreacting free shear layers behind the step. The growth of the vortices and the propagation of the flame were intimately linked. Vortex pairing was observed to be one of the mechanisms for introduction of fresh reactants into the shear layer and growth of the shear layer. Probe composition measurements of the flame showed that, in the recirculation zone, the reaction was above 99% complete, CO and unburnt hydrocarbons were above the equilibrium level, NO_x concentration was far below the equilibrium level and NO_2 comprised a negligible fraction of NO_x.

17. Key Words (Suggested by Author(s))	18. Distribution Statement
Vortex shedding Premixed Propane/air Turbulence Combustion	Unclassified - unlimited STAR Category 07

19. Security Classif. (of this report)	20. Security Classif. (of this page)	21. No. of Pages	22. Price*
Unclassified	Unclassified	212	A10

* For sale by the National Technical Information Service, Springfield, Virginia 22161